Scientific report; 99 - 04

KNMI

ASGAMAGE:
the ASGASEX MAGE experiment

Final report

ed. W.A. Oost

De Bilt, 1999

Koninklijk Nederlands Meteorologisch Instituut

Scientific report = wetenschappelijk rapport; WR 99 - 04

De Bilt, 1999

PO Box 201
3730 AE De Bilt
Wilhelminalaan 10
De Bilt
The Netherlands
Telephone + 31(0)30-220 69 11
Telefax + 31 (0)30-221 04 07

Editor: W.A. Oost

UDC: 551.506.24
551.526.63
551.551.8
551.46.062

ISSN: 0169-1651

ISBN: 90-369-2164-3

ASGAMAGE

THE ASGASEX MAGE EXPERIMENT

CONTRACT MAS3-CT95-0044

FINAL REPORT

MAY 25, 1999

TABLE OF CONTENTS

[1] Now: National University of Ireland, Galway

ASGAMAGE, THE ASGASEX MAGE EXPERIMENT

Contract MAS3-CT95-0044

Management report
over the period September 1, 1998 – March 1, 1999

Final report

General

The activities for the project have come to an in general satisfactory end. The most important issue in this period has been the Final Workshop, held in Brussels at the EC-premises on January 6, 7 and 8, 1999, in conjunction with the MAST Air-Sea-Ice workshop on January 7 and 8. The presentations made there constituted the basis for the contributions of the various parties to the Detailed Scientific Report. Important activities in this last period were furthermore the application and intercomparison of the two newly developed computer models, mentioned in the Management Report for the period March '98-September '98, describing the air-sea gas exchange process. These models, one developed at KNMI, the other at Risø, support each others outcomes well. An important conclusion from the KNMI model, which is specifically aimed at estimating and describing the effects of vertical concentration gradients, is that a simplifying assumption, needed for the data-analysis of an important measurement method may have led to underestimation of the CO_2 exchange at the water surface by some 15%. More information can be found under 1.2, in the Publishable Synthesis and in the Detailed Scientific Report.
The ASGAMAGE Internet site (http://knmi.nl/asgamage) has been visited regularly.

In what follows we will again use the subject headings of the Technical Annex.

1. OBJECTIVES and METHODOLOGY

1.1. OBJECTIVE 1: To find relationships between the transport coefficients for the gas fluxes and any relevant geophysical parameters.

Analysis of the ASGAMAGE data is still continuing, outside the project proper. Both the diffenretial tracer and the eddy correlation data now indicate that of the two main contenders for the relationship between the transfer velocity k_w and the wind the one due to Wanninkhof agrees best with the experimental results, especially at higher wind speeds. This conclusion is independently supported by results from FASTEX, a US supported air-sea gas exchange experiment on the Atlantic Ocean. There has been an order of magnitude improvement in the correspondence between the results of various measurement methods (see under 1.2), but the uncertainty in the data is still too high to detect dependencies that are more subtle than the one with the wind. The accuracy does allow the conclusion, though, that there is no significant dependence of k_w on atmospheric stability.

1.2. OBJECTIVE 2: To intercompare different methods and systems to measure the transfer velocity of trace gases over the sea.

As stated before there appears to be a genuine difference between the eddy correlation and differential tracer results, not caused by inadequate practices or instrumentation deficiences. Based on the data, the model results and the specific conditions of the measurements a number of factors have been identified that contribute to that difference as well as to the rather high spread of the eddy correlation data. As noted under 1.3. there appears to be a gas concentration gradient just below the water surface. This gradient may well be one of the main causes for the remaining difference between the eddy correlation results and the differential tracer outcomes. Another important cause of these differences is short term fluctuations in e.g. the wind speed. These are

averaged out in the differential tracer outcomes, due to their long (24 hours and longer) measurement times, but visible in the eddy correlation results.

1.3. OBJECTIVE 3: To find out whether and, if at all, under what conditions, there can be significant carbon dioxide stratification in the upper meters of the water column.

The results of the KNMI model study (see the general part) indicate the existence of a permanent vertical concentration gradient close to the water surface. The main part of this gradient, which is different for different gases and fluctuating in time with the CO_2 concentration as well as with other parameters, is too close to the surface to have been measured with the instrument configurations used during ASGAMAGE. As stated under 1.2 it may have been one of the main causes of the remaining differences between the eddy correlation and differential tracer results.

1.4. OBJECTIVE 4: To test new methods and new equipment for the measurement of air-sea fluxes of CO_2, N_2O, CH_4 and DMS.

There are, as should be expected at this stage of the project, no further developments in this area compared to earlier reports. The earlier information is repeated below, with some additional remarks.

New methods that have been applied during ASGAMAGE are

- The differential tracer method using non-volatile tracers and a large overdetermination of the system through the use of five different tracers
- The eddy correlation technique for DMS and O_3
- The relaxed eddy accumulation technique for DMS
- The inertial dissipation method
- The simultaneous use of two CO_2 fluctuation sensors to reduce experimental noise.

New equipment:

- The closed NOAA/CMDL ultrasensitive CO_2 detection system, used for eddy correlation, relaxed eddy accumulation and gradient measurements of the CO_2 flux.
- The latest version KNMI Infrared Fluctuation Meter (for eddy correlation measurements)
- The equipment needed for the new techniques described above.

The eddy correlation and relaxed eddy accumulation measurements with the NOAA/CMDL instrument have only yielded upper limits, due to the long inlet tube, an insufficient flow speed in that tube and an unexpected difference in the effective flow speeds of water vapor and CO_2 in the tube. The relaxed eddy accumulation technique (applied by MPIC and NOAA) had not been used over sea before; the application of the eddy correlation method to DMS and O_3 over sea was new too (MPIC). The differential tracer technique has been extended with non-volatile tracers (NUT, PML, UEA). For a review of the results the reader is referred to the Detailed Scientific Report.

2. TASK STRUCTURE OF THE PROJECT.

The task structure, as indicated in the Technical Annex was followed; see 4.

3.ROLE OF PARTICIPANTS

The participants have made their contributions as agreed in the contract.

4. DETAILED DESCRIPTION OF TASKS

4.1 Financial management (full contract period).

All payments (except the final 10%) were received by the coordinator's Institute and were distributed among the Participants. Financial reporting has been made as required with the exception that the report of UCG over the second year came in too late at the institute of the Project Co-ordinator to be added to the overall report over that year.

4.2 Project organization and implementation (months 1-11).

The mutual contract has been signed by all participants and its organizational contents implemented at the 1997 workshop.

4.2.1. Platform (MPN and ship) provision (months 0-4)

This activity has been succesfully concluded.

4.2.2. Organization of transport and lodging (months 0-4)

This activity has been succesfully concluded.

4.3. 1st Experimental phase (months 3-7)

This activity has been succesfully concluded.

4.3.1. Preparation (trans/port, facilities, months 3-5)

This activity has been succesfully concluded.

4.3.2. Measurement phase (month 5-6)

This activity has been succesfully concluded.

4.3.3. Dismantling (months 6-7)

This activity has been succesfully concluded.

4.4. 2nd Experimental phase (months 8-12)

4.4.1. Preparation (transport, facilities, months 8-10)

This activity has been succesfully concluded.

4.4.2. Measurement phase (months 10-11)

This activity has been succesfully concluded.

4.4.3. Dismantling (months 11-12)

This activity has been succesfully concluded.

4.5. Analysis and verification phase (months 6-19)

This activity has been succesfully concluded.

4.6. Interpretation phase (months 19-31)

A number of conclusions have been reached, the results mentioned under 1.1, 1.2 and 1.3 are based on them. The total amount of information obtained in the Project is such that the Interpretation phase is at present still being continued, after the formal end of the Project.

4.7. Publications (months 0-36)

The first publications in the open literature have been accepted; more have been submitted.

5. MANAGEMENT OF THE PROJECT.

5.1. Organization

The organization of the project has been succesfully concluded.

5.2 Data management

Project data are available at the data exchange facility at KNMI, where the participants have stored them. A separate set on CD-ROM is accompanying this report.

5.3, 5.4 Meetings and Milestones

The experimental phases and workshops have been executed according to plan. The final workshop took place in the period January 6-8, 1999.

5.5 Reports.

All reports have been duly delivered.

6. DISSEMINATION AND EXPLOITATION OF RESULTS.

An Internet site about the project, with information suitable for both professional and lay persons is available under http://knmi.nl/asgamage .

7. WORK PLANNING SCHEDULE

Progress has been as planned.

Research cruises

ASGAMAGE contained two experimental periods, the first from May 6 - June 7, 1996 (ASGAMAGE-A), the second from October 7 - November 8, 1996 ASGAMAGE-B). During the B-period the UK ship RRS Challenger participated in the activities. The vessel sailed on 16 October and was operating in the vicinity of the release site and the Meetpost from 17 October until 31 October with the exception of one period of poor weather from 27 to 29 October. Some surveys and CTD stations were also made close to the Meetpost in support of their activities. Data has been archived by BODC. Full details of the cruise and the data collected are given in the NERC Cruise Report for Challenger 129. ROSCOP forms for this cruise have already been submitted.

Oral and poster presentations

Graham, A. 1998. Acoustic measurement of surface waves .*Oceanography '98*. Southampton, U.K., 7-11 September 1998.

Graham, A. 1998. Sonar studies of shallow-water dynamics. *Coastal and Marginal Seas*. Paris, France, 1-4 June 1998.

Graham, A. 1999. Measurements of the marine bubble layer. *Air-Sea Interface Symposium.* Sydney, Australia, 11-15 January 1999.

Jacobs, C.M.J. and W.A. Oost, 1999: A model study of the air-sea transfer velocity of carbon dioxide. *Oral Presentation at the 24th General Assembly of the European Geophysical Society,* April 18-22, 1999, Den Haag (NL).

Jacobs, C.M.J. and W.A. Oost, 1999: ASGAMAGE in a bird's-eye view. *Accepted as an oral presentation at the 1999 Spring Meeting of the American Geophysical Union*, June 1-4, Boston (USA).

Jacobs, C.M.J., 1997 Air-sea flux and transfer velocity of CO_2. *Seminar presented at Risø National Laboratory,* November 1997, Roskilde (DK).

Jacobs, C.M.J., 1998: CO_2 fluxen door het zee-oppervlak. *Seminar presented at the Royal Netherlands Meteorological Institute,* September 17 1998, De Bilt (NL).

Jacobs, C.M.J., 1999: The narrowing gap between direct and indirect observations of the air-sea transfer velocity of CO_2. *Oral presentation at the ASGAMAGE workshop*, January 5-8, 1999, Brussels, (BE).

Jacobs, C.M.J., J.F. Kjeld, S.E. Larsen and W.A. Oost, 1999: Possible consequences of near-surface tracer gradients for the air-sea transfer velocity of CO_2: some results from ASGAMAGE. *Accepted as poster presentation at the 1999 Spring Meeting of the American Geophysical Union*, June 1-4, Boston (USA).

Jacobs, C.M.J., W. Kohsiek, W.A. Oost, C. van Oort, H. Wallbrink and E. Worrell, 1997: KNMI analyses of ASGAMAGE data and results: status September 1997. *Oral presentation* at the ASGAMAGE workshop, September 22-25, 1997, De Bilt (NL).

Kjeld, J.F. and S.E.Larsen. Modeling of the air-sea exchange of CO2. Presented at the Ph.D.-course on Carbon Dioxide and Methane between the surface and the Atmosphere, Naturhøjskolen, Rødkilde, Stege Denmark, 3-7 November 1997.

Larsen, S E (1998) Surface fluxes in Climate System. Abstracts volume, European Climate Science Conference, Vienna, 19-23 October 1998, Abstract Volume, EC, Brussels, Belgium.

Larsen, S E (1999) Autonomous system for monitoring air-sea fluxes. MAST Projects Meeting : Air-Sea-Ice studies, Processes, Modeling and Instrumentation. Brussels january 7-7 1999.

Leeuw, G. de, G.J. Kunz, S.E. Larsen and F. Aa. Hansen (1999). Analyses of CO_2 fluxes measured with micrometeorological and geochemical techniques. ASGAMAGE workshop, Brussels, 6-8 January, 1999.

Nightingale P.D. Measurements of air-sea transfer velocity using deliberate tracers. ASI Interaction Meeting, Brussels, Jan 1999.

Nightingale P.D., Upstill-Goddard, R.C., Malin G., Liss P.S., Watson A.J., Schlosser, P., Ho, D.T and C.S. Law, Field measurements of air-sea gas exchange via the deliberate release of multiple tracers, Spring AGU, Boston, USA, 1999 (Invited Talk).

Nightingale, P.D., Upstill-Goddard, R.C., Malin, G., Watson, A.J., Liss, P.S., Law, C.S., Schlosser, P. and Ho, D. (1999). Field measurements of air-sea gas exchange using multiple tracers. Abstract submitted to IUGG99, Birminghamn U.K.

Oost, W.A. and C.van Oort: *New data for heat and moisture fluxes at sea.* EGS conference The Hague, April 19-23, 1999.

Oost, W.A.: *ASGAMAGE - finding out about greenhouse gases* Poster, Lissabon, May1998.

Oost, W.A.: *ASGAMAGE, a comprehensive air-sea gas exchange experiment.* 1997 Joint Assemblies of IAMAP/IAPSO, Melbourne, Australia, July 1-9, 1997.

Oost, W.A.: *ASGAMAGE: Trying to come to grips.* MAST workshop Sea-Air Exchange: Processes and Modelling, Kjeller, Norway, June 11-13, 1997.

Oost, W.A.: *Micro-meteorology and measurement of air-sea fluxes of CO2 at a coastal site.* Presentation at "Ocean-Atmosphere Exchanges near Coasts", Meeting Royal Meteorological Society/Challenger Society, London, UK, April 21, 1999.

Sprung, D., C. Jost, and T. Reiner, Development and improvement of an Atmospheric Pressure Ionization Mass Spectrometer for trace gas flux measurements using the eddy covariance method, to be presented at European Geophysical Society, XXIV. General Assembly, The Hague, 1999.

Upstill-Goddard, R.C., Nightingale P.D., Malin G. (1997). Air-sea gas transfer velocities determined with volatile and conservative tracers: first results from the ASGAMAGE experiment, October 1996, Joint Assembly of IAMAS/IAPSO, Melbourne, Australia.

Upstill-Goddard, R.C., Nightingale, P.D., Malin G. Broadgate, W. and Schlosser, P. (1997). Air-sea gas exchange rates measured with volatile and conservative tracers : first results from the ASGAMAGE experiment, October 1996. EC workshop (poster): "Greenhouse gases and climate: the status of research in Europe".

Upstill-Goddard, R.C., Nightingale, P.D., Malin G., Schlosser, P., Ho, D. and Suijlen, J. (1999). Sea-air gas transfer velocities in the southern North Sea measured with volatile and conservative tracers. Abstract (invited presentation) submitted to Royal Meterorological Society / Challenger Society joint meeting: "Air-sea exchanges near coasts", London 21 April 1999.

Woolf, D.K and Bowyer, P.A. 1997. Air-sea exchange in near-saturation conditions. Progress in Chemical Oceanography. Southampton, U.K., 18 September 1997.

Woolf, D.K. 1998. Large eddies and bubble plumes in surface renewal and air-sea gas transfer. *EUROMECH 387 - Surface Slicks and Remote Sensing of Air-Sea Interactions,* Warwick, England, 7-9 April 1998.

Woolf, D.K. 1999. Turbulence in coastal waters and air-sea exchange. Royal Meteorological Society/ Challenger Society joint meeting: Air-sea exchanges near coasts. London, U.K., 21 April 1999.

Woolf, D.K., Graham, A. Hall, A.J., and Ward, N. 1997. Observations of physical processes related to air-sea gas exchange. Greenhouse Gases and their Role in Climate Change: The status of research in Europe. Orvieto, Italy, 10-13 November 1997.

Woolf, D.K., Graham, A. Hall, A.J., Johnson, D. and Ward, N. 1999. Measurement of breaking wave statistics with a sector-scanning sonar. Air-Sea Interface Symposium. Sydney, Australia, 11-15 January 1999.

Publications and manuscripts

Many of the publications mentioned below as well as more general information about the project can be found on the Internet at www.knmi.nl/asgamage.

Anderson, R.J. and Stuart D. Smith, 1998: Data Workshop Report from BIO - ASGAMAGE-B. In: The ASGAMAGE workshop, September 22-25, 1997. (ed. W.A. Oost) *KNMI Scientific Report* 98-02, Royal Netherlands Meteorlogical Institute, de Bilt.

Bowyer, P.1998: Measurements of total gas saturation, bubble population and acoustic scattering during ASGAMAGE by University College Galway. In: The ASGAMAGE workshop, September 22-25, 1997. (ed. W.A. Oost) *KNMI Scientific Report* 98-02, Royal Netherlands Meteorological Institute, de Bilt.

Cohen, L.H., A.M.J. van Eijk, G.J.Kunz, G. de Leeuw and M.M. Moerman, 1997: TNO Physics and Electronics Laboratory (TNO-FEL), the Netherlands. In: W.A. Oost (Editor): ASGAMAGE, the ASGASEX MAGE experiment. Contract MAS3-CT95-0044, Report over the period March 1, 1996 - March 1, 1997, pp. 6-8.

Dissly,R.W., J.Smith, and P.P. Tans, 1998: Final Report on the NOAA/CMDL Contribution to ASGAMAGE-B. In: The ASGAMAGE workshop, September 22-25, 1997. (ed. W.A. Oost) *KNMI Scientific Report* 98-02, Royal Netherlands Meteorological Institute, de Bilt.

Graham, A., 1998: Sonar studies of shallow-water dynamics. TOS/IOC meeting on Coastal and Marginal Seas, Paris, June 1-4. Proceedings in *Oceanography*, 11.

Graham, A., 1999:. Measurements of the marine bubble layer. Symposium on Air-Sea Interaction, Sydney, January 11-15. In press.

Graham, A., and D.Woolf, 1998: Air-Sea Exchange Processes and their Remote Measurement by the Southampton University Department of Oceanography. In: The ASGAMAGE workshop, September 22-25, 1997. (ed. W.A. Oost) *KNMI Scientific Report* 98-02, Royal Netherlands Meteorological Institute, de Bilt.

Hare, J. and Chr. Fairall, 1998: NOAA/ETL Water Vapor Measurements During ASGAMAGE-B. In: The ASGAMAGE workshop, September 22-25, 1997. (ed. W.A. Oost) *KNMI Scientific Report* 98-02, Royal Netherlands Meteorological Institute, de Bilt.

Jacobs, C.J.M.W.Kohsiek, W.A.Oost, C.van Oort, H.Wallbrink and E.Worrell, 1998: KNMI analyses of ASGAMAGE data and results: status September 1997 In: The ASGAMAGE workshop, September 22-25, 1997. (ed. W.A. Oost) *KNMI Scientific Report* 98-02, Royal Netherlands Meteorological Institute, de Bilt.

Jacobs, C.M.J. and W.A. Oost, 1998: Can breaking waves bridge the gap between direct and indirect observations of the air-sea transfer velocity of CO_2? *Submitted for Publication in Journal of Geophysical Research.*

Jacobs, C.M.J. and W.A. Oost, 1999: A model study of the air-sea transfer velocity of carbon dioxide. *Geophysical Research Abstracts*, **1**, 574.

Jacobs, C.M.J., 1999: The narrowing gap between direct and indirect observations of the air-sea transfer velocity of CO_2. This report.

Jacobs, C.M.J., G.J. Kunz, D. Sprung and M.H.C. Stoll, 1998: CO_2 in water and air during ASGAMAGE: concentration measurements and consensus data. *KMNI Technical Report,* **TR-209**. Available from KNMI, De Bilt, The Netherlands.

Jacobs, C.M.J., J. Hare, G.J. Kunz, S.E. Larsen, G. De Leeuw, W.A. Oost, D. Sprung, and M.H.C. Stoll,1999: Micrometeorological aspects of air-sea exchange of CO_2 during ASGAMAGE. *In preparation.*

Jacobs, C.M.J., J.F. Kjeld, S.E. Larsen and W.A. Oost, 1999: Possible consequences of near-surface tracer gradients for the air-sea transfer velocity of CO_2. *In preparation.*

Jacobs, C.M.J., W. Kohsiek and W.A. Oost, 1997: Direct determination of the air-sea transfer velocity of CO_2 during ASGAMAGE. *KNMI Scientific Report 97-06.* Available from: KNMI, De Bilt, The Netherlands

Jacobs, C.M.J., W. Kohsiek and W.A. Oost, 1999: Air-sea fluxes and transfer velocity of CO_2 over the North Sea: results from ASGAMAGE. *Accepted for publication in Tellus (In Press).*

Jacobs, C.M.J., W. Kohsiek, W.A. Oost, C. van Oort, H. Wallbrink and E. Worrell, 1997: KNMI analyses of ASGAMAGE data and results: status September 1997. *In: Oost (ed.), Report of the ASGAMAGE workshop, September 22-25, 1997. KNMI Scientific Report,* **98-02**, 20-32.

Jacobs, C.M.J., W.Kohsiek and W.A.Oost, 1997: Direct determination of the air-sea transfer velocity of CO_2 during ASGAMAGE. KNMI Scient.Rep. 97-06

Kjeld J.F. and S.E.Larsen, 1997: Air-Sea exchange of CO2, different estimation techniques. Annales Geophysicae. Suppl.II to vol 15.Abstracts from 22nd General assembly of EGS. Part 2 p C414.

Kjeld, J. F. and Larsen, S. E., 1998: Air-Sea Exchange of CO2. Proceedings of the SNF workshop, Svaleholm, Risø, Denmark (Eds. Hertel, O., Zlatev, Z., Larsen, S. E., Mikkelsen, T.) NERI, Roskilde, Denmark. pp 53-60

Kjeld, J.F. and S.E. Larsen, 1997: Air-Sea Exchange of CO2, different estimation techniques. Annales Geophysica, suppl. II To vol 15. Abstract of the 22nd General Assembly of the EGS. Part 2. p. C414

Kjeld, J.F., S E Larsen and H.E.Jorgensen, 1997: Diffusion model for Air-Sea exchange of CO2, case study result. 3rd EU Conference on Exchange Processes for the Continent/Ocean Margins in the North Atlantic, Vigo, Spain 14-16 May 1997. Abstract Volume.

Kohsiek, W., 1998: Measurement of CO_2 fluxes with the IFM during ASGAMAGE. In: *The ASGAMAGE workshop, September 22-25, 1997* (ed. W.A. Oost), *KNMI Scientific Report* **98-02**, Royal Netherlands Meteorological Institute, De Bilt, 33-37. (Also available on Internet: *http://www.knmi.nl/asgamage).*

Kunz, G J, G deLeeuw, S E Larsen, F Aa Hansen, S W lund, 1998: CO2 Gas concentrations, gradients and air-sea exchanges during ASGAMAGE (TNO-FEL Results). In: The ASGAMAGE Workshop, September 1997 (Ed. W A Oost) KNMI Scientific Report, WR98-02, 95-104.

Kunz, G.J., 1998: CO_2 gas concentrations, gradients and air-sea exchange during ASGAMAGE-B (TNO contribution). TNO Physics and Electronics Laboratory, Report FEL-98-C169.

Kunz, G.J., F. Aa. Hansen, S.W. Lund, S.E. Larsen and G. de Leeuw, 1998b: CO_2 gas concentrations, fluxes and air-sea gas transfer during ASGAMAGE-A. TNO Physics and Electronics Laboratory, Report FEL-98-C193.

Kunz, G.J., G. de Leeuw, S.E. Larsen and F. Aa. Hansen, 1997: In: The ASGAMAGE workshop, September 22-25, 1997. (ed. W.A. Oost) *KNMI Scientific Report* 98-02, Royal Netherlands Meteorological Institute, de Bilt.

Kunz, G.J., G. de Leeuw, S.E.Larsen, F.Aa.Hansen and S.W.Lund, 1998: CO_2 Gas Concentrations, Gradients and Air-Sea Exchange during ASGAMAGE (TNO-FEL results). In: The ASGAMAGE workshop, September 22-25, 1997. (ed. W.A. Oost) *KNMI Scientific Report* 98-02, Royal Netherlands Meteorological Institute, de Bilt.

Kunz, G.J., S.W. Lund, S.E. Larsen, F. Aa. Hansen and G. de Leeuw, 1998a: Air-sea CO_2 gas transfer velocity during ASGAMAGE-B. TNO Physics and Electronics Laboratory, Report FEL-98-C190.

Larsen S.E., F.Aa. Hansen, G.Kunz, G. deLeeuw, 1999: Recent micrometeorological flux results from platform- and ship measurements. EGS XXIV General Assembly, The Hague, 19-23 April 1999. Geophysical Research Abstract, Vol 1, number 2, p449.

Larsen, S E, F Aa Hansen, J F Kjeld, S W Lund, G J Kunz and G de Leeuw, 1998: Experimental and modeling study of air-sea exchange of Carbon dioxide. In: The ASGAMAGE Workshop, September 1997 (Ed. W A Oost) KNMI Scientific Report, WR98-02, 116-123.

Larsen, S E, F. Aa. Hansen, G,deLeeuw and G.J.Kunz, 1997: Measurement of fluxes of momentum, heat, water vapour and CO2 over water by inertial dissipation and co-spectral estimation. Annales Geophys. Suppl. II to Vol 15. Abstracts of 22nd Assembly of EGS., Part 2 p. C438.

Larsen, S.E. F.Aa. Hansen, J.F.Kjeld, G.deLeeuw and G.Kunz, 1997: Experimental and modelling work on CO2 exchange. Abstract Volumen: NILU/EC-MAST workshop on Air-Sea Exchange 11-13 June 1997. Abstract Volume.

Larsen, S.E., 1997: Rapporteurs Report on Ocean Working Group. Abstract Volume International Workshop Greenhouse gases and their role in climate change: The status of research in Europe, Orvieto, Italy, 10-13 nov, 1997. To appear in proceeding.

Larsen, S.E., 1998: Air-Sea exchange of gases: Experiments and modelling. Proc. NILU/MAST workshop on Air-Sea Exchange 11-13 June 1997, EU-DGXII-MAST report, EUR 17660 EN, 293.

Larsen, S.E., 1999: Autonomous system for monitoring air-sea fluxes. MAST Projects Meeting : Air-Sea-Ice studies, Processes, Modeling and Instrumentation. Brussels january 7-7 1999.

Larsen, S.E., F Aa Hansen, J F Kjeld & S W Lund, G J Kunz, & G deLeeuw, 1997: Air-Sea Exchange of gases: Experiments and modelling. Abstract Volume International Workshop Greenhouse gases and their role in climate change: The status of research in Europe, Orvieto, Italy, 10-13 nov, 1997.

Larsen, S.E., F.Aa.Hansen, J.Friis Kjeld, S.W.Lund, G.J.Kunz and G. de Leeuw, 1998: Experimental and Modeling study of Air-Sea Exchange of Carbon Dioxide (Risø results) In: The ASGAMAGE workshop, September 22-25, 1997. (ed. W.A. Oost) *KNMI Scientific Report* 98-02, Royal Netherlands Meteorological Institute, de Bilt.

Larsen,S.E.,F.Aa. Hansen and S. Lund, 1999: Analyses of CO2 fluxes measured with micrometeorological and geochemical techniques. ASGAMAGE Final Workshop, Brussels january 6-8 1999. To appear in KNMI-report

Leeuw, G. de, G.J.Kunz, L.H. Cohen, M.M. Moerman and A.M.J. van Eijk, 1997: ASGAMAGE, MAS3-CT95-0044, First Annual Report. In: W.A. Oost (Editor): ASGAMAGE, the ASGASEX MAGE experiment. Contract MAS3-CT95-0044, Report over the period March 1, 1996 - March 1, 1997, Annex I (7 pp.).

Nightingale, P. D. and Upstill-Goddard, R. C., 1995: Measurements of air-sea gas exchange using the dual tracer technique. In: *Report of the ASGASEX '94 workshop* (W. Oost, ed). Tech. Rept. No. TR-174, 62 pp, KNMI, De Bilt, The Netherlands.

Nightingale, P.D., G. Malin, C.S. Law, A.J. Watson, P.S. Liss, M.I. Liddicoat, J. Boutin and R.C. Upstill-Goddard, In-situ evaluation of air-sea gas exchange parameterisations using novel conservative and volatile tracers Global Biogeochemical Cycles (submitted).

Nightingale, Ph., R.Upstill-Goddard, G.Malin, D.Ho, P.Schlosser, W.Broadgate and T.Sjöberg, 1998: Measurements Made During Challenger 129: A Contribution To ASGAMAGE. In: The ASGAMAGE workshop, September 22-25, 1997. (ed. W.A. Oost) *KNMI Scientific Report* 98-02, Royal Netherlands Meteorological Institute, de Bilt.

Oost, W. and B.J.Huebert, 1996: ASGAMAGE: Can't we make better measurements of air-sea exchange? *IGACtivities Newsletter* 6, 4-6.

Oost, W., 1998: The Effect of Long Measurement Times on Flux Measurements at Sea. In: The ASGAMAGE workshop, September 22-25, 1997. (ed. W.A. Oost) *KNMI Scientific Report* 98-02, Royal Netherlands Meteorological Institute, de Bilt.

Oost, W.A., 1997: *ASGAMAGE: Trying to come to grips*. In: Proc. NILU/MAST workshop on Air-Sea Exchange, Processes and modelling. Kjeller, Norway 11-13 June 1997, EU-DGXII-MAST report, EUR 17660 pp.257-263.

Rapsomanikis,S., D. Sprung, T. Kenntner, M. Baumann, 1998: Intermediate report on the contribution of the Max-Planck-Institute for Chemistry Mainz to the ASGAMAGE project In: The ASGAMAGE

workshop, September 22-25, 1997. (ed. W.A. Oost) *KNMI Scientific Report* 98-02, Royal Netherlands Meteorological Institute, de Bilt.

Upstill-Goddard R.C., J. Barnes, W. Broadgate, F. Carse, R. Downer, D. Ho, M-L. Lauria, S. Leigh, G. Malin, P. Nightingale, T. Sjoberg and G. Uher, 1997: The ASGAMAGE experiment, 16 October-1st November 1996: Gas transfer velocities and biogenic gas fluxes in the southern North Sea. NERC CRUISE REPORT : *Challenger* 129.

Upstill-Goddard, R. C. Nightingale P.D., Malin G., 1997: Sea-air transfer velocities in the southern North Sea measured with volatile and conservative tracers: first results from the ASGAMAGE experiment, October 1996 (Solicited Paper). *Annales Geophysicae Pt II, Suppl. II,* 15. European Geophysical Society, The Hague, Netherlands.

PhD -thesis.

Kjeld, J.F. 1999. A model study of the Air-Sea Exchange of Trace gases and the Wind flow in complex terrain. PhD-thesis. University of Odense and Risø National Laboratory. 203 p.

PUBLISHABLE SYNTHESIS OF SCIENTIFIC RESULTS

The ASGAMAGE project formally started on March 1, 1996 and lasted until March 1, 1999. The name is a contraction of ASGASEX (for Air Sea Gas Exchange, an earlier project with partially the same participants) and MAGE (for Marine Aerosol and Gas Exchange), activity 1.2. of IGAC, the International Global Atmospheric Chemistry project, which in turn is part of the IGBP programme. Three problems lay at the root of the project:

- the importance of the carbon balance with respect to the global climate, the sizable share of the oceans in this balance and the size of the "missing sink", the difference between the sum of the known sources and sinks that can not be attributed to a known process or depository.
- the search for the cause of the order-of-magnitude discrepancy between the air-sea transfer velocity k_w for CO_2 found with chemistry oriented methods (based on e.g. ^{222}Rn, ^{14}C, deliberate tracers) and with the newly developed micrometeorological techniques, especially the eddy correlation method and
- the large uncertainties in the values for the transfer velocity (even without the micrometeorological results) in combination with the expectation that there are more geophysical parameters affecting air-sea gas exchange beside wind speed (the rôle of which is generally accepted). Micrometeorological methods, with their measurement times in the order of half an hour, could be of prime importance for the study of these other parameters, because their effects are largely averaged out during the measurement periods of the chemistry oriented methods, which are in the order of a day or more.

The project focused on four objectives:

1. To find relationships between the transport coefficients for the gas fluxes and any relevant geophysical parameters.
2. To intercompare different methods and systems to measure the transfer velocity of trace gases over the sea.
3. To find out whether and, if at all, under what conditions, there can be significant carbon dioxide stratification in the upper meters of the water column.
4. To test new methods and new equipment for the measurement of air-sea fluxes of CO_2, N_2O, CH_4 and DMS.

Objectives 1, 2 and 4 can be directly understood from the motives for the project. Objective 3 resulted from the earlier ASGASEX experiment in which strong fluctuations of the CO_2 fugacity with the tide had been found, that could be seen as an indication of vertical concentration gradients. This was of special importance for the second objective because in the analysis of the differential tracer method the assumption is generally made that concentration gradients within the water column can be neglected and that for air-sea gas transfer processes only the surface is important.

The ASGAMAGE participants and their nationalities are given in Table 1. Three institutes from the American continent participated in the project; they were not supported from EU funds.
The project contained two experimental periods, the first one from May 6 - June 7, 1996, the second from October 7 - November 8, 1996. During the first period measurements were only made at and around Meetpost Noordwijk (MPN), a research platform 9km off the Dutch coast, owned and operated by RWS-DNZ (figure 1). The second experimental phase was again at MPN, but this time the RRS "Challenger" also participated, operating in the wider neighbourhood of MPN. These latter activities were primarily aimed at a determination of air-sea gas transfer coefficients with the differential tracer method being made simultaneously with the micrometeorological experiments. A full description of the instrumentation used during both experiments is well outside the scope of this paper. Figure 2 gives an impression of the sensors operated at MPN. The activities on the "Challenger" were devoted to the differential tracer experiment (tracer preparation, tracer release, sampling, analysis) and meteorological observations.

	Table 1. Participating institutes and departments	Nationality
1	Royal Netherlands Meteorological Institute (KNMI), Department of Oceanography (Project leader)	the Netherlands
2	Department of Harbours and Public Works (RWS-DNZ), North Sea Directorate	the Netherlands
3	Max Planck Institut für Chemie (MPIC), Abteilung Biochemie	Germany
4	University College Galway (UCG), Department of Oceanography	Ireland
5	Risø National Laboratory (Risø), Department of Meteorology and Wind Energy	Denmark
6	TNO Physics and Electronics Laboratory (TNO-FEL)	the Netherlands
7	Southampton Oceanographic Centre (SOC), George Deacon Division	United Kingdom
8	University of East Anglia (UEA), School of Environmental Sciences	United Kingdom
9	University of Newcastle upon Tyne (NUT), Department of Marine Sciences and Coastal Management	United Kingdom
10	Southampton University Department of Oceanography (SUDO)	United Kingdom
11	Plymouth Marine Laboratory (PML)	United Kingdom
12	NOAA Environmental Technology Laboratory, Boulder, CO (NOAA-ETL)	USA.
13	NOAAClimate Monitoring and Diagnostics Laboratory, Boulder, CO (NOAA-CMDL)	USA
14	Bedford Institute of Oceanography, Dartmouth N.S. (BIO)	Canada

Figure 1. The Meetpost Noordwijk platform with the outrigger extended.

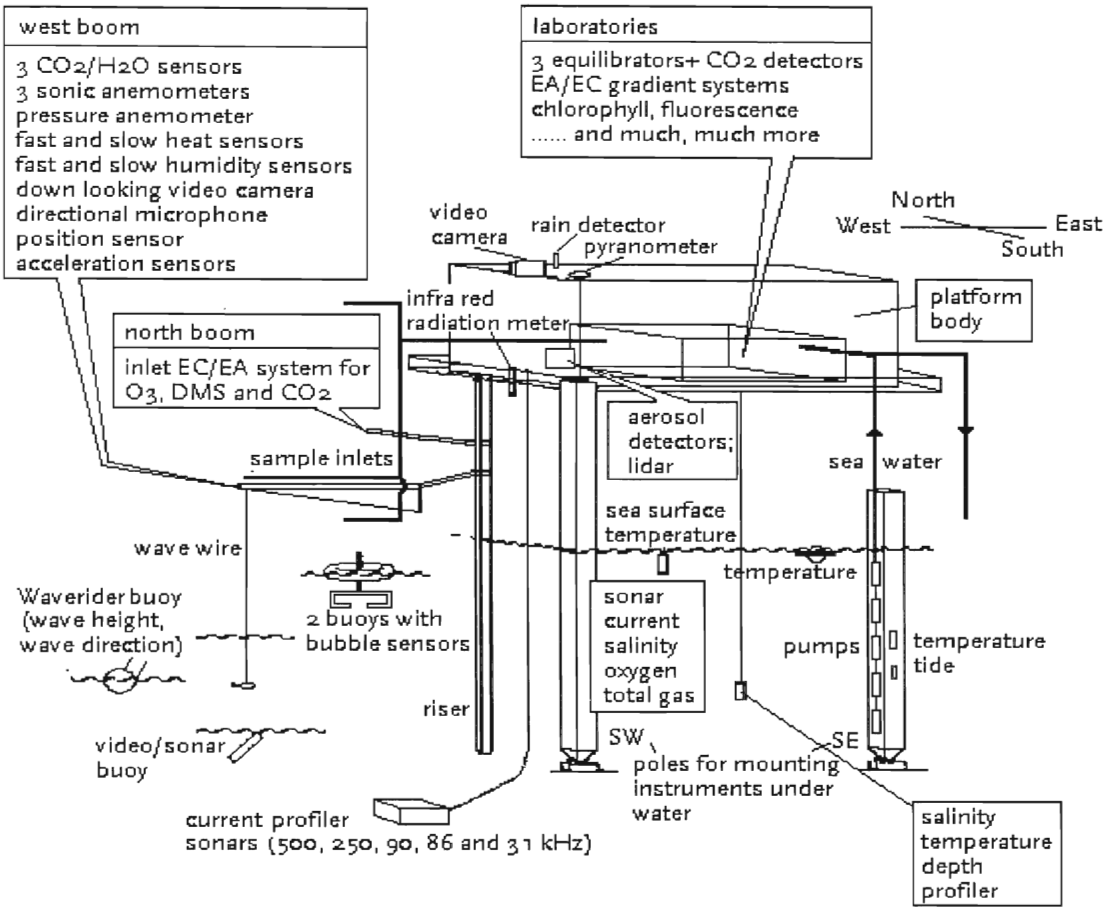

Figure 2. A schematic of Meetpost Noordwijk during ASGAMAGE, giving an impression of the instruments used during the experiments. "EA" (for eddy accumulation) and "EC" (for eddy correlation) are methods used to measure fluxes.

After the experimental phases the analysis and interpretation of the data were started. In behalf of the interpretation of the results two models were developed, a two-dimensional one, primarily aimed at estimating the effects of horizontal inhomogeneities on the results of the experiments and a one-dimensional one, specifically intended to estimate the effects of the various processes affecting air-sea gas transfer.

The one-dimensional model was developed at KNMI and specifically aimed at the study of the possible causes of the remaining discrepancy between the direct ec results and the tracer results on k_w. Crucial to the tracer method is a well-mixed water column. Simulations using this model suggest, however, that near-surface tracer gradients below the skin layer may cause the tracer methods to underestimate k_w by some 15% under conditions of strong turbulent mixing. A study with the two-dimensional model, independently developed at Risø, confirms the results of the one-dimensional model. If turbulence is suppressed - for example, by penetration of light into the water column - tracer gradients and therefore the difference with true value of k_w could become even greater.

The following conclusions can be drawn at the end of the project:

Concerning OBJECTIVE 1:

- Of the two main contenders for the relationship between the transfer velocity and the wind, the Liss-Merlivat and the Wanninkhof parameterizations, the one due to Wanninkhof agrees best with the experimental results, especially at higher wind speeds. This conclusion is independently supported by

results from GAS EX-98, a later, US supported, air-sea gas exchange experiment in the Atlantic Ocean.

- Despite a strongly improved accuracy of the micrometeorological results, reflected in an order of magnitude improvement in the correspondence between the results of various measurement methods, the uncertainty in the data is still too high to detect dependencies that are more subtle than the one with the wind.
- The accuracy of the data is nevertheless sufficiently high to allow the statement that there is no significant dependence of k_w on atmospheric stability.

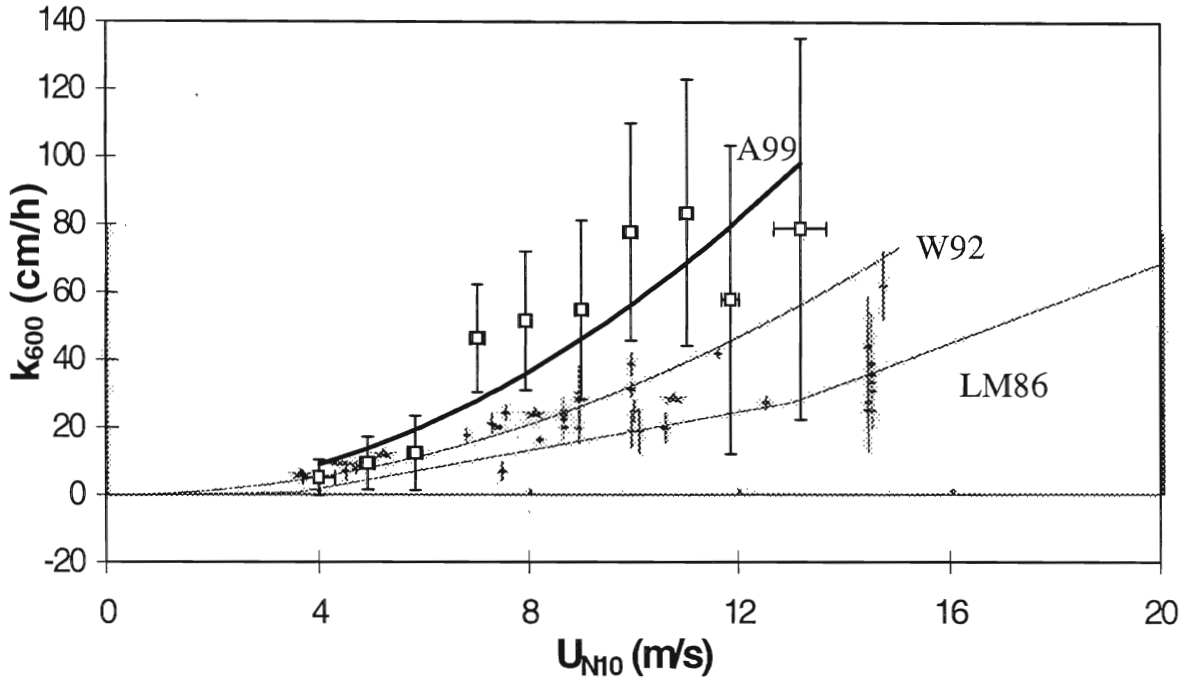

Figure 3: Air-sea transfer velocity of CO_2 normalised to a Schmidt number of 600 (k_{600}) versus wind speed at a height of 10m. Open squares: results from ASGAMAGE direct observations: averages over wind speed bins of 1 m/s (error bars denote 95% confidence limits); bold line, labelled A99: fit determined by Jacobs et al. (1999); dots and stars: results from ASGAMAGE multiple tracer and other field experiments. Solid lines labelled "W92" and "LM86" are fits proposed by Wanninkhof (1992) and Liss and Merlivat (1986), respectively.

Concerning OBJECTIVE 2:

- The order-of-magnitude difference between the transfer velocities found with the micrometeorological and with the differential tracer experiments is reduced to about a factor two (Figure 4).
- The remaining difference can be attributed to a number of well-defined causes and as such reflects the idiosyncrasies of the measurement methods.
- As noted below modelling results indicate a gas concentration gradient just below the water surface. This gradient is different for different gases. If indeed present it would have a small effect on the eddy correlation results. The differential tracer results would be affected to a much higher degree, causing an estimated 15% change in the values for the transfer velocity compared to the uniform situation.
- Another important cause of differences between the eddy correlation and differential tracer results is the daily trend in the data, which is averaged out in the differential tracer outcomes, due to its 24 hour (and longer) measurement times, but visible in the eddy correlation results.

Concerning OBJECTIVE 3:

- During ASGAMAGE no vertical carbon dioxide concentration gradients of the size seen in the 1993 experiment have been detected, neither at the platform, nor from the ship. Kunz et al. (1998) detected concentration fluctuations of about 15ppm, related to the tide
- The one dimensional model indicates the existence of a permanent vertical concentration gradient close to the water surface. The main part of this gradient is too close to the surface, however, to have been detected with the instrument configurations used during ASGAMAGE.

Concerning OBJECTIVE 4:
New methods that have been applied during ASGAMAGE are

- The differential tracer method using non-volatile tracers and a large overdetermination of the system through the use of five different tracers. This method has led to a higher accuracy of the final result. (Nightingale et al., 1999)
- The eddy correlation technique for DMS (MPIC).
- The relaxed eddy accumulation technique for DMS (MPIC)
- The inertial dissipation method (TNO-FEL and Risø, Kunz et al., 1998)
- The simultaneous use of two CO_2 fluctuation sensors to reduce experimental noise (TNO-FEL and Risø, Kunz et al., 1998).

New equipment used during ASGAMAGE:

- A closed ultrasensitive CO_2 detection system, used for eddy correlation, relaxed eddy accumulation and gradient measurements of the CO_2 flux designed, owned and operated by NOAA/CMDL.
- The latest version of the Infrared Fluctuation Meter for CO_2/H_2O eddy correlation measurements (KNMI, Kohsiek, 1998).
- Equipment for the new techniques indicated above, e.g. the APIMS (Atmospheric Pressure Ionization Mass Spectrometer) of MPIC

The eddy correlation and relaxed eddy accumulation measurements with the NOAA/CMDL instrument have only yielded upper limits, due to the long inlet tube, an insufficient flow speed in that tube and an unexpected difference in the effective flow speeds of water vapor and CO_2 in the tube. The relaxed eddy accumulation technique (applied by MPIC and NOAA) had not been used over sea before and is notoriously difficult to use there because of its high sensitivity to small misalignments. Much experience has been gathered, although the accuracy of the data was not yet sufficient to make them useful.
The application of the eddy correlation method to DMS over sea was new too (MPIC).
The differential tracer technique has been extended with non-volatile tracers (NUT, PML, UEA).
For a more extensive review of the results the reader is referred to the Detailed Scientific Report.

REFERENCES

Jacobs, C.M.J., W.Kohsiek and W.A. Oost, 1999: *Tellus B*, (in press).

Kohsiek, W., 1998. Measurement of CO_2 fluxes with the IFM during ASGAMAGE. In: *Report of the ASGAMAGE workshop, September 22-25, 1997* (ed. W.A. Oost), *KNMI Scientific Report* **98-02**, Royal Netherlands Meteorological Institute, De Bilt, 33-37. (Also available on Internet: *http://www.knmi.nl/asgamage).*

Kunz, G.J., S.W.Lund, S.E.Larsen, F.A.Hansen, G.de Leeuw, 1998: Air-sea CO_2 gas transfer velocity during ASGAMAGE-B. TNO report FEL-98-C190, 45 pp.

Liss, P.S. and L. Merlivat, 1986, *In: P. Buat Ménard (Ed.) The role of air-sea exchange in geochemical cycling*, 113-128, D.Reidel Publishing Company, Dordrecht.

Nightingale, P.D., G. Malin, C.S. Law, A.J. Watson, P.S. Liss, M.I. Liddicoat, J. Boutin and R.C. Upstill-Goddard, In-situ evaluation of air-sea gas exchange parameterisations using novel conservative and volatile tracers *Global Biogeochemical Cycles* (submitted).

Wanninkhof, R., 1992, *J. Geophys. Res.*, **97**, 7373-7382, 1992.

EXPLOITATION REPORT

An important result of ASGAMAGE is a better estimate of the inherent limitations of the methods in use to determine the transfer velocity k_w and therefore of the range of values in which k_w for CO_2 will lie. This will lead to a re-evaluation of the error limits of the oceanic sink in the Global Carbon Balance, and thus to a more realistic picture of the rôle the oceans play in the Global Change process. In the light of the post-Kyoto process the scientific and economic importance of this result needs little digression.
The clarification of the limitations of the present data and the identification of their causes are furthermore stimuli for new and more accurate measurements, which will lead to a narrowing of the error limits just mentioned. The ASGAMAGE participants will be the first, but hopefully not the only ones to exploit both the experimental and modelling results of ASGAMAGE to improve their instruments and analysis methods.
ASGAMAGE, by largely resolving the conflict between the chemistry based and micrometeorological methods, has become a stepping stone to a more accurate and better understood carbon balance.

ASGAMAGE Final Report

Contributions of the Royal Netherlands Meteorological Institute

Partner 1

Principal Investigator: Dr. W.A.Oost
Royal Netherlands Meteorological Institute,
P.O.Box 201, 3730 AE De Bilt, the Netherlands
Phone: +31 30 2206670; FAX +31 30 2210407
E-mail: oost@knmi.nl

Contributors: *Cor M.J.Jacobs, Wim Kohsiek, Cor van Oort and Wiebe A.Oost.*

Overview

The experimental contributions of KNMI to ASGAMAGE were centered around the measurements of the CO_2 flux with the eddy correlation (EC) method. To this end KNMI used a newly developed sensor, the Infrared Fluctuation Meter or IFM. In view of the existing controversy about the validity of the EC method for CO_2 fluxes much atteniton had to be devoted to the calibration of the instrument and a comparison with another fast responding CO_2 sensor. (W.K.)

During both ASGAMAGE experimental phases KNMI measured heat and moisture fluxes. These were necessary to be able to apply the so-called Webb correction (Webb *et al.*, 1980) to the EC data for the CO_2 flux. This produced a set of new values for the transfer coefficients for heat and for moisture, the Stanton number C_H and the Dalton number C_E. Because during the A-phase, in the spring, the atmospheric stratification was mainly stable and during the B-phase, in the fall, unstable KNMI could study stratification effects on C_H and C_E. This study provided new insights in the coherence of the various fluxes (W.O., C.J., C.v.O.).

The narrowing gap between direct and indirect observations of the air-sea transfer velocity of CO_2

Cor M.J. Jacobs

Introduction

Values of the air-sea transfer velocity (k) of CO_2 obtained with direct, micrometeorological measurements tend to be much higher than k values from indirect methods such as dual or multiple tracer experiments. During the ASGAMAGE field experiment, both types of measurements were performed in the same area. The direct method employed the eddy correlation (ec) technique to determine the CO_2 flux at Meetpost Noordwijk (MPN), a research platform 9 km off the Dutch coast in the North Sea. The ec-fluxes were combined with simultaneously measured air-sea concentration differences of CO_2 to determine k for CO_2 directly (Jacobs et al., 1999). In the same area a multiple-tracer experiment was performed using the UK research ship RRS "Challenger" from which k for CO_2 was determined indirectly (Nightingale et al., this volume). Results from both experiments are merged and shown in Fig. 1 as averages over wind speed bins, along with a fit from the ASGAMAGE ec-data determined by Jacobs et al. (1999). The figure also shows results from other field experiments, including the recent direct results from GASEX (Hare et al., this volume). Finally, the well-known fits of Wanninkhof (1992) and Liss and Merlivat (1986) are depicted. The direct ASGAMAGE and GASEX results show some agreement. They both follow the Wanninkhof (1992) fit at low wind speed. At some point (6 and 10 m/s, respectively) the increase of k with wind speed becomes much stronger than predicted by the Wanninkhof fit. Finally, k values from both experiments merge again at a wind speed greater than about 12 m/s. The tracer data follow the Wanninkhof fit up to $U_{10} \approx 10$ m/s. At higher wind speed, k according to the tracer data reaches only about half the value of k from direct method.
Some agreement between the methods emerges from the data, but differences are still too large to ignore. To investigate possible reasons for systematic differences between direct and indirect methods a modelling study was performed. The present contribution describes some of its results.

The model

The one-dimensional oceanic boundary layer model of Large et al. (1994) was used. This is a first-order closure (K) model with a countergradient correction term. The model allows for stabilisation of the water column, due to the penetration of light into the water column.
The model was adapted to the shallow depth of the North Sea, by incorporating a simple bottom boundary layer (BBL). The BBL is driven by velocity shear at the bottom, introduced by tidal currents that are simulated using a sinusoidal source function for momentum. Dissipation of wave energy at the bottom is ignored, which implies deep water waves. At MPN (average depth: 18 m) this condition is fulfilled if the wavelength at the peak of the wave spectrum is less than about 75 m. Usually, this criterion is met up to a wind speed of 14 -16 m/s (Oost, 1998).
An important extension of the model is the parameterisation for the effect of breaking waves on turbulence. (Bubble-mediated transport is not incorporated at present.) The parameterisation used here is based on Terray et al. (1996, 1997), who express enhanced turbulence by breaking waves in terms of dissipation of turbulent kinetic energy (tke):

$$\varepsilon = Eu_*^3/(\kappa d) \qquad (1)$$

where ε is the dissipation rate of tke, u_* is the friction velocity in the water, κ is the Von Kármán constant (0.4) and d is depth. Furthermore, E (≥ 1) is the enhancement factor, relative the to the "wall layer result" for κ in which case $E \equiv 1$. E can be scaled as (Burgers, 1997; Terray et al., 1997):

$$E = eH_s/d \qquad (2)$$

where H_s denotes significant wave height, which enters to scale the penetration depth of breaking waves. The scaling factor e that modulates E is taken to be a function of wave age (Terray et al., 1997), based on the data presented by Terray et al. (1996). At present the turbulent velocity scales (used to compute, for example, the turbulent diffusivity, K) of the model are adjusted by replacing u_*^3 by Eu_*^3. Then, the model formulation of turbulent transport becomes consistent with (1). The value of E is constant between the surface and depth d=0.6H_s (Terray et al., 1996) and can therefore never be larger than $1^2/_3e$. Observed relations between H_s and wind speed (U_{10}) and wave age and U_{10} at MPN lead to $e \approx 15$ at U_{10}= 8-10 m/s. The effect of breaking waves shows up at $U_{10} \approx 6$ m/s. This value of U_{10} is somewhat below the lower validity limit of U_{10} = 8m/s suggested by Terray et al. (1996). However, the influence of wave breaking is very small at U_{10} =6m/s and gradually increases with U_{10}.
The model was also extended to account for turbulent transport of passive dissolved gases. These tracers may be inert, like He and SF_6, or reactive CO_2. In the latter case, the slow hydration of CO_2 in water is taken into consideration, but chemical equilibrium between the concentration of HCO_3^- and CO_3^{2-} is assumed (cf. Emery, 1995).
A final major change to the model is the implementation of surface renewal theory to model the skin layer. According to this theory the flux of a tracer x across the skin layer, F_x, is given by:

$$F_x = (D_x/t_*)^{0.5}(C_b-C_i) \qquad (3)$$

where D_x is the molecular diffusion constant of x, t_* is the surface renewal time scale that characterises the residence time of fluid parcels in the skin layer, C_b is the bulk concentration of the tracer and C_i its concentration at the air-sea interface. The characteristic time t_* may be taken (Wick et al., 1996):

$$t_* \propto (\nu/\varepsilon)^{0.5} \qquad (4)$$

where• is the kinematic viscosity of water. The dissipation rate • is evaluated at the Kolmogorov microscale. It is taken equal to the buoyancy flux at the surface under convective conditions. Under the regime of shear driven turbulence• is computed from (1), using the roughness length in the water as the depth scale. The appropriate constants of proportionality are taken from Wick et al. (1996). The transition from one regime to the other is effectuated by taking the minimum value of t_* from the convective or the shear regime. Thus, t_* is controlled by the dominant turbulence production mechanism. Note that Wick et al. (1996) do not include wave breaking in their analysis. The present parameterisation provides a smooth transition between situations with and without wave breaking, without the need to introduce an extra regime (cf. Soloviev and Schlüssel, 1994).

The simulations

In the simulations presented here the model computes the tendency of longitudinal and lateral water speed (U and V, respectively), temperature, T, salinity, S, and concentration of some gaseous tracer, C.
Boundary conditions at the bottom are: C=C+, U=V=0, T=T+, S=S+, where + denotes the first model level above the seabed. The boundary conditions at the air-water interface are as follows: $C_o = H\,pC_a$, with H the solubility, pC partial pressure and with the subscripts o and a denoting "at the interface" and "in the air," respectively; salinity flux is $-QS_1$, where Q is water vapour flux (computed assuming a fixed relative humidity in the air) and S_1 is salinity at the first model level below the surface; T_a=T_0, so that the atmospheric stability is near neutral (small deviations from neutrality are due to the water vapour flux). Initially, a well-mixed water column is assumed with T=12 °C, S=31‰, U=V=0. The depth of the water column, h, is 18 or 40 m. The amplitude of the tidal current is 0.5 m/s, with two cycles per day. In the air, the wind speed at a height of 10 m, U_{10}, is constant. Simulations are performed for U_{10} = 2, 4, …, 16 m/s, respectively. Furthermore, the relative humidity of the air, used to compute Q, is 85% at a height of 10 m. In the case of temperature and salinity the conditions are forced to quasi-stationarity by defining a source term that exactly balances the surface flux.
Results from two sets of simulations with the general characteristics described above are presented. The first set simulates CO_2 fluxes and concentrations. It is intended as a model validation and to analyse the predicted contribution of enhanced turbulence by wave breaking to gas transport. Initial pCO_2 is 46 Pa in

the water and 36 Pa in the air, which were typical values near MPN at the end of the ASGAMAGE-B period. The concentration of CO_2 is forced to quasi-stationarity by taking the source term for carbon to balance the CO_2 efflux at the air-sea interface. Furthermore, a solar cycle is assumed that is valid for clear weather in May or October, near MPN (Holtslag and Van Ulden, 1983). The model results can be analysed in a way that corresponds to a direct determination of k using the ec-technique and are therefore denoted as the "ec-simulations." The second set is the simulation of a dual-tracer experiment in the North Sea, denoted as the "dual tracer simulations." In this set He and SF_6 are "released" in the same initial concentration ($4.15 \times 10^{-6} mg/m^3$), again assuming well-mixed conditions. Their concentration in the air is zero throughout the simulations. Simulations are performed assuming complete darkness, that is, without light penetrating into the water column, or with a realistic solar cycle for clear weather near MPN in May or October (Holtslag and Van Ulden, 1983). In the dual-tracer simulations there is no source term for the tracers in the water: the amount of tracer in the water will gradually be depleted.

Results

Figure 2 depicts k_{660}, the air-sea transfer velocity for CO_2 from the ec-simulations for October, normalised to a Schmidt number (Sc) of 660 (the salt-water value of Sc for CO_2 at a temperature of 20°C), as a function of U_{10}. It has been computed from the simulated surface flux of CO_2 and the concentration difference between air and water at a depth of 5 m. Total water depth is 18 m. Values are averages over 24 h.
Plain results from the model are shown as the diamonds. Without breaking waves k_{660} remains considerably smaller (dashes). It should be realised that the model does not include bubble mediated gas transfer. If one may assume that the total gas transfer is made up of independent contributions from direct and bubble mediated transfer (Woolf, 1997), a bubble contribution must be added to the results in order to compare the results with field observations. Here, the parameterisation of Woolf (1997) for the bubble-mediated part of k_{660} has been added and the sum of the model's k_{660} plus this bubble contribution is depicted as well (circles). It can be seen that the results with wave breaking agree rather well with the fit determined from direct observations by KNMI during the ASGAMAGE field experiment (Jacobs et al, 1999; Fig. 1; bold line). Without wave breaking the sum of k_{660} from the model and the bubble contribution (data not shown) agrees more with the Wanninkhof (1992) fit (dashed line). Because of the large uncertainty in the contributions from the bubbles and in the parameterisation of breaking waves it is fair to say that the present model predicts a quadratic fit of k_{660} on wind speed in between the fits from Wanninkhof (1992) and Jacobs et al. (1999). The results confirm that bubbles as well as turbulence characteristics under breaking waves need careful attention in order to be able to interpret the behaviour of k_{660}.
All results discussed above refer to 24-h averages, obtained at a constant wind speed. However, due to the water current the wind speed relative to the water varies slightly, which introduces a varying k_{660}. Examples of simulated diurnal variations are given in Fig 3. Most of such a variation can be resolved by means of direct methods to determine k because the averaging time of these methods is typically 1 hour or less. Expressing wind speed relative to water speed will at least partly remove the diurnal trends. However, indirect methods with their averaging period of – typically – 24 h or more, cannot resolve such a diurnal variation. This introduces an error in the measured k_{660} if there is a correlation between k_w and the air-sea concentration differences. Recent laboratory experiments indicate that such a correlation may exist (Liss et al, this volume).
Results of the dual tracer simulations are considered next. Results from the K-model are compared to results of a bulk model for the OBL. A bulk model exactly corresponds to the assumption made in tracer experiments that the water column is perfectly mixed, except for the skin layer. The concentration of a tracer, C, at any depth below the skin layer, is then given by:

$$C = C_n exp(-k\Delta t/h) \qquad (5)$$

where C_n the concentration at the start of each time step and k is the transfer velocity. The value of k is updated every time step and taken equal surface value from the detailed model during the corresponding

time step. In both cases k is computed from the concentration ratio of He and SF_6 (Nightingale et al, this volume).

$$k = -\frac{h}{\Delta t}\Delta\left[\ln\left(\frac{[\mathrm{He}]}{[\mathrm{SF}_6]}\right)\right]\left\{1-\left[\frac{Sc(\mathrm{He})}{Sc(\mathrm{SF}_6)}\right]^{0.5}\right\}^{-1} \qquad (6)$$

where • t is the time interval between two "samples" (here 2 hours). The simulated course of $\ln([He]/[SF_6])$ according to two models is depicted in Fig. 4 (depths: 18m and 40m, respectively; U_{10}=8 m/s). Results of the K-model are shown for complete darkness and with solar cycle in October, respectively. The most important feature of these results is the different slope • $\ln([He]/[SF_6])/\bullet$ t. This difference leads to k values that are typically 15% smaller for the K-model than for the bulk model. Another important feature is the deviation from linear behaviour if a solar cycle is present. The most likely cause of the differences between the two models is the occurrence of concentration gradients in the water column. To investigate this further the "degree of unmixing," $D_u = R(d)/R(d=2)$, (where $R(d)$ = $[He]/[SF_6]$ at depth d) is plotted as a function of depth in Fig. 5, for various times of the day, indicated in Universal Time Code (UTC). For the bulk model, D_u = 1 everywhere. However, D_u varies considerably for the K-model, especially just below the surface, and under strong insolation (see profile of 12 UTC). During tracer experiments in the field, concentration ratios are checked below a depth of 1-2 m or so and no large deviations have been found so far. The present model results are consistent with these observations, at least for the well-mixed situation in darkness, but suggest that concentrations should be checked in the one or two upper meters of the water column. Independent simulations at Risø by means of a 2-D model (Kjeld, 1999) confirm the results from the 1-D K-model (Fig. 6). Although the influence of light in the model might be exaggerated, the results nevertheless suggest that the influence of light should be considered in more detail in future experiments. The values of k according to the dual tracer simulations were compared to k values from the ec-simulations. Figure 7 shows the difference between the k values from the different simulations as a function of wind speed, expressed as the amount with which the simulated tracer-results need to be adjusted to obtain the ec-results. The difference for the relatively well-mixed conditions during complete darkness is about 15 %. Penetration of solar radiation may cause much larger differences between the two methods. Note that both methods suffer from the existence of a concentration gradient below the surface. However, the influence on the ec-method is less because the reactivity of CO_2 tends to reduce the gradients (data not shown) and the difference between the "observed" k with the surface value of k is only about 3% in this case.

References

Burgers, G., 1997, *J. Phys. Oceanogr.*, **27**, 2306-2307.

Emery, S., 1995, *in B. Jähne and E.C. Monahan (Eds.), Air-water gas transfer,* 25-35, AEON Verlag & Studio, Hanau.

Hare et al, this volume

Holtslag A.A.M. and A.P. Van Ulden, 1983, *J. Climate Appl. Met.*, **22**, 517-529.

Jacobs, C.M.J., W.Kohsiek and W.A. Oost, 1999: *Tellus B*, (in press).

Kjeld, J.F., 1999. *Model study of the air-sea exchange of trace gases and of wind flow over complex terrain.* PhD- thesis, Risø National Laboratory, Dept. Wind Energy and Atmospheric Physics (VEA), Roskilde.

Large, W.G., J.C. McWilliams and S.C. Doney, 1994, *Reviews of Geophysics*, **32**, 363-403.

Liss, P.S. and L. Merlivat, 1986, *In: P. Buat Ménard (Ed.) The role of air-sea exchange in geochemical cycling*, 113-128, D.Reidel Publishing Company, Dordrecht.

Liss, P.S., et al, This volume

Nightingale, P., et al., This volume

Soloviev, A.V. and P. Schlüssel, 1994, *J. Phys. Oceanogr.*, **24**, 1339-1346.

Terray, E.A., M.A. Donelan, Y.C. Agrawal, W.M. Drennan, K.K. Kahma, A.J. Williams III, P.A. Hwang and S.A. Kitaigorodskii, 1996, *J. Phys. Oceanogr.*, **26**, 792-807.

Terray, E.A., M.A. Donelan, Y.C. Agrawal, W.M. Drennan, K.K. Kahma, A.J. Williams III, P.A. Hwang and S.A. Kitaigorodskii, 1997, *J. Phys. Oceanogr.,* **27**, 2308-2309.
Wanninkhof, R., 1992, *J. Geophys. Res.*, **97**, 7373-7382, 1992.
Wick, G.A., W.J. Emery, L.H. Kantha and P. Schlüssel, 1996, *J. Phys. Oceanogr*, **26**, 1969-1988.
Woolf, D.K., 1997, *in P.S. Liss and R.A. Duce (Eds.), The sea surface and global change*, 173-206, Cambridge University Press, Cambridge.

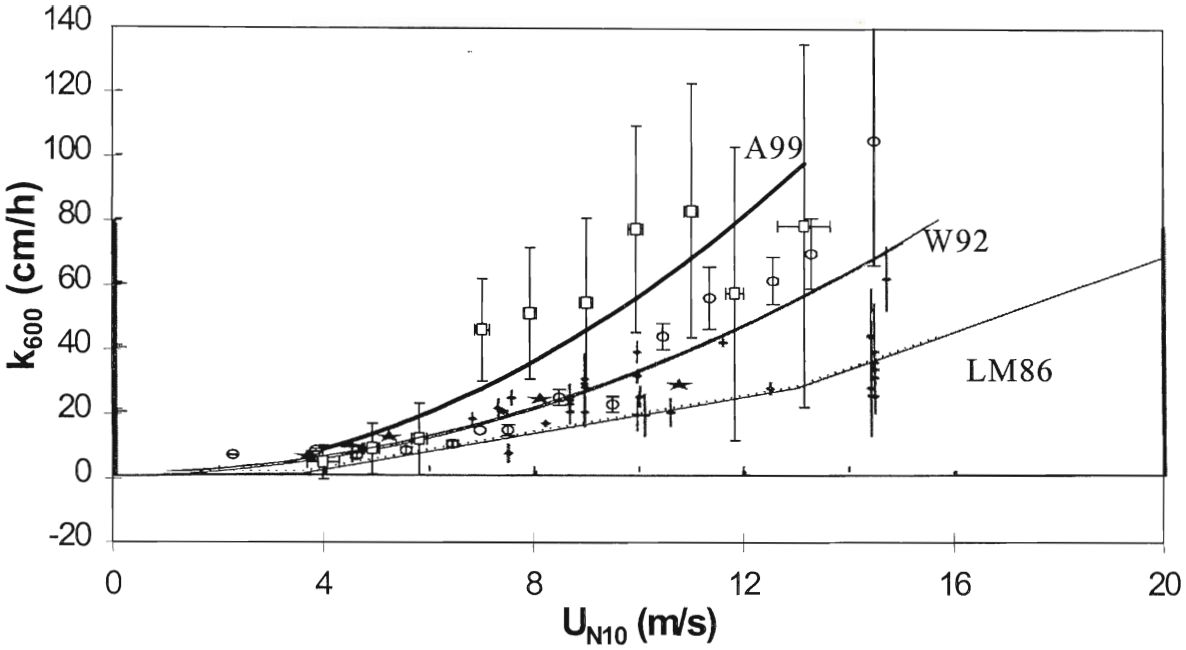

Figure 1: Air-sea transfer velocity of CO_2 normalised to a Schmidt number of 600 (k_{600}) versus wind speed at a height of 10m. Open squares: results from ASGAMAGE direct observations: averages over wind speed bins of 1 m/s (error bars denote 95% confidence limits); bold line, labelled A99: fit determined by Jacobs et al. (1999); dots and stars: results from ASGAMAGE multiple tracer and other field experiments (see Nightingale et al (this volume) for details); Solid lines labelled "W92" and "LM86": fits proposed by Wanninkhof (1992) and Liss and Merlivat (1986), respectively. Open circles: direct GASEX results (Hare et al, this volume).

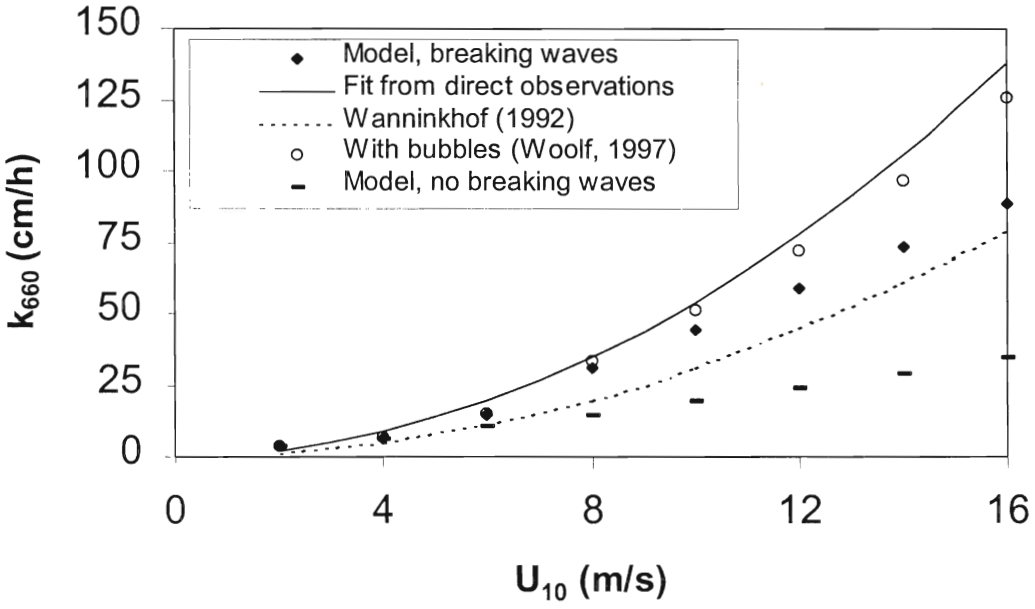

Figure 2: Air-sea transfer velocity for CO_2 normalised to a Schmidt number of 660 (k_{660}) versus wind speed at a height of 10m. Diamonds: model results with wave breaking; circles: sum of model results with wave breaking and an independent contribution from bubble mediated gas transfer according to Woolf (1997); separate dashes: model results without wave breaking; solid line: fit from direct ASGAMAGE observations (Jacobs et al., 1999) dashed line: Wanninkhof (1992) fit.

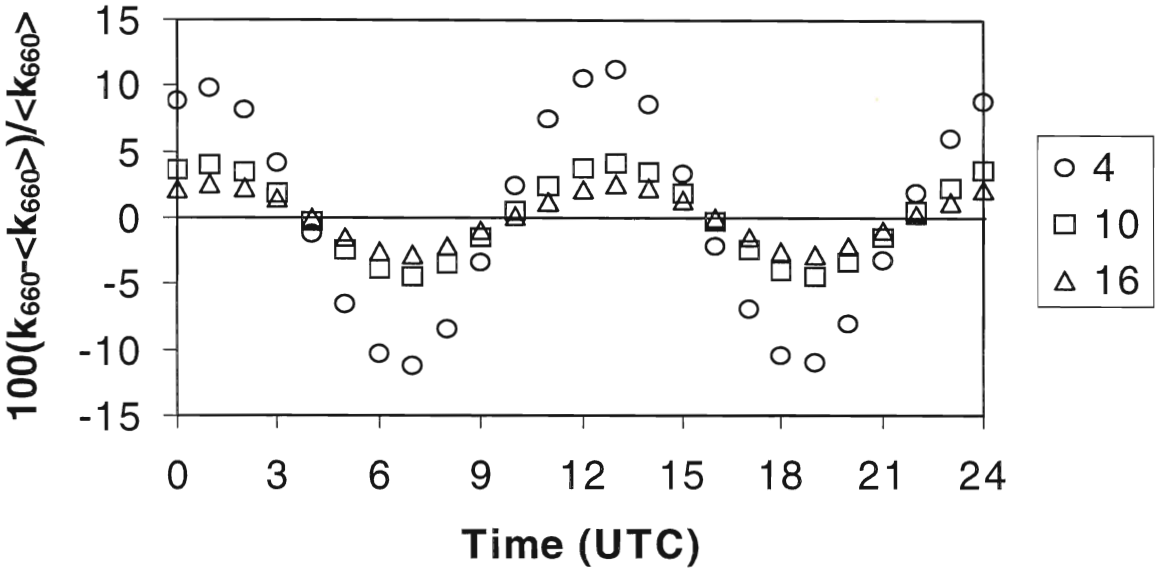

Figure 3: Simulated diurnal variation of k_{660}, expressed relative to its mean value. The wind speed at the height of 10 m is constant and taken to be 4 m/s (circles), 10 m/s (squares) and 16 m/s (triangles), respectively.

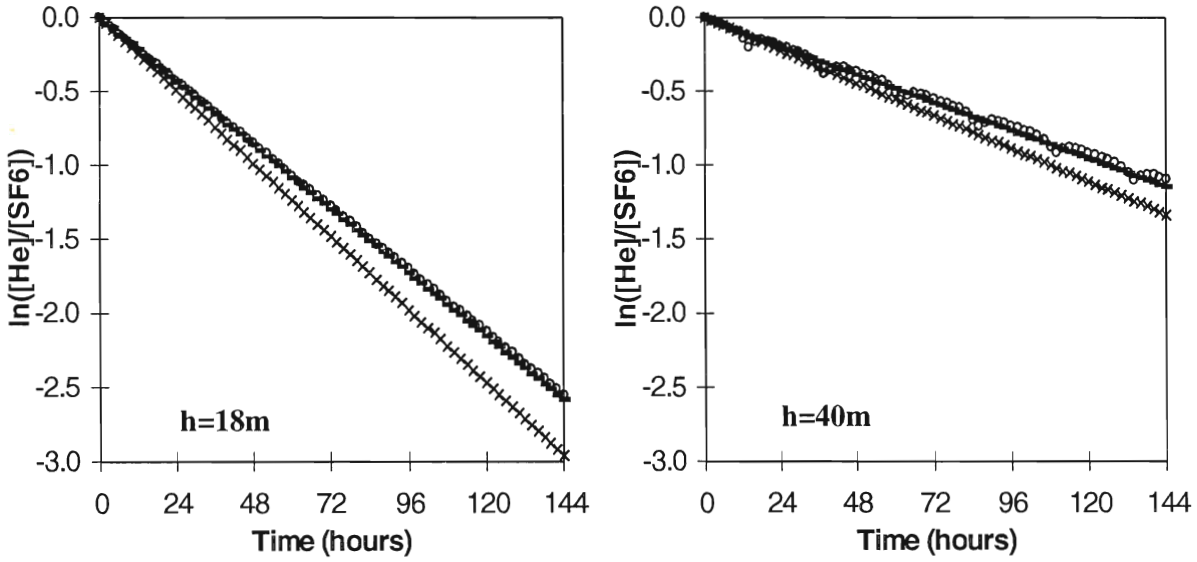

Figure 4: Simulated course of ln([He]/[SF_6] for a water depth of 18 m (left panel) and 40 m (right panel), respectively, and at a wind speed of 8 m/s. Crosses: results from bulk model (Eq. 5); dashes: results from *K*-model for complete darkness; circles: results from *K*-model with solar cycle typical for MPN under conditions of clear weather in October. The difference in slope • (ln([He]/[SF_6])/• *t* (see Eq. 6) from the two models is about 15%.

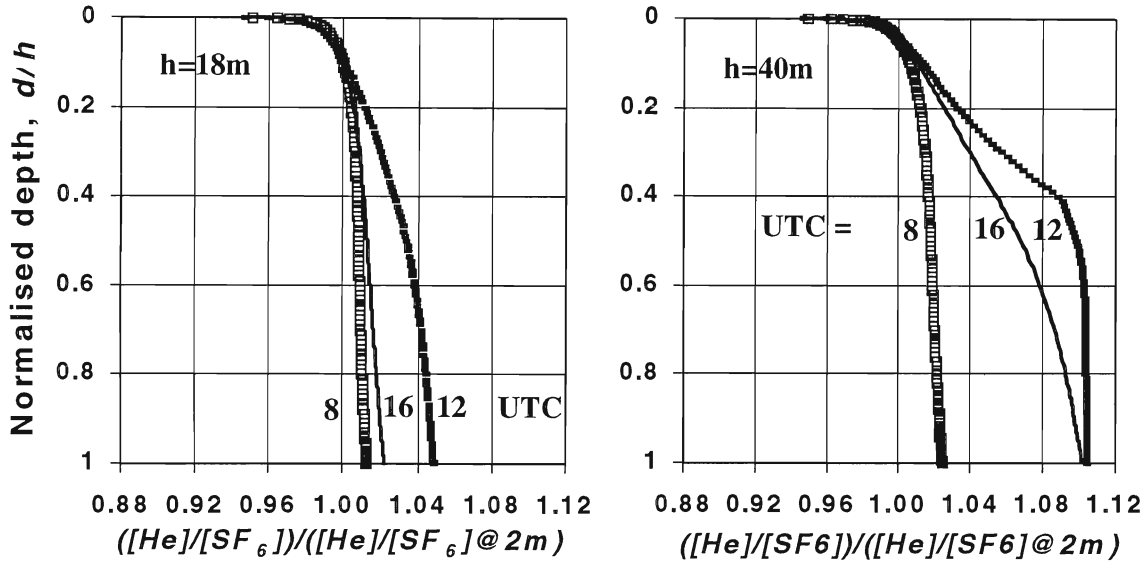

Figure 5. Simulated profiles of the "degree of unmixing" according to the *K*-model for water depths of 18 m and 40 m, respectively, at a wind speed of 8 m/s. The different profiles are valid for the time of day indicated in the labels.

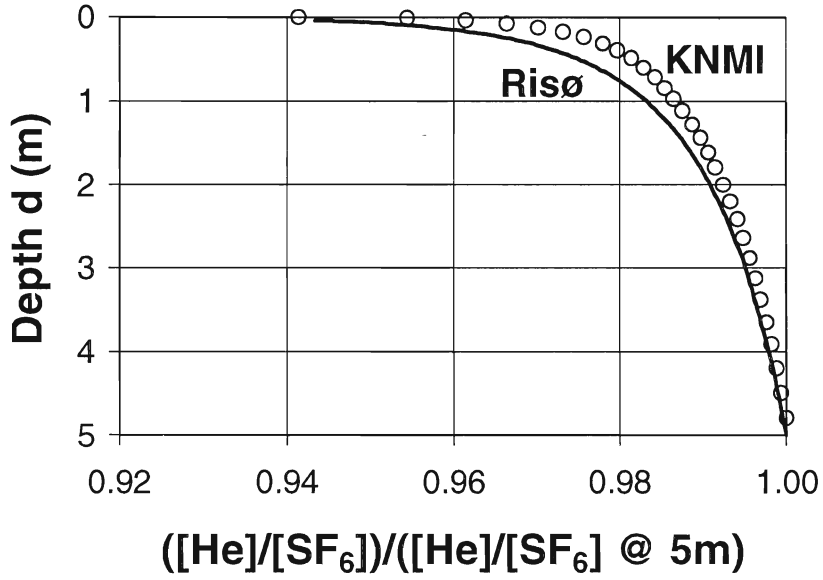

Figure 6: Comparison of simulated profiles of the "degree of unmixing" in the upper 5 meters of a water column from a 2-D model developed at Risø (Kjeld, 1999; solid line) and from the present model (circles). In both cases, the friction velocity in the air is about 0.3 m/s.

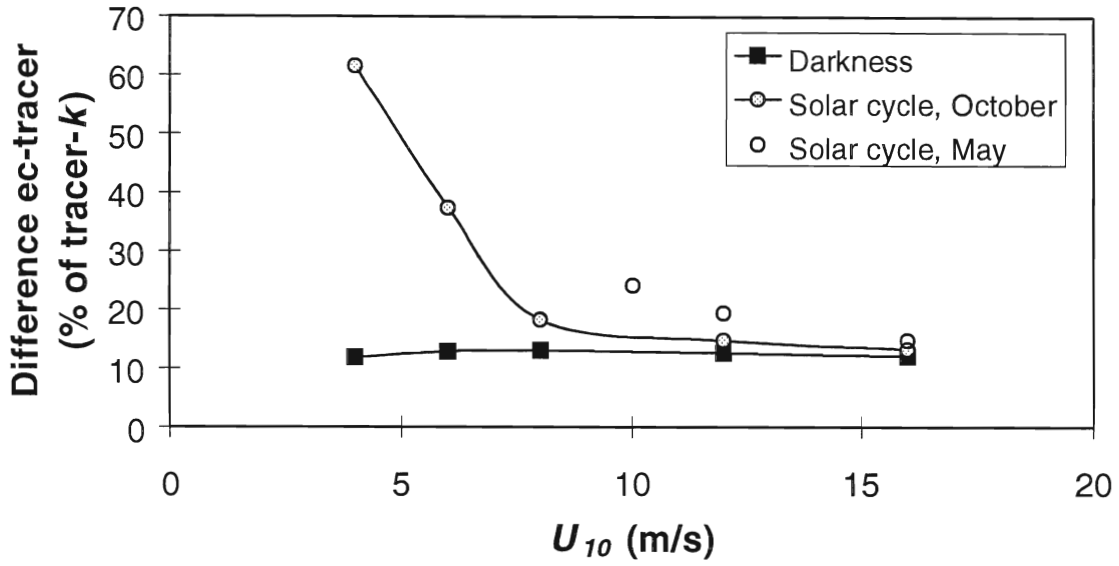

Figure 7: Amount by which k from the dual-tracer simulations has to be adjusted to obtain k according to the ec-simulations. The adjustment is expressed relative to the dual tracer values and given as a function of the wind speed at a height of 10 m. Closed squares: simulations for complete darkness; circles: simulations with solar cycle typical for MPN during clear weather in October (shaded symbols) or May (open symbols).

MEASUREMENT OF CARBON DIOXIDE AND WATER VAPOUR FLUXES DURING ASGAMAGE

W. Kohsiek

1. The IFM sensor

The IFM (Infrared Fluctuation Measurement) sensor is described by Kohsiek, 1991. The sensor used during ASGAMAGE is an improved version and differs from the instrument described in 1991 in the following aspects:
a two pass, 44 cm total length measuring cell with heated optics was employed. This cell was placed in a perspex cylinder that was ventilated by a small fan. Inside the cylinder was a fast response temperature sensor (thermocouple) as well. The purpose of the heating was to prevent moist on the optics, and the perspex cylinder acted to prevent droplets in reaching the optics. The temperature sensor was needed in order to apply the so-called Webb correction to the CO_2 measurements.
A liquid nitrogen cooled InSb detector was applied. Cooling was by means of a small Joule-Thompson cooler. This technique required the supply of compressed (100-200 bar) nitrogen gas to the sensor.
Several absorption/reference filter pairs were used during the experiment with the purpose to exploit the sensitivity of the CO_2 measurement to water vapour. The next configurations were employed:
a. 4.2 (s) and 2.3 micrometer
b. 4.2 (s) and 3.9
c. 4.2 (s) and 4.2 (b)
The 's' denotes a small passband filter, the 'b' a broad passband one. The 4.2 (s) and 4.2 (b) filters have nearly coincident centre wavelengths. This reduces sensitivity, but potentially gives the best rejection against water vapour cross-sensitivity.
Short (1.5 m) optical fibres were used with improved transmission at 4.2 micrometer.

The time resolution of the instrument was set at 10 Hz. Due to the perspex cylinder, and an internal delay, the response was delayed by about 0.2 s. This delay was acceptable since little flux was carried at frequencies above 1 Hz.

2. The NOAA sensor

This sensor is well described by Auble and Meyers, 1992. In contrast to the IFM, this instruments has an integrated optical absorption cell. The optics at one end of this cell are slightly heated (about 1 to 2 degree C above ambient), at the other end of the cell is an unheated mirror.

3. Calibration (IFM only)

The IFM was calibrated for CO_2 by means of mixtures of N_2 and CO_2 from gas cylinders. The CO_2 content of these gases was measured with a LICOR-6262 IRGA, which in turn was calibrated against a reference gas brought on board of the MPN by the group of NOAA. The accuracy of the procedure is estimated at 2 ppm. The reference gas of NOAA is believed to be accurate within a fraction of this number. A quadratic relation was fitted to the voltage output of the IFM versus the CO_2 density by means of regression. Following the same principle, the IFM was calibrated for water vapour. Known contents of water vapour were generated by means of a dew point generator (LICOR-610). Since the IFM is not an absolute instrument, regular baselining is needed during its operation. On MPN, baselining was done against the LICOR-6262 and the MPN humidity sensor for CO_2 and H_2O, respectively. Figure 1 presents calibration curves for CO_2 and H_2O. Note that different filter pairs as discussed above result in different calibration curves. The ordinate in these figures is optical

transmission. This quantity is related to the voltage output of the sensor by means of a linear relation, the coefficients of which are set by software commands.

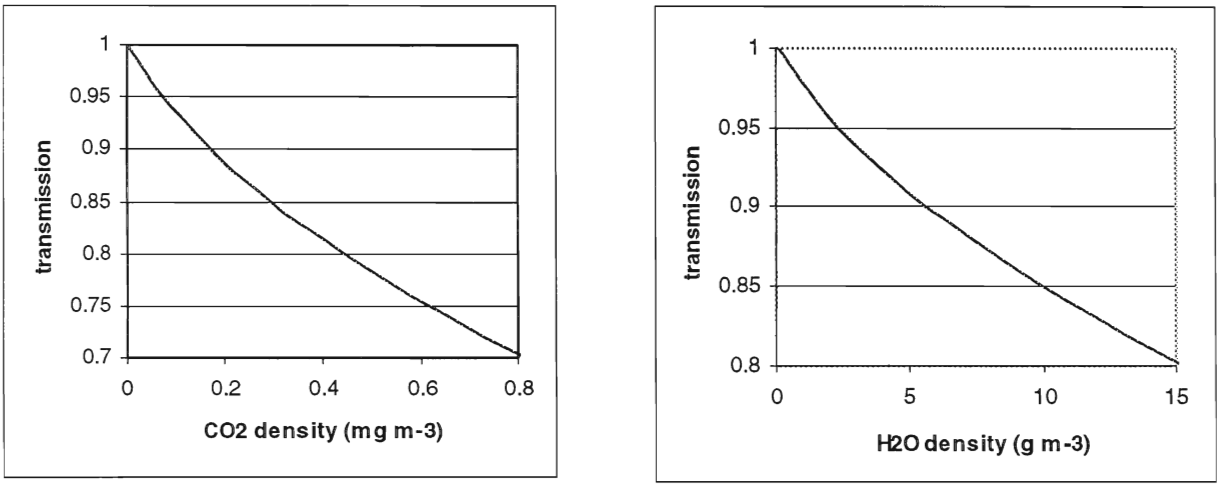

Fig.1 Calibration curves of CO2 and H2O (IFM)

4. Cross-sensitivity

Infrared gas sensors work after the principle of optical absorption at a wavelength that is specific for the gas of interest. Due to various reasons, other gases may affect the optical absorption as well. This phenomenon is referred to here as cross-sensitivity. With the open path sensors used during ASGAMAGE cross-sensitivity of CO_2 to water vapour is a matter of serious concern. Cross-sensitivity of water vapour to CO_2 is negligible, mainly because of the much larger fluctuations of the optical transmission in the water vapour band as compared to the fluctuations in the CO_2 band (Kohsiek, 1999). To get some feeling for the seriousness of the effect, let us suppose that a change in the water vapour density of 1 gm^{-3} gives an apparent change in the CO_2 density of 10^{-4} gm^{-3}. It can than readily be proven that a latent heat flux of 100 Wm^{-2} gives an apparent CO_2 flux of $0.4*10^{-5}$ $gm^{-2}s^{-1}$, a number which is to be compared with the real flux of CO_2 that ranged from 10^{-5} to 10^{-4} $gm^{-2}s^{-1}$ during ASGAMAGE. It is thus necessary to quantify cross-sensitivity down to an accuracy of, say, 10^{-4} .

After the measurements at MPN were finished, the IFM and a NOAA sensor were tested in the laboratory for cross-sensitivity. The sensing head was placed in a temperature controlled chamber and alternatively dry and moist air with the same CO_2 content was fed to the sensor. Details of the procedure are given by Kohsiek (1999). This led to the following results for the IFM:

a. the radiation levels in all three filters that are outside the absorption spectrum of water vapour show a response to the change in humidity
b. when the relative humidity of the moist air is high (over 80% in the test), a complex response is observed, which can not be expressed as a single number for cross-sensitivity. The cause of this response is sought in thin water layers on the optics that are absorbing differently in the CO_2 absorption band and the reference band. The phenomenon was absent when the 4.2 (b) filter was used as a reference
c. when the moist air was relatively dry (about 50% in the test), the cross-sensitivity was $4(\pm1)*10^{-4}$ gm^{-3}

CO_2 per gm^{-3} H_2O, a number that is close to the effect of pressure broadening, $3.3*10^{-4}$.

d. when using the 2.3 micrometer filter as a reference, the cross-sensitivity was negative. This is likely due to leakage of this filter at the 2.6 micron absorption band of water vapour.

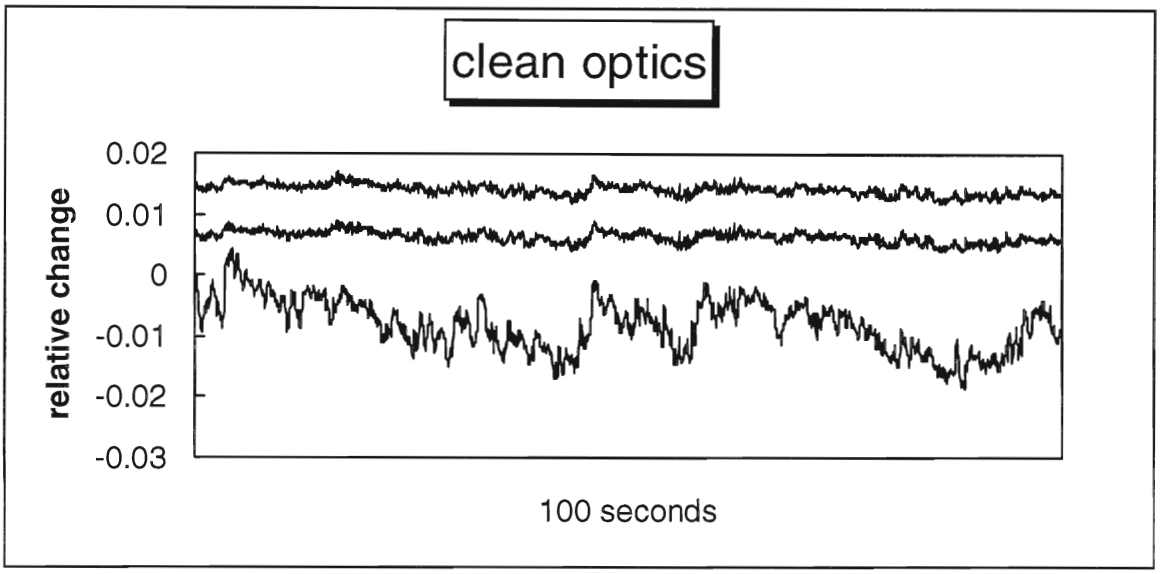

Fig. 2a. Water vapour response of the 4.2, 3.9 and 2.6 micron channel (top to bottom)

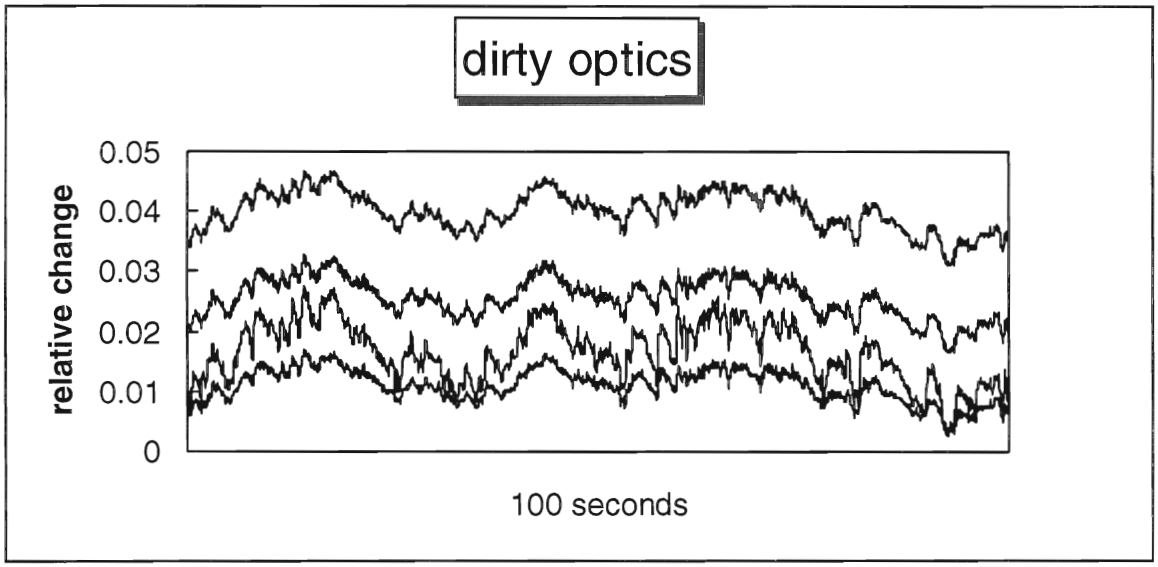

Fig. 2b. Water vapour response of the 4.2, 3.9, 2.6 and 2.3 micron channel (top to bottom)

In addition, an analysis of the radiation levels in the four individual filters during ASGAMAGE showed that the response to water vapour fluctuations of the three filters that are outside the water vapour absorption spectrum depends on the cleanliness of the optics (Fig. 2a,b). Such an effect can be expressed as a 'common mode' response, that gives the cross-sensitivity due to the response of a single filter, thus without taking into account the compensation effect of the other filter. After the optics were cleaned, a

common mode response of $200*10^{-4}$ was found, and after some days without cleaning it had gone up to $1000*10^{-4}$. Thus, a common mode rejection of 200 in case of clean optics, and of the order of 1000 with dirty optics is required to achieve the desired precision of $1*10^{-4}$ in the cross-sensitivity rejection. This illustrated the extreme demands that have to be put on common mode rejection.

Since the optics of the IFM were heated during the measurements at MPN, the air close to the optical surfaces was always at low relative humidity and cross-sensitivity is adequately accounted for by the pressure broadening correction. Cleaning was done on a regular base (once a day) only after the measurements had started for a while. This led to rejection of some of the data obtained with the 3.9 micron filter.The NOAA sensor was inspected in the same way. The optics of this sensor were not heated during ASGAMAGE, be it that part of the optical components were slightly above ambient temperature as mentioned above. When the relative humidity was less than 50% we

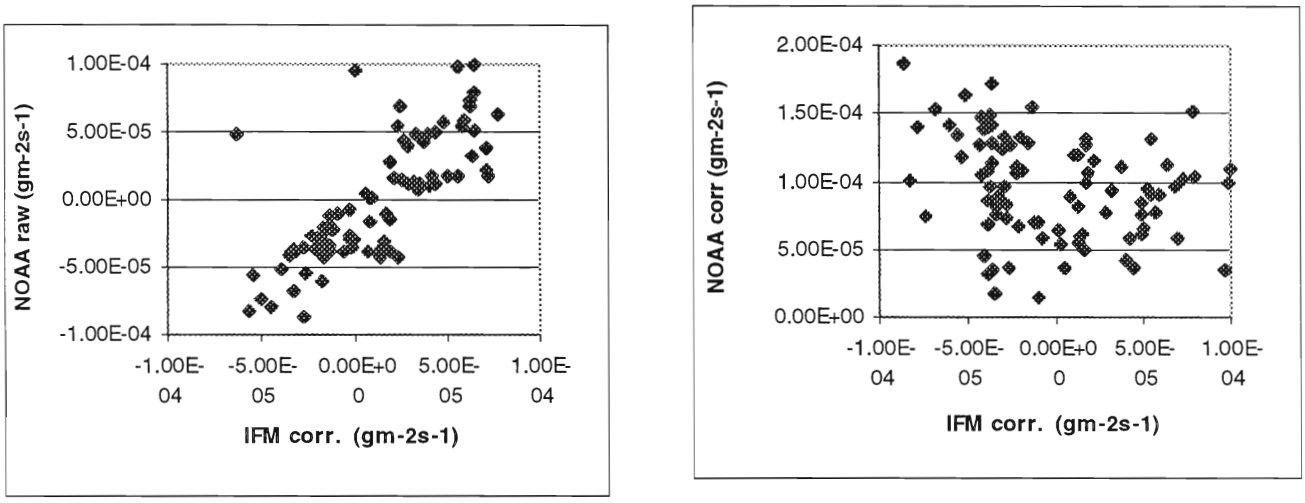

Fig.3 The effect of the cross-sensitivity correction on the CO_2 flux data of the NOAA sensor. The IFM data were corrected for cross-sensitivity. No Webb correction applied. Left figure: no correction; right figure: corrected.

found no cross-sensitivity at all, although an effect of pressure broadening was expected. At higher relative humidity, a negative CO_2 response set in, that should lead to corrections of 10 to20 ppm CO_2 when the relative humidity was above 80%. The nature of this response was not quite clear; as a working hypothesis, it is argued by Kohsiek (1999) that scattering of radiation by small droplets on the optics may be the cause. Anyhow, when we applied a corresponding correction to the ASGAMAGE measurements, it was found that the effect was adverse. Without correction, there was some agreement between the fluxes of the IFM and the NOAA sensor, but after correction the NOAA fluxes were shifted to unreasonably high values (Fig.3). Obviously, the laboratory result are not applicable to the field measurements. The reason for these conflicting results is as yet obscure.

5. Conclusions

When the humidity changes, the radiation level in all optical channels changes as well. Since the CO_2 concentration is calculated from the ratio of the radiation in the 4.2 micron absorption band and the radiation outside the absorption band, the CO_2 response depends on the rate of compensation of these two signals. It was found that this compensation should be in the order of 1000 or better, that is, the responses at the absorption wavelength and the reference wavelength should be equal within 1 part per 1000. This is for the case that the optics were not cleaned for several days; if regular cleaning is done, the required compensation is an order of magnitude less. In spite of these extreme demands, both the IFM and the NOAA sensor appear to have behaved properly. The IFM is heated and laboratory tests showed that in that

case the cross-sensitivity is equal to the effect of pressure broadening. The unheated NOAA sensor exhibited in the laboratory an appreciable cross-sensitivity at relative humidity higher than 50%; however, the results obtained with ASGAMAGE showed that better no correction be applied, in spite of the relative humidity that was always above 50%. This result is not well understood and requires further study.

6. References

Auble , D.L., and Meyers, 1992: An open path, fast response infrared absorption gas analyzer for H_2O and CO_2. *Bound.-Layer Meteor.*, **59**, 243-256.

Kohsiek, W., 1991: Infrared H_2O/CO_2 sensor with fiber optics. *Seventh Symposium on Meteorological Observations and Instrumentation, New Orleans, La, U.S.A., January 14-18, 1991,* pp. 352-355.

Kohsiek, W., 1999: Water vapor cross-sensitivity of open path H_2O/CO_2 sensors. *Submitted to J. Atmos. Oceanic Technol*

HEAT AND MOISTURE FLUXES DURING ASGAMAGE

W.A.Oost, C.M.J.Jacobs and C.van Oort

1. Introduction

During both ASGAMAGE experimental phases we measured heat and moisture fluxes to be able to apply the so-called Webb correction (Webb *et al.*, 1980) to the eddy correlation data for the CO_2 flux. This provided us with a set of new values of the transfer coefficients for heat and for moisture, the Stanton number C_H and the Dalton number C_E. An important characteristic of our data is the range of atmospheric stabilities covered, due to the two separate observation periods of the experiment. During the A-phase in the spring we had mainly stable situations, whereas during the B-phase, in the fall, the stratification was in general unstable.

2. The data

Our flux data were measured by KNMI and BIO, temperature and moisture values are based on data from other participants as well. All fast sensors for the flux measurements and some of the slower ones for the average temperature and humidity were located at the end of a 23m outrigger at the West side of the platform, to reduce flow distortion to a level that can be treated with confidence (Oost et al., 1994). Flow distortion corrections were only applied to the wind speed components; for scalar quantities, like temperature and humidity, the effects of flow distortion are negligible at the end of the boom.
Wind measurements were made with a 3-component Gill ultrasonic anemometer, type R2A, mounted on the outrigger. The fast humidity sensors were two custom-built instruments, a Lyman-α sensor and the humidity channel of an Infrared Fluctuation Meter (IFM, Kohsiek, 1998), designed and built by KNMI. The IFM was primarily intended to measure fluctuating CO_2 concentrations, but its humidity channel turned out to be an important asset. Temperature fluctuations were measured with K-type chromel-alumel thermocouples by KNMI and with a microbead thermistor by BIO. The latter sensor also provided average temperatures, whereas KNMI detected averaged values for humidity and air temperature with a separate sensor. Water temperatures were derived from a PT100 platinum resistance thermometer, mounted on a small float. All KNMI temperature and humidity sensors were calibrated in a climate chamber, both before the A- and before the B-phase.
The permanent hydro/meteo station on board MPN and sensors of TNO-FEL provided further air temperature, sea water temperature and humidity data. For sea water temperature we also used data from a CTD sensor, operated by UCG and SOC, and from a thermostring of NIOZ. The CTD data we used were usually from a depth of less then one meter, on one or two occasions slightly deeper. The data point of the thermostring we used was at a depth of one meter.
The KNMI group made 130 55 minute runs during the A-phase and 282 runs during the B-phase. All runs used have wind directions in the range 210°-270°-360° (SSW to N), to avoid runs affected by strong flow distortion. This directional range also certifies that the wind comes from the open sea, with a fetch of several hundred kilometers, reducing problems of horizontal homogeneity.

3. Results

3.1. Heat flux

Figure 1 shows the result for the Stanton number reduced to 10m height and neutral stratification, after the following types of runs had been deleted:

- runs during which the temperature difference between air and water was less than 0.8 °C or for which the relative error of the difference between the air and the water temperature (the sum of the

uncertainties in these temperatures, divided by the absolute value of their difference) was 0.2 or more (altogether 132 runs).

- runs with peak wavelengths of the surface waves larger than 75m (58 runs)
- runs with a wind direction outside the range 210°-360° (32 runs).

The first criterion is used to avoid the large uncertainties in C_H these data would introduce. The second category are data for which appreciable effects on the transport properties may be expected from the limited water depth (18m) at the platform (Oost, 1998). The third criterion removes data for which the flow distortion was too strong to correct with an acceptable accuracy.

Despite this pretty severe weeding out of the data the overall picture at first sight is pretty discouraging: the data show a very large spread and there is even an appreciable number of negative transport coefficients. We found an interesting structure, however, after we sorted the data according to the three stability categories shown in figure 1: stable ($z/L>0$, diamonds, category A), unstable ($z/L<0$, $T_a<T_s$, squares, category B) and "semi-unstable" ($z/L<0$, $T_a>T_s$, triangles, category C).

The data now group themselves into three coherent clusters with clear boundaries. Groups A and B contain data from both phases of the experiment, group C only data from the spring phase.

The stable data of group A form a consistent group, with low values for $C_{HN,10}$. They show an upward trend. The regression line is

$$1000 \times C_{HN,10} = 0.107 \times U_{N,10} - 0.77$$

(with $U_{N,10}$ in m/s) and the correlation coefficient R^2=0.64. If we compare this result with the values of Large and Pond (1982, LP82), we see that these authors also found lower values for stable than for unstable circumstances, but no indication for a trend. The values are different too: LP82 find 0.66, whereas our data average out at 0.29±0.23. However, LP82 cover a wind speed range 6-20 m/s, where we have a range from 7 to somewhat over 13 m/s. If we take the regression line, extrapolate it to 20 m/s and take the average over the range 6 to 20 m/s, we find a value of 0.64, close to the LP82 value.

This relationship of C_{HN10} with wind speed could be criticized, however. If we make the plot dimensionally correct by normalizing U_{N10} with the phase speed c_p of the waves in the peak of the wave spectrum, the stable data split into two clearly separated sub groups, one with $C_{HN10} \leq 10^{-4}$, the other with $C_{HN10} \geq 2.6\times10^{-4}$. All low values belong to runs made during the spring phase of the project, when both the air and the seawater temperature were 2°C lower than during the second phase in the fall. This could indicate an effect of either the water temperature or the average peak wave length, which in the fall period, was also almost twice the value in the spring (64.4m, respectively 35.5m).

The unstable data of group B ($z/L<0$, $T_a<T_s$, squares in figure 1) show a very loose structure. The regression line over the whole wind speed range is

$$1000 \times C_{HN,10} = 0.079 \times U_{N,10} + 0.471$$

with correlation R^2 = 0.37; the average value is 1.23±0.53. The value of 1.23 in itself is comparable to e.g. 1.13 in LP82, 1.1 in DeCosmo et al., (1996) or 1.18±0.19 in Smith et al. (1995). The most prominent characteristic of group B, however, is its huge spread compared to the other two groups. For a further assessment of group B, we have plotted all $C_{HN,10}$ data points as a function of wave age (c_p/u_*) in figure 2, which suggests a relationship between the heat exchange process and the wave field.

Still the most surprising results are the values for group C, runs that are unstable as far as the Monin-Obukhov length is concerned, but with a seawater temperature lower than the air temperature at measurement level. Despite numerous checks the accepted data points all remained negative. This rather surprising outcome is further supported by the fact that these negative values for C_H link up smoothly with the data from both the stable and the unstable group, as evident from figure 1. Our conviction that these negative transfer coefficients are real is strengthened once more by the systematic nature of the effect: almost all runs with $L<0$ and $T_a>T_s$ show this behavior, including most of those we deleted from further treatment on the basis of our selection criteria.

3.2. Humidity

In figure 3 we have plotted the Dalton coefficient $C_{EN,10}$, reduced to 10m and neutral stratification, as a function of $U_{N,10}$ after the following runs had been discarded:

- runs for which the absolute value of the difference between the specific humidity at the water surface and the one at measurement height was less than twice the standard deviation of the measurements, i.e. smaller than 0.00056 kg/kg (78 runs)
- runs with peak wave lengths longer than 75m (62 runs)
- runs with a wind direction outside the range 210°-360° (35 runs).

The numbers of runs discarded on the basis of the second and third criterion are different from those removed for the heat flux because we applied the criteria in the indicated order. Based on the Chauvenet criterion, which identifies outliers that would have a disproportionally large effect on the analysis result, assuming a Gaussian distribution, another 17 runs were not accepted.

We made the same division of the data in stability groups as in figure 1. It is clear from figure 3, that C_E behaves differently from C_H: the Monin-Obukhov length is the main determining factor and the data are split into a stable and unstable group, with neither of them showing a significant trend with wind speed.

The average value of C_{EN10} for the unstable group is 0.00110 ± 0.00022; the wind speed range is 2 to 18 m/s. This is identical to values fdound by deCosmo et al (1996), Smith et al (1995) and Large and Pond (1982).

The average value for the stable group is 0.00031 ± 0.00025, i.e. only marginally different from 0. The group as a whole contains a number of negative values, but none of these passed our selection criteria (the negative values had in general low humidity differences between water and air). We are not aware of comparable data in the literature.

4. Discussion

In our analysis we have given attention to every correction we could think of. Many of them were not significant (Webb, sensor separation, path averaging), others were applied to the best of our knowledge. We have furthermore been pretty strict in the rejection of dubious data runs and have used extensively the availability of simultaneous and co-located data from several sensors for the same quantity in our quality control procedures. These measures make that we consider our results as reliable.

That trust is further supported by the fact that our data confirm some earlier results from the literature. The difference between the values for C_{HN10} under stable and unstable circumstances has been noted before (Large and Pond, 1982). Our averaged results for C_H for both stable and unstable stratification and for C_E under unstable circumstances are well in line with those available in the literature. We see these results also as a confirmation that our results can be considered as deep water values, thanks to the selection of peak wave lengths shorter than 75m (Oost, 1998).

New, as far as the Stanton coefficient is concerned are

- the split of the data into two groups under stable conditions,
- the wave age dependence for unstable conditions and
- the negative values under well-defined atmospheric circumstances (Figures 6 and 7).

The stable data of group A show a well-defined trend with wind speed given earlier. Group A merges smoothly with group C (unstable, with stable temperature distribution). If we combine the two groups we find an only slightly different relationship

$$1000 \times C_{HN10} = 0.0814 \times U_{N10} - 0.0051$$

with a comparable, even slightly higher correlation coefficient: $R^2 = 0.70$.

We have our doubts, however, about the value of these parameterizations, basically because the trend with wind speed disappears when we normalize U_{N10} with c_p or u_*. We are then left with two groups of more or less constant values.

That bi-valued character of the stable data is difficult to interpret. We split the stable runs into two groups, according to their C_{HN10} values, and then checked all available parameters for differences. We found significant differences (of the order of 1.7 $\Sigma(\sigma)$, with $\Sigma(\sigma)$ the sum of the standard deviations within both

groups) between the air and water temperature and in the sea state (peak wave length) of the two groups. The difference in z/L between the two groups is much smaller (0.7 $\Sigma(\sigma)$), although we only found the dual character with runs under stable circumstances, indicating a relation with atmospheric stability. Which parameter or combination of parameters causes the difference between groups A_1 and A_2 cannot be decided without additional information.

C_{DN10} is related to C_{HN10}, so the obvious explanation for the wave age dependence of the unstable C_{HN10} values is that it is due to the wave age dependence of the drag coefficient, (Maat *et al.*, 1991, Smith *et al.*, 1992, Oost, 1998). The exponential fit

$$C_{HN10} = 0.0094\ (c_p/u_*)^{-0.64}$$

of figure 2 was chosen as the simplest one with a useful behavior in the high and low wave age limits. A similar fit to our values for the 10m neutral drag coefficient C_{DN10} (not shown) had an exponent -0.71, close to the present -0.64, whereas C_{HN10} should be roughly proportional to the square root of C_{DN10} i.e. have an exponent around -0.32. Hence the wave age dependence of C_{HN10} cannot be explained as due to the one of C_{DN10}.

Our most surprising results, however, are those in the C-category, the robustly negative values for C_H. Negative transport coefficients have been appearing for many years and have in general been attributed either to measurement errors or to gradients on space and time scales larger than those resolved by the experiment. The sharply defined conditions (unstable stratification, but air temperature higher than seawater temperature) under which we found the negative C_H-values and the fact that they were in many cases measured by two independent instruments made us accept them as real.

The negative values cannot be attributed to large scale gradients. Otherwise we would have to suppose that the characteristics of the group ($L<0$, $T_a>T_s$) are inextricably coupled to a specific phase of e.g. a helical roll, which in itself is already very improbable, because the indicated conditions were present during extended periods. But it even doesn't solve the problem: it simply transfers it to the **positive** values for C_E we find for the same runs.

The solution of the problem appears to lie in the fact that the measurements have been made in a high humidity environment. The physical meaning of the negative values for the transfer coefficient is that energy is being transported against the measured temperature gradient, the transport of sensible heat is increasing the temperature gradient. Conservation of energy then requires an additional energy source. The most obvious one is the conversion of latent heat into sensible heat through the condensation of water vapor just above the water surface. The relative humidity in that region is close to 100% and there is no reason to assume delayed condensation due to supersaturation, so in principle no objections exist to this explanation. A quantitative treatment of this effect is a matter of another study

REFERENCES

DeCosmo, J., K.B.Katsaros, S.D.Smith, R.J.Anderson, W.A.Oost, K.Bumke and H.Chadwick, 1996: Air-sea exchange of water vapor and sensible heat: the Humidity Exchange over the Sea (HEXOS) results. *J.Geophys.Res.* 101, 12001-12016.

Large, W.G. and S.Pond, 1982: Sensible and latent heat flux measurements over the ocean. *J.Phys. Oceanogr.* 12, 464-482.

Kohsiek, W., 1998. Measurement of CO_2 fluxes with the IFM during ASGAMAGE. In: *Report of the ASGAMAGE workshop, September 22-25, 1997* (ed. W.A. Oost), *KNMI Scientific Report* **98-02**, Royal Netherlands Meteorological Institute, De Bilt, 33-37. (Also available on Internet: *http://www.knmi.nl/asgamage).*

Maat, N., C.Kraan and W.A.Oost, 1991: The roughness of wind waves. *Boundary-Layer Meteorol.* 54, 89-103.

Oost, W.A., C.W.Fairall, J.B.Edson, S.D.Smith, R.J.Anderson, J.A.B.Wills, K.B.Katsaros and J.deCosmo: Flow distortion calculations and their application in HEXMAX. *J. Atmos. Oceanic Technol.*, 11, (1994), 366-386.

Oost, W.A., 1998: The KNMI HEXMAX stress data - a reanalysis. *Boundary-Layer Meteorol.* 86, 447-468.

Smith, S.D., R.J.Anderson, W.A.Oost, C.Kraan, N.Maat, J.DeCosmo, K.B.Katsaros, K.L.Davidson, K.Bumke, L.Hasse and H.M.Chadwick, 1992: Sea surface wind stress and drag coefficients: the HEXOS results. *Boundary-Layer Meteorol.* 60, 109-142

Smith, S.D., R.J.Anderson, O.Hertzman, Oost, W.A., W.Kohsiek, G.de Leeuw and G.J.Kunz, 1995: New measurements of eddy fluxes at the sea surface in ASGASEX. In: *Selected papers from the proceedings of the Third International Symposium on Air-Water Gas Transfer '95, Heidelberg. B.Jähne and E.Monahan, eds.,* AEON Verlag & Studio, Hanau, pp. 703-712.

Webb, E.K., G.I.Pearman and R.Leuning, 1980: Correction of flux measurements for density effects due to heat and water vapour transfer. *Quart.J.Roy.Meteor.Soc.* 106 (1980), 85-100.

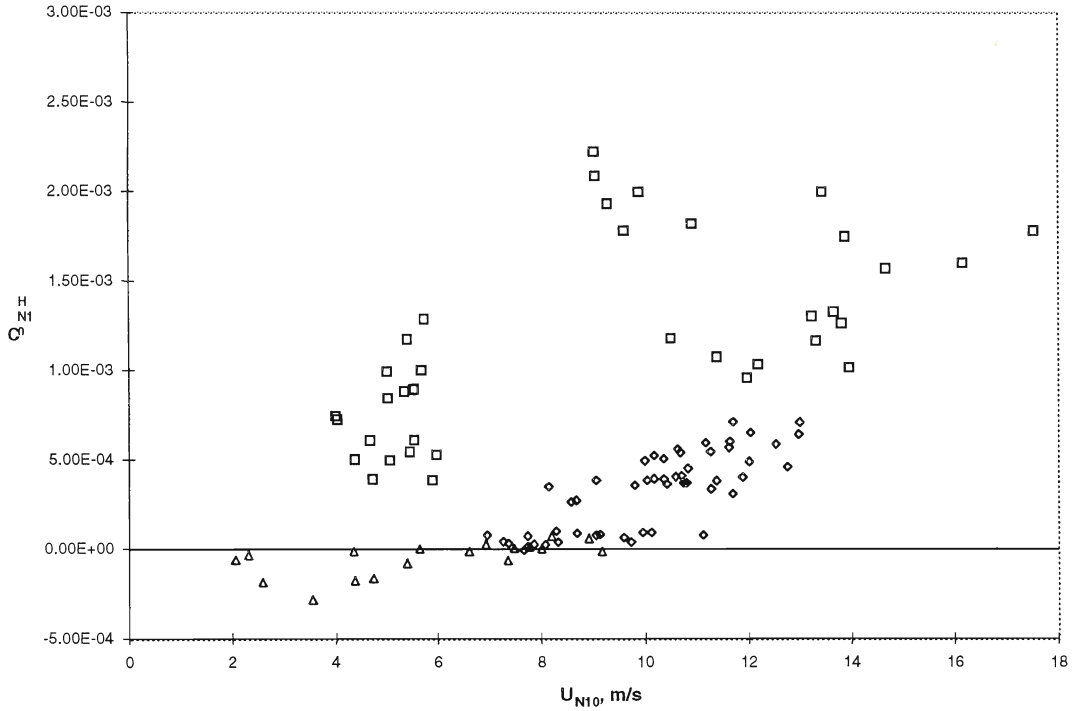

Figure 1 The heat transfer coefficient (Stanton number) as a function of the wind speed, both quantities reduced to 10m height and neutral conditions for three stability categories. Diamonds: Monin-Obukhov length L positive (stable stratification), air temperature higher than sea water temperature; squares: L negative (unstable stratification), air temperature below sea water temperature; triangles: L negative but air temperature higher than sea water temperature.

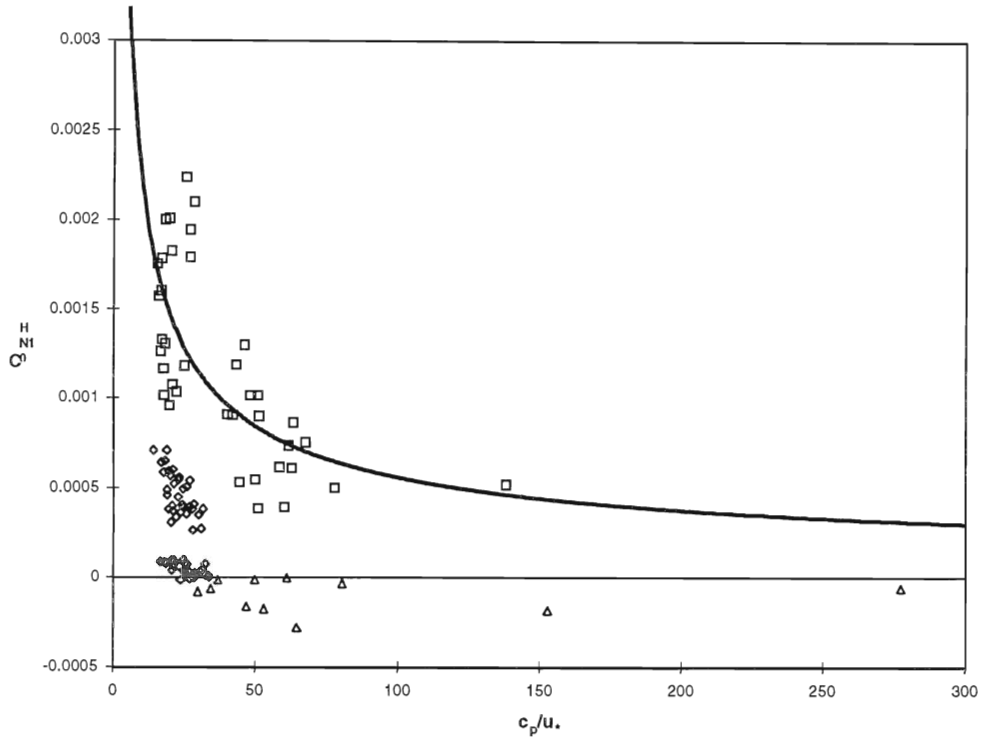

Figure 2. As figure 1, but plotted as a function of the wave age c_p/u_*, with u_* the friction velocity and c_p the phase speed at the peak of the wave spectrum.

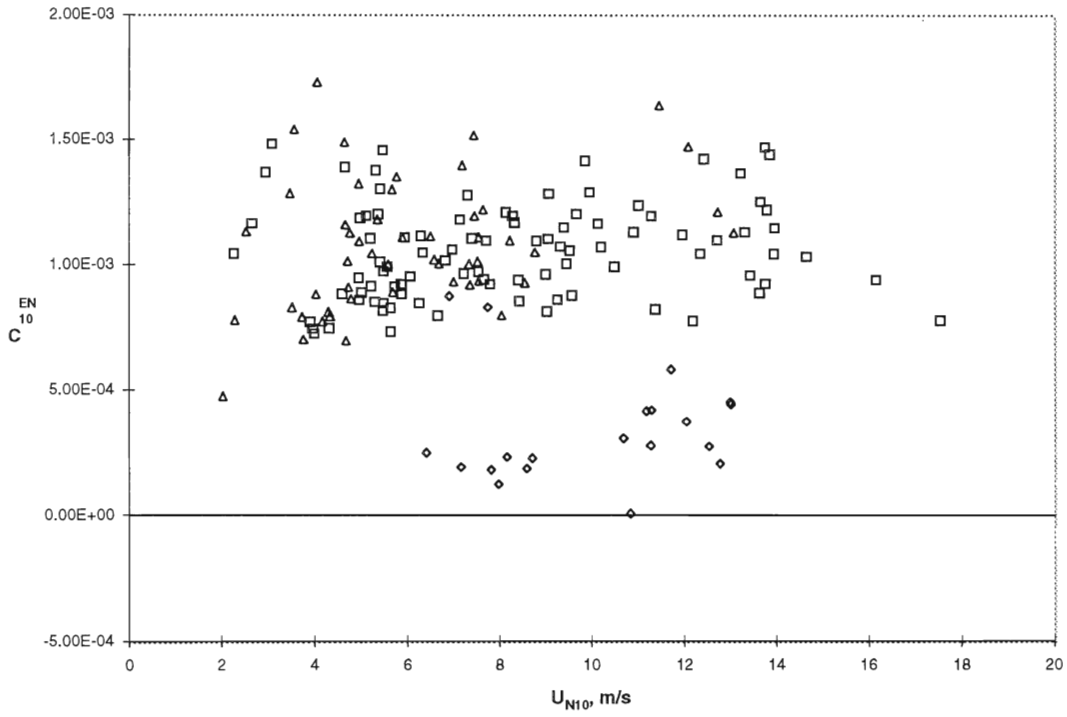

Figure 3 The humidity transfer coefficient (Dalton number) as a function of the wind speed, both quantities reduced to 10m height and neutral conditions for three stability categories. Conventions as in figure 1.

ASGAMAGE Final Report

Contribution of the Max-Planck-Institute for Chemistry Mainz

Partner 2

Principal Investigator: Dr. T.Reiner
Max Planck Institut fuer Chemie, Abt.Biogeochemie, Postfach 3060, 55020 Mainz, Deutschland
Phone: + 49 6131 305-422; FAX + 49 6131 305-487
E-mail: reiner@mpch-mainz.mpg.de

Contributors: D. Sprung, S. Rapsomanikis, T. Kenntner, T. Reiner

Introduction and Overview

The work of the Max-Planck-Institute for Chemistry (MPIC) aimed at contributing to the ASGAMAGE objective no. 4: "To test new methods and new equipment for the measurement of air-sea fluxes of CO_2, N_2O, CH_4, and DMS". Measurements were carried out on the research platform Meetpost Noordwijk (MPN), 9 km off the Dutch coast in the North Sea, during the ASGAMAGE field phases A and B in spring and fall 1996, respectively. The main interest was the determination and comparison of dimethyl sulfide (DMS) fluxes using different measurement techniques, including a novel Atmospheric Pressure Ionization Mass Spectrometer (APIMS) system for fast and sensitive measurements of atmospheric trace gases. The APIMS measurement technique was further developed and the performance of the APIMS instrument was further characterised and improved by laboratory measurements and a short field test campaign in Bellheim, Upper Rhine valley, Germany.

Determinations of sea air fluxes of DMS performed so far have used the so-called bulk method. This method indirectly infers the flux, F, from the off-equilibrium conditions between the concentration of DMS in water and that in air:

(1) $$F = k\,(c_w - c_a/H)$$

Here, c_w is the concentration in water, c_a the concentration in air, H the Henry's law constant, and k the transfer velocity. Since DMS is highly supersaturated in sea water, the air concentration of DMS can be neglected and equation (1) reduces to:

(2) $$F = k\,c_w$$

The DMS flux can then be calculated from the measured concentration of DMS in sea water and the transfer velocity. The transfer velocity k depends on the Schmidt number, Sc, and on the horizontal wind velocity, u. Several models exist, which parameterise the dependence of k on the wind velocity (e. g. Liss and Merlivat, 1986, Wanninkhof, 1992). However, in addition to wind speed other factors like bubbles and breaking waves may also affect k.

In order to reduce the uncertainty related with the indirect determination of DMS fluxes using the bulk method, means have been sought to measure DMS fluxes directly using micrometeorological methods.

One possibility is the eddy correlation method. In this technique, the covariance between the fluctuations of the vertical velocity, w, and the concentration of the gas in air, c_a, is measured. The trace gas flux is obtained by:

(3) $$F = w' c_a'$$

The primed values w' and c_a' denote deviations from the mean vertical wind velocity and the mean concentration in air, respectively. The eddy correlation technique requires fast and precise measurement techniques, which are able to measure trace gas concentrations in air at frequencies of 1 s^{-1} or faster. So far, the eddy correlation technique has been applied for sea air flux measurements of gases like H_2O and CO_2.

An alternative to the eddy correlation technique is the technique of relaxed eddy accumulation. In this technique air is conditionally sampled in two different reservoirs, depending on whether the vertical velocity is upward or downward. Instrumental requirements on measurement frequency are less demanding for the relaxed eddy accumulation than for the eddy correlation technique. The flux can be obtained by:

(4) $$F = b(z/L)\, \sigma_w\, (c_{up} - c_{down})$$

Here, b is a stability dependent factor (depending on the Monin-Obukhov stability parameter z/L), σ_w the standard deviation of the vertical wind velocity, and c_{up} and c_{down} the concentrations measured in samples of upward and downward moving air parcels, respectively.

Measurements on Meetpost Nordwijk during ASGAMAGE A and B

Experimental

Measurements on Meetpost Nordwijk (MPN) were performed during the ASGAMAGE phases A and B in spring and fall 1996. Micrometeorological parameters were measured with a frequency of 21 Hz by a sonic anemometer, which was deployed on the North boom of MPN at a height of about 6.5 m above sea level. Water vapour was measured with a LICOR hygrometer. Sea water concentrations of DMS were obtained using a gas chromatographic system with flame photometric detection (GC/FPD) as described by Andreae et al. (1994). Water samples were taken from a depth of two meters. The sea water DMS measurements provided the basis for flux estimates using the bulk method (see below).

A similar detection system, combined with DMS preconcentration by absorption on gold wool in a quartz tube, was used for measuring DMS concentrations in air. Upward and downward moving air masses were conditionally sampled on two separate gold wool tubes, selected by the vertical wind measurements of the sonic anemometer. These measurements were used to calculate the flux using the relaxed eddy accumulation method.

In addition to these measurements, an attempt was made to use a novel Atmospheric Pressure Ionisation Mass Spectrometer (APIMS) for high frequency trace gas measurements and flux measurements using the eddy correlation technique.

Results

Bulk method: Figures 1 (a) and (b) show the DMS concentration in sea water measured at MPN during the ASGAMAGE phases A and B. Very high DMS concentrations of more than 10 nmol/l were measured at the beginning of the campaign. DMS concentrations remained high around 4 nmol/l throughout phase A. In

contrast, DMS concentrations measured during phase B (Fig. 1(b)) were much lower, rarely exceeding 1 nmol/l, and steadily decreasing.

From the measured sea water DMS concentrations DMS fluxes were calculated using equation (2) and the Liss and Merlivat (1986) wind speed parameterisation. The Schmidt number dependence was accounted for following the work of Turner et al. (1996). Very high DMS fluxes were observed at the beginning of the campaign, driven by the high sea water DMS concentrations (Fig. 2 (a)). During the fall campaign, DMS fluxes reach values up to 7 $\mu mol/m^2/d$ (Fig. 2(b)), which are due to high wind speeds of up to 18 m/s.

Relaxed Eddy Accumulation: Relaxed Eddy Accumulation measurements were only attempted during the ASGAMAGE A phase. The concentration differences measured between upward and downward moving air parcels (conditional sampling) are shown in Figure 3. Figure 3 also shows expected concentration differences, which were calculated using the DMS fluxes estimated by the bulk method. The measured concentration differences are of the same order as the calculated ones, but occasional large discrepancies are also evident. These differences may be due to experimental problems related with the sampling and the analysis of the air DMS samples on MPN.

Eddy Correlation Measurements: Eddy correlation flux measurements were attempted using the APIMS instrument on MPN. It was the first time that this instrument was used under the measurement conditions of a measurement platform like MPN. Technical problems prevented the new instrument from gathering any data during ASGAMAGE phase A. During ASGAMAGE phase B DMS fluxes were too low (cf. Fig. 2(b)), so that no significant cross correlation between the measured DMS and the measured wind speed could be observed. After the end of the field phases ASGAMAGE A and B the APIMS instrument and measurement technique was further developed, which will be described in the following section.

Development of an APIMS instrument for atmospheric trace gas and flux measurements

Measurement technique

Atmospheric trace gas measurements by the APIMS technique rely on the production of specific product ions by ion molecule reactions between atmospheric trace gases and reactant ions produced by an ion source (cf. Carroll et al., 1981). The MPIC APIMS instrument uses a corona discharge in atmospheric air for the production of reactant ions. Reactant ions undergo ion molecule reactions with atmospheric trace gases in the atmospheric pressure ionisation chamber before they are drawn through a 0.25 mm diameter inlet orifice into the ≈1 Torr pressure decluster chamber. Here the ions are accelerated by electric fields and enter the high vacuum mass spectrometer chamber through another aperture. A vacuum ion optics system focuses the ions into the quadrupole rod system, where the ions are mass-analysed and detected by a conversion dynode/channel electron multiplier detector.

For certain applications gases may be mixed with the air in order to produce particular reactant ions. For example, for the detection of DMS, benzene vapour is added to the air (Spicer et al., 1996), resulting in the production of $C_6H_6^+$ reactant ions (mass 78 amu, atomic mass units). DMS is ionised by a charge transfer reaction:

(5) $\quad C_6H_6^+ + DMS \rightarrow DMS^+ + C_6H_6$

The DMS^+ product ion (mass 62 amu) is detected with the mass spectrometer. Other trace gases that can be measured with the APIMS technique include SO_2, organic and inorganic acids, ammonia, acetone, and other organic compounds with a high proton affinity. Very recently, the suitability of an APIMS system for

atmospheric trace gas flux measurements using the eddy correlation technique was investigated by Shaw et al. (1998).

Laboratory calibration

Figure 4 shows a calibration curve for DMS obtained in our laboratory. A linear relation between the abundance of DMS^+ (mass 62 amu), normalised to the abundance of the reactant ion $C_6H_6^+$ (mass 78 amu), can be found. Normalisation of the product ion to the abundance of the reactant ion makes the signal independent of variations of the total ion source current and leads to a more stable signal. Similar calibration curves have been obtained for other gases. In the meantime the APIMS instrument has been equipped with an in-field calibration source.

Sampling system

Since the APIMS is a big and heavy instrument, it has to be housed separately and the sample air has to be brought to the instrument via a relatively long sampling line. For the measurements described here the sampling system consisted of a 12 m long, 3/4" diameter PFA teflon tube. The sample air was pulled through the teflon tube by a high speed (400 l/min) mechanical pump to minimise wall effects on the measured chemical components. From the main sampling line a small volume was branched off via a short piece of 1/4" diameter tubing, leading into the APIMS. The delay time of this system was about 2 s.

Response time

For eddy correlation measurements the system response time must be fast enough to resolve short time trace gas fluctuations of the order of one second and less. The system response time includes the response time of the measurement system (the APIMS) and the sampling system.

Figure 5 shows the system response of the APIMS when acetone is added to the sample air flow at the sample tube inlet. Acetone is measured using the proton transfer reaction of $H_3O^+(H_2O)_n$ reactant ions with acetone, leading to protonated acetone ($H^+(CH_3)_2CO$). The count rate of $H^+(CH_3)_2CO$, measured with the mass spectrometer, is proportional to the acetone concentration in the sample air.

The rising time of the acetone signal is about 0.7 s. If the acetone supply is turned off, the acetone signal measured with the APIMS drops down to ambient levels with about the same response time as it has risen before. This shows that a measurement cycle of 1 Hz can be used with the APIMS system as far as the restricting factor of the response time is concerned. The response times for increasing and for decreasing concentrations are almost identical, showing that - at least for acetone - memory effects due to absorption and desorption of acetone on the sampling line walls are small.

Field test of the APIMS system

In order to further characterise the APIMS measurement system and the sampling system, field measurements have been performed at a measurement site in Bellheim (Upper Rhine valley, northwest of Karlsruhe). These measurements took place in fall 1998 on a field with 10 cm high barley shoots. Sample air was taken from a 4 m high tower using a 12 m long, 3/4" diameter PFA teflon tube as described above. On the tower an ultra sonic anemometer (Gill Instruments) was deployed providing the measurements of the vertical velocity used for eddy covariance measurements. The delay (about 2 s) time was calculated from the geometry of the sampling system and the sample air flow rate. This calculation was in good agreement with the results determined by the covariance function of the vertical velocity and the chemical compounds measured by the APIMS.

In order to be able to compare the performance of the APIMS system with other, more established, measurement techniques, we have used the ability of the APIMS to measure water vapour. Water vapour is measured with the APIMS using the hydration equilibrium between O_2^- and $O_2^-H_2O$ ions:

(6) $$O_2^- + H_2O + M \quad \leftrightarrow \quad O_2^-H_2O + M$$

M is an inert collision partner like N_2 or O_2. The equilibrium reaction (5) takes place in the atmospheric pressure ion source region of the APIMS. The water vapour concentration is proportional to the ratio of $O_2^-H_2O$ and O_2^- and can be obtained from a measurement of the relative abundance of these ions:

(7) $$(H_2O) = \frac{1}{K_{eq}} \frac{(O_2^-H_2O)}{(O_2^-)}$$

Here, K_{eq} is the equilibrium constant for hydration of O_2^-.

The APIMS water vapour measurements were calibrated with a closed path sensor based on IR absorption (LICOR 6000). The APIMS measurements of the water vapour fluctuations were compared with the water vapour fluctuation measurements of the closed path LICOR system and open path measurements conducted with a Krypton lamp (Campbell Scientific, UV absorption). The Krypton lamp was located close to the inlet of the sampling tube 4 m above the ground. For the closed path LICOR system a similar sampling tube as for the mass spectrometer was used.

Figure 6 shows a comparison of the power density spectra obtained with the three different techniques: the APIMS, the LICOR, and the Kr lamp system. The spectra have been computed using a Fast Fourier Transform (FFT) algorithm, and they have been normalised by dividing by the variance of their time series. Very good agreement between the LICOR system and the Krypton lamp can be observed. The basic features of the LICOR and Krypton lamp spectra are also reflected in the APIMS power density spectrum. In particular, all three spectra show similar structures at the low frequencies between 0.001 and 0.01 Hz and the –5/3 slope toward higher frequencies, which is characteristic of the inertial subrange of turbulence spectra (cf. Shaw et al., 1998).

Summary and Conclusions

We have measured sea air fluxes of DMS on the research platform MPN during the ASGAMAGE phases A and B in spring and fall 1996 using the bulk method. These measurements showed very large fluxes in spring and much smaller fluxes in fall. During ASGAMAGE A an attempt was also made to measure DMS fluxes using the relaxed eddy accumulation method. The fluxes inferred from the relaxed eddy accumulation method were of the same order as those estimated by the bulk method, but also showed some larger discrepancies.

Eddy correlation measurements of DMS fluxes on the research platform were attempted using an APIMS for fast and sensitive atmospheric DMS measurements. However, these first attempts on MPN failed due to technical problems with the new instrument. After the ASGAMAGE field phases the APIMS instrument was further developed both in the laboratory and in the field. An intercomparison of water vapour flux measurements with the APIMS and two other techniques at a field measurement site in southern Germany yielded good agreement between the three different techniques and demonstrated the capability and suitability of the APIMS instrument for future trace gas eddy correlation measurements.

References

Andreae, T. W., M. O. Andreae, and G. Schebeske, Biogenic sulfur emissions and aerosols over the tropical South Atlantic: 1. Dimethylsulphide in sea-water and in the atmospheric boundary layer, J. Geophys. Res., 99, 22819-22829, 1994.

Carroll, D. I., I. Dzidic, E. C. Horning, and R. N. Stillwell, Atmospheric pressure ionization mass spectrometry, in Applied Spectroscopy Reviews, 17, 337-406, 1981.

Liss, P. S., and L. Merlivat, Air-sea gas exchange rates: Introduction and synthesis, in The role of sea-air exchange in geochemical cycling, edited by P. Buat-Menard, 113-127, Reidel, Dordrecht, 1986.

Spicer, C. W., D. V. Kenny, E. Chapman, K. M. Busness, and C. M. Berkowitz, Observations of dimethyl sulfide over the western North Atlantic using an airborne tandem mass spectrometer, J. Geophys. Res., 101, 29,137-29,147, 1996.

Shaw, W. J., C. W. Spicer, and D. V. Kenny, Eddy correlation fluxes of trace gases using a tandem mass spectrometer, Atmos. Environ., 32, 2887-2898, 1998.

Turner, W. M., G. Malin, P. D. Nightingale, and P. S. Liss, Seasonal variation of dimethyl sulphide in the North Sea and an assessment of fluxes to the atmosphere, Mar. Chem., 54, 245-262, 1996.

Wanninkhof, R., Relationship between gas exchange and wind speed over the ocean, J. Geophys. Res., 97, 7373-7381, 1992.

(a)

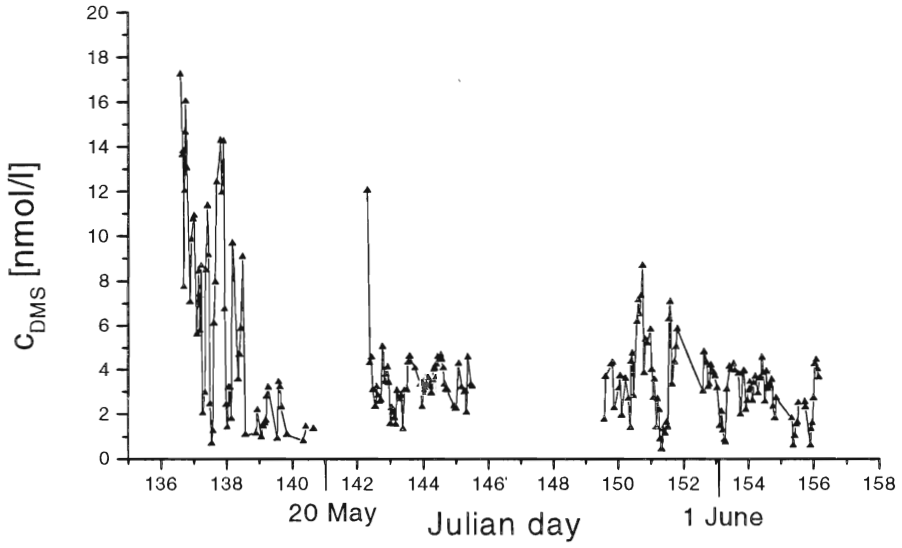

(b)

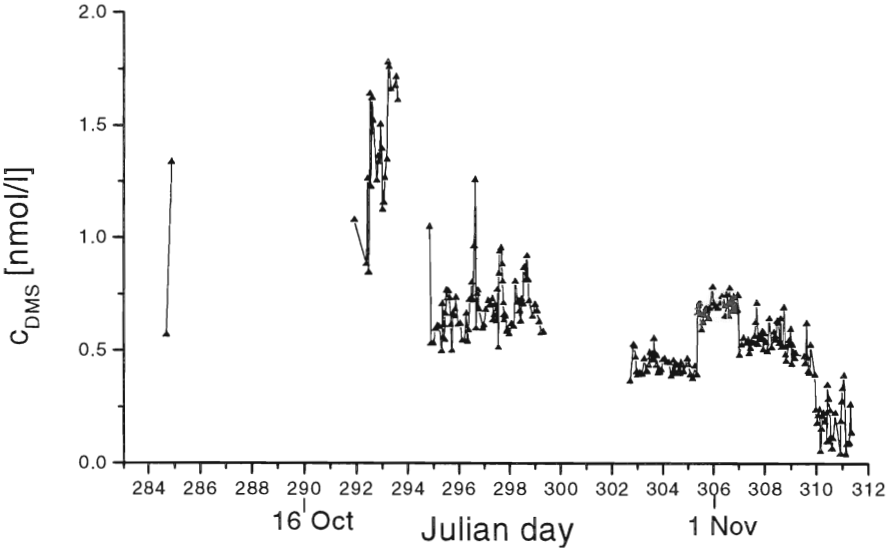

Figure 1. DMS concentration in sea water during ASGAMAGE A (a) and B (b).

(a)

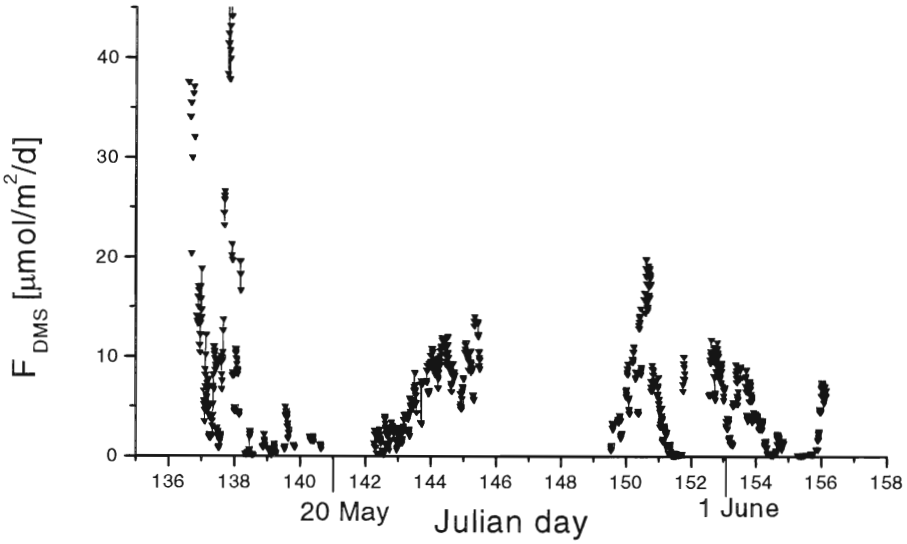

(b)

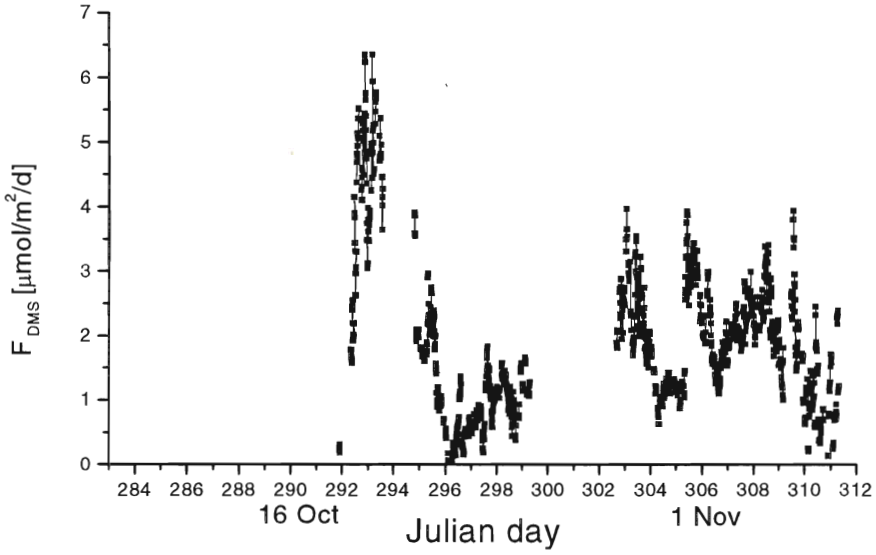

Figure 2. DMS fluxes calculated from the measured sea water DMS concentration using the Liss and Merlivat (1986) wind speed parameterisation. (a) ASGAMAGE A, (b) ASGAMAGE B.

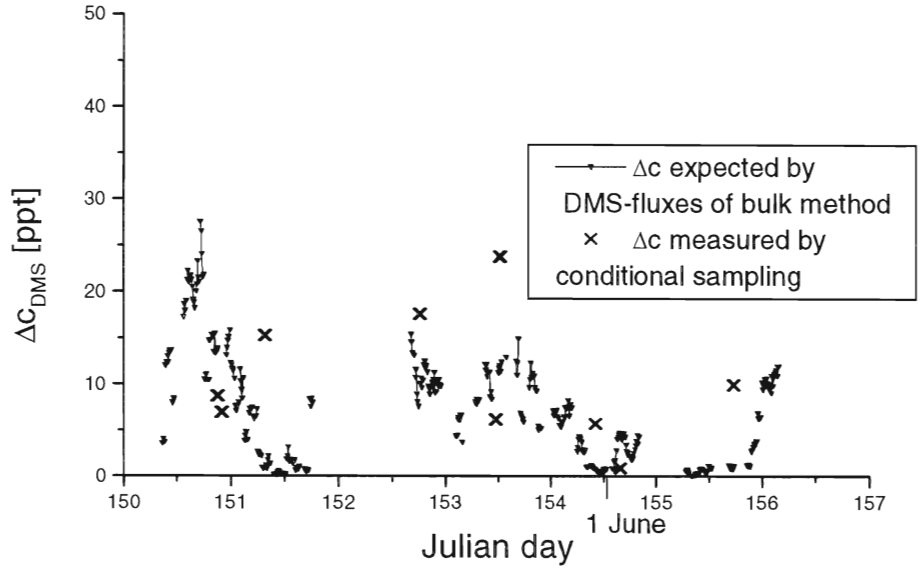

Figure 3. Comparison of the expected and measured DMS concentration differences between upward and downward moving air parcels for ASGAMAGE A. The expected concentration differences are calculated from the flux values obtained by the bulk method.

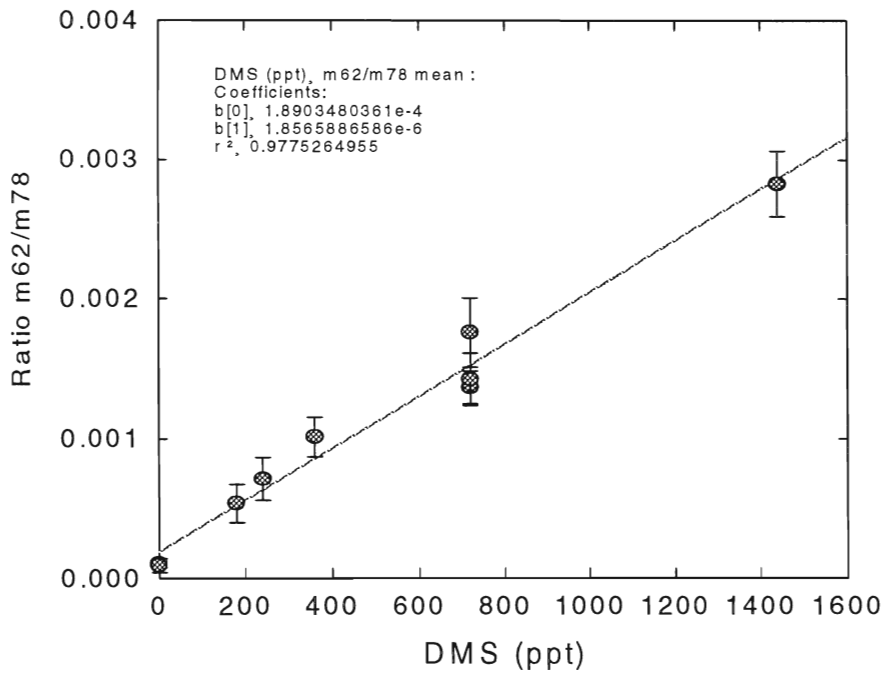

Figure 4. Laboratory calibration of DMS (further explanations see text).

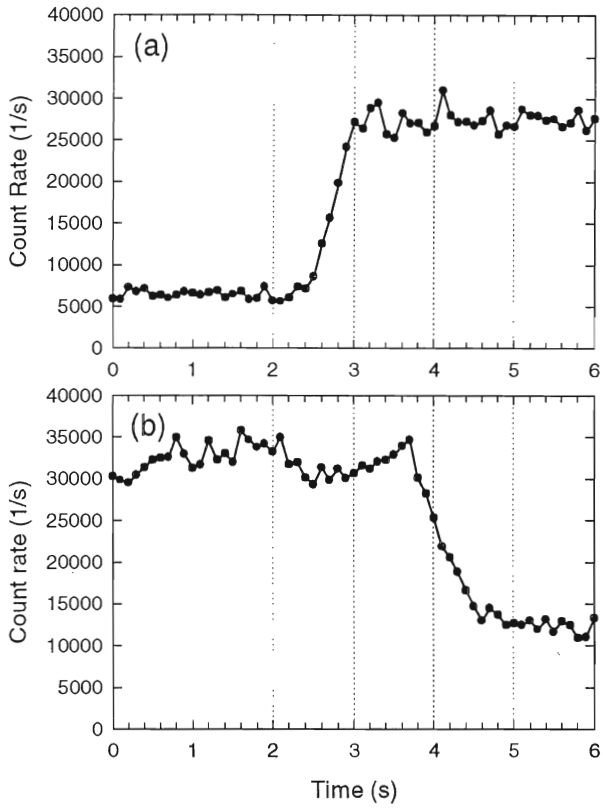

Figure 5. Response time of the APIMS system for acetone: (a) increasing concentration, (b) decreasing concentration. The ordinate shows the count rate of protonated acetone measured with the APIMS, which is proportional to the concentration of acetone in the sample air.

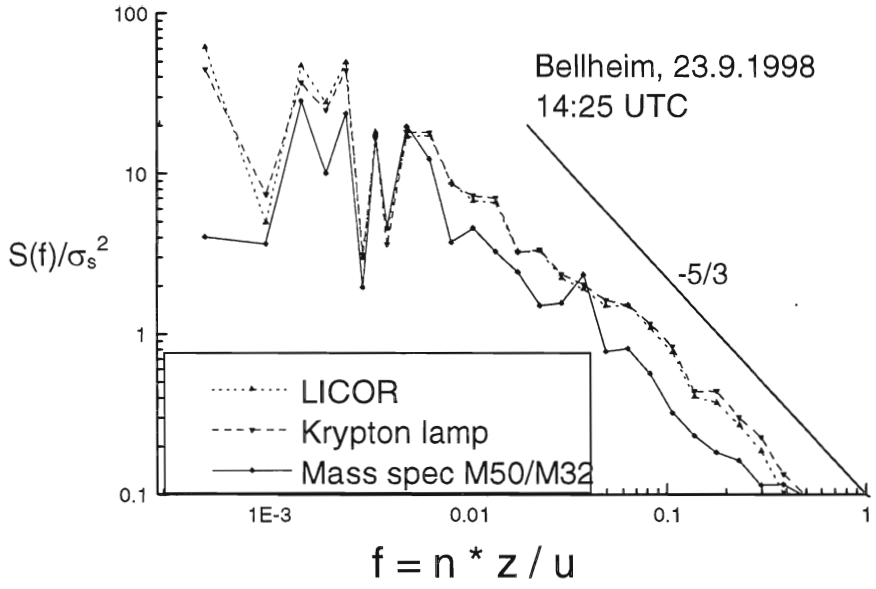

Figure 6. Power density spectra for water vapour measurements with the APIMS, a LICOR system, and a Kr lamp system. The abszissa gives the normalised frequency (n = measurement frequency, z = heigth above ground, u = mean horizontal wind speed).

ASGAMAGE Final Report

Contribution of TNO Physics and Electronics Laboratory

Partner 3

Principal Investigator: Dr. G. de Leeuw
TNO Physics and Electronics Laboratory
P.O. Box 96864, 2509 JG The Hague, The Netherlands
Phone: +31 70 3740462/0460; FAX +31 70 3280961
E-mail: deleeuw@fel.tno.nl

Contributors: Gerrit de Leeuw and Gerard J. Kunz

CO_2 flux measurements using micro-meteorological and geochemical techniques during ASGAMAGE.

Gerrit de Leeuw and Gerard J. Kunz

Work done in co-operation with *Søren Larsen, Finn Aa Hansen and Søren Lund, Risø National Laboratory, Roskilde, Denmark*

1. Introduction

The TNO Physics and Electronics Laboratory (TNO-FEL) participated in the ASGAMAGE project with the objective to contribute to developing methods for measurements of CO_2 fluxes over sea. A system was built for geo-chemical measurements of CO_2 fluxes, based on an equilibrator and an infra-red CO_2/H_2O measuring device. This system was used to measure CO_2 concentrations in water and in air. Together with Risø National Laboratory a micro-meteorological system was developed to directly measure CO_2 fluxes based on a sonic anemometer and two CO_2/H_2O fluctuation meters. The latter method can be used for analysis with eddy correlation techniques, or spectral methods including inertial dissipation.

TNO-FEL participated in both ASGAMAGE field experiments that were conducted on Meetpost Noordwijk (MPN). The first one, ASGAMAGE-A, took place from May 6 to June 7 in 1996, and was aimed at the study of processes affecting the exchange of gases between the water and the atmosphere. The second experiment, ASGAMAGE-B, focused on the measurement techniques and was conducted from October 7 to November 8. In addition to measurements of CO_2 fluxes, fluxes of momentum, heat and water vapour were measured, as well as size distributions of bubbles in the water and aerosols in the air. A lidar system was used to characterise the boundary layer structure. Measurements of bubbles, aerosols, and meteorological parameters were described in the first annual report [De Leeuw et al., 1997] and will no further be discussed here.

The main effort was on the flux measurements, and in particular the analysis of the CO_2 fluxes. The analysis presented in this report is focused on the geo-chemical measurements, profiles of CO_2 concentrations in the air, and micrometeorological flux measurements. Extensive descriptions of the ASGAMAGE experimental data and the analysis were presented in Kunz [1998] and Kunz et l. [1998a, b].

2. Experiments

2.1 Micro-meteorological measurements of fluxes of momentum, heat, water vapour and CO_2

In a close co-operation with Risø National Laboratory, partner 3, a micro-meteorological flux package has been assembled consisting of a Solent sonic anemometer and two Advanet CO_2/H_2O fluctuation meters. The signals of the two Advanets were used together to reduce the noise and thus increase the sensitivity of the CO_2 measurements. Both eddy correlation, inertial dissipation and spectral analysis techniques were applied to derive the fluxes from the measured signals [Larsen et al., 1996].

To reduce the influence of flow distortion, the instruments were mounted on the long boom extending west from the MPN. As a consequence, measurements could only be made when the wind was from westerly directions. The signals were recorded with the DAQ system developed by Risø, consisting of an A/D converter and processing software running on a PC.

2.2 Geochemical measurements of CO_2 fluxes.

As an alternative for the direct measurements of the CO_2 fluxes by the eddy correlation or inertial dissipation techniques, they can also be determined from the difference of the partial pressures of CO_2 in water and in air. This requires a value for the exchange coefficient for CO_2, available in the literature. However, fluxes determined from micro-meteorological methods and geochemical methods are often significantly different. One of the objectives of the ASGAMAGE project was to simultaneously measure the CO_2 fluxes with both methods to understand the observed discrepancies. When consensus can be reached in the results from both methods, they can be combined to derive experimental values for the exchange coefficients.

For ASGAMAGE, TNO-FEL built and applied an equilibrator system to measure the CO_2 partial pressures in seawater, together with those in air. The CO_2 concentrations were measured in seawater pumped up from different depths under the platform, to determine the CO_2 gradients in the sea. Seawater was continuously sprayed into the headspace of an equilibrator that was built after the design of Bakker et al. [1996]. Small samples of the air in the equilibrator headspace were analysed in a LI-COR CO_2/H_2O analyser, model LI-6262. Air samples were taken at levels of 2, 6, 12 and 30 m above mean sea level, using sampling tubes for continuous aspiration. A computer-controlled valve system has been built to consecutively sample air from the equilibrator headspace and from the outside-air aspiration tubes.

The equilibrator system was completed only briefly before the start of ASGAMAGE-A, and in fact improvements were continuously made during the experiment. Also during ASGAMAGE-B some modifications were made. However, all of these did not drastically alter the results and we feel confident with the data acquired during both experiments.

3. Results

3.1 CO_2 concentrations in water and in air

Concentrations of CO_2 in water and in air are presented in Figure 1. Figure 1a shows the molar fractions of CO_2 in water and in air measured during ASGAMAGE-A, in Figure 1b results are presented for ASGAMAGE-B. During ASGAMAGE-A the concentrations in water were ca. 200 ppm at the start of the experiment, and increased with ca. 100 ppm in the second week to a value of circa 300 ppm. These values are significantly lower than in the air, where the concentrations were circa 365 ppm. During ASGAMAGE-B the concentrations in air were similar to those in ASGAMAGE-A, although significant excursions to much higher values were observed. Those in water varied between 400 and 500 ppm. Hence, during ASGAMAGE-A the fluxes will have been directed into the water, while during ASGAMAGE–B they will have been from the water into the atmosphere.

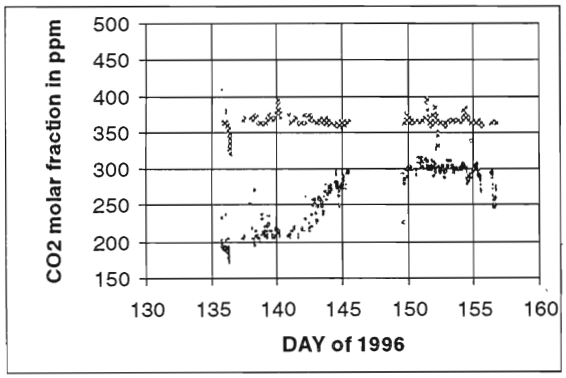

a

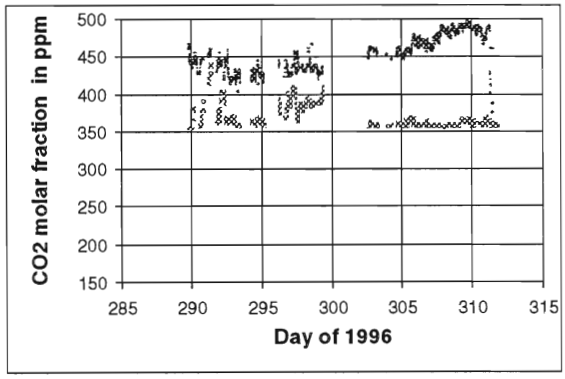

b

Figure 1. CO_2 molar fractions in water (circles) and in air (diamonds) during ASGAMAGE-A (a) and ASGAMAGE-B (b)

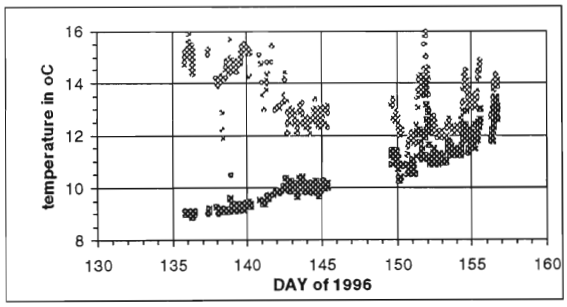

Figure 2. Temperature of water (squares) and air (plusses) during ASGAMAGE-A

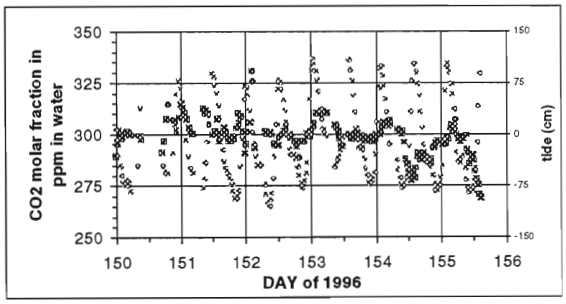

Figure 3. Fluctuations of CO_2 molar fraction in water during days 150-156 of ASGAMAGE-A (left vertical axis) and tidal fluctuations (right vertical axis).

Taking a closer look at the ASGAMAGE-A data, in relation to the ambient conditions, we see that the strong rise in the CO_2 concentrations in the water is associated with a rise in the water temperature starting on day 140 (Figure 2). An explanation for this effect could be enhanced biological activity producing CO_2, but we have no experimental evidence to confirm this assumption. Furthermore, the CO_2 partial pressure in water remains fairly constant at ca. 300 ppm after day 150, while the water temperature is seen to increase by another 2-3°C. Hence a correlation between the CO_2 partial pressure in water and the water temperature does not follow from this data.

The ASGAMAGE-A data in Figure 1a are quite variable. Zooming in on this data shows a regularity fluctuation with a period of ca. 12 hours. In Figure 3, the data for days 149-157 are plotted on an enhanced scale, together with the tidal variations of the water level. The variations in the CO_2 molar fraction appear to trace the tidal fluctuations quite well, but they are somewhat out of phase, with the peaks in the CO_2 partial pressures lagging behind. Also for days 141-147 such tidal fluctuations in the CO_2 molar fractions were clearly observed.

In the rest of this report we will mainly focus on the data from ASGAMAGE-B, starting with a brief overview of the meteorological conditions. Wind speed, air temperature and water temperature during ASGAMAGE-B are plotted in Figure 4. The wind speed in the first two weeks was generally lower than 10 m/s, with excursions to 15 m/s by the end of the first week. In the last two weeks, the wind speed was generally higher than 10 m/s. The water temperature gradually decreased from about 15°C to circa 13°C, while the air temperature was in general lower than the water temperature, except during a few days in the second period. Hence, the thermal stratification was generally unstable to neutral, or possibly slightly stable at the end of the third week.

The CO_2 data for ASGAMAGE-B in Figure 1b show strong variations in the air for days 290-300, while thereafter they are fairly constant at about 365 ppm. The high values of the CO_2 partial pressures during these initial 10 days are mainly associated with off-shore wind directions bringing air from the Rotterdam and Antwerp harbour areas. Likely, in these areas CO_2 is produced from industrial activities. The CO_2 partial pressures in either water or air, nor the partial pressure difference, as measured during ASGAMAGE-B, show a clear correlation with the water temperature or the air-sea temperature difference.

The partial pressures in the water measured during ASGAMAGE-B vary strongly with the wind speed during this period, see Figure 5. Possibly, the high wind speeds caused mixing of the water column, bringing CO_2 from larger depths to the surface. The high CO_2 partial pressures in air at low wind speeds are associated with the off-shore wind directions mentioned above. Apart from these wind directions, the CO_2 partial pressures in the air are independent of wind speed and vary slightly around 365 ppm. As a consequence, also partial pressure difference between water and air is completely determined by the variations in the water, and hence became more negative as the partial pressures in water increased. As shown in Figure 6, and can also be derived from the data in Figure 5, the partial pressure difference apparently reaches levels at elevated wind speeds, above ca. 15 m/s, where they become relatively independent of wind speed. Presumably, at these wind speeds CO_2 is well-mixed over the water column. It is noted that this discussion is highly speculative, supported by only a small data set in which in fact also some data points are observed which do not follow the general trend discussed in this section.

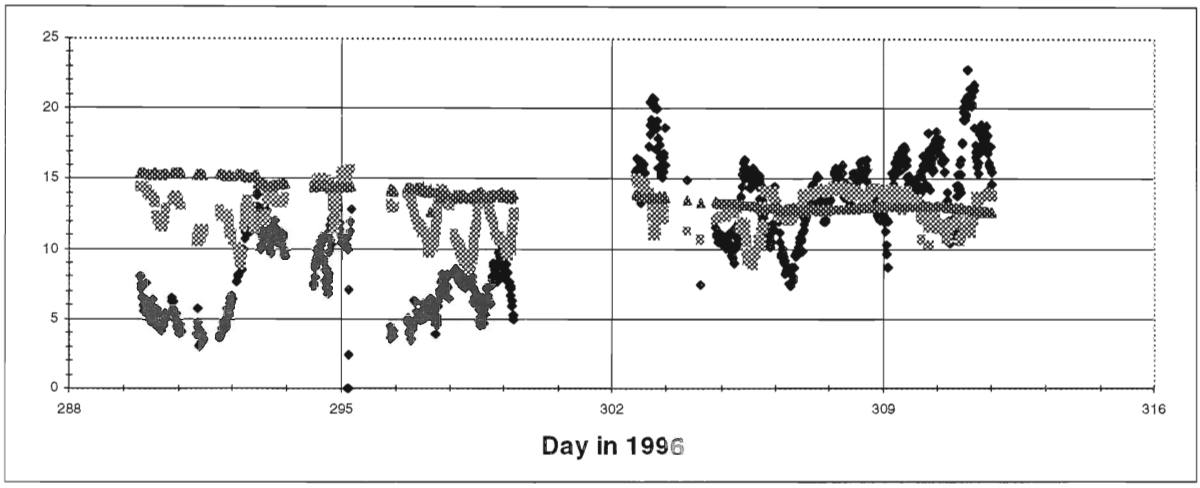

Figure 4. Wind speed (plusses) in m/s, water temperature (triangles) and air temperature (squares), both in °C, measured during ASGAMAGE-B

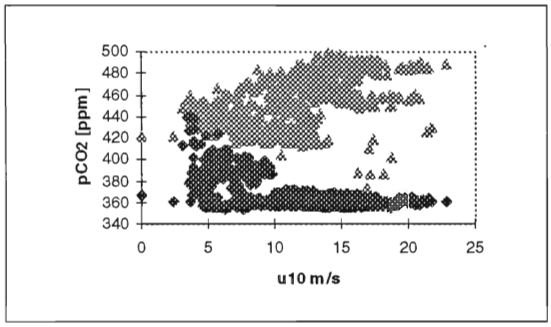

Figure 5. Partial pressure of CO_2 in water (triangles) and in air (plusses), plotted as function of wind speed u_{10} (i.e. wind speed at the reference height of 10 m above sea level).

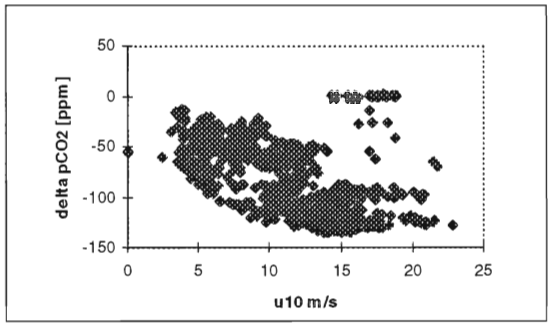

Figure 6. Partial pressure difference of CO_2 (air minus water) as function of wind speed u_{10}

3.2 Gradients of water vapour and CO_2 in the air.

Water vapour concentrations and CO_2 partial pressures in air were measured during ASGAMAGE-B at four levels: 2, 6, 12 and 30 m. The aim of these measurements was to determine the gradients and from these, to determine the fluxes. The results for water vapour in Figure 7 show that often a gradient is observed. In the second week of ASGAMAGE-B, when the wind was from land, gradients were quite strong, with a difference in the mixing ratio between 2 m and 30 m of up to about 2.5 g/kg on day 297! The low mixing ratios at the highest level of 30 m may have been associated with dry air masses transported from land accompanied with little mechanical mixing at the relatively low wind speed of 5-10 m/s. On the other hand, the sea was relatively warm with respect to the air with air-sea temperature differences between 0°C and more than –5°C, indicating neutral to strongly unstable stratification, which should imply strong thermal mixing by advection! The gradients between 6 and 30 m were much smaller than between 2 and 30 m, hence most of the convective flux may have been in the lowest levels. However, the elevated mixing ratios may have been an artefact, as discussed in the following paragraph.

The water vapour gradients during the rest of ASGAMAGE-B were generally smaller, with differences in mixing ratio of 1g/kg between 2 m and 30 m. In the last week some very high mixing

ratios were observed at the lowest level of 2 m. It cannot be ruled out that some water had entered the tubing through which the sample air was aspirated. Likewise, some water vapour in the tubing may have been responsible for the elevated concentrations at the 2 m level in the second week.

Highest mixing ratios were observed on days 294 and 307-310. On these days days, the atmosphere was neutrally stratified, thus prohibiting thermal mixing and trapping the moist marine air in the lower layers.

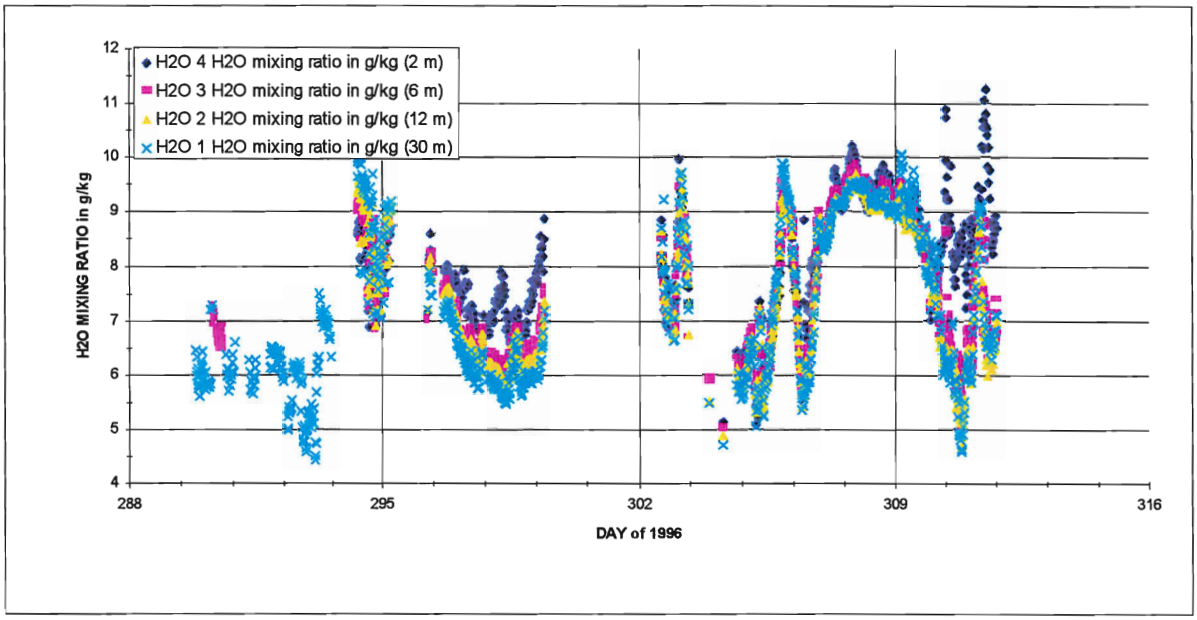

Figure 7. Water vapour mixing ratios measured during ASGAMAGE-B at 2, 6, 12 and 30 m above mean sea level (see legend).

CO_2 partial pressures in the air at 2, 6, 12 and 30 m are shown in Figure 8. Unlike the water vapour profiles, gradients are very small and the values at the different levels can hardly be discerned. In Figure 9 the partial pressure differences have been plotted, together with the air (at 30 m) – water partial pressure difference. The latter increased significantly in the second half of the ASGAMAGE-B experiment. Hence also the fluxes are expected to increase, leading to partial depletion of the atmospheric partial pressures near the surface. At the heights at which the measurements were carried out, with the lowest level at 2 m, no such effect was observed. In fact, the partial pressure differences in this period were ca ±0.5 ppm, while in the first period they were ca ±1 ppm. Possibly, mechanical mixing due to the higher wind speeds in the second period reduced the gradients.

Another observation is that the signs of the gradients were in general not consistent with the expected direction of the flux. The gradients scatter strongly around zero, although at times trends may be present. For example on days 298-300, the gradients seem to be positive on average, with partial pressures at the higher level up to ca. 0.5 ppm for all combinations shown in Figure 8. These positive gradients are contrasting the negative air-sea partial pressure differences. Also there appear to be days in which the gradients between different levels show consistent trends, but the signs for these levels are opposite. An example is for days 307-308, where the trends in the gradients between all combinations of levels tend to decrease. The partial pressure difference between 30 m and 12 m changes from slightly positive to slightly negative, while below 12 m the gradients remain slightly positive. Although likely all these variations are within experimental error, the trends are rather clearly present.

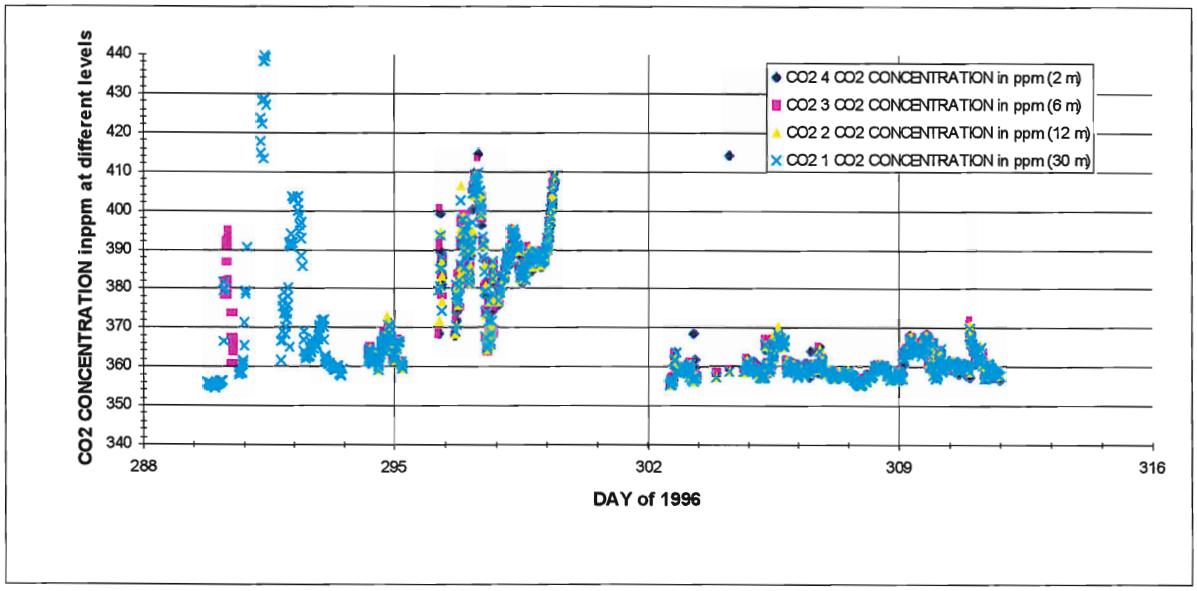

Figure 8 CO_2 partial pressures in air at 2, 6, 12 and 30 m above mean sea level (see legend).

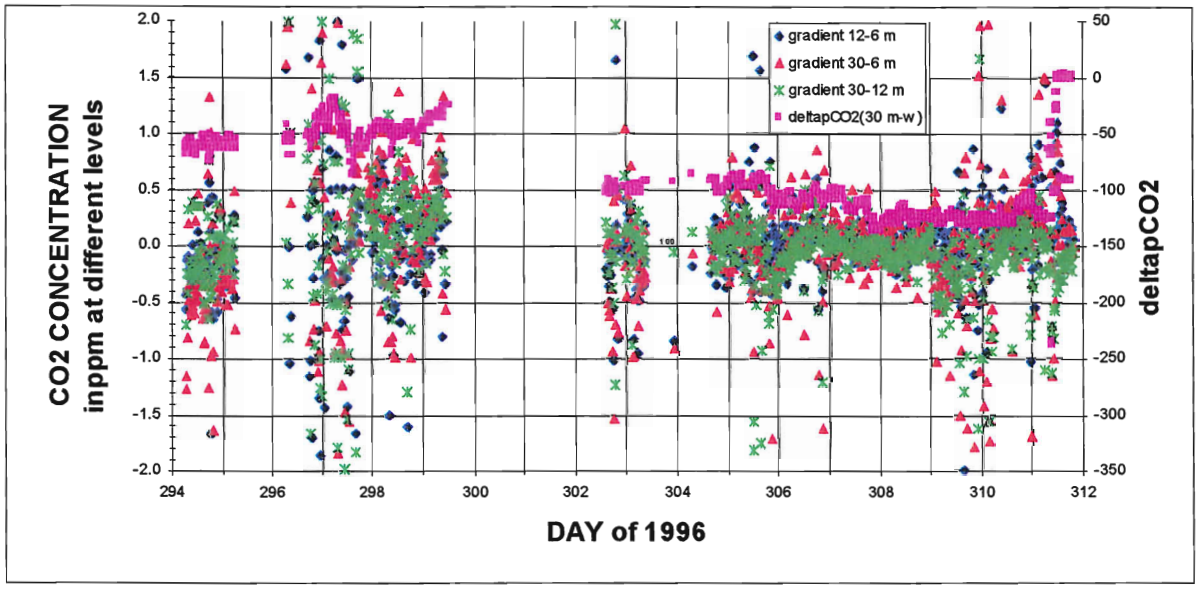

Figure 9. Differences in CO_2 partial pressures measured at 12 and 6 m, 30 and 6 m, 30 and 12 m (all left vertical scale), and 30 m minus the partial pressure in water (right scale). See legend.

The CO_2 partial pressure profiles show that the 'expected' trends are not obviously present in the data, also in cases where the water vapour mixing ratios clearly vary toward the water surface. The difference between water vapour and CO_2 is in the exchange rate. Water vapour, for which the sea is usually a source, is readily exchanged between the water and the atmosphere, which sustains a gradient near the sea surface. Water vapour transported away from the surface by diffusion is readily replaced by evaporation. For CO_2 this is not the case, because the exchange between the sea and the overlying atmosphere is much slower. Even for the large air-sea partial pressure differences of almost −150 ppm observed during ASGAMAGE-B, the exchange is too slow to sustain a significant gradient near the surface. Due to diffusion the gas is mixed over the boundary layer and the gradients are negligibly small. Although trends in the gradients are clearly present, their signs often predict a different direction of the flux than expected from air-sea partial pressure differences.

3.3 Micro-meteorological flux measurements and derived transfer rates

Micro-meteorological fluxes were measured together with Risø. Part of the analysis was carried out while Gerard Kunz from TNO-FEL was at Risø. Both eddy correlation and spectral analysis methods were applied, and advantage was taken of two Advanet CO_2/H_2O fluctuation meters to reduce the noise in the CO_2 signals. Results from the different analysis methods were presented in Kunz et al. [1998a]. Inter-comparisons were made between the results from the different methods and they were also compared with those from the Oakridge sensor. For water vapour both sensors agree very well, but for CO_2 the results obtained with the Advanets appear too high. Consequently, also the transfer coefficients derived from the Advanet results with the measured air-water partial pressure differences will be too high.

The reason for the high fluxes from the Advanet sensor are not completely clear. Obviously the high noise level of the Advanets have a large influence, but also other factors seem to play a role. For instance, as indicated in Kunz et al. [1998a], the air-flow measurements appear perturbed for the majority of the measurements with winds from south-westerly, as evidenced from the variances and the values for the friction velocities. It is in this wind sector that also the CO_2 fluxes appear high. For westerly and north-westerly winds the CO_2 fluxes are much lower and appear to be close to the expected values.

Exchange rates derived from the fluxes measured in W-NW winds are in reasonable agreement with those found by other ASGAMAGE participants. This conclusion applies to selected data, for which also other fluxes show reasonable values.

4. Conclusion

The analysis of the ASGAMAGE data set presented in this final report was aimed at the determination of the CO_2 fluxes between water and atmosphere. Three methods have been applied: geochemical measurments, profile measurements and, together with Risø (partner 3), micro-meteorological methods.

The results from the geochemical measurements appear quite good [Jacobs et al., 1998]. Presented data show large fluctuations of the partial pressures, especially in water, and smaller fluctuations that appear correlated with the tide. Partial pressures in air were generally around 365 ppm, and the occurrences of significantly higher values are associated with wind coming from apparent source regions.

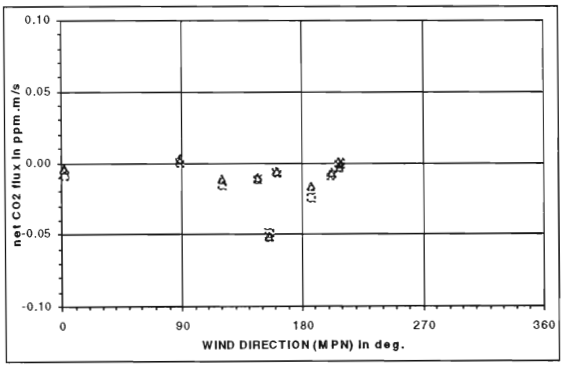

Figure 10. Selected CO_2 fluxes during ASGAMAGE-B. Data are for wind directions between 240 and 330°, and apparently unperturbed meausurements

The profile measurements appear very difficult. Although trends were found in atmospheric gradients, they could not be associated with the expected flux direction, and often the sign was reversed from the expected value. Gradients observed were on the order of 0.05-0.1 ppm.

For micro-meteorological measurements several methods were tried. In particular the two-sensor method was applied in an attempt to reduce the sensor noise to a level where signals could reliably be analysed. However, the Advanet sensors are not sensitive enough for reliable measurements over sea, where fluxes are very low. Only after very careful selection of data points, some results could be obtained that are close to expected values.

The ASGAMAGE projects has resulted in the development of new sensors with much higher sensitivity which are much more suitable for direct measurements of CO_2 fluxes over sea than the Advanet sensors. Hence the application of the Advanet sensors for this purpose, even with the two-sensors method, is not worthwhile pursuing.

In conclusion, the ASGAMAGE project has lead to a better understanding of the application of sensors and techniques for measurments of CO_2 fluxes over sea. The equilibrator system developed by TNO-FEL yields good-quality data.

References

Bakker, D.C.E., H.J.W. de Baar and U.V. Bathmann (1996). Changes of carbon dioxide in surface waters during spring in the Southern Ocean. Deep-Sea Res., Spec. Iss. (in press).

Larsen, S.E., F. Aa. Hansen, G. de Leeuw and G.J. Kunz (1996). Micrometeorological fluxes of CO_2, bubbles, heat, humidity and momentum in the marine atmospheric surface layer during OMEX. OMEX final annual workshop (Brussels, 20-22 May, 1996), p. 47.

ASGAMAGE Final Report

Contributions of the Risø National Laboratory, Denmark

Partner 4

Principal Investigator:

Dr.S.E.Larsen
Risø National Laboratory,
Postboks 49,
DK 4000 Roskilde,
Danmark
Phone + 45 4677 5012; Fax + 45 4677 5970
E-mail: metsol@risoe.dk

Measuring and modeling fluxes of especially Carbon Dioxide in the marine atmospheric surface layer during ASGAMAGE. Final Report.

S. E. Larsen, F. Aa. Hansen, J. F. Kjeld & S. W. Lund
Wind Energy and Atmospheric Physics, Risø, Roskilde, Denmark
In cooperation with:
G. J. Kunz & G. de Leeuw
TNO-FEL,The Hague, The Netherlands

1. Introduction

Air-sea exchange of slowly dissolving gases is still associated with considerable uncertainties. The transfer-velocity relations based on the Liss and Merlivat(1986), and the Wanninkhof(1992) studies offer integration of many data sets, and seems satisfactory integration of these data, although with substantial scatter, and with substantial systematic difference between the two suggested regression expressions. Also, the small transfer rates implied by these relations indicate that in the natural environment fluxes and concentrations will often not be in the equilibrium, implicitly assumed when employing the transfer velocity relations. Within the ASGAMAGE project, the Riso group participated in both the ASGAMAGE field experiments at Meetpost Nordweijk (MPN), and simultaneously through a phd-sproject (Kjeld,1999) carried out model studies of the exchange processes.

The first of the field campaigns, ASGAMAGE-A, took place from in 1996, from 6 May until June 7. The second experiment, ASGAMAGE-B, was carried out from 7 October to 8 November in 1997. In both experiments, the Riso cooperated closely with the team from TNO with a joint instrument packet to measure the turbulent fluxes of momentum, heat water vapour and CO2, as seen in Figure 1. It consisted of a sonic anemometer- thermometer to measure the turbulent velocity and temperature fluctuations, and two Advanet Infra Red absorption instruments to measure the turbulent fluctuations of H2O and CO2. Two Advanets were used in an effort to improve the signal/noise ratio of the Advanet CO2 measurements, for which it at the start of the project was known that the S/N ration was marginal.

The modeling study was performed especially to evaluate the role of inhomogeneity and instationarity in the air and the water for the air-water exchange of different trace gases including of course as the most important Carbon Dioxide. The reason for this objective was that the exchange rate formulation, normally used as a basic assumption has that the exchange takes place between a well mixed water body and a well mixed air body, with the only gradient being present at the interface. The modeling efforts have to a large extent been performed in cooperation with the group from KNMI.

2.Determination of fluxes.

The common method for determination of the air-sea exchange of gases is application of the exchange-coefficient method, where the exchange is determined from the difference in concentration between the air and the water, that is

$$F = k_p \bullet (C_{w0} - \alpha C_{a0}), \qquad (1)$$

where C_{w0} and C_{a0} are the concentrations close to the surface at the water and the air respectively.α is the dimensional Ostwall solubility coefficient, $\alpha = K_H RT$, with K_H being the Henry's law constant. The gas exchange coefficient, k_p, has been determined empirically and theoretically by several authors. Empirical expressions are found in Liss and Merlivat (1986) and Wanninkhof(1992), while theoretical evaluation are found Coantic (1986) and within ASGAMAGE by the work of Jacobs and Oost, using surface renewal theory. In general the authors find k_p to grow with wind speed, or u_*, in a power between 1 and 2, dependent on the velocity interval and the authors. Also a dependency on the Schmidt Number, $Sc = \nu/D$, in the power between -½ and -¾, with a typical value being -2/3. Woolf(1997) relates k_p to the bubble production at the surface in a way that captures the velocity and Sc dependency described above and add a bubble dependency related to the solubility of the individual gases. One source of uncertainty when using (1) is that it in practice always must be used between practical measuring positions in the water and the air, eg. 10 m and -5 m.

Here we shall concentrate on the use and development of micrometeorological techniques either as alternative to (1) or for comparison with results derived from (1). Until recently large differences have existed between fluxes estimated by micrometeorological methods and the transfer-velocity methods. The differences have at times exceeded an order of magnitude. In Larsen et al. (1996) we presented measurements from the cruising with substantially less difference between the different flux estimation techniques, and further reported on the first use of the co-spectral method for ship measurements.

The micrometeorological methods employed included eddy-correlation, eddy co-spectral and inertial dissipation methods based on use of sonic anemometers and the Advanet IR water vapor and CO_2 absorption measurements. Figure 1 shows the three key-instruments used for the micrometeorological flux estimation, a Gill sonic anemometer/thermometer and two Advanet CO_2/ H_2O Infra- Red(IR) absorption sensors. Two CO_2 sensors were used to improve the marginal Signal/Noise with cross-correlation between the two sensors, a method that will remove non-common noise between the two sensors. The method is illustrated on Figure 2, where the CO_2 concentration power spectrum is estimated as power spectrums from each of the sensors and as a Co-spectrum between the two signals. The distance between the two sensors will only affect the correlation between the signals for the frequency being larger than about 1 Hz, as was found by comparing the corresponding signals for humidity, where the signal/noise ration is much better.

The basic micrometeorological method for flux estimation is the eddy correlation between the vertical velocity and the concentration fluctuations.

$$F = \rho_o < w'\gamma' >, \qquad (3)$$

where ρ_o is the density of the air and γ stands for concentration of any of the scalars, T, q or q_{CO2}, or also the horizontal velocity u, if F is the flux of momentum.
Here we have further employed the eddy-co-spectral method and the inertial dissipation method, both being less sensitive to flow-distortion induced by the platform and its motion.

The co-spectral methods employs the low frequency part of the co-spectra, fCo(f) to derive fluxes:

$$< w'\gamma' > \approx 5\, f\, Co_{w\gamma}(f) \quad for\ 0.01 < n < 0.1\ , \qquad (4)$$

Here f is the frequency in Hz, while n is the so-called normalized frequency, n = fz/U, where z is the measuring height and U the mean wind speed, γ again stands the horizontal velocity u, or for any of the scalars, T, q or q_{CO2}.

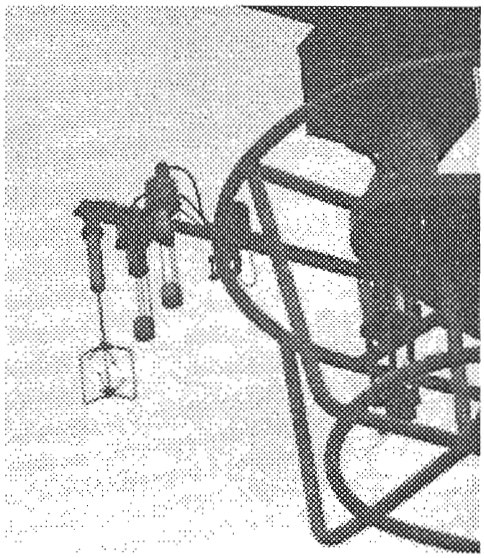

Figure 1. Sensor packet used for micrometeorological estimation of the CO_2 flux, showing a sonic anemome-ter/thermometer and two Advanet CO_2/H_2O sensors.

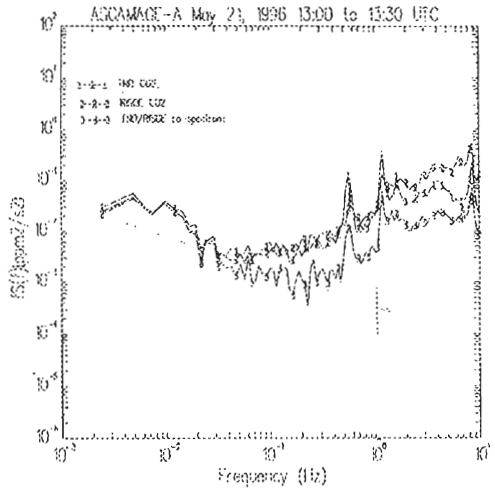

Figure 2. Co-spectral and power spectral estimation of the CO_2 power spectrum for the dissipation and method during the MAST-ASGAMAGE-A.

The inertial dissipation method employs the laws for high-frequency small scale turbulence to derive the fluxes from estimates of the dissipation, derived from the high frequency inertial range of the power-spectra, S(f) . The general formulation for the dissipation estimates of an arbitrary scalar flux can be found from the following expressions:

$$u_* = [\frac{f\, S_u(f)}{\alpha}]^{1/2} [\frac{2\pi}{U}\frac{\kappa\, z}{\phi_\varepsilon} f\ ]^{1/3}\ , \qquad (5)$$

$$|< w'\gamma' >| = [\frac{\alpha}{\beta}\frac{\phi_\varepsilon}{\phi_{N_\gamma}}\frac{f\, S_\gamma(f)}{f\, S_u(f)}]^{1/2} u_*^2\ ,$$

It is understood that the spectral values have to be taken within the inertial sub-range. α and β are the Kolmogorov constants for the velocity and the scalar spectra respectively, $\phi_\varepsilon = \phi_\varepsilon(z/L)$ is the Monin-Obuchov similarity function for the velocity dissipation, while ϕ_N is the similar function for the scalars. L is the Monin-Obuchov stability Length-scale and z the measuring height.

From the micrometeorological point of view equation 3 is the basic definition of the turbulent flux, while (4) and (5) derives the fluxes from the scaling laws that have been found to be valid in the atmospheric surface layer, they are thus less basic than equation 3. Their advantage is that they in a number of ways a less susceptible to flow distortion, platform motion and simple signal noise than is equation 3. Comparing equation 4 with equation 5, the dissipation method must be considered more generally valid than the co-spectral method because the characteristics of the inertial sub-range is a more universal feature of surface layer turbulence than is the intensity of the co-spectrums around their peak value.

Also equation 3 can, however, not be considered the final definition of the vertical flux, since it neglects the transport by the mean vertical wind speed. Especially for trace gases with small fluxes, due to the importance of a high surface resistance, as CO_2, the vertical mean speed can contribute substantially to the total vertical flux.
This correction to (5) is called the Webb Correction and is by now reasonable well established. For species with very small fluxes it account for that even extremely small average vertical velocities may contribute significant to the total flux. The existence of the correction can be argued several ways. Building on (5) we can formulate the total flux, for a gas with concentration C + c', as:

$$F_t = <(W + w')(C + c')> = WC + <w'c'>. \qquad (6)$$

In (6) the second term correspond to (3), while the first term reflect transport by the mean vertical velocity. W is generally so small that it can not be measured, the absolute value being typically less than 1 mm/sec. Typically W is derived from the continuity equation for the dry air, ρ:

$$\frac{\partial <\rho>}{\partial t} + \frac{\partial}{\partial x_i}(<\rho u_i> - D\frac{\partial <\rho>}{\partial x_i}) = 0. \qquad (7)$$

To simplify (7) we neglect the molecular diffusivity, and further assume stationarity and horizontal homogeneity. The remaining term involves the vertical gradient of $<\rho w>$. Since that term is zero at the surface equation 7 reduces to: $<(W+w')(<\rho> + \rho')> = 0$, or:

$$W = -<w'\rho'> / <\rho> = <w'T'> / <T> \qquad (8)$$

where T is the temperature. For the mixing ratio for CO_2 we find the detailed expression for the Webb correction to have the form:

$$F_{qCO_2} = <w' q_{CO_2'}> + 1.61 <q_{CO_2}> <w'q'> + (1 + 1.61 <q>) <q_{CO_2}> \frac{<w'T'>}{<T>}, \qquad (9)$$

where we can normally neglect the water vapor mixing ratio, q, compared to 1.

A consequence of (9) is that the statistical uncertainty on experimental estimates of the total flux becomes fairly large, as it is determined by a sum of three covariance estimates. The actual analysis is compli-cated as it will depend on the actual magnitude of each term and also on the degree of correlation between the different fluxes. A detailed error analysis has to the author's knowledge never been done.
It is worthwhile to consider the continuity equation in a little more detail, since the Webb-correction opens for other sources of uncertainties, than the pure statistical. If we in (7) now accept instationarity and horizontal inhomogeneity along the x-direction, the equation reads:

$$\frac{\partial <\rho>}{\partial t} + \frac{\partial}{\partial x} <\rho u> + \frac{\partial}{\partial z} <\rho w> = 0. \qquad (10)$$

We integrate from z_0 to Z to obtain:

$$Z\frac{\partial <\rho>}{\partial t} + ZU\frac{\partial <\rho>}{\partial x} + Z<\rho>\frac{\partial U}{\partial x} + <\rho> W + <\rho' w'> = 0$$

Next, we use the equation of state to replace the air density with pressure and temperature.
We finally replace ∂ with Δ to evaluate the different terms:

$$W = \frac{<w'T'>}{T} - \frac{Z}{\Delta X}\Delta U - \left(\frac{ZU}{\Delta X} + \frac{Z}{\Delta t}\right)\left(\frac{\Delta p}{p} - \frac{\Delta T}{T}\right) \qquad (11)$$

With Z= 10 m, ΔX = 100 Km and ΔU = 5 m/s, the second term in (11) is seen to be of the order of the leading Webb term, which is typically of the order of 1 mm/s or less. This means that the physics behind the Webb cor-rection can make interpretation of local micrometeorological measurements of gas fluxes difficult.

3. Discussion of the Experimental results

The flux and turbulence results from ASGAMAGE-A and ASGAMAGE-B, obtained by the TNO/Riso team are described in Kunz et al(1998a, 1998b). The results are included in the ASGAMAGE data base, managed by KNMI. The data are presented in the two reports cited above, and has been included in the overall ASGAMAGE data base. The Riso/TNO data were actually best from in ASGAMAGE-A. But there was agreements between the ASGAMAGE participants on focusing first on the data when the best and the most CO2 sensors were available, which was during ASGAMAGE-B. In the process organizing and improving the data- base, part of the data have been reanalyzed in response to the problems appearing when different data sets were compared and integrated.

Reanalysis of data from the TNO/Riso data set
In the context of setting up the data base plots of data were exchanged between the coordinator TNO and the participant about the differences and similarities between the different data sets. Below is shown special plots connected with the CO_2 fluxes.
From the data illustrated on Figures 3 and 4 and from evaluation of the logbooks, we have found that our

sonic w data should be increased by 10%, because this correction to sonic data had not been included in the data base. Also a number of TNO/Riso runs should be removed because the logbooks indicated uncertainty about the occurrence of rain, instrument performance, boom vibrations or movements. These runs are, following the KNMI numbering system:
KNMI: 12-27 (Signals looks strange). KNMI: 32-49 (due to precipitation), KNMI: 76-79 (precipitation is likely). KNMI: 172-176 (precipitation). KNMI: 204, 205, 209-212, and 229 (precipitation and boom work).

Finally a number of runs have reanalyzed with a new soft-ware system with improved noise reduction features. The runs for reanalysis were chosen based on the wind direction, Figures 3,4 and on logbook entries. Both KNMI

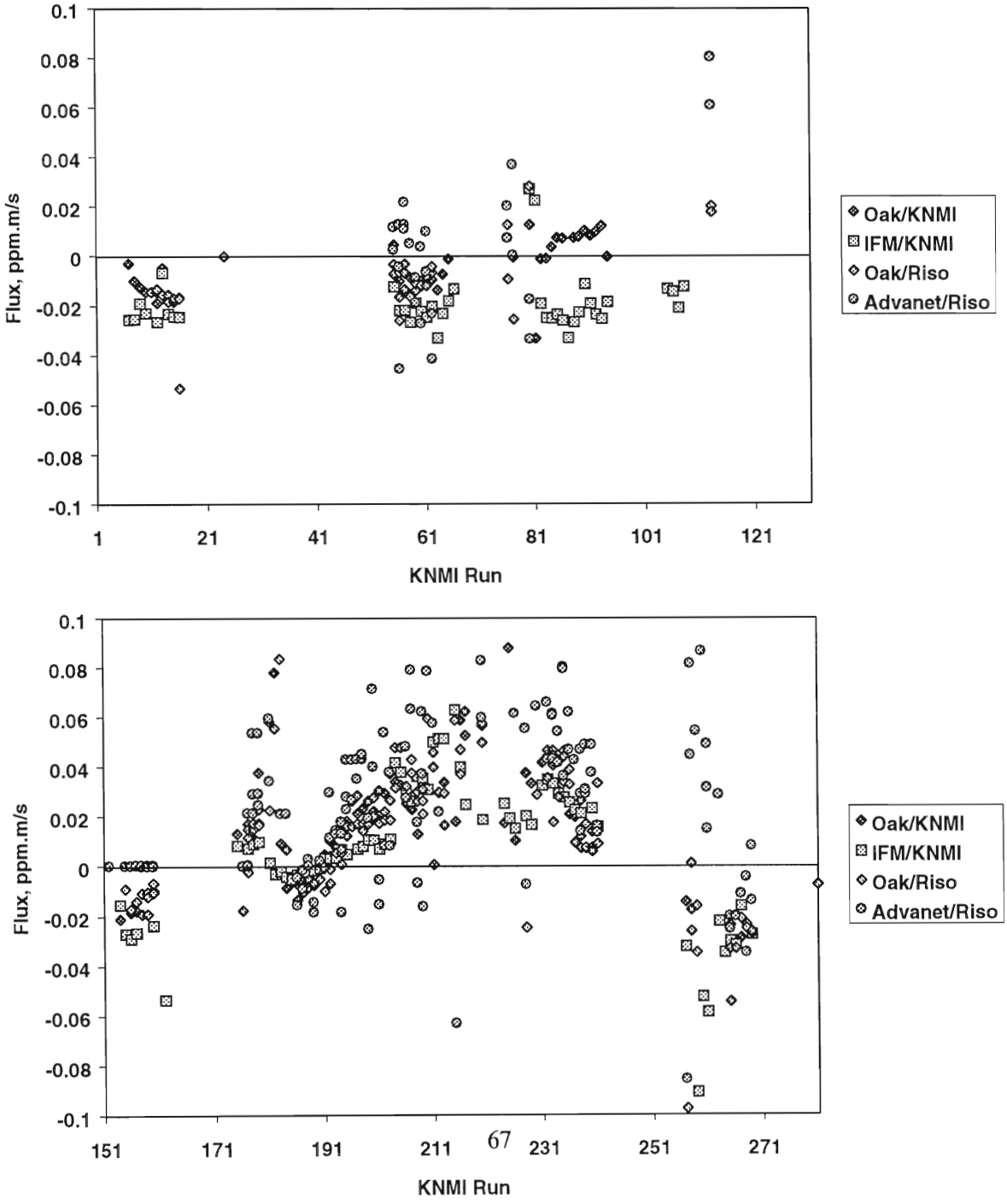

Figure 3 : Raw fluxes, reflecting reflecting result from different groups and instruments.: NOAA data with KNMI processing: dark blue diamonds; IFM data with KNMI processing: red squares; NOAA data with Risø processing: light blue diamonds; Advanet data with Risø processing: green circles. Upper: runs 1-131; lower:
runs 151-281, all during B period. Filtering: winddirection > 220 degrees; 0.5 < CDN < 4; ΔpCO_2 available; IFM data available. (Figure produced by Cor Jacobs, TNO, in January 1999)

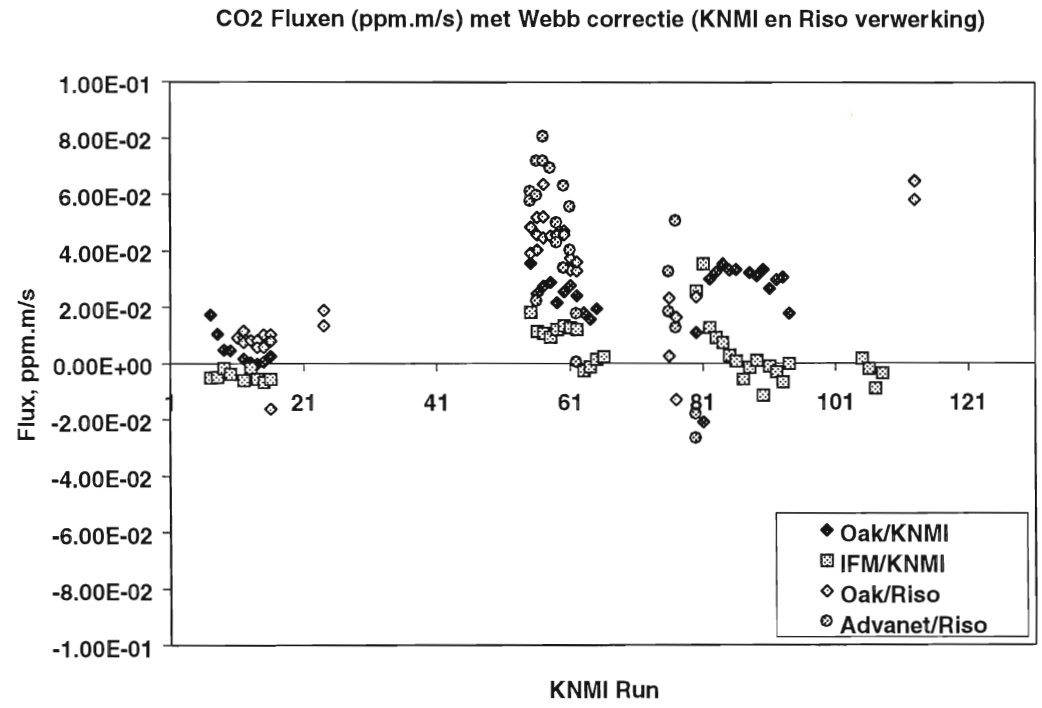

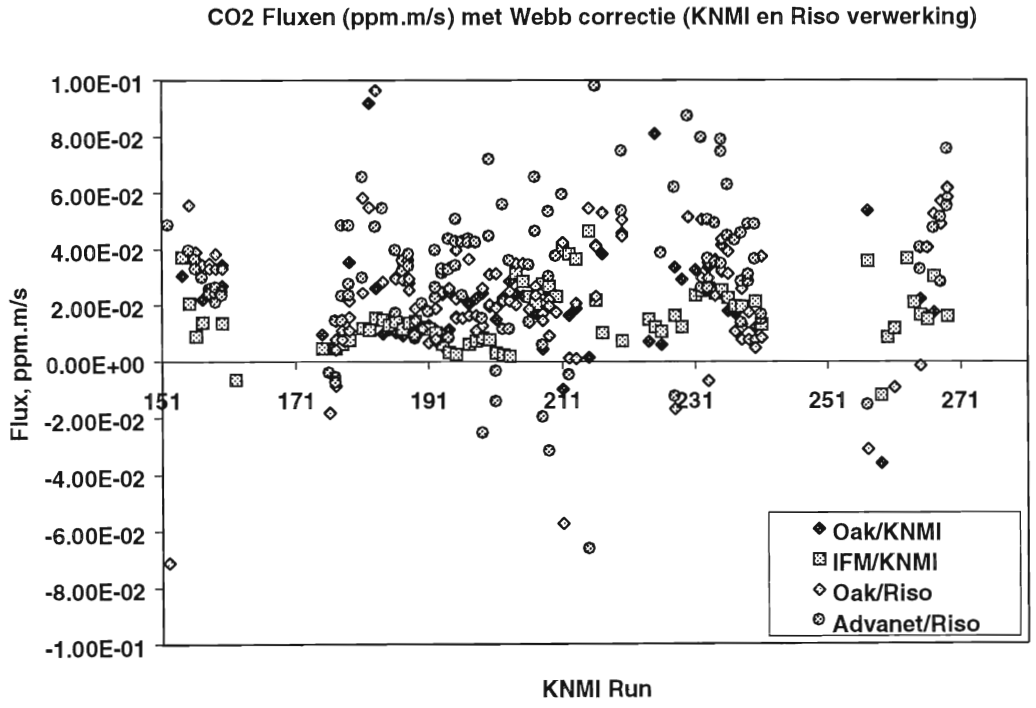

Figure 4: As in Figure 3, but for CO_2 fluxes with Webb correction applied.

and BIO participants noticed fairly large scatter in the CO_2 flux data for the wind direction larger than 270 degrees, while we (Kunz et al, 1998a) noticed that wind directions around 220 degrees gave rise to problematic highly variable lux values. Results of the fairly promising reanalysis is presented in Table I.

KNMI Run	date,hr	W.DIR.	new raw 1	new raw 2	New cor 1	new cor 2
55	10.19.06	310	-0,001	-0,0246	0,01	0,01
58	10.19.08	310	-0,0165	-0,0275	0,05	0,005
60	10.19.10	305	-0,015	-0,0222	0,018	0,017
62	10.19.13	295	-0,012	-0,013	0,01	0,013
205	11.02.09	226	0,006	0,027	0,0304	0,0259
209	11.02.13	230	0,059	0,0522	0,0388	0,037
215	11.02.20	230	0,002	0,001	0,0241	0,0162
218	11.02.23	230	0,015	0,0404	0,0378	0,0345
226	11.03.06	220	0,012	0,0152	0,0179	0,0149
230	11.03.13	224	0,06	0,04	0,0319	0,0223
233	11.03.17	228	0,0425	0,0339	0,0318	0,0276
239	11.03.21	223	0,03	0,0122	0,0185	0,0273

Table 1. Result of reanalysis of a number of runs selected on basis of wind directions an dissimilarities between the different data sets, as described in the text. New raw 1 and 2 mean new estimates of the raw CO_2 fluxes measured as ppm m/s , 1 is estimated from the average of two co-spectra between w and CO_2 following equation 4, while 2 is estimated from the dissipation method, equation 5, and using both the Advanet and the Oak Ridge sensors for estimating both the average co-spectrum and the dissipation estimate, as described in the text. The new cor estimates are based on the raw estimates and the Webb correction, using co-spectral estimates and dissipation estimates respectively,- again using both the Advanet and the Oak Ridge sensors. However, it should be pointed out that the estimation is dominated by the Oak Ridge sensor, because the correlation techniques used automatically favors the sensor with least noise.

4. Modeling

To study the behavior of the air-sea flux for inhomogeneous and non-stationary conditions, we have developed a diffusion model considering the vertical diffusion in the water and in the air and the chemical buffer in the water as well the Webb corrections in the air. Basically, the model looks as follows:

$$\frac{\partial C}{\partial t} + U\frac{\partial C}{\partial x} = -\frac{\partial Flux}{\partial z} - \alpha(C - C_{eq}), \qquad (12)$$

$$Flux = WC + < w'c' > - D\frac{\partial C}{\partial z}$$

In these equations, $\alpha(C\text{-}C_{eq})$ accounts for the buffer effect in the water, with α being 10-20 sec-1 for $C < C_{eq}$

0.025-0.04 sec-1[-1] for $C > C_{eq}$. In the air α is zero. Average values are indicated by capital letters, while lower case letters are used to describe the turbulent part of the variables. In the air the mean vertical velocity, W, is derived from the formulation for the Webb correction to the measured/modeled raw turbulence fluxes. The turbulent part of the flux is determined through a turbulence diffusivity closure.The model is constructed to match the transfer velocity expression if conditions are homogenous and stationary by stipulating the exchange across the interfacial layer to be described by the exchange coefficient expression. This concept is based on that the transfer coefficient method models situations where all the air-water concentration difference is found at the air-water interface, a situation that is most closely approximated for stationary and horizontally homogenous situations. Also, the empirical transfer rates are well in according with transfer rates derived from first principles characteristics of the surface processes (Coantic, 1986) and the work by KNMI in this report. The model solves for the flux-concentrations between an upper and a lower boundary, corresponding to typically to the levels for the water and the air inlets for the concentration measurements in an experimental situation.

The model of (12) have been solved for numerous different situations with perturbations of the concentrations at the upper or lower boundaries, with the perturbations typically being formulated as Gaussian perturbations of different horizontal scales.

From the model computations we can draw a number of conclusions (Kjeld, 1999):

For CO_2 the equation for the water is dominated completely by the chemical buffer, meaning that the advection-diffusion terms in the (12) are negligible in the water. On the other hand this means that knowledge about C_{eq} all the way to the surface becomes very important for estimating the surface exchange, if the [1]concentrations are known at some depth. Ceq can be estimated from the total Dissolved Inorganic Carbon, DIC, alkalinity, salinity, ph and temperature. In the air, however, the advection-diffusion part is always important for the flux-profile relation ships.

Taking the true exchange rate as given by (1), the exchange rates estimated by (1) by use of concentrations at the typical measuring levels, at ±5-10 meter, or by micrometeorological methods. The different flux estimates agree for perturbations of scales larger than 3-5 km. For smaller scales the different estimates start disagrees, with the micrometeorological method being more sensitive, as illustrated from figure 3. This aspect can be understood in the light of a simplified stationary version of (12):

$$U \frac{\partial C}{\partial x} = - \frac{\partial}{\partial z} (WC - \kappa u_* z \frac{\partial C}{\partial z}), \qquad (13)$$

where we have parametrized the turbulence flux by use of a standard formulation for the neutral turbulence diffusivity. In the atmospheric surface layer the vertical gradients of both C and W are very small for homogeneous conditions. For W due to the general formulations for a surface layer and for C because the largest gradient will be found in the water, and especially at the water-air interface. Therefore the vertical fluxes determined at a given height in the air can be more sensitive to an advection term on the left hand side (13), than will the gradients in the water and at the water-air interface.

Finally, we mention that for other trace gases, the flux profile relations in the water is more directly sensitive to the advection-diffusion aspects of a concentration perturbation, because the species are non-reactive in the water.

In Figure 4, we show as an example the concentration profiles for He and SF_6 at different phases of the pertur-bation, indicated by an arrow. These aspects of the difference between flux-profile relations for different species and different concentration cloud sizes may have consequences for the use of dual tracers . This aspect of our ASGAMAGE research have been coordinated with a similar research at KNMI and is discussed further in Jacobs et al (1999).

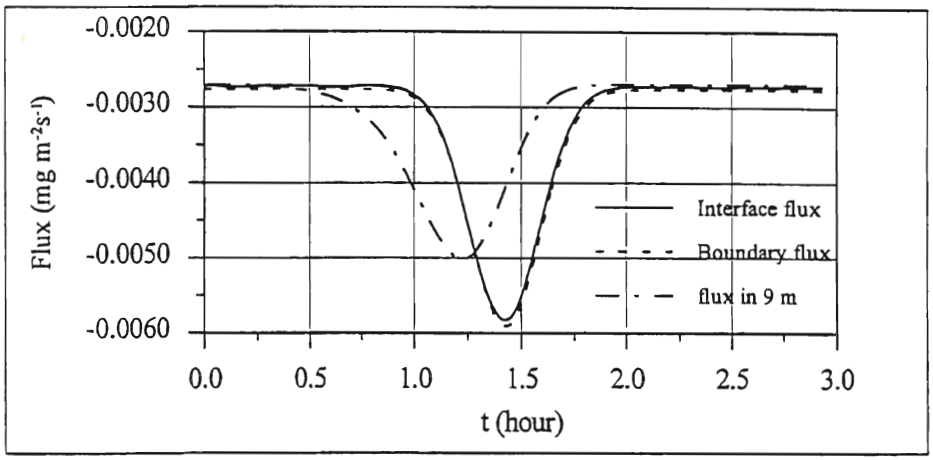

Figure 5. Model computation of the different estimates of the air-water CO_2 flux in responce to a Gaussian concentration perturbation at 6 meters depth. The perturbation has a horizontal scale of 1 km and is drifting by the measuring position with a wind induced current corresponding to a $u_* = 0.3$ m/s.The Boundary fluxes are those one would abtain from measurements of the CO2 concentrations a 6 meters depth and 10 meters height, while the interface flux is estimated from (1) and the flux in 9 meter is estimated from the concentration vertical concentration gradient.

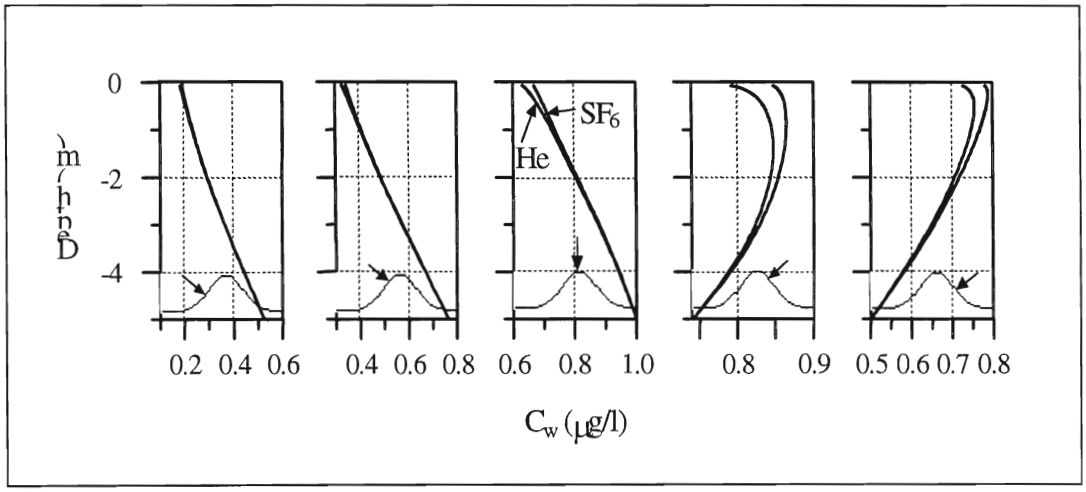

Figure 6. Concentration profiles for He and SF_6 for relative to the phase of a 1 km concentration perturbation drifting by a measuring point with an wind driven current corresponding to an $u^* = 0.3$ meter/sec. The phase of the perturbation is indicated by an arrow on the Gaussian form for each profile in the figure.

5. Discussions and Conclusions.

The micrometeorological methods have been found to deliver results that in average are getting closer to the transfer-velocity method from the ASGAMAGE results. Hence the road seems now open for more detailed comparisons between the two methods allowing for experimental studies of the importance of instationary and inhomogeneous situations for the air-sea exchange of CO2. Such situations have also been studied by means of simple diffusion models combined with the description of the carbonate buffer system. Although simplistic, this modeling concept has allowed for exploratory analysis of the air-ocean exchange of CO2 for transient conditions. Some of the model results indicate that, one should generally not expect very close real time similarity between the different flux estimation methods. A reason for this is the sensitivity of the micrometeorlogical method to inhomogeneity and instationarity as presented in this report. Other reasons for such sensitivity may be found in the Webb correction that also has been shown to be sensitive to inhomogeneity and instationarity. We conclude that more work in understanding and clarifying these aspects of air-sea exchange under inhomogeneous and instationary conditions would be useful.
Although the micrometeorological method has been found work reasonably for all the different flux interpretation method, summarized in the present report, much sensor and system improvement still need to be done before the measuring systems used can be considered mature. Both the sonic and the CO_2 systems used were found to perform less well than expected and desired. For the Advanet CO_2 sensor specifically the sensitivity to contamination and the badly determined sensitivity of the CO2 channels to water vapour concentrations have been problematic. Future work within the measurement field will involve improvement of the CO_2 sensor, a possibility already documented during the ASGAMAGE project by the Oak-Ridge and the IFM sensor applied in ASGAMAGE B. Also improvement of the Sonic anemometer-thermometer could be well-come, especially with respect the temperature measurements. With this said, however, the Advanets as presented in figures 3 and 4 did not really give much average larger values than the other instrunemts, Oak Ridge and IFM. It gives much more scatter primarily due to the smaller S/N ration for Advanet and due to the fairly badly cross talk between the humidity and the CO_2 channel. However, with the changes in the TNO/Riso contribution to the database, described under the reanalysis section, the similarity will be enhanced.

6. References.

Coantic, M. (1986) A model of Gas Transfer across Air-Water Interfaces with Capillary Waves. J.Geophys. Res.,Vol.91, No.C3, 3925-3943.
Larsen, S. E., F.Aa. Hansen, G.De Leeuw and G.J.Kunz, 1996 Micrometeorological estimation of fluxes of CO2, heat, humidity and momentum in the marine atmospheric surface layer during OMEX. In: OMEX Final Report, SubProject F (ULB, Brussels, Belgium), F,1-F,37.

Liss, P.S. and L.Merlivat (1986) Air-Sea Exchange Rates: Introduction and Synthesis. In: The Role of Air-Sea Exchange in Geochemical Cycling. (p.Buat-Menard Ed.) D.Reidel Publishing Company, 113-127.
Wanninkhof, R. (1992) Relationship Between Wind Speed and Gas Exchange over the Ocean. J.Geophys. Res., Vol.97, No.C5, 7373-7382.
Woolf, D K (1997) Bubbles and their role in air-sea gas exchangeIn: The Sea and the Global Change (Ed.s P S Liss and R A Duce) Cambridge University Press (In Press), 173-205.

Project publications.

Jacobs, C.M.J., J.F.Kjeld, S.E.Larsen and W.A.Oost (1999). Possible consequences of near-surface tracer gradients for the air-sea transfer velocity of CO_2: Some results from ASGAMAGE. Spring meeting of the American Geophysical Union, 1-4 June 1999, Boston. Session A11 (Air-sea Interaction).
Kjeld, J.F. (1999) A model study of air-sea exchange of trace gases and wind flow in complex terrain. PhD Thesis, University of Odense and Risø National Laboratory, 203 p.
Kjeld, J.F. and S.E.Larsen. Modeling of the air-sea exchange of CO_2. Presented at the Ph.D.-course on Carbon Dioxide and Methane between the surface and the Atmosphere, Naturhøjskolen, Rødkilde, Stege Denmark, 3-7 November 1997.
Kjeld, Jørgen F. and Søren E Larsen (1997): Air-Sea Exchange of CO_2, different estimation techniques. Annales Geophysica, suppl. II To vol 15. Abstract of the 22nd General Assembly of the EGS. Part 2. p. C414
Kunz, G J, G deLeeuw, S E Larsen, F Aa Hansen, S W Lund (1998). CO_2 Gas concentrations, gradients and air-sea exchanges during ASGAMAGE (TNO-FEL Results). In: The ASGAMAGE Workshop, September 1997 (Ed. W A Oost) KNMI Scientific Report, WR98-02, 95-104.
Kjeld, J. F. and Larsen, S. E., 1998. Air-Sea Exchange of CO_2. Proceedings of the SNF workshop, Svaleholm, Risø, Denmark (Eds. Hertel, O., Zlatev, Z., Larsen, S. E., Mikkelsen, T.) NERI, Roskilde, Denmark. , 57-63.
Kjeld, J.Friis, S E Larsen and H.E.Jorgensen (1997). Diffusion model for Air-Sea exchange of CO_2, case study result. 3rd EU Conference on Exchange Processes for the Continent/Ocean Margins in the North Atlantic, Vigo, Spain 14-16 May 1997. Abstract Volume.
Kunz, G.J., S.W.Lund, S.E.Larsen, F.Aa.Hansen and G.deLeeuw (1998b) CO_2 gas concentrations, fluxes and air-sea gas transfer during ASGAMAGE-A. TNO Physics and Electronics Laboratory, Report FEL-98-C193.
Kunz, G.J., S.W.Lund, S.E.Larsen, F.Aa. Hansen and G.deLeeuw (1998a) Air-sea CO_2 gas gas transfer velocity during ASGAMAGE-B. TNO Physics and Electronics Laboratory, Report FEL-98-C190.
Larsen, S.E., F Aa Hansen, J F Kjeld & S W Lund, G J Kunz, & G deLeeuw, 1997. Air-Sea Exchange of gases: Experiments and modelling. Abstract Volumen International Workshop Greenhouse gases and their role in climate change: The status of research in Europe, Orvieto, Italy, 10-13 nov, 1997.
Larsen, S E (1999) Autonomous system for monitoring air-sea fluxes. MAST Projects Meeting : Air-Sea-Ice studies, Processes, Modeling and Instrumentation. Brussels january 7-7 1999.
Larsen, S.E., 1997. Rapporteurs Report on Ocean Working Group. Abstract Volumen International Workshop on Greenhouse gases and their role in climate change: The status of research in Europe, Orvieto, Italy, 10-13 nov, 1997. To appear in Orvieto proceeding.
Larsen,S.E., F.Aa. Hansen, G.de Leeuw and G.J.Kunz, 1997b. Measurements of fluxes of momentum, heat, water vapor and CO2 over water by inertial dissipation and co-spectral estimation. 3rd EU Conference on Exchange Processes for the Continent/Ocean Margins in the North Atlantic, Vigo, Spain 14-16, May 1997. Abstract Volume.
Larsen, S.E., F.Aa.Hansen, J.F.Kjeld, G.deLeeuw, and G.J.Kunz, 1997c. Experimental and modelling work on CO2 exchange. Proceeding of the NILU/MAST Workshop on Air-Sea Exchange, Oslo, Norway,

11-13 June, 1997. Abstract Volumen.

Larsen, S.E., F.Aa. Hansen, J.F.Kjeld, S.W.Lund, G.J.Kunz and G.deLeeuw, 1997d. Air-Sea Exchange of Carbon Dioxides: Experiments and modelling. Presented at "Greenhouse Gases and their Role in Climate Change: Status of Research in Europe". Orvieto, Italy, Nov. 10-14, 1997. Abstract Volume.

Larsen,S.E.,F.Aa. Hansen and S. Lund (1999).Analyses of CO2 fluxes measured with micrometeorological and geochemical techniques. ASGAMAGE Final Workshop, Brussels january 6-8 1999. To appear in KNMI-report

Larsen S.E.,, F.Aa. Hansen, G.Kunz, G. deLeeuw (1999) Recent micrometeorological flux results from platform- and ship measurements. EGS XXIV General Assembly, The Hague, 19-23 April 1999. Geophysical Research Abstract, Vol 1, number 2, p449.

Larsen, S E, F Aa Hansen, J F Kjeld, S W Lund, G J Kunz and G de Leeuw (1998) Experimental and modeling study of air-sea exchange of Carbon dioxide. In: The ASGAMAGE Workshop, September 1997 (Ed. W A Oost) KNMI Scientific Report, WR98-02, 116-123.

Larsen, S E, F. Aa. Hansen, G,deLeeuw and G.J.Kunz (1997). Measurement of fluxes of momentum, heat, water vapour and CO2 over water by inertial dissipation and co-spectral estimation. Annales Geophys. Suppl. II to Vol 15. Abstracts of 22nd Assembly of EGS., Part 2 p. C438.

Larsen, S.E. (1998). Air-Sea exchange of gases: Experiments and modelling. Proc. NILU/MAST workshop on Air-Sea Exchange 11-13 June 1997, EU-DGXII-MAST report, EUR 17660 EN, 293.

Larsen, S E (1998) Surface fluxes in Climate System. Abstracts volume, European Climate Science Conference, Vienna, 19-23 October 1998, Abstract Volume, EC, Brussels, Belgium.

Larsen, S E (1999) Autonomous system for monitoring air-sea fluxes. MAST Projects Meeting : Air-Sea-Ice studies, Processes, Modeling and Instrumentation. Brussels january 7-7 1999.

ASGAMAGE Final Report

Contributions of
the University of Southampton, School of Ocean and Earth Science

Partner 5

PARTICIPANT INFORMATION:

Partner: **"SUDO"**
University of Southampton,
School of Ocean and Earth Science[1]
United Kingdom

Principal Investigator: Dr. David Woolf
School of Ocean and Earth Science
Southampton Oceanography Centre
European Way
Southampton SO14 3ZH
Tel. 44 1703 593038
Fax. 44 1703 593059
E-mail dkw@soc.soton.ac.uk

Co-Principal Investigator: Dr. Duncan Purdie

Other Investigators Dr Angus Graham
Mr Andrew Bedford
Mr Nicholas Ward
Mr David Johnson

Guest Investigator Dr Craig McNeil
Institute of Ocean Sciences
Patricia Bay, Sydney
Vancouver Island, B.C.
Canada
(formerly LODYC, Paris, France)

CONTENTS

1 Introduction

The contribution of SUDO must first be placed in the context of the objectives of the ASGAMAGE project:-

Project Objectives

(i) To find relationships between the transport coefficients for gas fluxes and any relevant geophysical parameters, such as wave geometry, whitecap coverage and bubble fluxes and spectra.
(ii) To compare different methods and systems to measure the transfer velocity of trace gases over the sea.
(iii) To find out whether and, if at all, under what conditions, there can be significant carbon dioxide stratification in the upper metres of the water column.
(iv) To test new methods and new equipment for the measurement of air-sea fluxes of carbon dioxide, nitrous oxide, methane and dimethyl sulphide.

The participation of SUDO has been directed primarily to objective (i), with some minor contributions to objectives (ii) and (iii). Most of the experimental methods were designed to describe as fully as possible wave breaking and the resulting bubble clouds (objective 1). Thermal imagery was also used to investigate directly surface renewal processes. Currents, temperature, salinity, dissolved oxygen and fluorescence were measured at various depths. The main experimental accomplishments are described in the next three sections. The implications of the observations are discussed in Section 5. Additional measurements are summarised in Section 6, and presentations listed in an appendix.

2 Acoustic Measurement of the Vertical Distribution of Bubbles

The vertical pencil-beam sonar system was designed to measure the volumetric backscatter from bubbles at four frequencies in a narrow conical section. Data have been analysed from the experimental campaign of autumn 1996, ASGAMAGE B, when components at three of the four frequencies were operational. (In ASGAMAGE A, only two of the frequencies were operational).

A full description of methodologies and objectives may be found in the Twelve-Month Report. Observations are described in the Twelve and Twenty-Four Month Reports, and in the proceedings of the Project Workshop (De Bilt, September 1997) relayed in the Workshop Report. Here we summarise methods and concentrate on summarising statistics of the bubble distribution for selected periods. A total of 23 periods, each of 30 minute duration, span eight days of ASGAMAGE B and the coincident cruise of RRS Challenger. (The relationship of our measurements to coincident measurements of gas exchange by other partners

Sonar Characteristics

An important characteristics of this sonar system is that each of the individual sonars was carefully calibrated, and also the sonars are well-matched so they each measured the acoustic cross-section of a similar population of bubbles at a different frequency. Extensive measurements of the sensitivity and directional properties of each sonar system were made for the range of target ranges and strengths of interest, at the unique calibration facility at Wraysbury Reservoir, England. These are used to describe the relationship of the volume backscattering cross-section of the bubbles at each range, $M_v(z)$, to the root-mean-square (rms) backscatter pressure induced at the sonar after a given time delay, P_b. Since the return at the sonar at a particular delay depends on attenuation of the

beam from transmission to that time, the cross-section must be calculated at progressively large delays, at each increment including the result of attenuation by scatterers at shorter ranges. The limits within which a practical inversion can be achieved are limited. Minimum values of M_v sufficiently above noise levels to be inverted decrease with increasing depth, taking values at the distance of the sea surface from the sonars of about $5\times10^{-8}m^{-1}$ at 86kHz, $10^{-7}m^{-1}$ at 250kHz and $5\times10^{-7}m^{-1}$ at 500kHz. A practical definition of the maximum value at which the accuracy of the inversion would be acceptable is that the calculated correction for attenuation be no more than the uncorrected value. This translates typically to a maximum value of $M_v \sim 0.1m^{-1}$. These limits are of great practical significance. In particular, it is found that it is impossible to infer the distribution of bubbles within the densest bubble clouds.

Pencil beams were achieved through a Mills-cross configuration of two side-scan transducers. Beam axes were within 2° of the vertical. The 86-kHz pulse power envelope is e-folding from 150μs (equivalent to a variation in target range of 0.11m) after transmission, with time constant 40μs. The other pulses are approximately square, and of 90μs duration. Ninety-five percent of the mean-square backscatter pressure will originate from within 2.5° of the axis for 86-kHz sonar (3.5° for the 250-kHz, 6.5° for the 500-kHz axis). The beam characteristics of each sonar are far from identical, but the pulses are sufficiently short and the beam sufficiently narrow that each samples a similar population, unless the population varies over horizontal scales <0.5m or vertical scales < 0.1m. Each of the sonars was operated at a pulse repetition rate of 4Hz.

The narrow-beam sonars were deployed on the seabed 100m from the platform, cross-stream of the major tidal axis (which lay along 50°), and thus well away from the zone of platform-perturbed flow. Winds were measured by a cup anemometer and vane, 28m above sea level, and calibrated to sonic standard. Currents were profiled by a 1.5MHz acoustic-doppler-current-profiler placed on the seabed 70m cross-stream of the platform. Significant-wave-height was measured with a wave staff. Ten-minute averages were found. Wave period was measured with the multi-frequency sonar system, using a real-time paper record generated prior to digitisation. The temperatures of the air and surface water were recorded.

Analysis

A set of twenty-three data periods, each of half an hour, has been compiled from the autumn experiment. It is representative of the range of environmental conditions encountered while waves were breaking and sonars were operational. Periods and conditions are described in Table 1. The periods lie within a group of 8 days in October. Winds (at 10m) range from 5-12ms^{-1}, significant wave heights from 0.3-2.0m, and dominant wave periods from 3-6s.

The digitised images were first processed to extract the wholly subsurface bins, the surface identified by the steep signal gradient, and the vertical component of the orbital wave motion removed. The images were sampled to yield temporal and spatial resolutions of 2s and 25cm, respectively.

When values of M_v obtained at the three frequencies comfortably exceed noise levels, and are lower than the thresholds at which coherent-scattering effects are manifest, they may be inverted to yield the bubble concentrations at the corresponding point in the beam. The backscattering is related to the total bubble number density, n_v, and normalised bubble size density, g, according to

$$M_v = n_v \int_0^\infty \sigma_b \, g \, da , \qquad (1)$$

where σ_b is the backscattering cross-section of a bubble of radius, a. Cross-section σ_b is calculated as a function of frequency and hydrostatic pressure according to the method and parameter values of Medwin (1977). The basis of the "multi-frequency method" is that the functional dependence of cross-section on radius is quite specific to each acoustic frequency. In particular, for each frequency

there is an exceptionally high cross-section about a different resonant radius (~7μm at 500kHz, ~14μm at 250kHz, ~40μm at 86kHz). Useful information on the size distribution of bubbles can therefore be inferred, particularly of the small bubbles. As measurements at only three frequencies are available, the form of the bubble size distribution is prescribed, so that only the peak radius, a_p, remains, along with n_v, to be determined. The redundant measurement then allows the accuracy of the inversion model to be checked.

A leading source of uncertainty lies in the form of instantaneous bubble size density to be adopted, but fortunately there is information from earlier studies on likely distributions. The instantaneous size distribution and any point in a bubble cloud was assumed to falls off as radius^{-5} at large radii, and follow a cubic dependence on radius for the smallest bubbles. Since only two frequencies were necessary to define a peak radius, the quality of the model could be assessed, by comparing the solutions from two possible pairs.

Observations: Bubble statistics and statistical dependence on environmental conditions

Environmental conditions

The dependence of the bubble statistics on environmental parameters is investigated. Wind and sea state are represented by:-

Wind speed at 10m, W_{10}
Significant wave height, H_s
Wavelength of the dominant waves, λ

Inversion

The near surface population is of most direct relevance to gas exchange. Scattering at a fixed depth of 0.4m, corresponding to the second subsurface bin (the first at which there can be no contamination from backscatter directly from the surface) can be calculated for each set of acoustic pulses. Bubble concentrations close to the surface are frequently too large to be measured accurately, as the signal exceeds the limit for accurate inversion described earlier. Similarly, there are often occasions within a half-hour period when the scattering is too close to noise levels for accurate inversion. The fractions of each period when one or other of the criteria for satisfactory inversion is not satisfied at 0.4m is shown in Figure 1. The fractions are plotted against the mean wind speed. The probability of inversion failing due to too low a level of backscattering, P-, falls with increasing wind speed, while the probability of failure due to breakdown of the approximation of incoherent scattering, P+, rises. Logarithmic least-squares regression yields the relations

$$P- = (5\pm46)\times10^{3} W_{10}(\text{m s}^{-1})^{-5.4\pm1.6} H_s(\text{m})^{0.2\pm1.7} \lambda(\text{m})^{0.1\pm1.8} \text{ and}$$

$$P+ = (7\pm66)\times10^{-9} W_{10}(\text{m s}^{-1})^{6.2\pm1.8} H_s(\text{m})^{0.4\pm1.8} \lambda(\text{m})^{0.4\pm2.0}.$$

The probability of very low scattering is more often greater than the probability of very high scattering, but as explained below the occasions of very high scattering are of much greater consequence.

The large number of sample values for each measurement period allows a fairly thorough statistical description of scattering in each period. Standard descriptions include the mean and higher moments about the mean (variance, skewness and kurtosis) of any scattering characteristic (e.g., cross-section at a particular acoustic frequency, bubble concentration, surface area of bubbles, void fraction). Coefficients of variation and skewness are defined here as $\xi_2^{1/2}/\xi_1$ and $\xi_3/\xi_2^{3/2}$ respectively, where ξ_i denotes the i^{th} moment about the mean. Additionally, the median of any characteristic can be calculated. If each sample value was known accurately, every statistic could be calculated without difficulty. As described in the previous paragraph however, the main characteristics of the bubbles often can not be estimated with any degree of confidence. Further, the distribution of bubbles is typically highly skewed such that most of the bubbles (number, area and volume) in a given period are contributed by a small fraction of samples. If most of the bubbles should be contributed by a few samples, but the bubble concentrations are so high in these cases that these samples are excluded from calculations because inversion is unsatisfactory, then the calculated mean and higher moments will be much less than the true values. This problem will occur even if there are only a few samples within a measurement period that can not be inverted due to high scattering. Excessive-scattering events occurred at wind speeds of only 6m/s. These events are probably frequent enough to effect the calculated moments at wind speeds above 9m/s. The mean concentration within a period can be highly dependent on one, or a few, especially large (or intense) breaking wave events; another consequence of the highly skewed distribution. The median is relatively robust at high wind speeds. The median can be calculated successfully unless either the scattering is too low in more than half the samples, or is too high in more than half the samples. The former condition is found at low wind speeds, but at moderate and high wind speeds the medians can be found. For moderate and high wind speeds, the median is generally a more robust and reliable statistic than the corresponding mean or any of the higher moments.

Scattering at greater depths is less likely to exceed acceptable limits. Bubble statistics at depth are therefore less degraded by caveats than near-surface values. It is also important to describe the depth distribution of bubbles, since all the submerged bubbles contribute to gas exchange and the attenuation of the clouds with depth is indicative of the strength and character of vertical mixing.

Dependence of backscatter on depth and environmental conditions

Specimen profiles of statistics of the volumetric backscattering cross-section, the median and measured moments of up to third order, are shown in Figure 2. Coefficients of variation and skewness are defined here as $\xi_2^{1/2}/\xi_1$ and $\xi_3/\xi_2^{3/2}$ respectively, where ξ_i denotes the i^{th} central moment (ie. that about the mean). Scattering falls exponentially with depth to a depth of about 4m, higher moments falling less fast than lower moments, so that coefficients rise. Below this, the fall-off of moments, though erratic, is typically more rapid, the fall-off of the mean comparable to that of the median. (Means are never less than two orders of magnitude above noise levels, these given in the following subsection.)

In low winds, profiles typically extend below the deepest bubbles. In parameterising the bubble backscatter profiles have been assessed only to a depth, D_l, at which the measured mean ceases to fall monotonically over intervals of 0.5m (that is, two bins).

There is often a zone close to the surface in which measured means fall below true values due to the exclusion of samples with the highest scattering. A dual-law fit is therefore firstly applied to the plots, taking the mean to fall off in two distinct zones above D_l, each zone characterised by a different e-folding depth. The fit is weighted by standard errors, log-linear and least-squares, with the depth of the upper zone included as a free variable. The fit is accepted if the difference between the two e-folding lengths identified is an order of magnitude or more greater than their combined standard error (as is the case for Figure 2). The e-folding depth then adopted is that of the lower zone. A single log-linear fit is otherwise applied.

In other figures, the fall-off of the median with depth may be faster than exponential, the e-folding depth gradually decreasing, perhaps due to a truncation of bubble clouds by stratification in the water column. The fitting procedure described above is also applied to the median, with the e-folding depth of the upper zone that retained where the two-fold fit is accepted. An unweighted fit is applied to the coefficients of variation and skewness. The coefficients of variation and skewness invariably increase slowly with increasing depth.

The dependence of backscattering on environmental conditions is investigated by calculating logarithmic regression fits of mean backscatter (weighted by standard errors) to wind speed and characteristics of the dominant waves. The only variable with which scattering cross-sections are clearly correlated is wind speed.

At 5.4m the mean backscatter is described by,

$$\xi\{M_v\}(m^{-1})=(1\pm9)\times10^{-23}W_{10}(ms^{-1})^{15.8\pm1.8}H_s(m)^{-0.1\pm1.5}\lambda(m)^{1.7\pm1.9} \quad \text{at 86kHz}$$

$$\xi\{M_v\}(m^{-1})=(2\pm11)\times10^{-16}W_{10}(ms^{-1})^{7.8\pm1.1}H_s(m)^{0.9\pm1.2}\lambda(m)^{1.1\pm1.2} \quad \text{at 250kHz}$$

$$\xi\{M_v\}(m^{-1})=(6\pm68)\times10^{-8}W_{10}(ms^{-1})^{5.1\pm1.9}H_s(m)^{0.5\pm2.1}\lambda(m)^{-2.5\pm2.5} \quad \text{at 500kHz}$$

At 0.4m the median backscatter is described by,

$$m\{M_v\}(m^{-1})=(2\pm13)\times10^{-8}W_{10}(ms^{-1})^{5.9\pm1.0}H_s(m)^{0.8\pm1.0}\lambda(m)^{-1.0\pm1.1} \quad \text{at 86kHz,}$$

$$m\{M_v\}(m^{-1})=(2\pm11)\times10^{-11}W_{10}(ms^{-1})^{6.4\pm0.9}H_s(m)^{0.2\pm0.9}\lambda(m)^{0.1\pm1.0} \quad \text{at 250kHz}$$

$$m\{M_v\}(m^{-1})=(7\pm49)\times10^{-15}W_{10}(ms^{-1})^{9.2\pm1.3}H_s(m)^{-0.9\pm1.4}\lambda(m)^{0.8\pm1.6} \quad \text{at 500kHz.}$$

A statistically significant dependence of higher moments of M_v on wind speed is seen at 86kHz, these increasing less fast with wind speed than lower moments, so that the coefficients of variation, c_v, and skewness, c_s, tend to diminish with wind speed,

$$c_v\{M_v\}=(2\pm8)\times10^{3}W_{10}(ms^{-1})^{-2.0\pm0.8}H_s(m)^{0.4\pm0.9}\lambda(m)^{-0.4\pm1.0}$$

$$c_s\{M_v\}=(4\pm15)\times10^{2}W_{10}(ms^{-1})^{-1.4\pm0.7}H_s(m)^{0.2\pm0.7}\lambda(m)^{-0.1\pm0.9}$$

Coefficients at the other frequencies overlap these values to within errors.

The attenuation depth (over which M_v may be expected to fall by a factor e), D_m, also depends on forcing conditions. Values of D_m found from profiles of $\xi\{M_v\}$ show little correlation with wind speed, but a statistically significant scaling with significant wave height is seen at 86 and 250kHz, as can be seen from Figure 3a. A linear regression yields the relation

$$D_m(m)=(0.40\pm0.06)H_s(m)+(0.12\pm0.08)$$

When D_m is derived from profiles of $m\{M_v\}$, values are comparable, but show an approximately square law dependence on wind speed, as can be seen from Figure 3b, a logarithmic regression yielding the relation

$$D_m(m)=(7\pm7)\times10^{-4}W_{10}(ms^{-1})^{2.0\pm0.2}H_s(m)^{-0.4\pm0.2}\lambda(m)^{0.6\pm0.2} \quad \text{at 86kHz}$$

$$D_m(m)=(5\pm6)\times10^{-3}W_{10}(ms^{-1})^{1.8\pm0.2}H_s(m)^{0.0\pm0.2}\lambda(m)^{0.1\pm0.3} \quad \text{at 250kHz}$$

Values at 500 kHz overlap those at 250kHz to within errors.

Dependence of bubble statistics on depth and environmental conditions

The distribution of bubbles at a given depth (obtained from the measurements at three frequencies) is calculated throughout each period (excepting inversion failures). The concentration of bubbles and two bulk bubble parameters, integrated over all bubble sizes, are computed. The void fraction, v_f, or volume fraction of the fluid that is air, is given by the following,

$$v_f = \tfrac{4}{3}\pi n_v \int_0^\infty a^3 g \, da . \qquad (2)$$

Integrating this over depth yields the upward displacement of the surface by the bubbles. The total surface area of the bubbles under unit sea-surface area is also calculated

Bubble statistics in one of the measurement periods are illustrated in Figure 4. The dependence of the measured mean radius on depth is shown in Figure 4a. The fractional change of radius per unit depth ic calculated by linear regression. Profiles of the medians of bubble concentrations and void fraction shown in Figures 4b and 4c, and are subjected to error-weighted log-linear regression fits

The mean bubble radius at 0.4m ranges from 29±2μm in a low wind (run 3) to 76±2μm in a higher wind (run 16). It is a factor of 1.7±0.1 greater than the peak radius, compared to a factor 1.05 fixed for each instantaneous distribution. (Only periods where inversion is successful on at least one occasion in four have been included). Bubbles contributing most to the total bubble surface area at 0.4m depth are of radius 2.1±0.2 times the peak, and bubbles contributing most to void fraction, a factor 3.0±0.2 times the peak. Measurements of mean radius change with depth in a way that appears best correlated with wave slope, as shown in Figure 5, an increase in radius with depth seen if waves are gently sloping, a decrease in radius if waves are steep.

The medians of bubble concentration and void fraction of bubbles at 0.4m depend on environmental conditions according to the relations

$$m\{n_v\}(m^{-3})=(4\pm26)\times10^{-3}W_{10}(m\,s^{-1})^{7.2\pm1.4}H_s(m)^{-0.2\pm1.3}\lambda(m)^{0.0\pm1.5},$$

$$m\{v_f\}=(6\pm44)\times10^{-20}W_{10}(m\,s^{-1})^{10.5\pm1.5}H_s(m)^{-1.8\pm1.4}\lambda(m)^{1.2\pm1.5}.$$

Maximum values saturate, in winds exceeding 6 - 7ms^{-1}, at values of around 100cm^{-3} and 10^{-5}, respectively.

The e-folding depth associated with $m\{n_v\}$ generally lies within the range of e-folding depths of $m\{M_v\}$ observed over the three frequencies. The e-folding depth associated with $m\{v_f\}$ is typically 80% of the corresponding value for $m\{n_v\}$.

The dependence of bubble statistics on wind speed is shown in Figure 6. The total bubble surface area, A_b, integrating over all depths and bubble sizes, and as expressed as a fraction of the sea surface, increases with wind speed, as can be seen from Figure 6a, a least-squares fit to medians yielding the relation

$$m\{A_b\}(\%) = (7\pm48)\times10^{-10}W_{10}(m\ s^{-1})^{6.9\pm0.9}H_s(m)^{0.1\pm0.9}\lambda(m)^{0.2\pm1.1}.$$

The corresponding relation for the mean surface area is significantly different,

$$\xi\{A_b\}(\%) = (2\pm6)\times10^{-5}W_{10}(ms^{-1})^{4.4\pm0.6}H_s(m)^{0.4\pm0.6}\lambda(m)^{0.1\pm0.5}$$

The upward displacement of the surface by the bubbles, z_b, also increases with wind speed, as can be seen from Figure 6b, the regressive fit given by

$$m\{z_b\}(m)=(5\pm31)\times10^{-17}W_{10}(m\ s^{-1})^{8.2\pm1.2}H_s(m)^{-0.4\pm1.2}\lambda(m)^{0.7\pm1.4}$$

Figure 7 shows the time-series of $m\{A_b\}$ and wind-speed, with the corresponding transfer velocity time-series obtained by other partners (led by KNMI) shown for comparison in Figure 8.

Interpretation

Parameters of the bubble concentration and its associated acoustic backscattering generally depend on the wind speed more than any other environmental factor. This is true, for example, of the volume backscattering strength whether means, which are sensitive to especially high values such as those close to a breaking wave, or medians are considered. Mean values derived at 5.4m exhibit more variability about the trend than do medians at 0.4m. This reflects the different measurement depths, in addition to the statistical characteristics of the estimators, as bubble concentrations at 5.4m depend on downward advection and diffusion of bubbles from the surface, as well as the generation of bubbles. Other factors, not yet fully investigated, such as the total gas saturation, will also affect the dispersion and evolution of the bubbles. At 86kHz and 5.4m, the characteristic volume backscatter cross-section increases as wind speed to the power 16, at least twice the power observed at 0.4m, primarily due to the dispersion terms. Environmental dependence at the higher acoustic frequencies are generally similar, but depend less on depth. The greater sensitivity to depth at the lowest frequency can be attributed to the greater sensitivity of the fairly large bubbles that are resonant at 86kHz to the strength of dispersion.

The strong dependence on wind speed is carried over to the bubble statistics. Number density, surface area and void fraction are highly sensitive to wind speed, and the mean bubble radius is generally lower at low winds. The maximum scattering that can be successfully inverted can be exceeded in wind speeds as low as 6m s^{-1}. The "saturation condition" typically corresponds to bubble concentrations of about 100cm^{-3}. This concentration corresponds to a characteristic distance between neighbouring bubbles of about a tenth of the largest acoustic wavelength. Conveniently, this situation also corresponds to when a breakdown of the approximation of incoherent scattering is approached, further reason to abandon inversion at excessive scattering. Unfortunately, in many cases the majority of the surface area and void fraction will be "hidden" because the corresponding samples are rejected by the inversion criteria.

In many cases, the statistical dependence on environmental conditions can be expressed solely in terms of wind speed. There is some evidence of sensitivity to the dominant wave characteristics in other cases. Two key parameters of wave breaking, or at least of the breaking of the dominant waves, are:

Wave slope, α, defined as the ratio of H_s to λ, and

Wave age, γ, defined as the ratio of the phase speed of the dominant waves, c, to W_{10}

For linear waves in deep water, $c=(g\lambda/(2\pi))^{1/2}$, where g is the acceleration due to gravity, and γ thus scales as $W_{10}^{-1}\lambda^{1/2}$. The convective velocity associated with Langmuir circulation may be expected to scale with a speed,

$$v_L, = \gamma^{-1/2}\alpha c,\ v_L^2$$

thus scaling with the product of wind speed and Stokes drift, as consistent with current theories of the circulation (Leibovich, 1983; Plueddemann et al., 1996). The Langmuir velocity may consequently be expected to scale as $W_{10}^{1/2}H_s\lambda^{-3/4}$.

The mean bubble radius usually decreases with increasing depth, which may be expected as a combined result of compression, partial dissolution and dispersion. (We have constructed

numerical models of this process which demonstrate this effect [Woolf, 1995]). The measured mean bubble radius may, rather surprisingly, increase with depth if waves are gently sloping (Figure 5). The dominant slope is far less than the slope necessary for wave breaking, and the surprising depth dependence of mean radius suggests a very different mode of bubble generation might be dominant. The most strongly scattering clouds and the related attenuation depth of the mean backscatter scales with the significant wave height (Figure 3a). In contrast, the attenuation depth of the median of backscatter (Fig. 3b) is closely related to wind speed. The picture that emerges is one where the dominant waves may determine the depth of the deepest clouds, but little else. It appears that both the characteristics of wave breaking and the dispersion in the surface waters are determined primarily by the wind speed. This situation may be expected for a "steady state" between momentum transfer at and below the sea surface and the wind stress (or "momentum flux input") applied. It is not obvious that a "steady state approximation" is generally satisfactory in a coastal situation, but this data set implies the approximation is fair. The breaking of dominant waves might be expected to contribute significantly to the total entrainment of bubbles, and dispersion directly associated with the largest breaking waves may be expected to a depth of order of the significant wave height (Rapp and Melville, 1990). As described above, we would expect the characteristic speed of Langmuir circulation to depend on dominant wave characteristics. Langmuir circulation is expected to play a key role in vertical dispersion, but in the wind and wave conditions encountered here this did not introduce a strong wave dependence into attenuation depths.

The underestimate of mean bubble concentrations due to the inability to process cases of high scattering severely undermine our efforts to estimate the influence of these bubbles on gas exchange. The mean statistics better reflect the values prevailing during wave breaking, when much of the bubble-mediated transfer of the relatively soluble gases may take place. Indeed a simple estimate of gas transfer can be made from the surface area of submerged bubbles alone. (We shall return to this subject in Section 5, but in short: the area of submerged bubbles must be significant compared to the sea surface area in order to make a large contribution to the total exchange). The median of bubble area can be calculated in most cases. At low to moderate winds, when both statistics can be estimated with reasonable confidence, the mean bubble area is typically a factor 25 times the median; factors ranging from half to twice these values. The coefficient of variation decreases with increasing wind speed, implying that the factor between mean and median will decrease as wind speed increases. (Note however, that variance and higher moments will also be underestimated by excluding high scattering samples). Figures 6-8 show that the highest median of submerged bubble area was approximately 1%, while the highest calculated mean was approximately 2%. The true peak value of submerged bubble area among the measurement periods was probably ~ 10%. The high sensitivity to wind speed suggests that the area of submerged bubbles will exceed the sea surface area in very high winds (> 20m/s). The implications of these observations will be discussed in Sections 5 and 6.

3 Acoustic Measurements of Breaking Waves

The experimental method described in the previous section is effective in describing the vertical distribution of bubbles, but any inferences that are made about the frequency and scale of breaking, and the related flux of bubbles into the surface waters are relatively indirect. We have developed relatively novel acoustic methods that have the potential to yield direct information on wave breaking and bubble injection. A 500kHz sector-scanning sonar was mounted on the Southwest "sensorpalen" of the platform. This is a side-scan sonar that sweeps in the azimuth, at any moment measuring backscatter from a very narrow range of angles in the azimuth, but a wide range in the vertical. The sonar is aligned to have greatest sensitivity to an angle above the horizontal, and will measure surface and near-surface scattering from immediately above the instrument out to maximum range (usually set at 50m or 100m). This commercial sonar was equipped with a display and control console. In addition, the system was customised for this project to transfer both control parameters and the raw data in real time to a personal computer, through a dual serial card. This sonar proved to give a wealth of information. Obvious features included scattering from the opposite face of waves, "active" breaking wave crests, bubble trails behind the crests (often exhibiting modulation by vortices), and the organisation of diffuse bubble clouds by Langmuir circulation. Data from this sonar has been used firstly, to develop an acoustic analogue of "whitecap coverage" that has traditionally been measured optically; and secondly, to investigate the relationship of wave breaking to the wave field. A simple hydrophone was deployed approximately 100m from the platform during ASGAMAGE A. This hydrophone detects wave breaking immediately above the instrument *via* the noise generated by breaking. Both the sector-scanning sonar and the hydrophone were validated by analysis of simultaneous video recordings of the same area of sea surface measured by each acoustic instrument.

A Sector-Scanning Sonar I : Acoustic Whitecap Coverage

Whitecap coverage is traditionally measured by analysing film or video observations of the sea surface. Whitecaps are identified as relatively reflective areas of the sea surface in diffuse daylight (as opposed to "sun glint"). One problem with traditional whitecap coverage measurements is the difficulty of establishing a consistent criterion for identifying "whitecap" in widely varying lighting conditions. (In any case, whitecap coverage can not be measured in the dark). Another problem is that the measured whitecap coverage may be sensitive to the surface behaviour of bubbles, and therefore a relatively poor measure of bubble injection. High-frequency side-scan sonars are highly effective in detecting breaking waves, because they give an exceptionally strong return from active breaking waves (Thorpe and Hall, 1983). The return is largely from the very high concentrations of bubbles very close to a breaking wave that are of greatest interest in terms of gas exchange. It is impossible to calibrate the instrument to give an absolute measurement of the bubble distribution, but the sonar can yield a relative measure of scattering. This method uses an "active" instrument as opposed to the "passive" traditional method; this almost entirely eliminates the sensitivity to ambient (optical or acoustical) conditions. The return is dependent on the depth of the sonar and the range of the scatterers. We have analysed data from ASGAMAGE B when a 500kHz sonar was in a fixed position on the Southwest sensorpalen, 14 metres below mean sea level. Variations in depth associated with the tidal range (~2 metres) and large waves are not very significant compared to the mean depth, therefore the data from the entire experiment is treated as a self-consistent set (scattering from a given range at different times during the experiment can be simply compared). There is an adjustable gain setting on the sonar that greatly affects the recorded signal, but a single gain setting was used for most of the measurement periods.

A suite of analysis programmes has been written to visualise and analyse the statistical features of the acoustic data. The first stage of analysis is simply to generate "images" from the recorded acoustic returns. Simple images are formed with time as the "x-ordinate", range as a "y-

ordinate" and the scattering strength displayed at each time and range as a shade of the pixel on a grey-scale. The grey-scale can be selected either customised for each measurement period, or set on the basis of data from a single measurement period that is set as the standard. The former choice optimises the images for the purpose of visualisation, but the latter option is used to define a consistent definition of "whitecap coverage". In either case the grey-scale is set by first taking the logarithm of the signal, then "normalising" the result to a mean of 127 and a standard deviation of n (= 30 or 40) for each range within the measurement period, as follows: If "p" = log (signal) for a given pixel, "m" is the mean value of log(signal) for all pixels at the same range as p, and "s" is the standard deviation of log(signal) for the same pixels, then the normalised value for each pixel, p*, is given by,

$$p^* = 127 + (p - m).(n/s)$$

The range of p* is limited to 0 (black) – 255 (white) on an 8-bit grey scale.

A typical image (from a fairly windy period) of a single sweep of the sonar is shown in Figure 9a. This sweep was the sixteenth of the measurement period, 1700-1800 on Julian Day 308 (November 3, 1996). All sweeps were in the quadrant from which the wind was blowing. The wind was fairly steady at 16m/s from 230°. Scattering from zero to 50 metres range is shown. The surface waves immediately above the instruments give a strong return (at a range of approximately 14 metres). In common with traditional, optical measurements of whitecap coverage, areas of high scattering associated with breaking wave crests are fairly evident. (Especially in this quadrant, where breaking waves form a characteristic track on sonar images; see Section 3B). Unfortunately however (again in common with the traditional method) when one attempts to automatically calculate whitecap fraction by setting a simple intensity threshold, one finds that for any choice of threshold, a large fraction of the scattering satisfying the threshold is not associated with breaking wave crests. Bubble clouds in various stages of evolution are evident in the images, from breaking wave crests to relatively diffuse clouds organised over time scales of minutes by Langmuir circulation. Extensive analysis of the distribution of scattering in sample images and experimentation with trial algorithms were conducted in search of an optimal automatic algorithm for estimating "whitecap coverage". Note that it is not important for this measure of whitecap coverage to be similar to the traditional measure. It is only important that breaking waves are uniquely and consistently identified in any measurement period to which the algorithm is applied. The breaking wave crests are more distinct than the more mature clouds and appeared more feasible to automatically detect. Whitecap measurement by video also largely measures breaking wave crest, so the acoustic measurement might be a similar if not identical measure to the video measurement.

A first analysis of data from several diverse measurement periods suggested that in any short period the distribution of scattering at a given range was close to a log-normal distribution (and by corollary, the normalised values, p*, followed a Gaussian distribution). It is not surprising that the signal distribution was close to log-normal; where a response depends on the multiplicative effect of a large number of factors this is the limiting behaviour. We investigated the hypothesis that most of the scattering (characteristic of the sea surface) followed a log-normal distribution and the only significant deviation from this distribution would result from additional scattering by bubbles. If this was the case, the distribution of low levels of scattering might follow a log-normal distribution, while the frequency of high levels of scattering might exceed this distribution by a value proportional to "whitecapping". A programme was written that fitted a log-normal distribution to the distribution of lower values of scattering, and calculated the difference between the actual frequency of high scattering and the predicted frequency. Unfortunately, this method proved to give highly inconsistent results, including negative values of whitecapping in many cases.

We attempted to find a simple algorithm for detecting breaking wave crests. As already noted, a simple intensity threshold alone was found to be too crude. Breaking wave crests are characterised by sharp gradients in scattering intensity, particularly at the front (Thorpe and Hall, 1983). This suggested that a gradient operator might be suitable for detecting the crests, but this also proved to be an impractical method.

We further investigated the distribution of scattering in images. If the variation in scattering was wholly incoherent, then the distribution of neighbouring pixels would be similarly distributed (same mean, standard deviation, skewness) to the general population of pixels. Before making such a comparison, pixels at a range less than or close to the range of the sea surface are excluded from the population, as the distribution in this region are clearly different (see for example Figure 9a). We compare the moments of 5x5 samples with the moments of the population. The relative values of sample moments and population moments are found to correlate with the value of the pixel at the centre of the sample. In particular, the mean and standard deviation of samples centred on pixels of high value ($p^* > 170$, where $n = 30$) are generally higher than the general population.

In order to test whether the special properties of samples centred on high value pixels were peculiar to breaking wave crests, we laboriously identified pixels on a few images that were definitely associated with breaking wave crests. One of the images is shown in Figure 9. The image in Figure 9b is a modified version of Figure 9a, with crest areas marked in white, and the remainder of the image transformed to a restricted grey-scale (from mid-grey to black). The values of each pixel in the marked crest areas, and the moments of the 24 (5x5 – centre pixel) nearest neighbours of each of these pixels were compared to the statistics of the remainder of the population. It was found that not only were the selected pixels fairly high in value, but also the mean and standard deviation of their nearest neighbours were high. The standard deviation of 24 nearest neighbours are generally lower than the standard deviation of the population, but the standard deviation of the neighbours to marked pixels is generally nearly as high or higher than that of the general population. It appears that the properties of neighbouring pixels can be useful in designing an automatic algorithm. The performance of a prototype algorithm is described below.

The algorithm has been applied to several images in minor variants, as we have experimented with the algorithm in search of an optimal form. We describe here the application of one variant to the image featured in Figure 9. In this case, the image had initially been normalised to a standard deviation of 30 for the hour-long measurement period. Two threshold conditions for pixels are set. The first threshold is a value of 170 for the pixel itself. The second threshold is a standard deviation of 25 for the 24 nearest neighbours of the pixel. The pixels that satisfy both thresholds are identified in black in Figure 9c. Excluding the sea surface and targets at less range, most of the identified pixels appear to be genuine candidates for breaking wave crests, and include over 50% of the area identified manually (Figure 9b). In respect of the major crest areas, the algorithm is stricter than the manual approach, but lower thresholds admit many relatively diffuse features. The algorithm identifies a number of smaller features that may be smaller breaking wave crests, but can not be readily validated. The smaller features can be reduced in number by the use of an additional size filter. Variants include a filter that excludes pixels that have less than 3 qualifying pixels among their 8 nearest neighbours, and one that eliminates features consisting of less than a chosen number (e.g., 16) contiguous pixels. The latter filter is computationally very demanding but is highly effective. One of these filters has been applied to generate the image shown in Figure 9d.

The algorithm including a size "16" filter has been applied to the entire measurement period described above. Only features beyond 16m range are included in the calculation of "whitecap coverage". The time series of whitecap coverage for the 130 sweeps in this measurement period is shown in Figure 10. The whitecap coverage is highly variable on a wide range of time scales, with occasional strong peaks in whitecapping, though the wind was quite steady. We are satisfied that this is a real phenomenon as it accords with both manual inspection of the same data, and casual experience on the platform. It is necessary to analyse very many images within a measurement period in order to achieve a representative value. The mean whitecap coverage in this hour was 0.27%. In the following hour, the mean coverage rose to 0.37% though the wind speed declined slightly. This method does appear capable of making a valid measurement of whitecapping, and with an adequate data set may be used to investigate the environmental dependence of whitecapping. Further by calculating the areas of contiguous features and with the analysis of breaking wave spectra described in the next section, it should be possible to investigate

scales of whitecapping and their relationship to wave spectra. The algorithm is computationally demanding, and it is necessary to maintain "quality control" over the measurement periods analysed, but given time a useful analysis of all the data gathered in ASGAMAGE B can be achieved.

B Sector-Scanning Sonar II: Wave Spectra

Processing

As described in the previous section, the simplest image processing software simply plotted the data in cartesian co-ordinates (time and range). More advanced image processing software was used to plot the data in polar co-ordinates (compass angle and distance). Two options were implemented. Firstly, "distance" was simply defined as range (calculated from the time delay of returning pulses and the sound velocity); this essentially recreates the real-time display on the console monitor. Secondly, horizontal distance is used, where this distance is calculated from range and water depth assuming scattering is predominantly from the mean sea surface. The images shown in this report are the product of the first option.

As already described, a wealth of features can be seen in the images. Approximately normal to the wind direction the most obvious features are bands of high scattering aligned approximately parallel to the wind. These can be identified with the rows of bubbles organised by Langmuir circulation. In the general direction of the wind, the most conspicuous features are long and curved. These curved paths are described by the intersection of the rotating sonar beam and linear wave fronts travelling at their characteristic phase speed.

These curved features have been studied using a specially-written image processing suite. The suite is designed to estimate the speed and direction of the wave fronts, and the phase position of the highest scattering associated with these wave fronts. The theoretical basis of the suite is as follows. The intersection point of a position of constant phase on a linear surface wave front and the rotating beam will depend on the speed and direction of the wave front, the rotation of the sonar, the depth of the sonar and the current (which will advect surface waves. Also, if the waves obey the linear surface wave dispersion relationship, the path of intersection points of preceding and following waves of the same frequency can also be calculated. If water depth and current speed are entered, three points on the track of a single wave uniquely determine the entire track, and the speed and direction of the wave. Alternatively, the tracks of a wave and the set of waves preceding and following it can be determined by two points on one wave and a third on another of the set. The processing suite plots each image in compass and range co-ordinates, together with an additional "instruction and results" panel. Two examples are shown in Figures 11 and 12. The sonar details are read from the data files. The speed and direction of the current is entered by the operator. The depth is found by clicking on the surface return on the image. The operator then clicks two points on the image with the mouse that he/she identifies as being on the "primary" feature. At this point, the computer chooses a default value of the wave propagation direction and plots the complete track of the feature and preceding and following waves. The operator then adjusts the wave angle by key strokes. After each adjustment, the computer recalculates the phase speed and wavelength of the waves (reporting these on the screen) and replots the tracks on the image. The operator uses his/her judgment to optimise the wave properties by matching the calculated tracks to the primary feature and any secondary features (preceding or following waves of the same set). At completion, the estimated wave properties are saved, and the operator can attend to the next major feature on the image, or the next image. For some data, it was possible to estimate the wave properties either using a single feature, or using two or more members of a set. In this case, both sets of estimates were retained and used as an *ad hoc* test of the method as a whole and the linear dispersion relation. The phase of the feature is estimated by noting the intersection of the calculated tracks and the surface return from the waves as they pass immediately above the sonar, as illustrated in Figure 13. The slope of the waves can also be measured at this instance.

A total of 13 measurement periods (one of 28 minutes duration, the rest lasting one hour) taken in a wide variety of conditions have been carefully analysed. In the case of three successive periods, covering 1632-1900 on day 308 (note the analysis of the same period described in Section 3A), additional activities were organised. Video measurements to the Southwest of the platform

were made with the KNMI system. Also, surface wave data from a wave wire on the main measurement boom was copied from KNMI and analysed.

Results

The sonar data and synchronous video have been carefully compared. It is not trivial to make this comparison, since the video records surface phenomena in a fairly wide field of view, while the sonar is sensitive to both surface and sub-surface scattering, but only in a very narrow horizontal arc. Many features recorded by the video are outside of the field of view of the sonar, while many strongly scattering features appearing on the sonar images have no noticeable surface counterpart on the video record. Nevertheless, we are satisfied that the video record validates the description of the sonar features given below.

The validity of the linear dispersion relationship is tested by comparing direct measurements of the phase speed with a phase speed derived from the apparent wavelength of the features using the dispersion relationship (see above). The results are shown in Figure 14. These results show a great deal of scatter, but cluster sufficiently to the theoretical relationship to validate the dispersion relationship and the processing method.

Two types of feature are identified (Types I and II). Prime examples of each are shown in Figures 11 and 12.

Type I features are characterised by a fairly sharp gradient in front with a broad fuzzy trail behind (e.g., Figure 11). Similar features have been noted before, in data from fixed side-scan sonars (e.g., Thorpe and Hall, 1983). These features have invariably been analysed for waves approaching the sonar. The sharp gradient is a characteristic of breaking waves, while the trail behind is the bubble plume left behind by the advancing breaking waves. The phase position of the highest scattering is typically close to the crest (Figure 15). Subsidiary curves in front of most of the major features are probably associated with the breaking of shorter waves on the front of larger waves when they are overtaken by the primary wave. The statistics of the features measured with the analysis method are the characteristics of the larger waves. It is important to note that wave breaking in deep water is immediately a form of wave-wave interaction, and we are only able to measure the larger of any wave pair. The measured slope of the primary waves is shown in Figure 16. These waves are generally steep, invariably steeper than the dominant wave slope, but not as steep as the kinematic condition for incipient wave breaking of a single wave (Longuet-Higgins, 1975). The waves all propagate in a relatively narrow sector about the wind direction. A histogram of the phase speed of the primary waves normalised by the dominant wave phase speed is shown in Figure 17. Three-quarters of the waves have a phase speed between 60% and 80% of the phase speed of the dominant wave, with a mean fraction of 66%. It is relatively rare for a dominant wave to break. These results are quite similar to the results reported by Ding and Farmer (1994) using a far larger and more expensive acoustic technology.

Type II features are relatively thin and symmetrical with no evidence of a bubble plume left in the wake. These features have been measured for both approaching and receding waves. An example of the imaging of receding waves is shown in Figure 12. A large set of fairly short waves (the wind speed was only 6m/s, and the fetch was only 10km) are very clearly imaged. Sets of approaching waves were never as clearly imaged, but there are many examples of individual waves forming distinct features. Irrespective of the propagation direction, the peak scattering was concentrated on the opposing face of the wave. "Wave imaging" by radars or sonars viewing the sea surface at an oblique angle is a common phenomenon, but the modulation seen in this case is remarkably extreme. We have attempted to simulate the observed scattering patterns simply be calculating the effect of tilt modulation on relatively uniform rough surface scattering. These simulations fail to recreate the very strong modulation observed in the data. It is necessary for there to be relatively intense scattering in a narrow sector of the wave. In the case of receding waves, it is not surprising for there to be strong scattering from the front face of a steep wave, as parasitic capillary waves might be expected here. The imaging of the back of approaching steep waves is

more mysterious. The properties of these waves are quite similar to the Type I waves, but Type II waves are generally slightly shorter than Type I waves.

The relationship of the two types of imaged waves to the overall wave field (measured by the wave wire) is investigated. In this period on day 308, the wind had been blowing strongly from the Southwest for some time. The power spectrum of the waves (Figure 18) is characteristic of a wind-driven sea, with a clear peak at a period of approximately 7 seconds. The power spectrum follows a frequency^{-4} dependence up to approximately the peak frequency and then steepens significantly. Again this is a common characteristic of wind-driven seas. As already discussed, wave breaking generally occurs at frequencies greater than the dominant frequency. We find the very interesting result that Type I waves are entirely restricted to the region of the spectrum with a frequency^{-4} dependence.

Conclusions

Type I features can be identified with the primary waves involved in large-scale wave breaking and bubble entrainment. It is practical to measure the characteristics of these waves. There is some indication that the spectrum of primary waves is intimately connected with the overall wave spectrum. In combination with measurements of whitecap area, the methods described above give detailed information on scales of breaking and whitecapping.

C Hydrophone

A hydrophone for detecting surface wave breaking was deployed during ASGAMAGE. (This was an early prototype developed by Craig McNeil and David Farmer of IOS Sidney, Canada. The instrument has since been developed further and applied to ice detection). The hydrophone was deployed away from the platform to avoid the numerous acoustic sources associated with the platform. The sea surface immediately above the hydrophone could be viewed from the platform and for one period a video recording of this are was taken with the KNMI video equipment operating at maximum zoom. The instrument samples the noise level every 0.2seconds. A sample portion of the hydrophone data overlapping with the "video calibration" is shown in Figure 19. The data is characterised by numerous spikes, presumably associated with surface breaking of various intensities, and at various ranges from the instrument. Calibration was difficult at the large range, but some coincidences between the video and hydrophone were found.

4 Thermal Imagery of the Sea Surface

Processes within the microlayer have been relatively little studied considering their primary role in air-sea gas exchange. This state of affairs can be explained by the inaccessibility of this very thin (~100 micrometres) layer to most methods. One of the few suitable tools is radiometry which can probe a surface layer of similar, lesser or greater depth according to the wavelength chosen. In particular, thermal imagery can be used to investigate turbulence impinging on the sea surface - "surface renewal patterns". Measurements with two different IR imaging cameras during ASGAMAGE_A. One of the cameras (borrowed from TNO-FEL) is a medium-wave IR camera with a 64x64 element detector, and a very high resolution and repetition frequency. This recorded similar surface patterns as reported by Jaehne and Haussecker (1998) in similar conditions. The other camera is a scanning longwave (thermal) imager viewing a much larger surface area (~100m^2). Supplementary measurements included solar radiation and downward infrared radiation using a solarimeter and pyranometer on the helicopter deck.

Night-time measurements with the thermal IR camera in a moderate wind (6-8m/s) show evidence of the importance of fairly large-scale (~ 1 metre) organised turbulent structures, and suggest that the process of air-sea exchange is remarkably dynamic and variable on time scales of a few minutes. (*In* Graham and Woolf, 1998). The original images do not usually show any distinct features (apart from an occasional breaking wave as described below). Special processing software was written. First, images are geometrically corrected yielding a 128x128 field of 0.05m resolution pixels. Secondly, the images are filtered in search of any underlying coherent variations. The small-scale (0.1-1 metre) fluctuations slightly exceed the thermal noise, but generally any coherent fluctuations are not sufficiently large to extract from the white noise. Larger scale (1-6 metre) fluctuations can be extracted and show evidence of vortices aligned with the wind. These vortices may be part of a spectrum of similar motions extending from large-scale Langmuir circulation to much smaller scales (Melville *et al.*, 1998). The smaller scale motions are more significant to surface renewal and air-sea gas exchange. The metre-scale fluctuations are closely related to the smaller-scale fluctuations. It may be possible to investigate small-scale surface renewal indirectly by measuring the related large-scale motions.

The amplitude of the metre-scale fluctuations varies enormously on time scales of a few minutes. Heat fluxes were automatically averaged every ten minutes, but there is no reason to expect such large fluctuations in the net heat flux. It seems likely that the variations in metre-scale fluctuations have a dynamical origin – perhaps associated with wave breaking which also varies greatly on these time scales.

Thermal imagery is also a powerful tool in the study of breaking waves. Thermal images of breaking waves are characterised by a "hot" high-emissivity crest ahead of a warm patch which

implies enhanced surface renewal (see also Jessup *et al.*, 1997). Laboratory experiments have demonstrated the impressive ability of surfacing plumes to renew the surface.

5 Wave Breaking and Gas Exchange

As described in the general summary of the project and the detailed contributions of other partners, the accuracy of gas transfer velocity estimates is insufficient to examine the environmental dependence beyond noting the broad relationship with wind speed. Nevertheless, it is interesting to assess the role of wave breaking and bubble clouds in gas exchange. The methods described in this report should be capable of describing in some detail, the environmental dependence of wave breaking and bubble cloud development. The most mature of the technologies described in this report is that used to measure the vertical distribution of bubbles. This technology is approaching its theoretical limits, and these limits seriously compromise the ability of this technology to describe the near-surface distribution of bubbles, especially when wave breaking is most intense (which of course are the most interesting occasions). We can use the results described in Section 2, and especially those summarised in Figures 7 and 8 to describe the empirical inter-relationships of the bubbles, wind speed and gas transfer velocities. Two periods when the measured transfer velocity of carbon dioxide was rapidly declining coincide with periods when both wind speed and bubble areas were also declining. It is not possible to separate the general influence of the wind speed from the specific influence of the bubbles. It is possible to place an upper limit on the contribution of the bubbles, simply on the basis of surface area of the bubbles as a fraction of the sea surface (Thorpe, 1982: Woolf, 1993). As the surface area probably does not exceed 10% of the sea surface area during the measurement periods (wind speeds up to 11.7m/s) the maximum likely contribution to gas transfer velocity by "bubble-mediated" transfer is ~ 4cm/h. This contribution will increase rapidly with increasing wind speed. The breaking waves and bubbles may also contribute to gas transfer velocity by other mechanisms, but these other mechanisms are unlikely to be more effective than the bubble-mediated mechanism.

5 Other Measurements

SUDO also made measurements of dissolved oxygen, temperature, salinity, fluorescence and chlorophyll during ASGAMAGE A. Dissolved oxygen and chlorophyll are both related to the carbonate chemistry of the same waters. Dissolved oxygen also contributes significantly to the total gas concentration measured by another partner.

ASGAMAGE A was during a biologically productive period with fairly high chlorophyll levels particularly in lower salinity waters (Bedford and Purdie, 1996). In spite of this there is little evidence of large net production or depletion of dissolved oxygen (in particular, there is no evidence of a diel signal in oxygen as might be expected. There is some relationship of oxygen to the tidal signal, which had a minor influence on total gas concentrations. There is evidence of periodic stratification (salinity dominated) especially in the latter half of the experiment

During ASGAMAGE B, current profiles were measured with a sea floor ADCP and profiles of salinity and temperature were occasionally measured with a CTD from the platform (Graham and Woolf, 1997). Both the CTD and the ADCP results show evidence of stratification in the first half of the experiment (days 289-298).

References

Bedford, A.P. and Purdie, D.A. 1996. Monitoring of dissolved oxygen and chlorophyll-a in the surface waters. ASGAMAGE Data Report.

Ding, L.and Farmer, D.M. 1994. Observations of breaking surface wave statistics. *J. Phys. Oceanogr.*, **24**, 1368-1387.

Graham, A. and Woolf, D. 1997. Profiles of current, temperature and salinity. ASGAMAGE Data Report.

Graham, A. and Woolf, D. 1998. Air-sea exchange processes and their remote measurement by Southampton University Department of Oceanography. In: The ASGAMAGE Workshop, September 22-25, 1997. (ed. W.A. Oost) *KNMI Scientific Report 98-02*, Royal Netherlands Meteorological Institute, de Bilt.

Jaehne, B. and Haussecker, H. 1998. Air-water gas exchange. *Ann. Rev. Fluid Mech.*, **30**, 443-468.

Jessup, A.T., Zappa, C.J., Loewen, M.R. and Hesany, V. 1997. Infrared remote sensing of breaking waves. *Nature*, **385**, 52-55.

Leibovich, S. A. 1983. The form and dynamics of Langmuir circulation. *Annu. Rev. Fluid Mech.*, **15**, 391-427.

Longuet-Higgins, M.S. 1975. Integral properties of periodic waves of finite amplitude. *Proc. Roy. Soc. London* **A342**, 157-174.

Melville, W.K., Shear, R. & Veron, F. 1998. Laboratory measurements of the generation and evolution of Langmuir circulations. *J. Fluid Mech.*, **364**, 31-58.

Pleuddemann, A. J., Smith, J. A., Farmer, D. M., Weller, R. A., Crawford, W. R., Pinkel, R., Vagle, S. & Gnanadesikan, A. 1996. Structure and variability of Langmuir circulation during the Surface Waves Processes Program. *J. Geophys. Res.*, **101**, 3525-3543.

Rapp, R.J. and Melville, W.K. 1990. Laboratory measurements of deep-water breaking waves. *Philos. Trans. Roy. Soc. London*, **A331**, 735-800.

Thorpe, S.A. 1982. On the clouds of bubbles formed by breaking wind-waves in deep water, and their role in air-sea gas transfer. *Phil. Trans. Roy. Soc., London*, **A304**, 155-210.

Thorpe, S.A. and Hall, A.J. 1983. The characteristics of breaking waves, bubble clouds and near-surface currents observed using side-scan sonar. *Cont. Shelf Res.*, **1**, 353-384.

Woolf, D.K. 1993. Bubbles and the air-sea transfer velocity of gases. *Atmosphere-Ocean*, **31**, 517-540.

Woolf, D.K. 1995. Vertical mixing in the upper ocean and air-sea gas transfer. In *Air-Water Gas Transfer*, ed. B. Jaehne and E.C. Monahan, pp. 59-67. Hanau, Germany: AEON.

Table Captions

Table 1

Environmental conditions prevailing for the selected data set. The data periods are 32 minutes in duration each, commencing at the time specified. Directions describe wind origin, θ, and the heading of the current with respect to that of the wind, $\Delta\theta_c$, positive to its right. Bounds are measures of the spread within a measurement period. The ranges of the current, v, reflects systematic change over the data period. Otherwise, the spread is taken to reflect statistical fluctuation, so the error given is the standard deviation within the period. Phase speed, c, is calculated from the dispersion relation for linear waves, $c=(gT/(2\pi))\tanh(2\pi D/(cT))$, where g is the acceleration due to gravity, T is the dominant period and D is the mean water depth, 18m. Significant wave height is denoted by H_s. The salinity was typically 31 psu. Heavy rain was observed during run 18, and some precipitation may also have occurred during runs 14, 15 and 21.

run	start (J day 1996)	wind		waves				current		air-sea temper-ature diff. (°C)
		W_{10} (m s^{-1})	θ (deg.)	H_s (cm)	T (s)	W_{10}/c	$H_s/(cT)$ $\times 10^{-2}$	v (cm s^{-1})	$\Delta\theta_c$ (deg)	
1	290.8438	4.6 ± 0.2	186 ± 7	48 ± 2	4.0 ± 0.2	0.7	1.9 ± 0.2	17 ± 5	-75 ± 40	-1.7
2	296.4201	4.9	204 ± 2	80 ± 4	5.1 ± 0.2	0.6	2.0 ± 0.2	53 ± 3	13 ± 6	-1.3
3	296.5417	5.5 ± 0.2	222	68 ± 4	4.5	0.8	2.2 ± 0.2	29 ± 2	10 ± 15	-0.9
4	297.7813	5.8 ± 0.4	108 ± 4	29	2.9	1.3	2.2 ± 0.4	64 ± 6	-62 ± 8	-1.2
5	293.8701	6.5 ± 0.5	251 ± 3	129 ± 4	5.0 ± 0.2	0.8	3.3 ± 0.3	34 ± 5	-29 ± 8	0.2
6	295.6910	6.7 ± 0.3	322 ± 3	170 ± 5	5.7	0.8	3.4 ± 0.2	31 ± 3	85 ± 6	-0.8
7	297.7188	7.0 ± 0.4	116 ± 2	35	3.0	1.5	2.5 ± 0.2	53 ± 8	-69 ± 5	-0.5
8	292.3201	7.3	181 ± 3	60	3.0	1.6	4.3 ± 0.3	36 ± 6	20 ± 5	-4.5
9	297.9188	7.6	128	38	3.0 ± 0.2	1.6	2.7 ± 0.4	20 ± 14	89 ± 16	-2.9
10	295.6049	8.0 ± 0.2	322 ± 2	201 ± 7	5.7 ± 0.3	0.9	4.1 ± 0.5	52 ± 4	87 ± 6	-0.7
11	293.5285	8.9	287	179 ± 6	6.0	1.0	3.3 ± 0.2	54 ± 3	120 ± 4	-1.0
12	295.5299	8.9 ± 0.3	318 ± 2	198 ± 21	5.8 ± 0.3	1.0	3.9 ± 0.6	10 ± 4	145 ± 56	-0.7
13	292.5097	9.6 ± 0.3	194	90 ± 3	4.2 ± 0.2	1.5	3.3 ± 0.3	64 ± 3	-128 ± 2	-1.7
14	294.6729	9.8 ± 0.5	228	133 ± 8	5.2	1.2	3.2 ± 0.2	42 ± 7	-159 ± 8	0.2
15	292.7049	10.2 ± 0.3	184	147 ± 6	4.4	1.5	4.9 ± 0.3	76 ± 3	31 ± 4	-2.4
16	292.5403	10.3 ± 0.2	187 ± 2	108 ± 10	4.4	1.5	3.6 ± 0.4	60 ± 3	-122 ± 5	-1.2
17	293.2444	10.5 ± 0.2	300	182 ± 9	5.4 ± 0.5	1.3	4.1 ± 0.6	68 ± 3	-80 ± 4	-0.7
18	292.6306	10.6	190	123 ± 6	4.6 ± 0.3	1.5	3.7 ± 0.5	10 ± 6	-66 ± 52	-1.4
19	292.8295	11.4 ± 0.3	205	165 ± 8	5.0	1.5	4.2 ± 0.3	32 ± 4	16 ± 5	-2.4
20	295.3132	11.4 ± 0.5	320 ± 2	183 ± 2	4.9 ± 0.4	1.5	4.9 ± 0.8	43 ± 5	-100 ± 6	-0.3
21	294.8035	11.5	207 ± 3	153 ± 3	4.9	1.5	4.1 ± 0.2	69 ± 2	17 ± 5	-2.7
22	295.2472	11.5 ± 0.7	311	152 ± 12	5.3 ± 0.2	1.4	3.5 ± 0.4	7 ± 5	74 ± 18	0.9 ± 0.2
23	292.8208	11.7 ± 0.4	204	165 ± 9	4.6 ± 0.2	1.6	5.0 ± 0.5	37 ± 5	14 ± 5	-2.5

Figure 1

Logarithmic plots of the probability of backscatter levels invalid for inversion occurring at 0.4m depth as a function of (10m) wind speed. Crosses denote the probability that levels are too low, yielding fit A, asterisks showing the probability that levels are too high, yielding fit B.

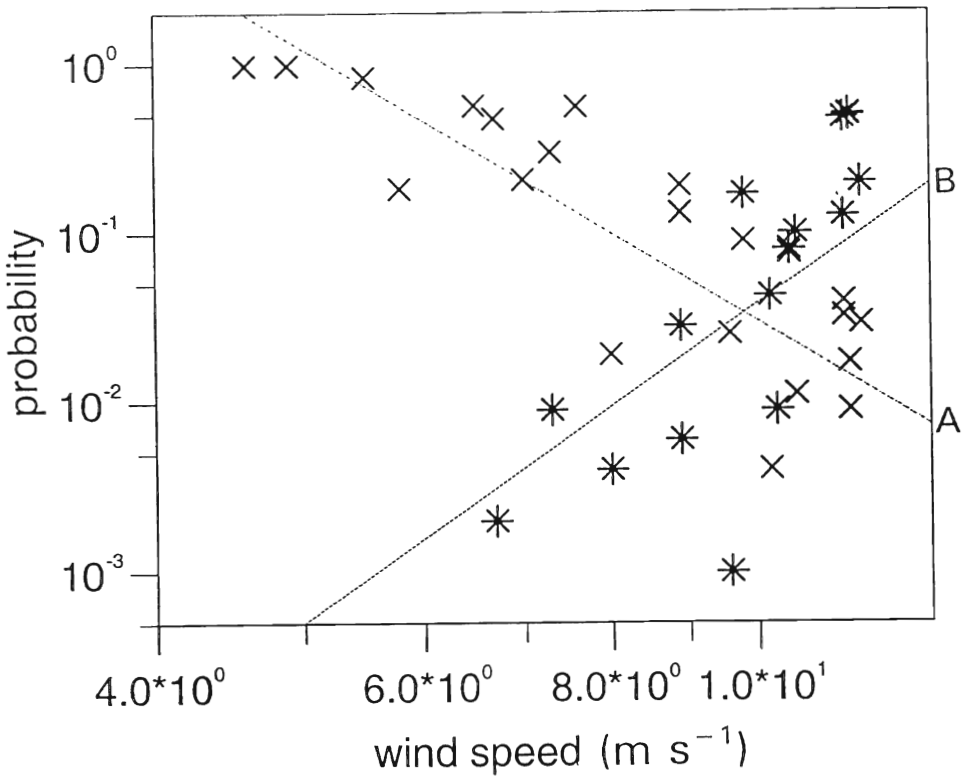

Figure 2

Statistics of the backscatter at 86kHz in run 14. Median and measured moments are shown, crosses and asterisks showing mean and median normalised by their values at 0.4m, 1.8×10^{-3} m^{-1} and 0.92×10^{-3} m^{-1}, respectively. Squares and stars show coefficients of variation and skewness, respectively. The attenuation depth of the mean = 0.51±0.02 m below a depth of 3.7m (as found from fit A). The attenuation depth of the median = 0.64±0.01 m (fit B). The attenuation depth of the mean = 1.33±0.03 m closer to the surface. The coefficients of variation and skewness grow exponentially with depth with a characteristic scale of 2.4m (fits C and D).

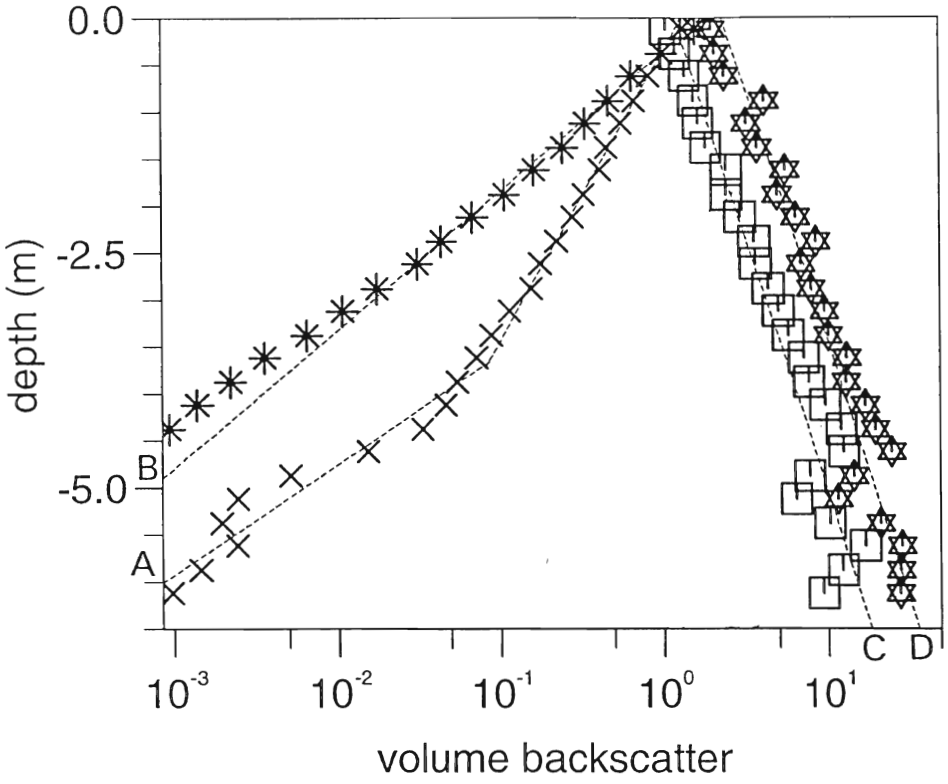

Figure 3

Dependence of the attenuation depth of backscatter at 86kHz (Crosses) and 250kHz (Squares) on conditions. a) Plot of the attenuation depth of the mean against significant wave height, b) Logarithmic plot of the e-folding scale of the median against (10m) wind speed. The top-right cross in (a) shows the standard error of the data.

(a)

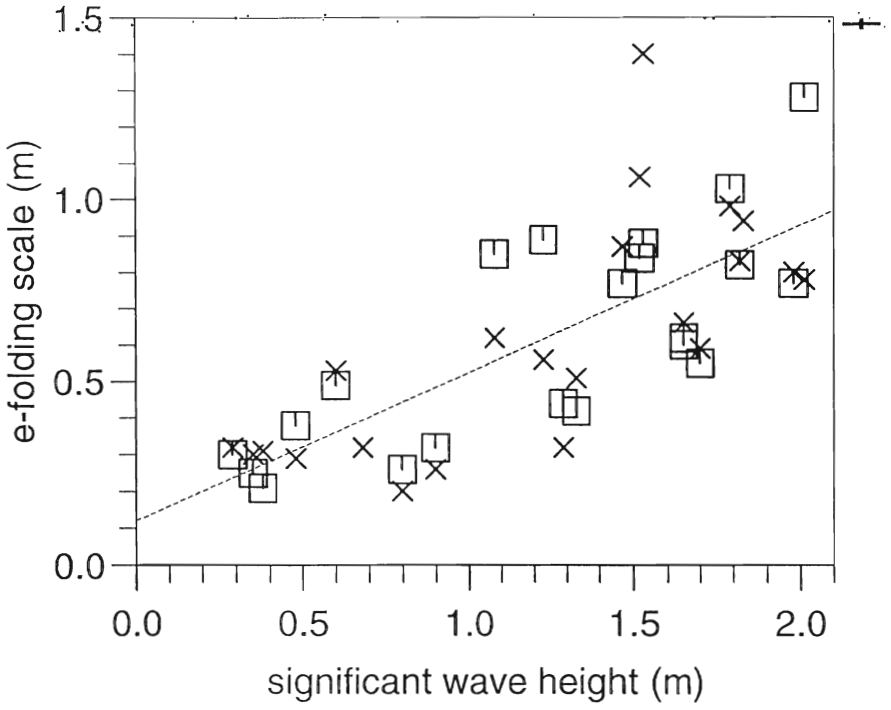

(b)

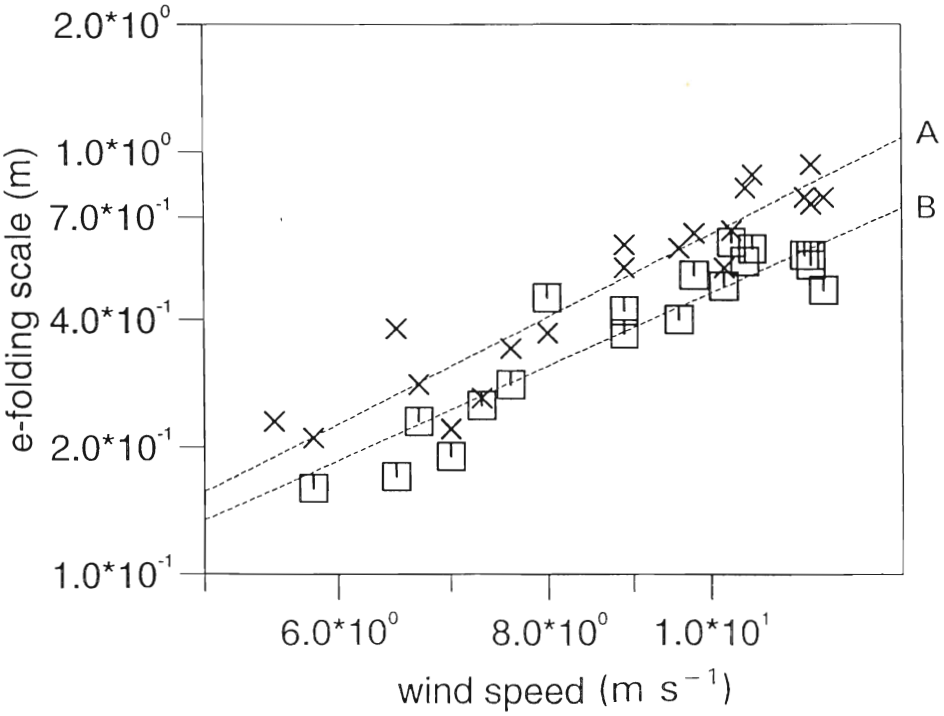

Figure 4

Profiles of bubble statistics in run 14: as normalised by values at 0.4m. a) Measured mean bubble radius, with standard errors, b) median of bubble concentration; c) median of void fraction. Dashed lines show least-squares fits weighted by standard errors, constrained to take the value calculated at 0.4m. Mean bubble radius and median of bubble concentration at 0.4m are 43μm and 59dm^{-3}, respectively. Medians could not be calculated below 2m. Net trends with depth are a decrease in mean radius of 7±1% m^{-1}, and attenuation depths of bubble concentration and void fraction of 0.58±0.02 m and 0.48±0.01 m respectively.

(a)

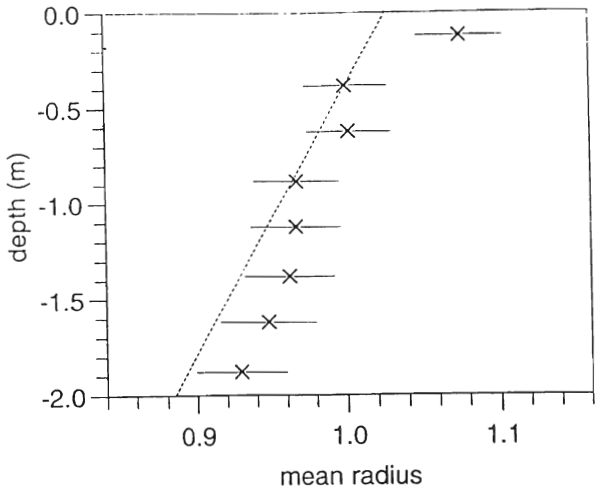

(b)

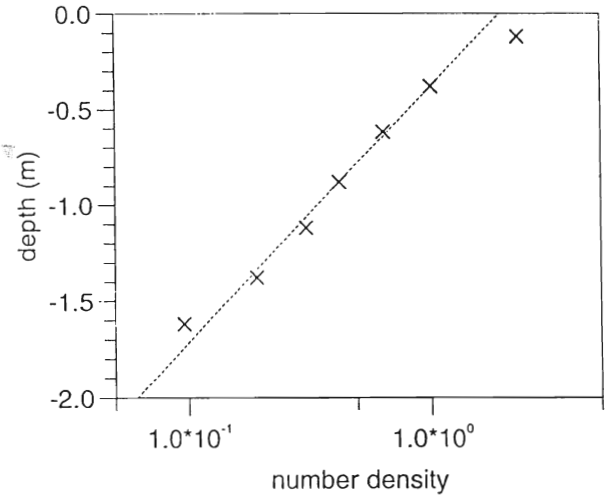

(c)

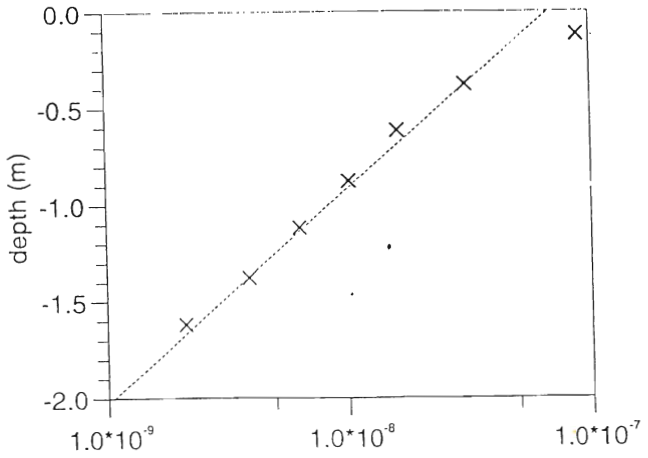

Figure 5

Plot of the mean fractional increase in bubble radius per unit depth, with standard errors, against wave slope (the ratio of significant wave height to dominant wavelength).

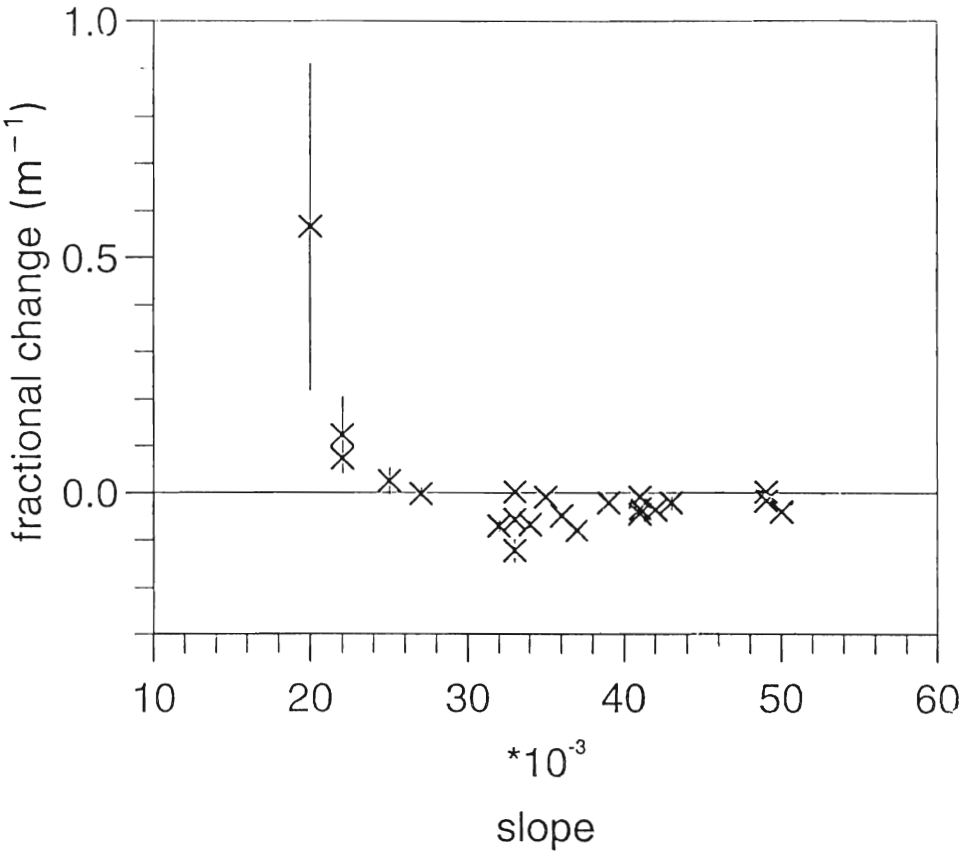

Figure 6

Plots of bubble statistics integrated over all depths and bubble sizes against (10m) wind speed. a) Total bubble surface area, as a fraction of the sea surface. b) Upward displacement of the sea surface by bubbles. Means (Circles) and medians (Stars).

(a)

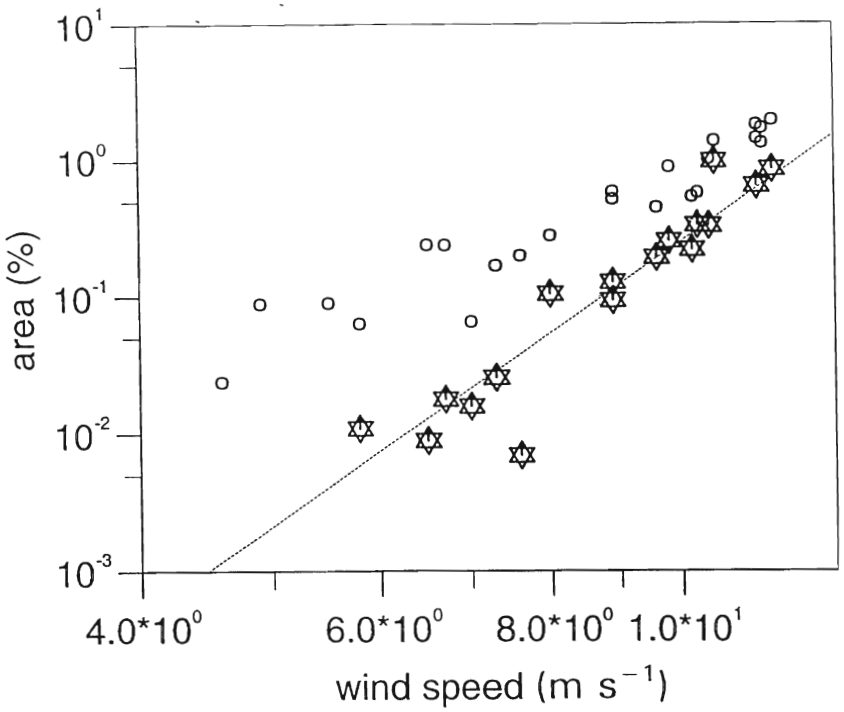

(b)

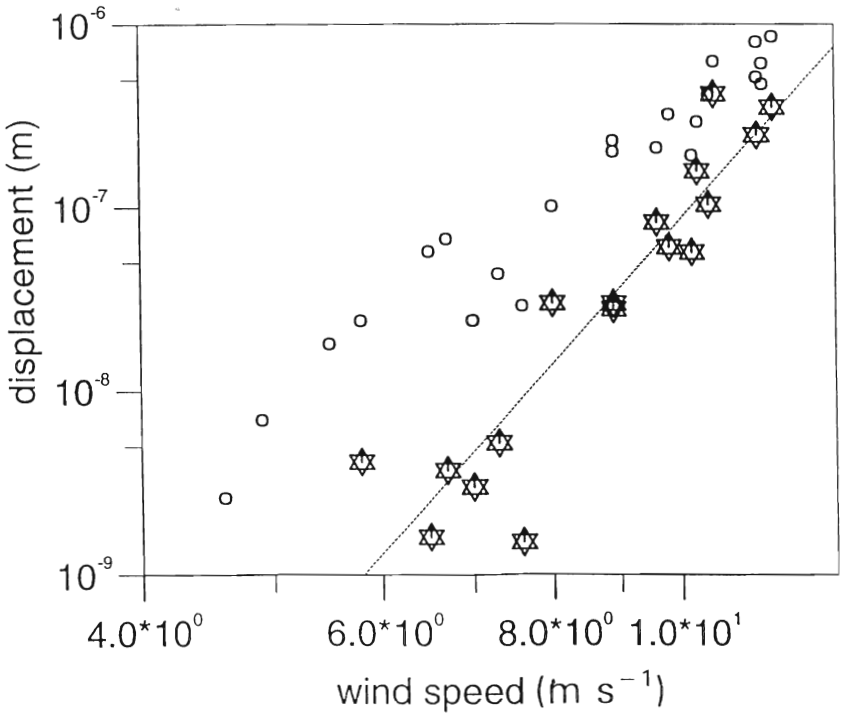

Figure 7

Time series of a) median of total bubble surface area, b) corresponding values of (10 m) wind speed. Times are Julian day in 1996. Bubble areas are expressed as a fraction of the sea surface. The dashed lines are added to make the sequence clear.

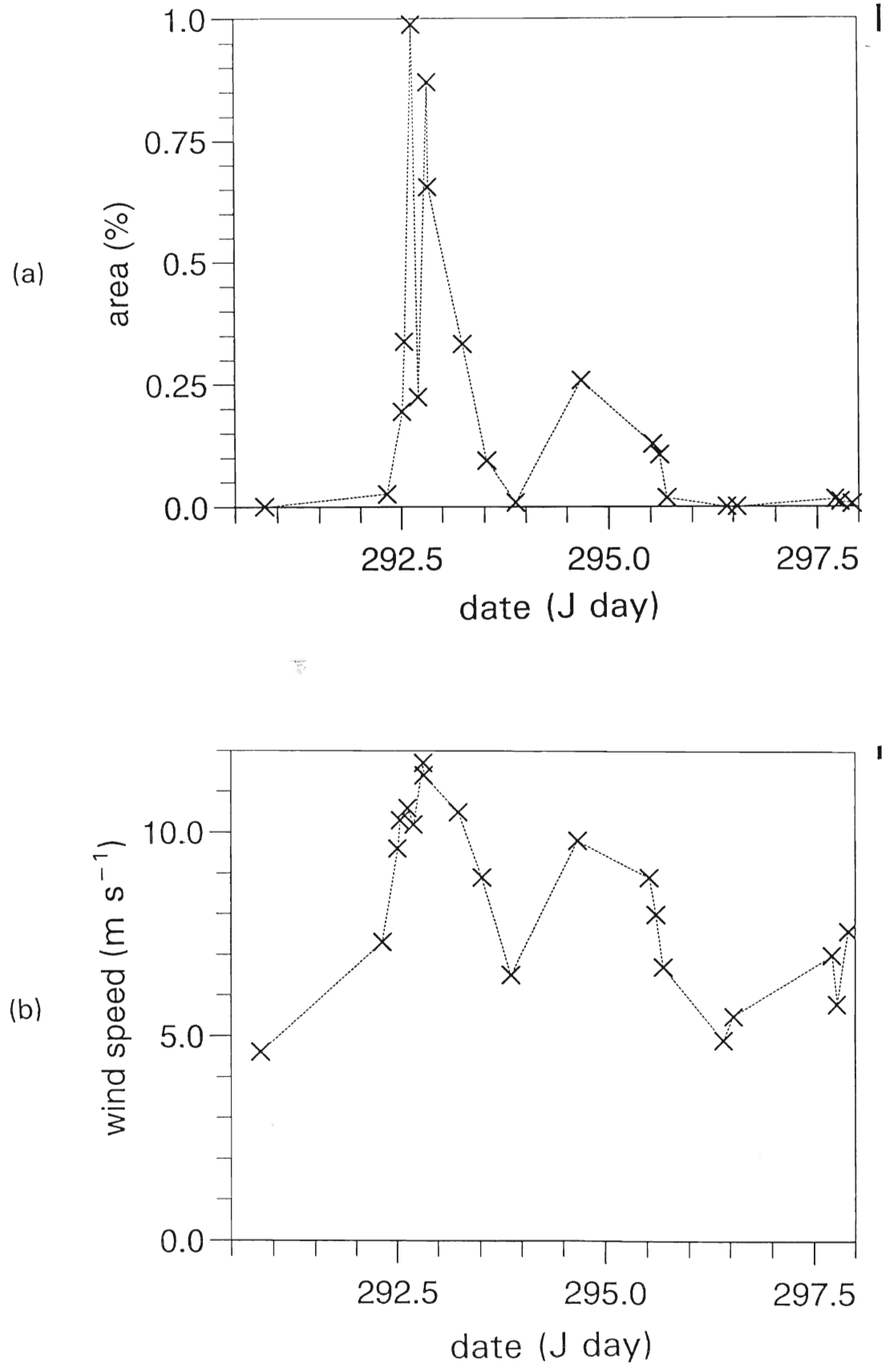

Figure 8

Time series of a) CO_2 transfer velocity, and b) wind speed.

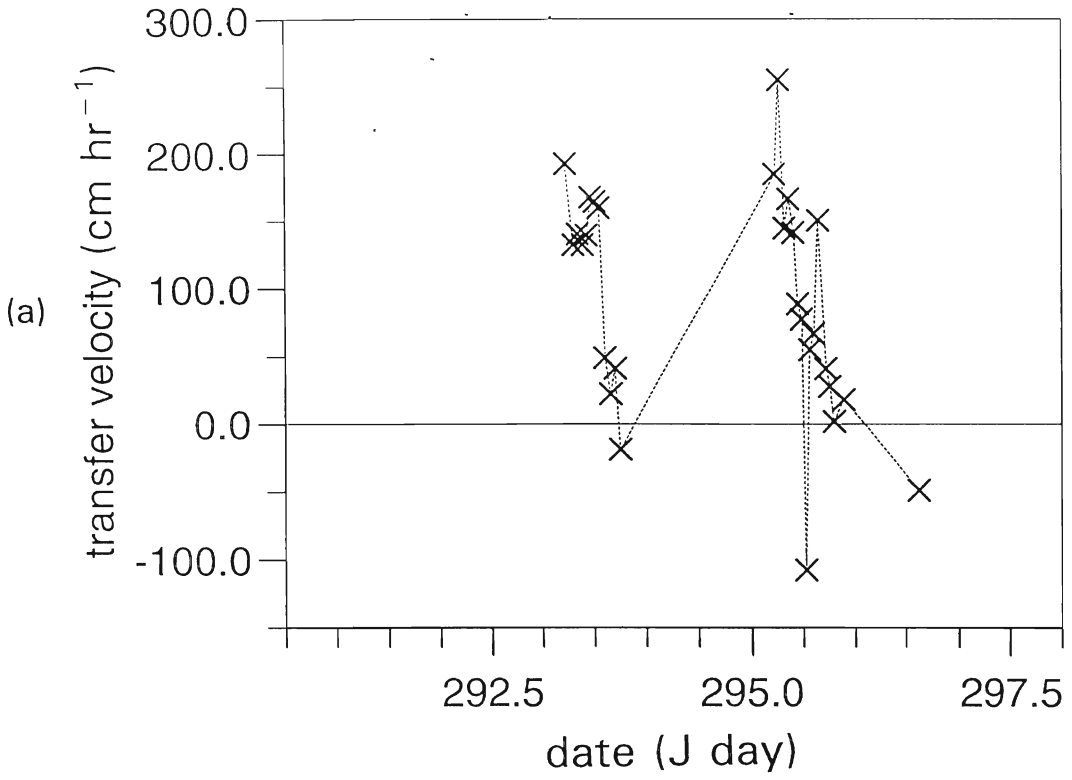

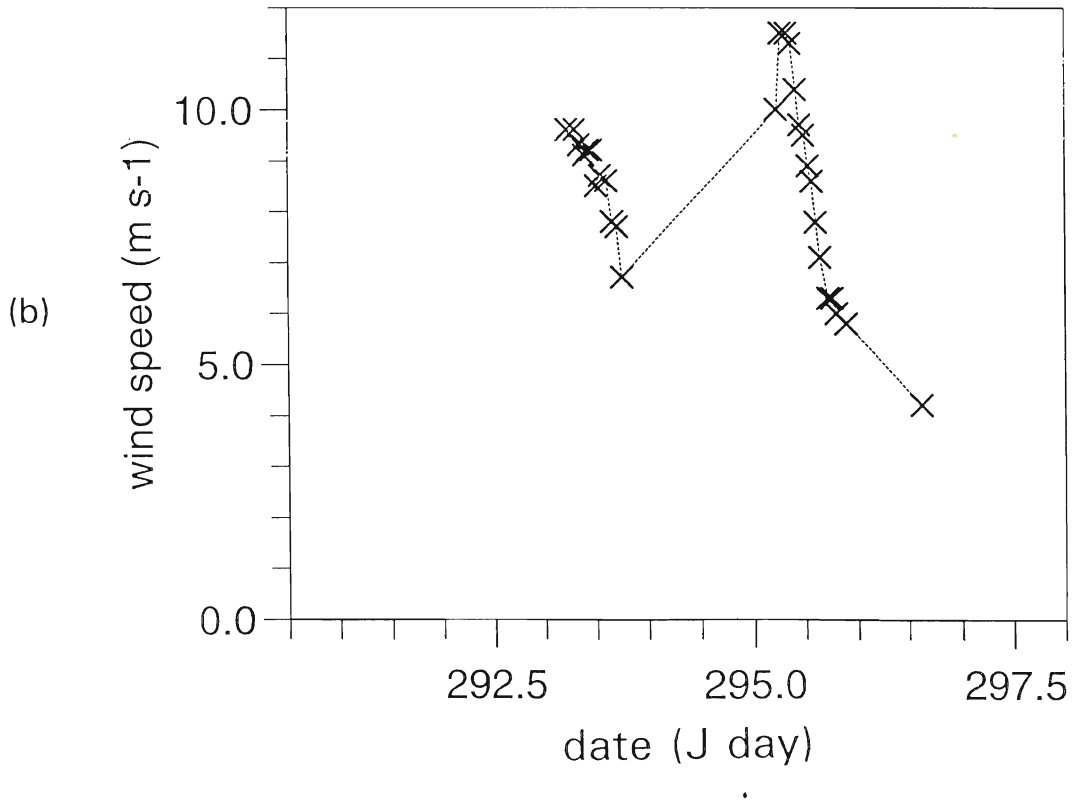

Figure 9

A single sweep of the sector-scanning sonar analysed to retrieve acoustic whitecap coverage. This sweep was the sixteenth of the measurement period, 1700-1800 on Julian Day 308 (November 3, 1996). All sweeps were in the quadrant from which the wind was blowing. The wind was fairly steady at 16m/s from 230°. Scattering from zero to 50 metres range is shown. The surface waves immediately above the instruments give a strong return (at a range of approximately 14 metres).

a) The original images is formed with time as the "x-ordinate", range as a "y-ordinate" and the scattering strength displayed at each time and range as a shade of the pixel on a grey-scale. The grey-scale is set by first taking the logarithm of the signal, then "normalising" the result to a mean of 127 and a standard deviation of n (= 30 or 40) for each range within the measurement period. The range of p* is limited to 0 (black) – 255 (white) on an 8-bit grey scale.
b) Areas manually identified as belonging to breaking wave crests are labelled in white. The remainder of the image has been compressed to a limited grey scale from mid-grey to black.
c) Areas detected by an automatic "whitecap algorithm" are shown in black.
d) The result of the image shown in c) additionally subjected to a size filter

Figure 10

Time series of "whitecap coverage" in the measurement period, 1700-1800 on Julian Day 308 (November 3, 1996). Whitecap coverage was measured with the automatic algorithm demonstrated in Figure 9, for each of 130 successive sweeps. Percentage whitecap coverage is plotted on the y-ordinate, sweep number on the x-ordinate.

9a)

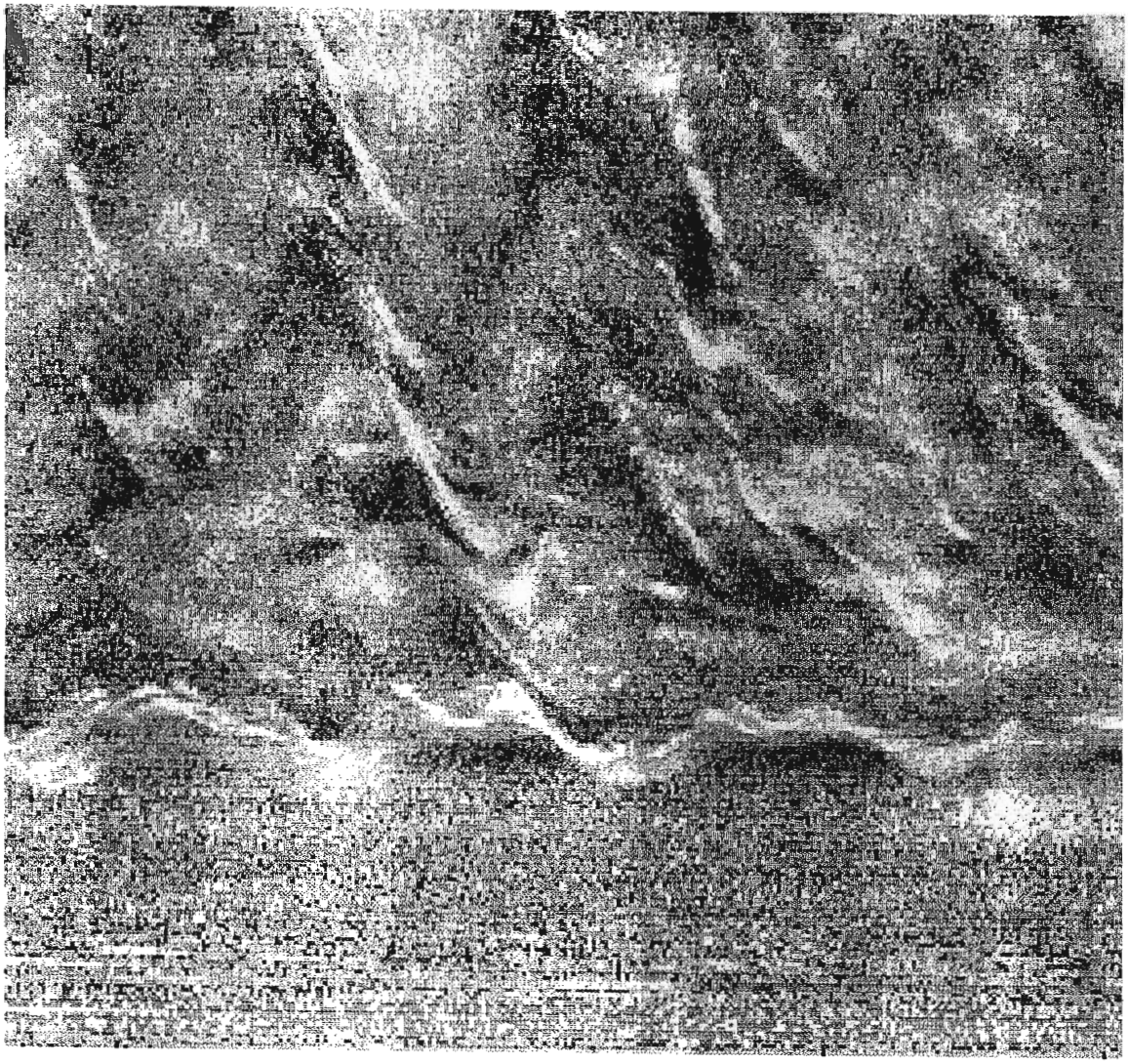

96)

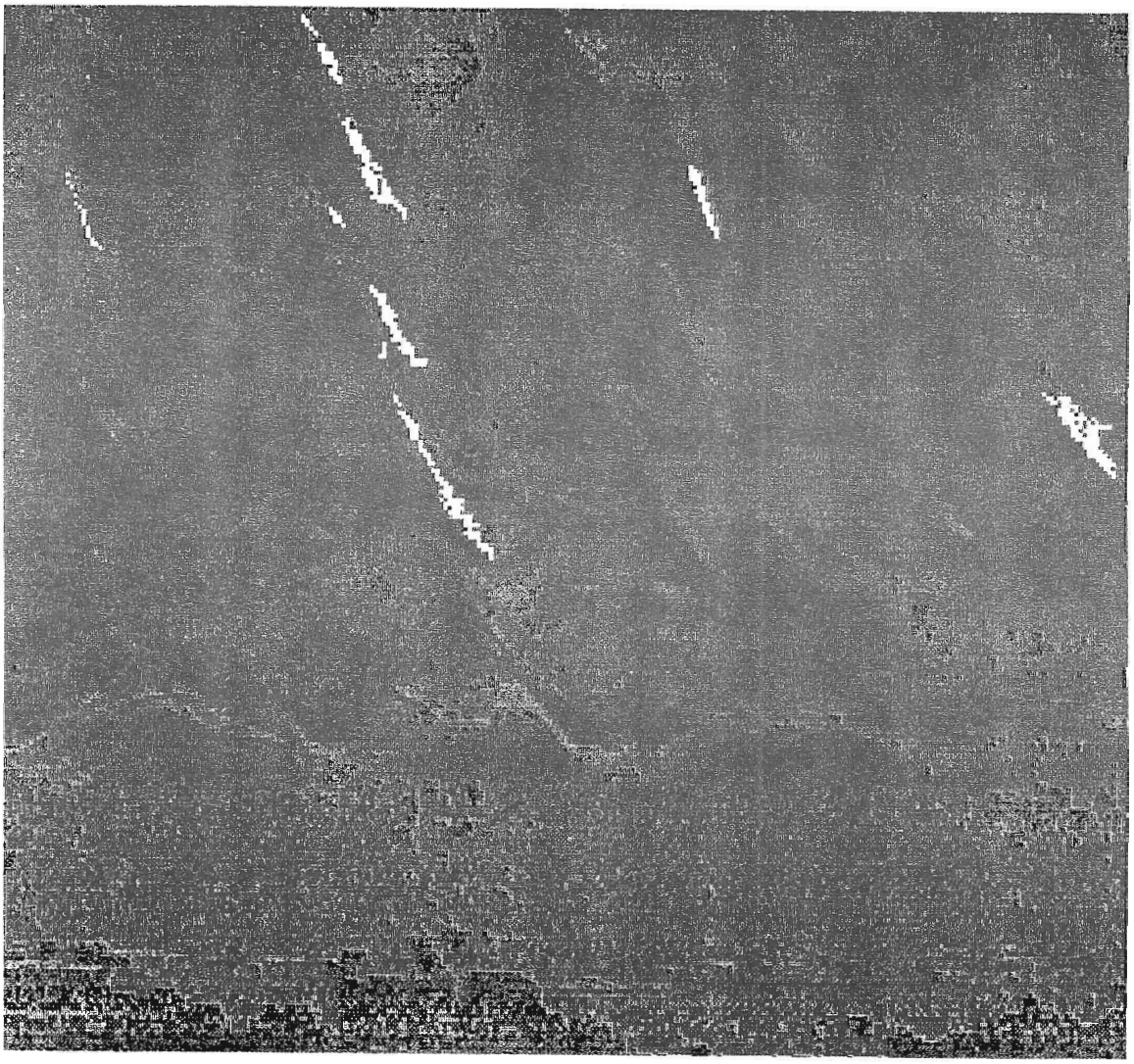

9c)

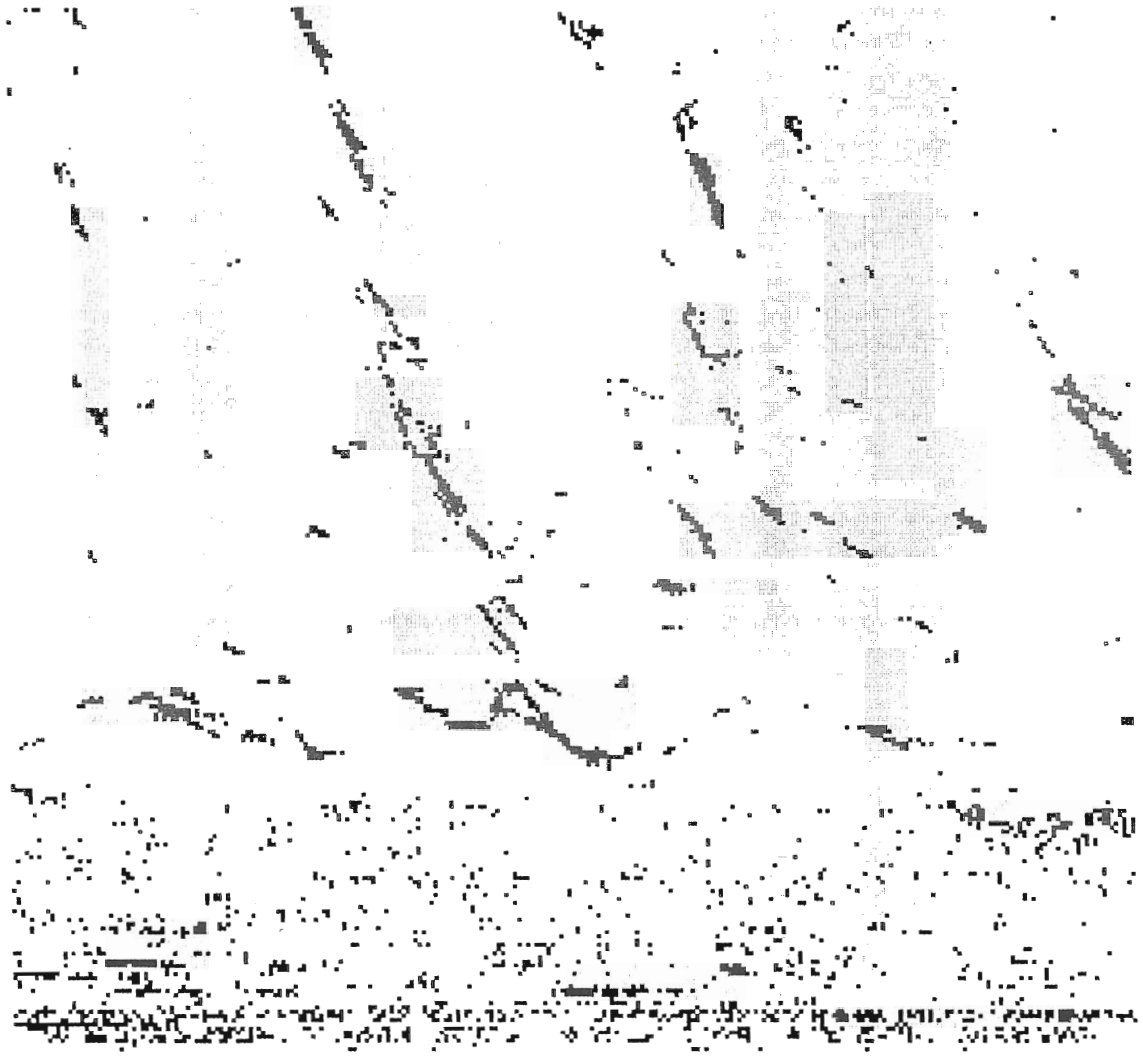

9d)

10)

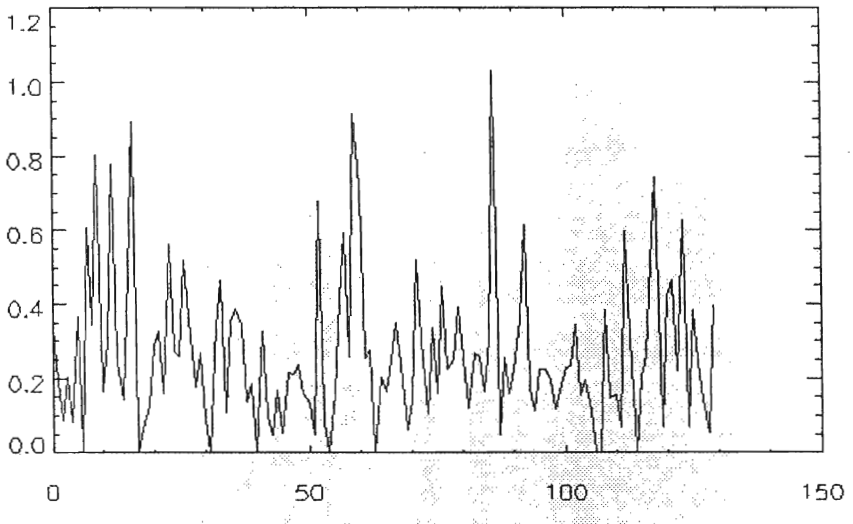

Figure 11

Approaching waves in the Northwest quadrant. An image is shown together with an additional display by the image-processing software. This image shows large Type I features. The software has been used to match the estimated wave statistics to the image features.

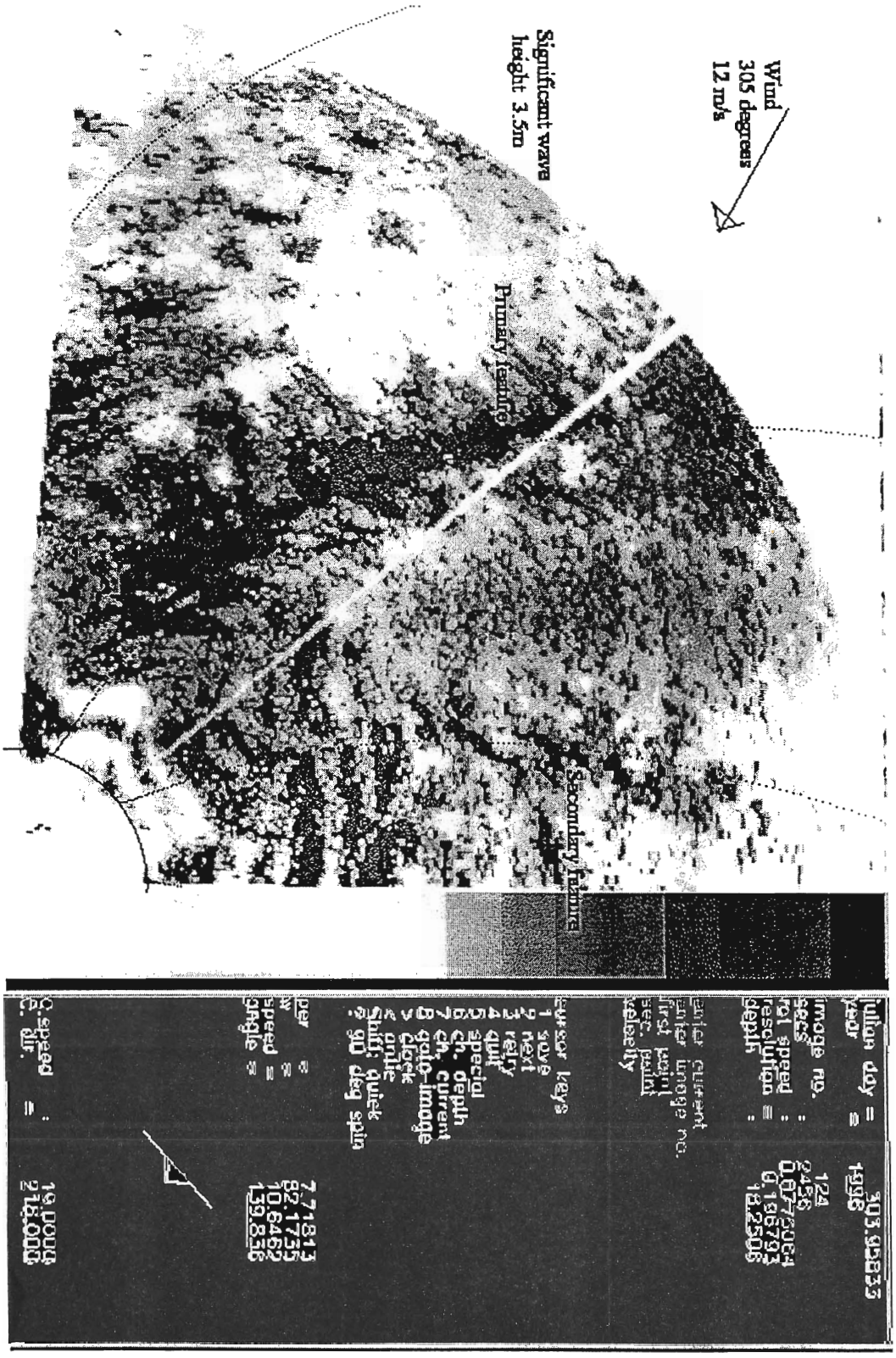

Figure 12

Receding waves in the Northwest quadrant. An image is shown together with an additional display by the image-processing software. This image shows a large set of Type II features. The software has been used to match the estimated wave statistics to the image features.

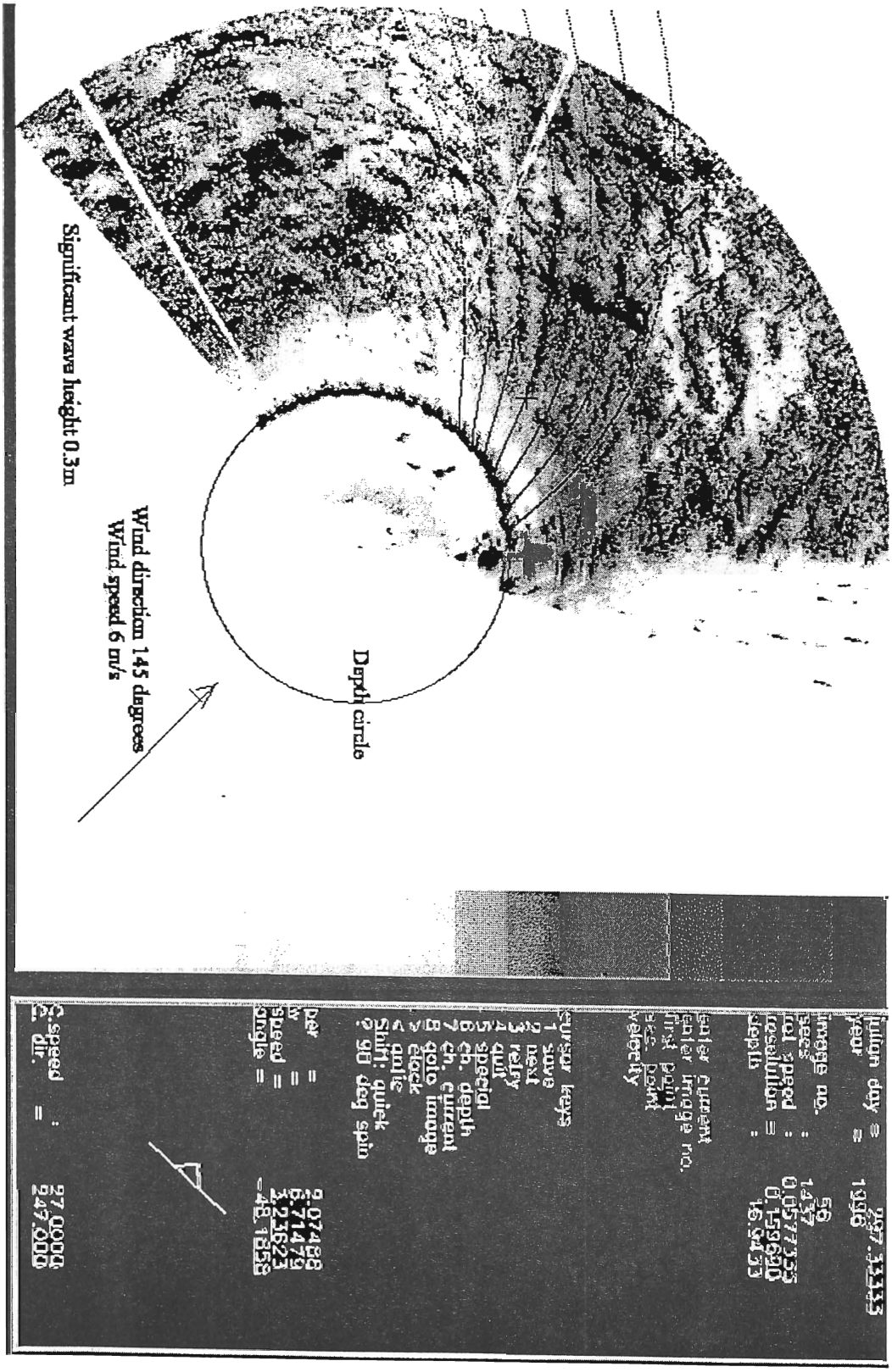

Figure 13

Measurement of wave amplitude and phase position.

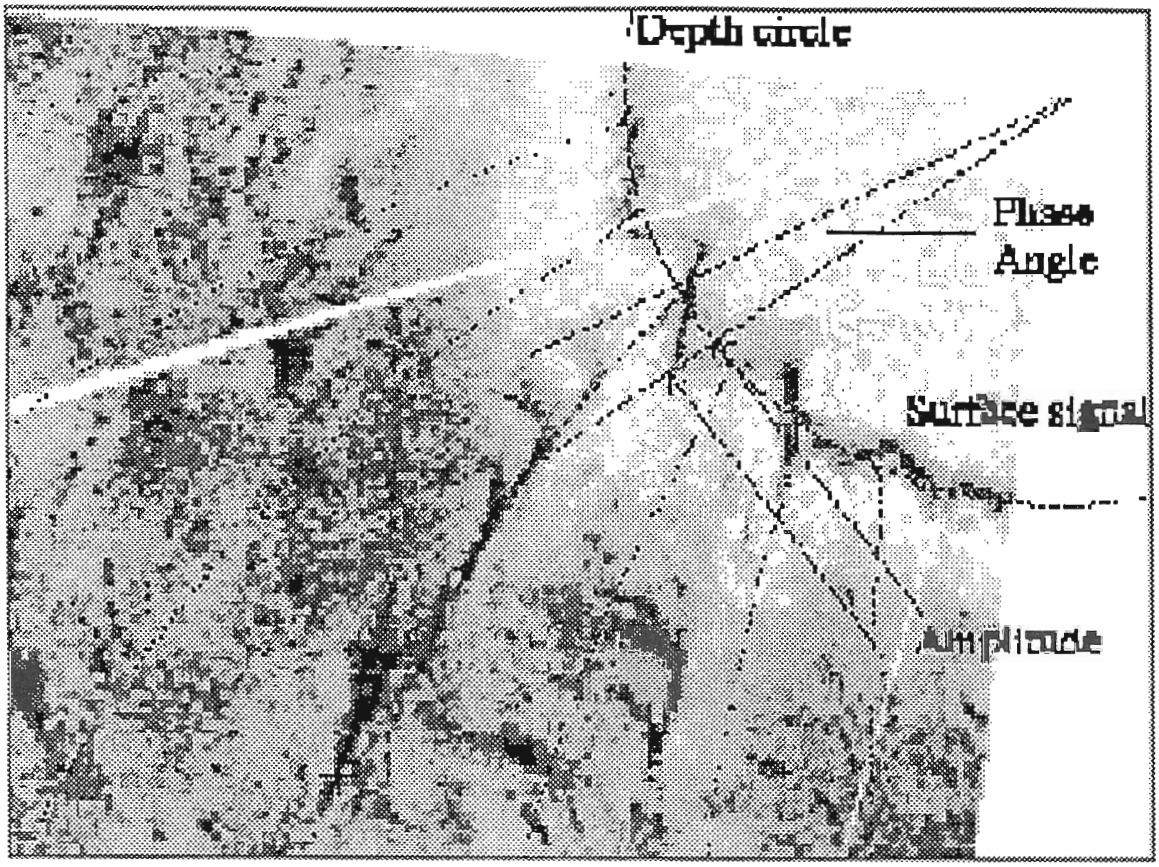

Figure 14

Dispersion relation. The dashed line is the theoretical relationship. The solid line is a linear regression fit.

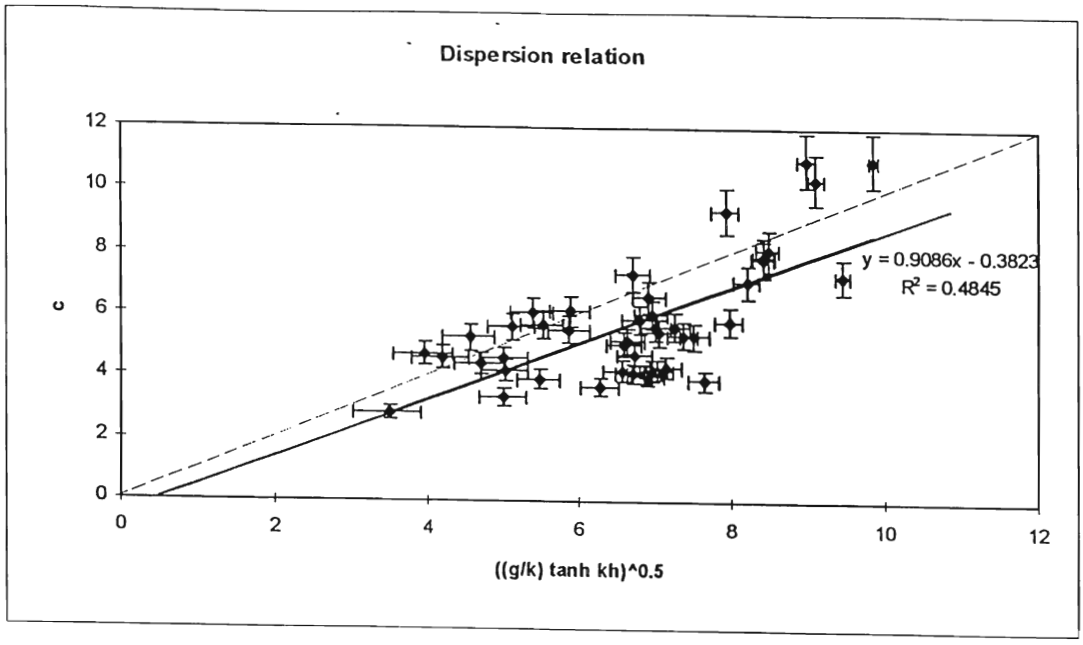

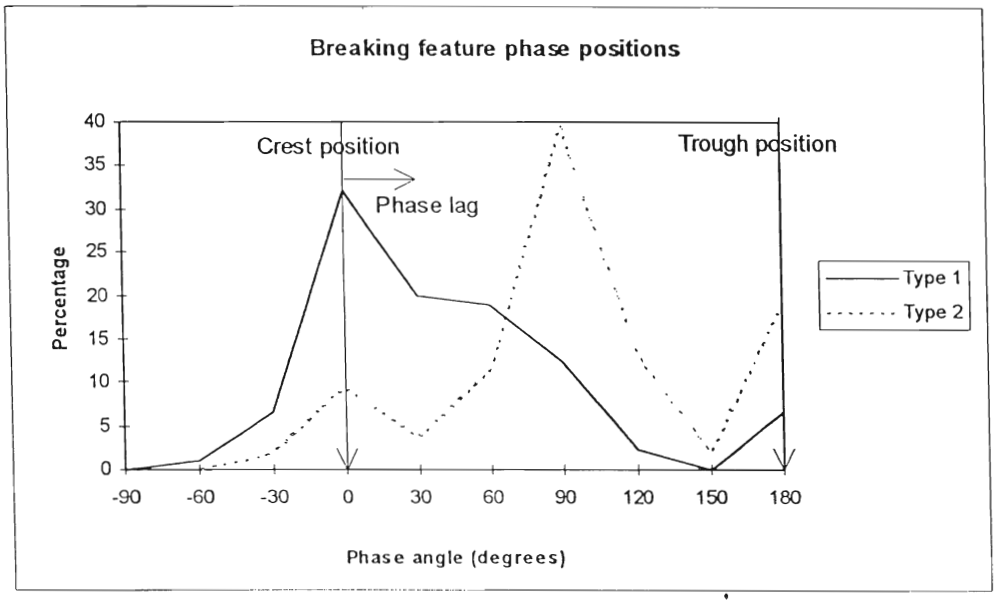

Figure 15

Breaking event phase position

Figure 16

Slope of wave associated with breaking events, S, plotted against the dominant wave slope, Sd, for the period.

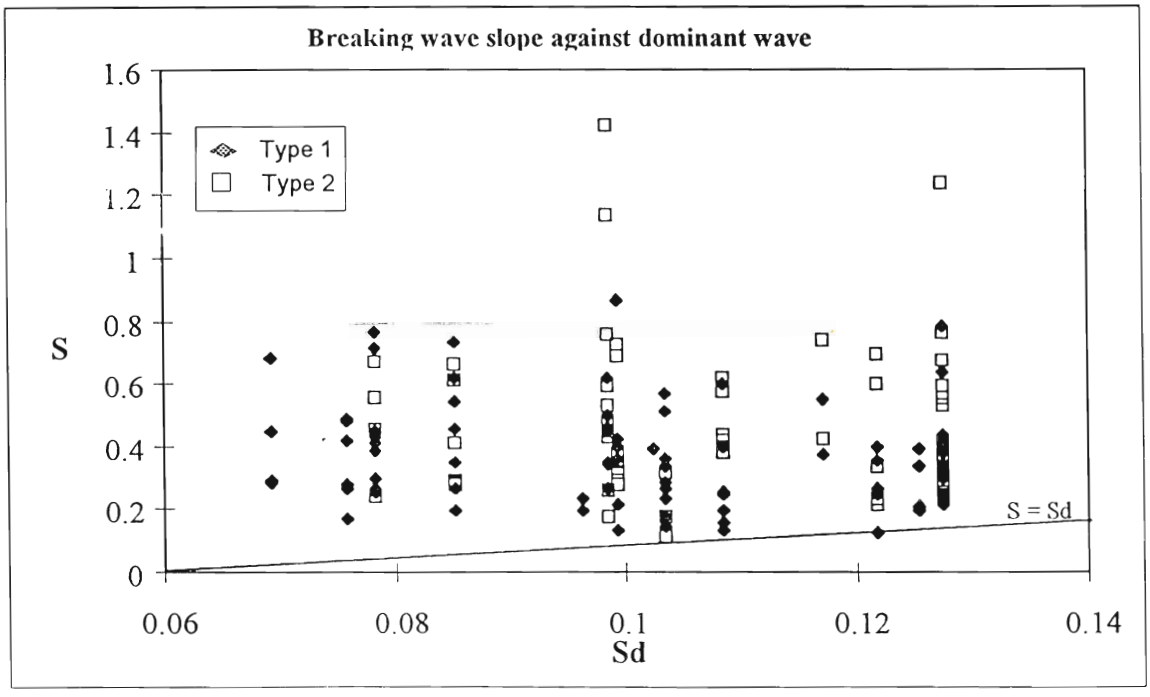

Figure 17

Phase speeds of breaking events normalised by dominant phase speed.

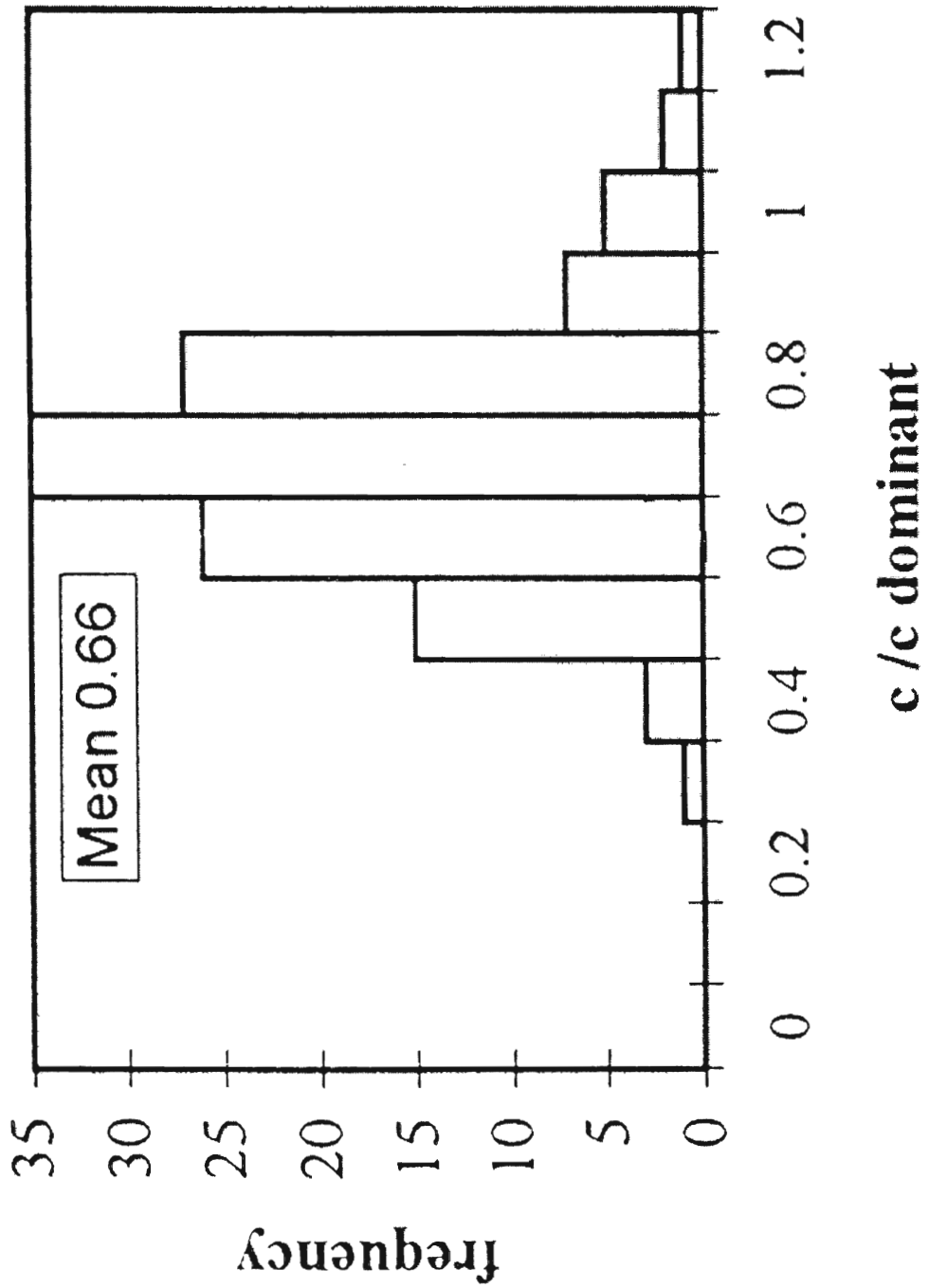

Figure 18

Frequency spectrum of surface waves on Julian Day 308, with frequency of waves forming features in this period indicated by arrows (Type I above spectrum, Type II below spectrum). For reference, lines indicating power law relationships with exponents of –4 and –5 are included.

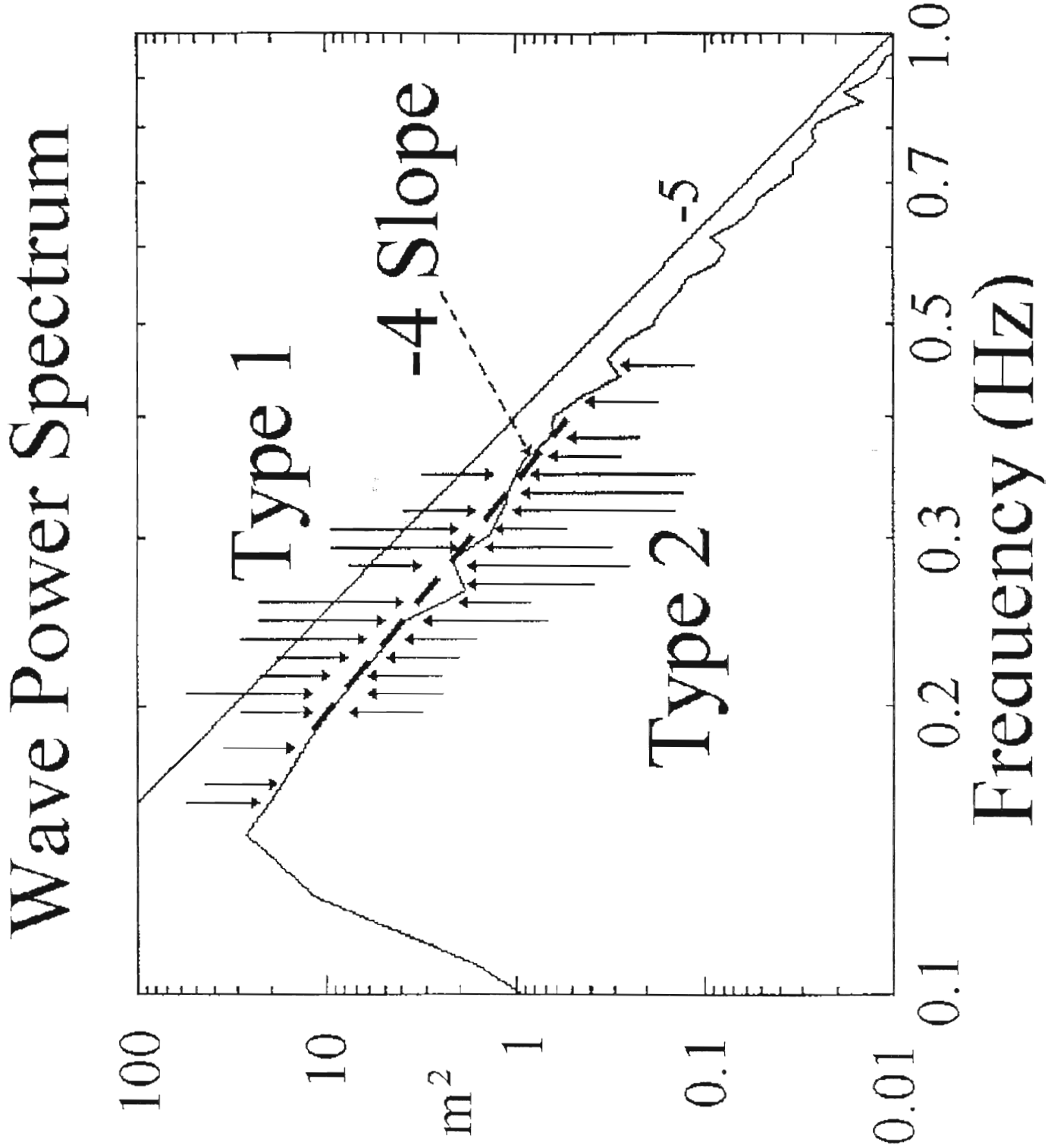

Figure 19

Graph showing a time series of the noise level measured by the hydrophone. The period of a "video calibration" is also shown.

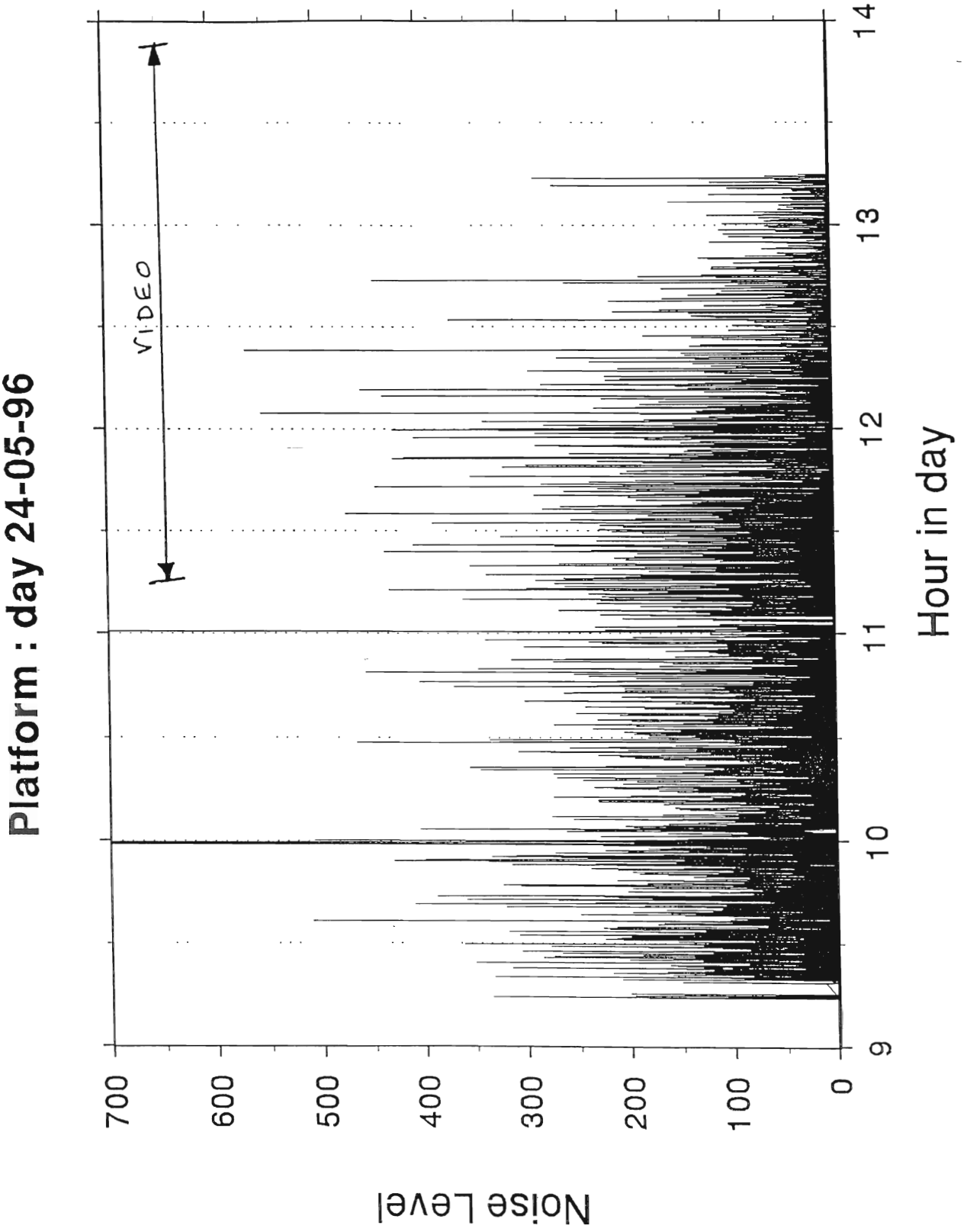

ASGAMAGE Final Report

Contributions of University College, Galway (National University of Ireland, Galway)

Partner 7

Principal Investigator:

Dr. P. Bowyer
Department of Oceanography
University College Galway
Galway, Ireland
Phone: + 353 91 524411; FAX + 353 91 525005
E-mail: Peter.Bowyer@ucg.ie

Overview

Peter Bowyer, Ferren MacIntyre

Work done as part of the ASGAMAGE experiment is presented.

The analysis of the acoustic results to produce a detailed picture of near surface scattering is presented. In this section, results from the upwardly pointing sonar deployed in ASGAMAGE-A are presented. The image analysis algorithms are described in detail and the measurements of near surface scattering cross section are presented (F.M.).

Video measurements of bubble populations were not successful during the ASGAMAGE experiments, but the experiments were continued in waters off Ireland and a paper (submitted to Journal of Geophysical Research) presenting measurements of large bubble statistics near the surface is presented here (P.B.)

Finally, Total gas saturation measurements made during both phases of the ASGAMAGE experiment are presented: data from the second experiment is used to model and parameretize supersatuation and transfer velocity and are presented as a paper (P.B. and D. Woolf).

ASGAMAGE Upward-Looking Sonar Data Analysis

Ferren MacIntyre & Peter Bowyer

The ASGAMAGE sonar data — some 24 100-MB ZIP disks — represents the first attempt to separate echoes from the sea surface itself and echoes arising from bubble clouds immediately subjacent. This attempt required stretching the envelope of transducer design by what seemed small amounts, from 300 to 500 kHz, for instance, and from 100-ms to 16-ms pulse length. In the event, these both proved to be much larger steps than expected, in terms of manufacture, mounting, calibration, and data analysis. Nonetheless, the effort succeeded.

Program development

The data-analysis program is portably written in MATLAB 5. It is reasonably automatic, but still requires occasional human intervention for one important aspect. As the kite depth varies, so does the best location for the short signal-free region used to determine the amount of electronic noise to subtract. As with many image-analysis problems, as task which is trivial for the human eye is well beyond the reach of algorithmic determination. An outline of the algorithm is presented in the Appendix.

Data analysis

Data reduction — including subsidiary operations such as expanding compressed files — requires about 300% of observation time on a 225 MHz machine, where it uses some 70Mb of memory (much of which is for image storage).

The surface half of an exemplary raw data block is shown in Fig. 1, where up in the ocean is down in the image. [A] is the kite, [B] the surface, and [C] an intermittent second echo of the surface which appears when the orientation of the kite and (random) surface slope permits.

The region between the kite and the line [D] is discarded. The heavy line at the kite is the outgoing pulse. Adjacent to this, in the high-intensity region [E] between the kite and line [D] — and near the kite at [7] on the left of Fig. 2 is a region of intermitdtent, anomalous, and occasionally intense signal. This, which appears to grow upward from the kite, and later retreat toward it, is a not uncommon occurrence, but is probably not 'real' bubbles. It might be a plankton swarm (although the acoustic impedance of plankton is so close to that of seawater that this appears unlikely), or it might be a region in which a cloud of bubbles had recently dissolved. The tendency of near-kite noise to appear in wave troughs [F] is not understood, but there appears to be some correlation with the 2nd surface echo, and this might be a result of the additional energy of a standing wave.

This unexplained signal might represent a recurring problem with acoustical measurements, in which rectified diffusion appears to regenerate bubbles from 'bubble ghosts' — gas-saturated organic particles which are produced when a surfactant-coated bubble dissolves. (Acoustic bubble counts are usually higher than optical counts for this reason.) Attempts to make this distance interactive and data-responsive failed, so 30 pixels are summarily dropped adjacent to the kite, representing an astonishing 1.04 m in which realistic bubble counts cannot be expected. This cutoff appears to lose some real data — at [G] in the block illustrated — and includes some probably spurious data at [H], but seems a reasonable compromise for automatic data reduction. The distance from the surface to [D], rather than the physical location of the kite, is reported as 'the kite depth' in Fig. 2.

Data after reduction is shown in Figs. 2 and 3. Fig. 2 is a summary of 20 data blocks, each consisting of 1024 sonar echoes (2^10, for the benefit of Fourier transforms). At 34.1 sec per block, Fig. 2 covers 11.4 minutes of observation.

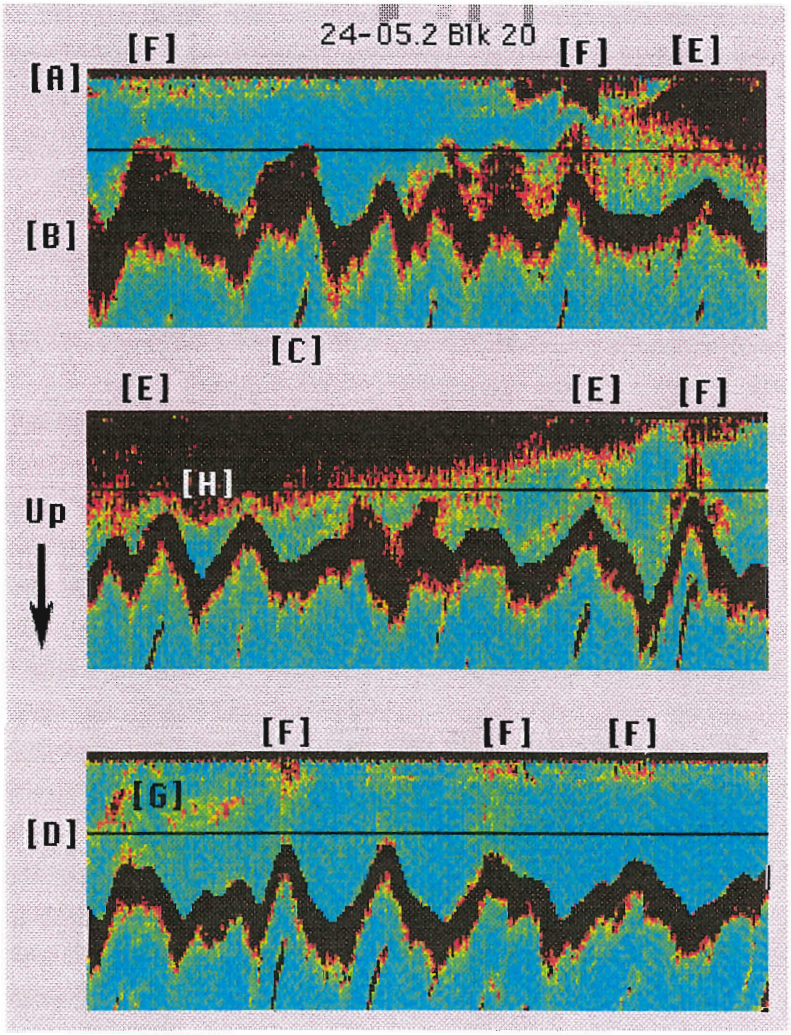

Fig. 1. 34 seconds of raw data (near-surface half). The panels represent one continuous sequence.

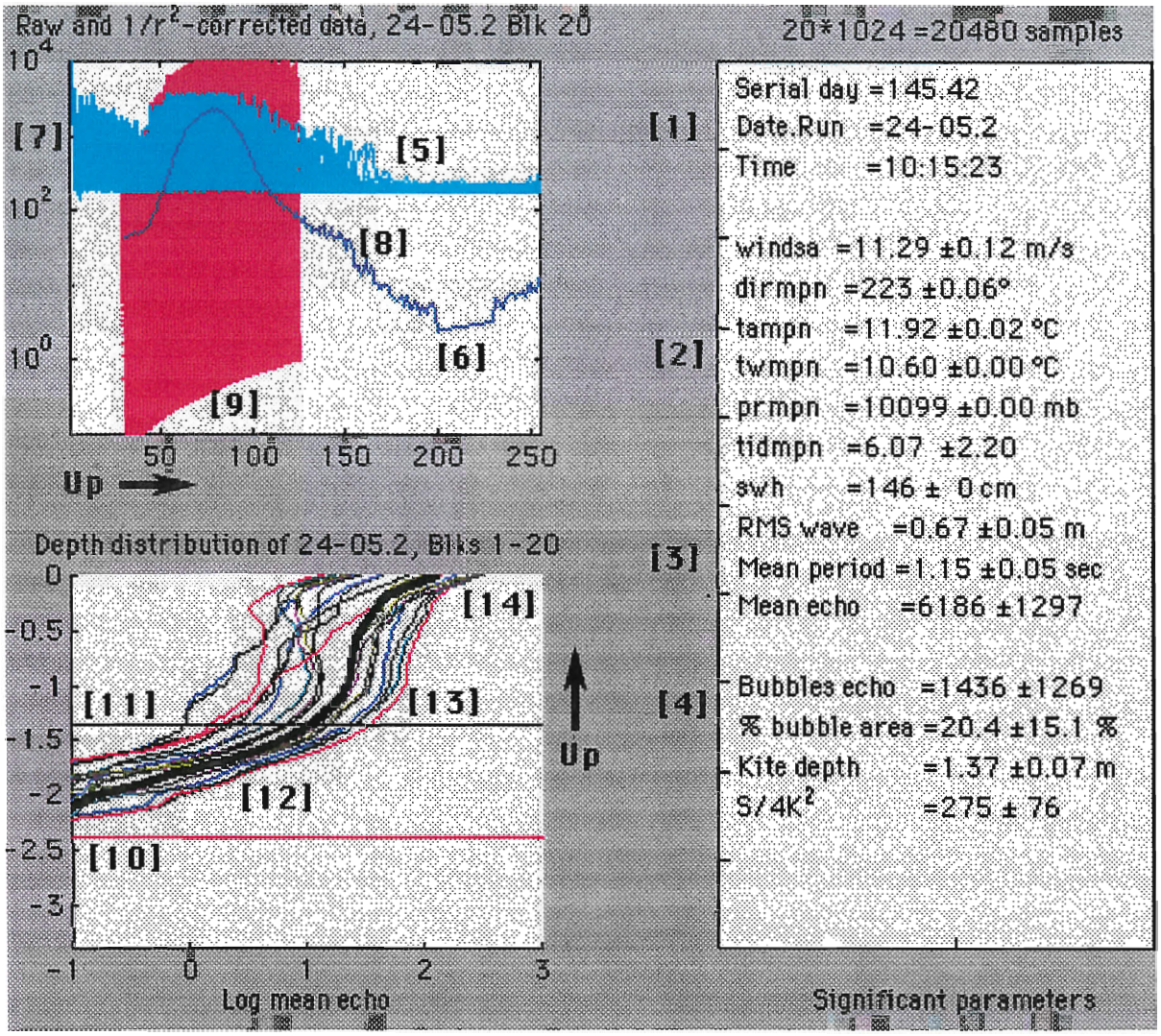

Fig. 2. 20-block (11.4 minute) Data Summary The right-hand panel contains several types of data. The 1st 3 lines [1] identify the run by serial date, calendar date and run number, and time at the start of the bock. The next 7 lines [2] present auxiliary data recorded on the tower as the mean and standard deviation of the block of 20 runs. In order, these are sonic-anemometer wind speed, wind direction, air and water temperature, tidal phase, and significant wave height. The next 3 lines [3] are data derived from the sonar analysis: root-mean-square wave height, mean wave period, and mean surface-echo strength. The mean wave period is derived from a 70-term Fourier/inverse-Fourier analysis, and omits both high-frequency noise (ripples) and periods longer than 30 seconds, both of which are evident on visual examination of the raw data. The next 2 lines contain the meat of the analysis [4]: the mean integrated strength of the echo from all bubbles within the water column, and this same number as a percent of the surface echo. The surface echo is an indeterminate function of instantaneous surface slope and curvature, while the echo from a calm sea can be taken as the 'instrumental response'. It may develop, upon further analysis, that the distance-scaled instrumental response is the correct normalizing function for counting bubbles. The last 2 lines are the mean kite depth, and a derived acoustical-strength function S/4K^2 which may yet prove useful.

The graph at the upper left in Fig. 2 shows the data for the last block in the series of 20. At [5] is the raw data (1024 echoes overlaid), perched on a surprisingly flat instrumental/environmental noise of undetermined origin. The mean of a 30-pixel stretch from the data-free area at [6] is subtracted individually for each echo, and any negative values are set to 0.1 for the logarithmic display. (The best location for this region is the bit that sometimes requires human intervention.)

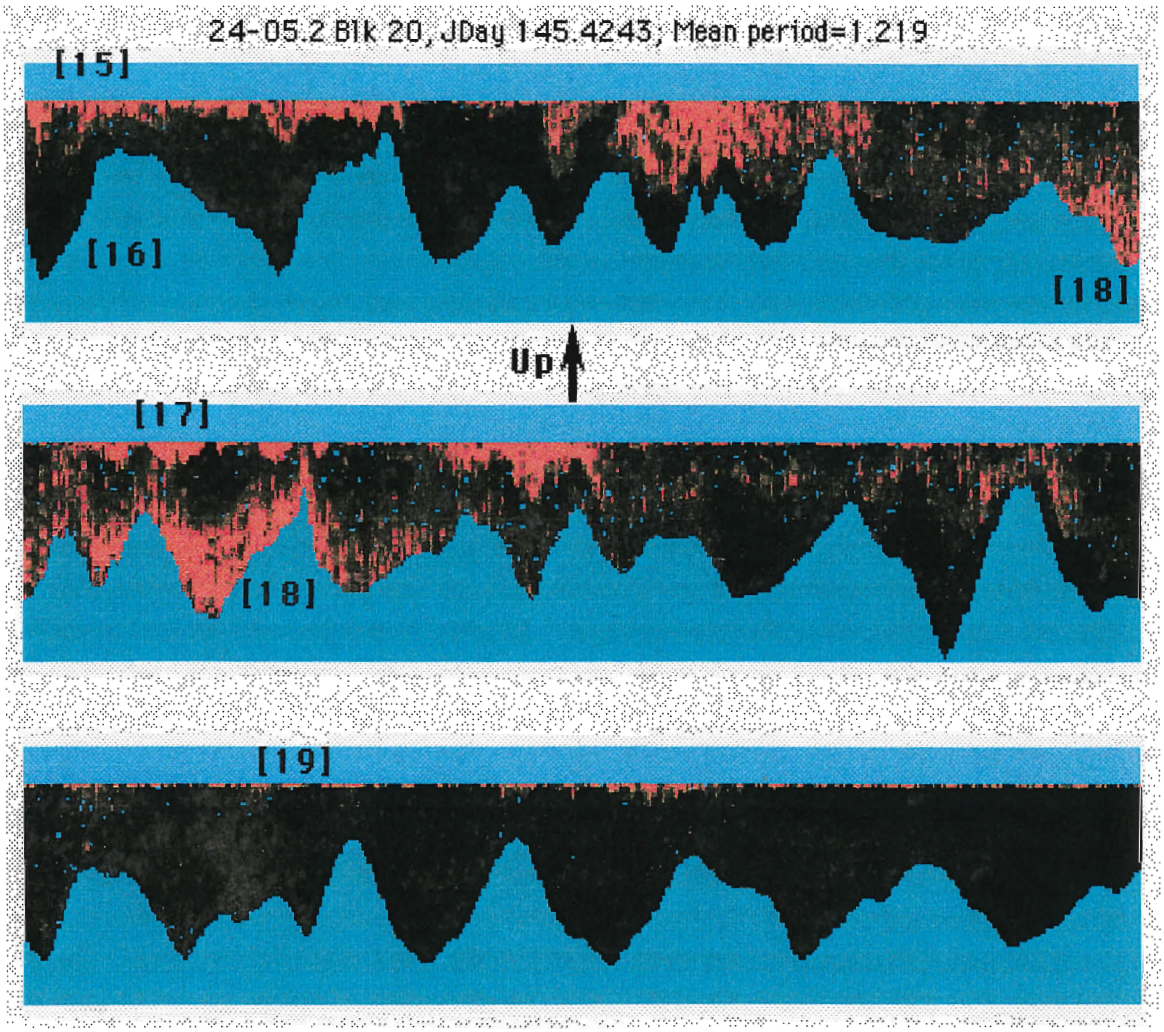

Fig. 3. Flattened-surface bubble distribution. The bubble clouds are tidally advected durng sampling. (The occasional cyan pixels among the tawny bubble clouds mark a particular echo-intensity level in the color map.)

The truncated, noise-subtracted data is then corrected for the distance-squared reduction of sound intensity. The average echo for the block is shown shown at [8], and the depth-overlap of signal and noise is particularly in evidence in this average. To reduce processing time, only the left-most portion of the data is retained [9], again shown with all echoes overlaid: this has been normalized to a point near the surface after the distance-squared correction. The curved lower boundary of this data shows the parabolic correction: notice that it extrapolates to join the 'noise-free' region [6]. The lower-left plot in Fig. 2 shows the bubble distribution (in terms of echo strength) vs depth in meters for each of the 20 blocks. The heavy line is the mean datum. The lower horizontal line [10] is the maximum kite depth during the run of 20 blocks, the upper horizontal line [11] is the mean depth. The sharp roll-off of the data between these lines [12] is an artefact: there are fewer echoes in the block mean below the mean kite depth, but the 4-decade logarithmic scale greatly over-emphasizes the real importance of this region. The artefact also continues for some distance above the mean depth [13].

Figure 3 is the processed version of Fig. 1. Because we are interested in the distribution of bubbles with distance from the instantaneous surface, the surface has been flattened here [15]. The kite depth at the bottom [16] is a vertically reflected mirror mage of the wave profile.

We see, in Fig. 4, bubble-cloud formation at the surface [17], deeper signals [18] which are remnants of the ambiguous response noted at [E] in Fig. 1, and superficial (1-pixel deep, ≤ 3.4 cm)) foam patches [19].

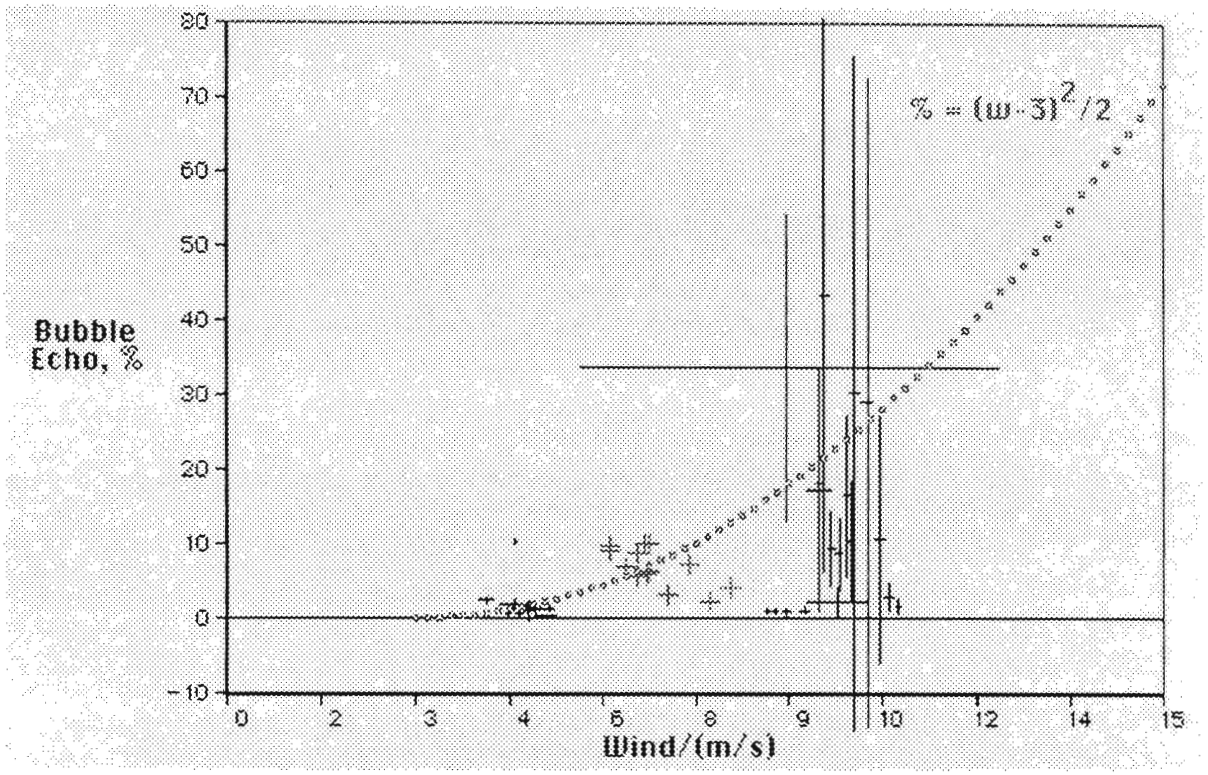

Fig. 4. Bubble surface area (normalized against superjacent sea surface area) vs wind speed. The curve, in this early version, is merely an eyeball fit.

Results

The principal result, at this stage, is the graph of Fig. 4 which plots the bubble surface area (as a percent of superjacent sea-surface area) vs wind speed. The 1-significant-figure parabola through 3 data clusters is % = 0.5(w - 3)^2, in reasonable agreement with other measures of bubbles vs wind speed.

The crosses at the data points span 1 standard deviation in all directions: the large increase at high wind speeds is real and merely reflects the sporadic nature of breaking waves. Additional parameters available from the tower data — such as tidal velocity, wave height, etc. — might ultimately reduce the experimental scatter.

Instrumental details

Not surprisingly, between the changing surface geometry, the presence of bubbles at the surface itself (foam patches), the shape of the acoustical pulse (recon-structed from verbal descriptions in Fig. 5), and the angular response of the transducer (Fig. 6), it is difficult to pinpoint the exact location of the surface.

Transducer construction and calibration left something to be desired. The 2-dimensional far-field angular response is shown in Fig. 6: the only way to reconstruct anything approximating the complex lobes shown here is by misaligning the 8 separate transducers in the arms of the Mill's cross structure by amounts of half a degree, but the complexity defeated every attempt to obtain a more exact mathematical model of the transducer. Given the symmetry of the Mill's cross design, we presume that the response in a plane at right angles to that of Fig. 6 was similar in shape, if different in detail.

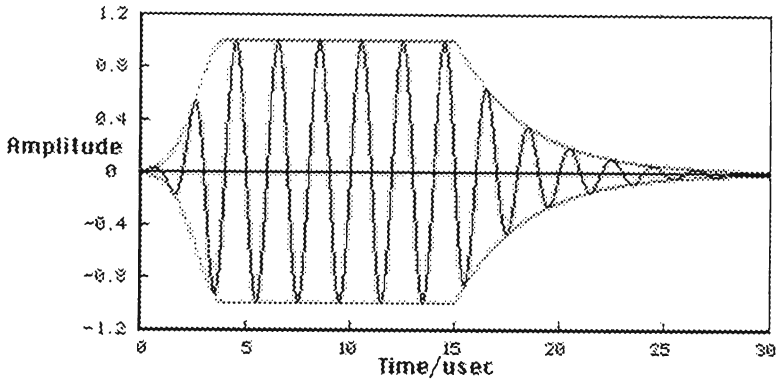

Fig. 5. Reconstruction of acoustical pulse shape. The electronic driving pulse had a rectangular envelope; the shaping appears to result from the impedance of and energy storage in the transducer.

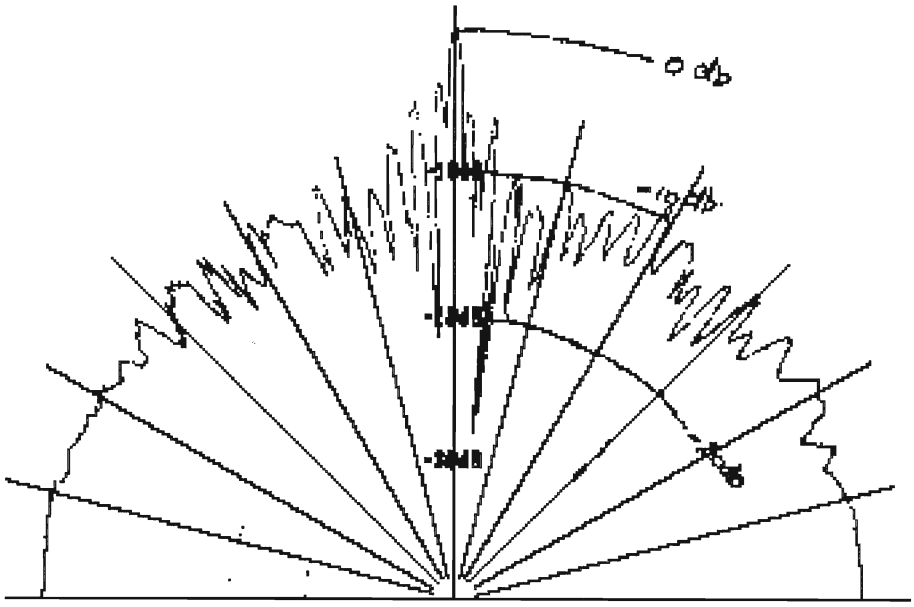

Fig. 6. Far-field calibration of transducer at 500 kHz by MOD Underwater Acoustic Calibration Centre Wraysbury. '3-db beamwidth = 1.5°, 6-db = 1.8°. Task # RE PV 346, 25Jul94'.

Given these problems, the attempt to locate the surface exactly is reduced to picking an arbitrary point on a steep slope of the increasing signal at [14] in Fig. 2. The actual point is a judgement call, and was estimated by allowing a bit of steep slope to appear in runs in which visual examination showed the presence of occasional foam patches at the surface. Some particularly calm-surface runs suggest that the chosen point may overestimate bubble fraction by a percent or 2.

There are a number of curious noise signals in the data: Indeed, the first few months of data analysis were devoted to squelching these as they showed up. Each new disk seemed to introduce a novel type of noise. The one shown in Fig. 7 appeared early, and was known colloquially as 'Radio 4'. It is as a fairly regular high-frequency noise superimposed on the data, which could on occasion be partially removed by setting its Fourier components to the background level. However, the perversity of inanimate objects is such that Fourier removal was inadequate because as can be seen in Fig. 7, the noise increased just below the surface (up in the ocean is down in the picture), doing its best to mimic the sort of bubble distribution one was hoping to detect.

Radio 4's most characteristic feature was its instantaneous switching. While it lasted for hours once it appeared, it switched on and off between one acoustical pulse and the next. If this is truly a

subharmonic of a radio signal (aliasing of the acoustical sampling frequency precludes any determination of the true frequency of the 'Radio 4' signal), it seems to represent pick-up by a ground-loop in the kite instrumentation leads.

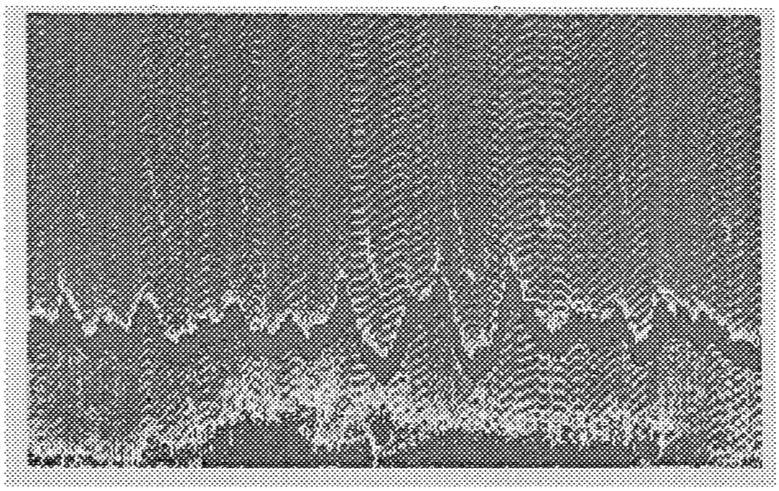

Fig. 7. 'Radio 4' noise in the original data record.

A 2nd noise source, which seems to be purely electronic and susceptible of removal if it could be identified, is the 'pedestal' indicated by the high base-line at [5] in Fig. 1. This is probably idiosyncratic to the data-collection system, and might have been eliminated if it had been noticed before deployment.
No attempt has been made to include 2nd-order corrections for such things as signal attentuation by bubbles in the path. As hinted in the caption in Fig. 4, the distribution of a particular echo intensity may be of interest. However, we do not attempt to make use of this in the present analysis because there is no way to distinguish between a strong return from a large bubble and the sum of weaker returns from small bubbles. The depth distribution of the particular 'cyan' intensity seems to offer no clues.

Recommendations
The transducer design required that the 8 individual transducers of each Mill's cross arm be epoxied to a substrate. The state of the art has advanced somewhat since the kite was built, and today the individual transducers would be made from a single block, thus ensuring a much more exact alignment. The existing transducer should be replaced.
Absolute far-field calibration is not required: more useful information can be obtained by relative autocalibration in a small tank. Echo strength from a flat water surface as a function of kite depth and 2-axis orientation is all that is needed.
Some way of measuring instantaneous kite orientation — a pair of 'digital bubble levels' — would be helpful in understanding what the transducer was examining at any moment.
Photographs of the kite in operation show that when it is near the surface (but still entirely submerged) it creates enough turbulence at the surface to generate its own bubbles. This appears to have happened in some of the runs. Between this ability, and the ease with which the kite appears to create its own near-field signal (which is identical to echoes from bubbles), it should preferably be flown a meter below the expected penetration depth of bubbles.
It should not be necessary, these days, to caution against ground loops! Next time we wire a kite, remember: One ground point only, to which all shields lead, and only one shield connected at the kite itself.
Given the bandwidth of the human eye/brain retina, there is no substitute for visual imagery. It would be an immense asset if the acoustical data were accompanied by video recordings. A sophisticated touch would be to illuminate only the acoustical beam, so that one saw exactly what the transducer was responding to. (This is not necessarily trivial to implement!)

APPENDIX
ASGAMAGE A-Kite Bubble-sonar-analysis Algorithm

A. Read disc; Preprocess data.

1. Select Run (tape/disc) and Block of 1024 samples
2. Obtain date and time for given block
3. Read appropriate raw data from disc
4. Get auxiliary data for this time (wind, waves, temperature, etc.)
5. Average the 1024 samples
6. Remove outgoing sound 5 pixels above near-kite minimum in average response
7. Zerobase by columnwise subtraction of maximum noise in data-free area
8. Set negative values of zerobased data to 0
9. Correct for r-squared dependence and normalize to surface response
10. Select a data strip extending 20 pixels above normalization point

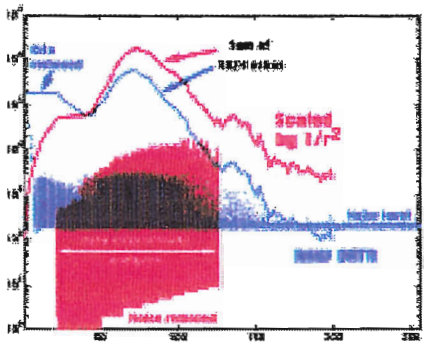

Fig. A1. Raw data (blue) and working data (red).

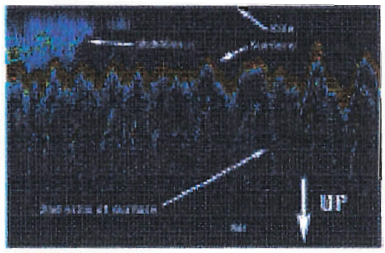

Fig. A2. Zero-based, noise-subtracted,

B. Locate and smooth surface for wave power spectrum

11. Find maximum signal in each column
12. Take 20% of maximum, or some higher intensity, as indicating surface
13. Replace individual weak signals with mean of neighbors
14. Find raw surface as pixel closest to kite and larger than chosen detection level
15. Use differential to detect and correct glitches
16. Reconstruct surface by integrating smoothed differential
17. Smooth with 5-pt running average
18. Calculate rms wave height

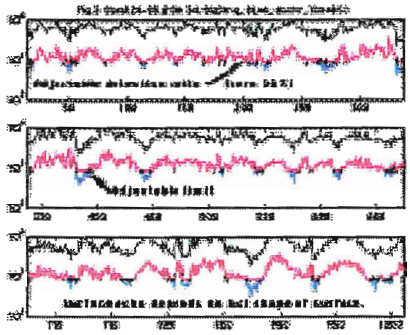

Fig. A3. Signal strength.

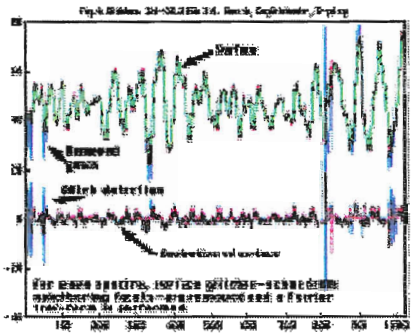

Fig. A4. Surface displacement and its differential.

19. Do FFT and 70-term IFT reconstruction for final smoothing
20. Determine kite depth as mean of distance to surface

21. Determine wave period from zero-crossings of inverse Fourier transform
22. Take 30-second subsample of IFT for power spectrum

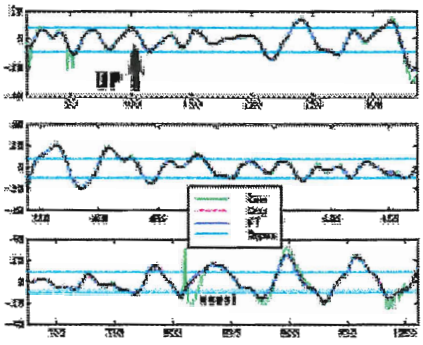

Fig. A.5 Inverse Fourier Transform

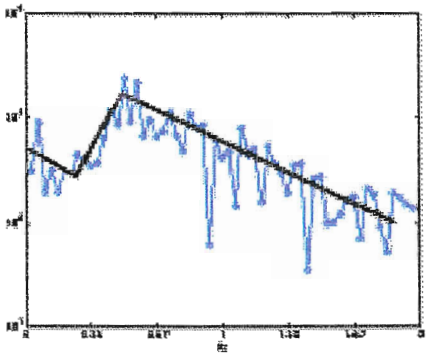

Fig. A.6 Wave power spectrum

C. Align surface, determine bubble area

23. Smooth raw surface with 3-point running mean
24. Align surface by moving surface echo to a common plane
25. Average this echo. In a quiet sea, this is the instrument response
26. If bubbles present, integrate echo from surface to kite for total bubble echo
27. Normalize echo to surface echo.
28. Publish.

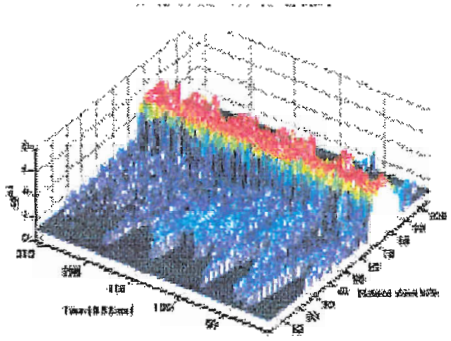

Fig. A.7. Aligned surface

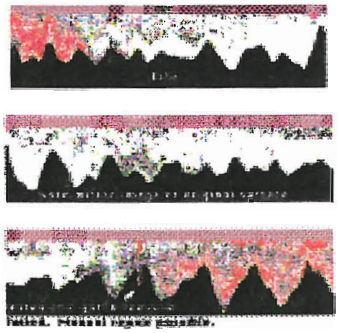

Fig. A.8 Flat surface withi bubble clouds.

Video measurements of near surface bubble spectra

Peter Bowyer

Abstract

Large bubbles (>300μm)have been observed at depths of between 10cm and 1.2m using a small video camera attached to a surface following float. In salt water, bubble spectra are presented for limited fetch and open sea conditions and in fresh water, for limited fetch conditions. The void fractions and areas of the observed bubbles are calculated. Measurements were made in a limited range of wind conditions (greater than Beaufort force 5). Video records were analysed by eye which introduced some uncertainty in the measured size and limited the number of sampled
bubbles.

1 Introduction

Large bubbles are of great importance for the enhancement of the exchange of soluble gases between the sea and air at higher windspeeds (Woolf, 1997, Keeling, 1993). However the number of measurements of the population of large bubbles in the field is limited. In addition, because large bubbles tend not to reach any great depth and to return to the surface a short time after their production in breaking waves, measurements need to be made near the surface for a long enough time to see some breaking waves.

Many experimental determinations of air sea gas transfer rates have been made in fresh water tanks. Fewer bubbles are produced by breaking waves in fresh water than in salt water (Cartmill and Su, 1993) and their size spectrum may be different (Bowyer, 1992). To aid extrapolation of fresh water results to the ocean, it is of interest to compare bubble production in fresh and salt water breaking waves in the field.

Medwin and Breitz (1989) used an acoustic resonator to measure the number of bubbles of radius <250 μm.at a depth of 30cm below a spilling breaker in Monterey Bay. They found a bubble size spectrum which had a slope of -2.7 for bubbles of radius >60 μm. In the laboratory, Cipriano and Blanchard (1981) have measured the bubble production by a wier in the laboratory. They found the bubble spectrum to have a slope of -1.5, which was similar to the spectrum measured by Bowyer (1992) from a jet of water falling into a small tank. Cartmill and Su (1993) used a similar device to that of Medwin and Breitz to measure bubble populations in a large wave tank. They found that a spectrum with a slope of -3 was a good fit to the measurements for bubbles of radius 100-1200 μm. These results are not necessarily inconsistent, since measurements of concentration (Medwin and Breitz, Cartmill and Su, this paper) give more weight to the smaller bubbles which have a longer residence time.

Large bubbles influence gas transfer by increasing the contact area between the atmosphere and ocean. The transfer velocity of large bubbles is in the range 30-40cm/hr (Woolf, 1993). The gas in a bubble comes into equilibrium with the gas in the water with a timescale which depends on the gas under consideration and the bubble size. This timescale is of the order 1s for bubbles of radius 1mm (Keeling, 1993) and CO2, and of the order 40s for a less soluble gas such as nitrogen, during which time the bubble would have risen 25cm (CO2) and 10m (N2). Therefore if the residence time of the large bubbles is <1s, the enhancement of gas transfer by 1mm bubbles can be approximated as the area of bubbles times the transfer velocity. A complicating factor here is
that the larger bubbles tend to occur in groups shortly after the passage of breaking waves: this may affect their residence time and their gas transfer. To allow for this process a measure of the time variation of large bubble concentrations is needed.

2 Apparatus

2.0.1 Surface following float

These are shown in figure 1. For all deployments, except the one off Valentia Island, a triangular rig was used. The rig, supported by trawl floats sat at the surface and was attached to a vertical frame which held the camera assembly and the screen; these were able to be moved up and down the frame as required. The float was tethered by the front frame, but the exact position depended on the deployment and was found by trial and error.

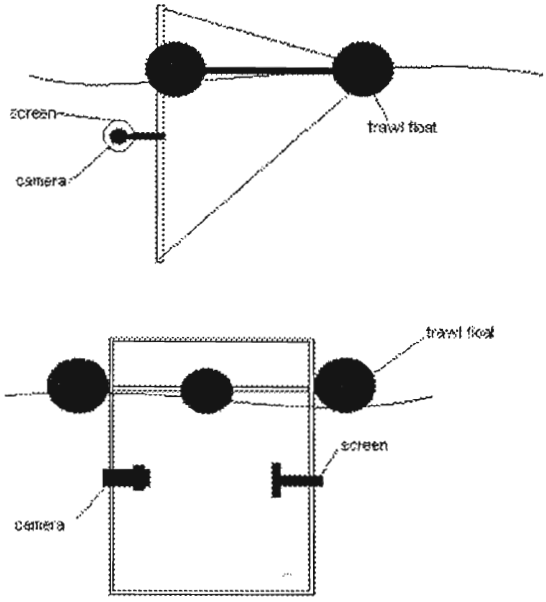

For the Valentia deployment, a simpler surface following spar was used, without a screen.

Figure 1: Surface following floats.

2.0.2 video cameras and recorders

A simple monochrome board camera was used (Radionics, Dublin). The resolution of the camera was 370 TV lines and it was equipped with an automatic shutter capable of working in light levels of >0.5 lux. A 16mm lens at f4 was focused at between 10 and 20cm in air(13 and 26 cm in water, depending on the deployment) using an extension ring: these settings corresponded to fields of view of between 2 and 4cm across in water.

The camera was housed in a waterproof case made from a 5 cm internal diameter ABS union, with a length of 20cm and an outside diameter of 15cm.

The pictures were recorded on standard VHS tape on a four head Mitsubishi video recorder which had a good freeze frame facility for analysis.

3 Method

3.1 Deployments.

Four deployments are presented, two at sea (Valentia and North Sound), one in a harbour at Dingle and one in fresh water (Kilbeg Pier, Lough Corrib).

Location	date	wind/waves	fetch	depths of measurement	salinity
Dingle Harbour	11/97	B7-8; 20cm	1.2km	10cm, 20cm,30cm	salt (30S)
North Sound	11/97	B5; 2m	unlimited	10cm	salt(34.8S)
Off Valentia Island	5/98	B5-6; 2.5m	unlimited	60cm, 120cm.	salt(35.0S)
Kilbeg Pier	2/98	B6-8; 20cm	1.0km	10cm, 20cm	fresh

Table 1: summary of the deployments presented in this paper.

At sea, the rig was deployed off the stern of the R.V.Celtic Voyager, and gaffed out using a boathook to a position just to windward and 3m off the stern of the vessel, which enabled measurements to be made in water which was not in the wake of the boat and also out of the
wind shadow of the boat. Careful note was made of the periods when the rig was judged to be in clear water and orientated into the waves.
For the Valentia deployment, the spar buoy was held away from the stern of the boat by a light boom and stayed to prevent sideways movement: the camera was pointed aft.

For the Dingle Harbour deployment the wind was blowing from the stern of the boat which was tied up outside two trawlers. The rig was gaffed out from the stern of the boat into undisturbed water 3-4m abeam.

For the fresh water deployment, an anchor was placed 40m to windward of the end of a pier and the rig was pulled out to the anchor using a light rope.

The scale was measured in the water using a ruler strapped in the field of view. Depth of field was measured by taking a video of a ruler held at 45 degrees to the camera.

3.2 Analysis of the data

Firstly, periods when the rig was correctly orientated and away from the influence of the ship were identified. For these periods, the video was played back one frame at a time and the bubbles counted and sized by eye. More than 5000 frames were analysed for each condition.

Bubble sizes were measured on the video screen and scaled. For elliptical bubbles, the radius was taken to be the average of the major and minor axes.

Bubbles were sorted into bins whose upper size limit was sqrt{e} (about 1.65) times their lower limit. This rather coarse binning was deemed necessary because of the uncertainty in the size measurements. The bin size was then calculated on the basis of a power law spectrum of slope -2.5. This caused the bin size to be shifted slightly from the average of the upper and lower bin radii. Time series of bubble sizes, and blank frames were recorded.

4 Results.

4.0.1 Bubble spectra

These are shown in figures 2-3

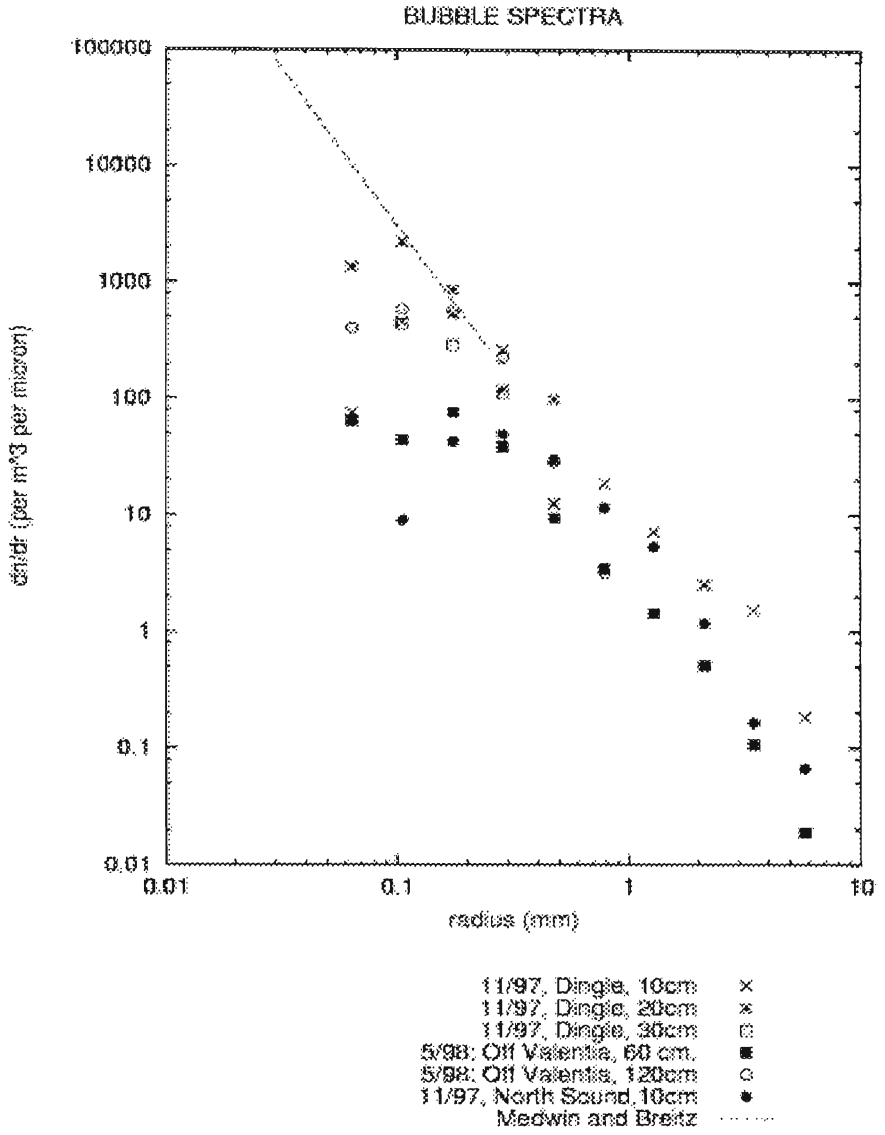

Figure 2: Bubble spectra measured at the salt water locations. Medwin and Breitz(1989) included for comparison.

All bubble spectra have a peak at about 0.1mm, which reflects an inability to detect smaller bubbles and is an artefact.

In Dingle Harbour the rapid variation of the bubble spectrum with depth is apparent. No bubbles of radius >1mm are observed at 20cm depth. Medwin and Breitz' spectrum is a good approximation at these depths.

The open sea measurements off Valentia show bubbles of radius 6mm at 60cm depth but no bubbles of radius >1mm were seen at 120cm. The wave height here was about 2m, and these observations are consistent with the breaking wave plume penetrating to half the wave height, as observed by Rapp and Melville (1990).

Fresh water data is shown in figure 3.

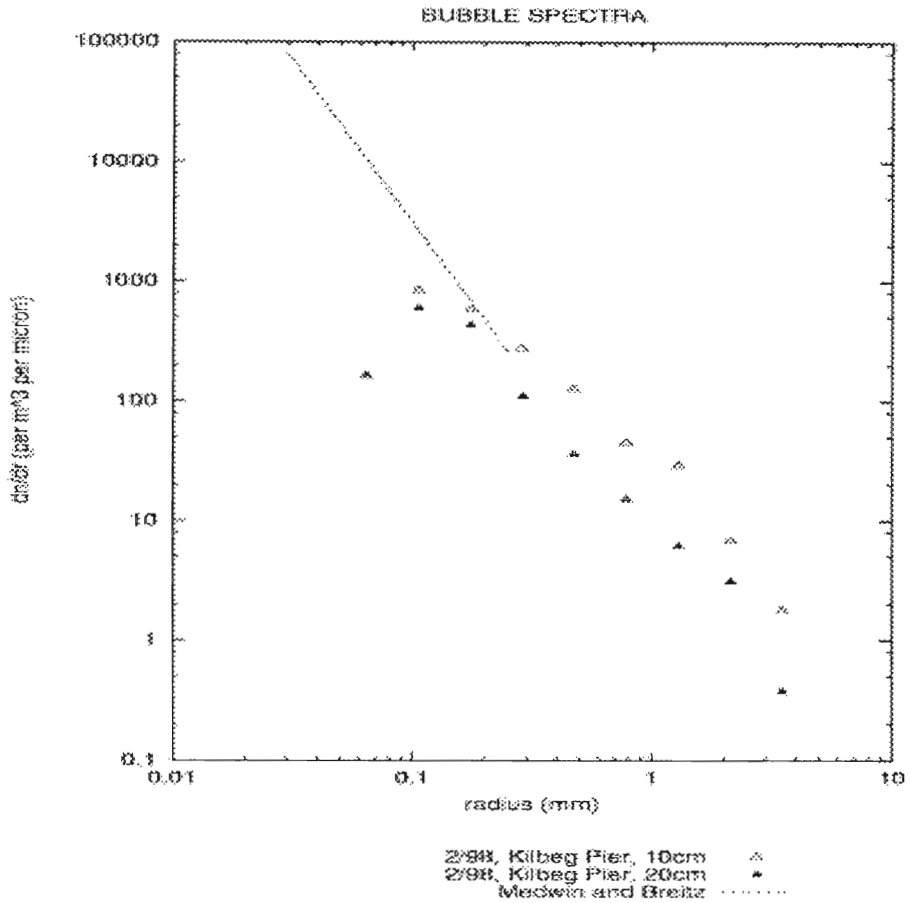

Figure 3: Bubble spectra in fresh water.

In this case there is a sharp decline in bubble population with depth, which may reflect the wave height of 15 cm. In addition there is a smaller spectral slope in the surface spectrum between 0.3mm and 1mm, which may reflect a change in the production of bubbles in fresh water compared to salt water. However the bubble numbers at 10 cm depth are not too far from the bubble numbers observed in similar conditions in Dingle

4.0.2 Cumulative distributions of bubble area and bubble volume.

The bubble spectra above are calculated by dividing the total number of bubbles in a particular size range by the total volume sampled. These measurements say nothing about the probability of seeing a particular void fraction or bubble area in the sample volume. Because the large bubbles occur just after breaking waves, the probability of seeing them is quite small and most of the frames contain few or no bubbles. Figures 4 and 5 show the same measurements as figures 2 and 3 but presented as cumulative distributions of bubble number, area and volume.
The slope of these graphs indicates the fraction of the sample frames that contain a given volume or bubble area.

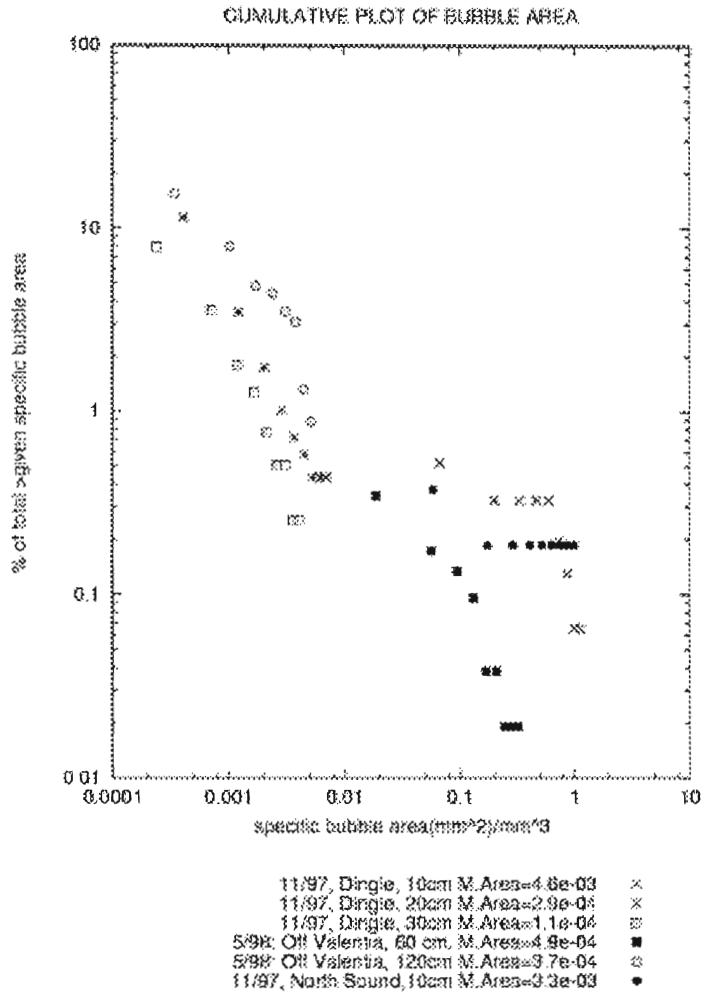

Figure 4: Cumulative distribution of bubble surface area.

The mean areas must be multiplied by the e-folding depth of the bubble concentrations, so that in Dingle, the total area of the bubbles is 70% of the surface area, assuming an e-folding depth of 15cm.

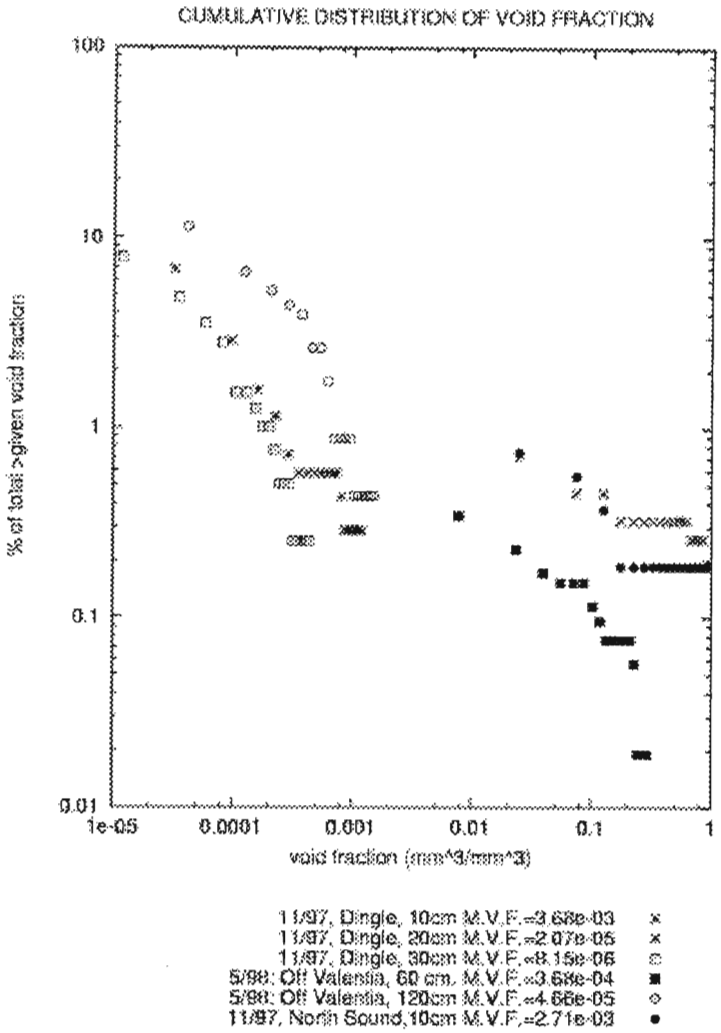

Figure 6: Cumulative distribution of void fractions.

The cumulative volume distributions show the probability of a given void fraction in the sample volume. At depths >20cm in the limited fetch conditioins in Dingle Harbour and >60cm in open sea conditions, void fractions $>2.10^{-3}$ are not seen. For the shallower measurements there is a 0.5% chance of seeing a void fraction of >0.1.

5 Discussion

5.1 Void fraction

Lamarre and Melville (1991) observed void fractions of 20-30% at a time of 0.1-0.2 periods after a laboratory breaking wave near the surface,decreasing to about 1% after 0.9 periods. In the shallower measurements above, a void fraction of 1% is exceeded about 1% of the time. In Dingle, for example, the fraction of waves which were breaking was between 20% and 50%. If the laboratory data is applied in these conditions, void fractions of 1% should be visible for about 1/3 of the time. In fact they were observed for about 1/30 of this time: this may be because not all bubble plumes penetrate to 10cm, and the waves are spilling breakers as opposed to the steep plunging breakers used by Lamarre and Melville (in the absence of wind).

5.2 Bubble Area

This quantity must be integrated over depth to give the total bubble area in a given situation. For Dingle, an e-folding depth of the order of 10cm can be assumed and this gives a total surface of 0.46.

This translates to a bubble induced exchange velocity of 0.46 K_w where K_b is the bubble transfer velocity, i.e. about 20cm/hr if K_w is assumed to be 40cm/hr.

Acknowledgements
This work was supported by the EU ASGAMAGE Project, MAS3-CT95-0044. The assistance of the crew of the Celtic Voyager, Tom Furey and Tom Creaven was much appreciated.

References

Bowyer P.A. The rise of bubbles in a glass tube and the spectrum of bubbles produced by a splash. Journal of Marine Research; 50(4); pp 521-543; 1992 .

Lamarre, E.; Melville, W. K. Void-fraction measurements and sound-speed fields in bubble plumes generated by breaking waves. Journal of the Acoustical Society of America; 95(3); pp 1317-1328; 1994 .

Cartmill, J. W.; Ming Yang Su, Bubble size distribution under saltwater and freshwater breaking waves. Dynamics of Atmospheres & Oceans; 20(1-2); pp 25- 31; 1993 .

Woolf, D. K. Bubbles and the air-sea transfer velocity of gases. Atmosphere-Ocean; 31(4); pp 517-540; 1993 .

Cipriano, R.J., and D.C. Blanchard, Bubble and aerosol spectra produced by a laboratory "breaking wave", J. Geophys. Res., 86, 8085-8092, 1981.

Medwin, H. and N.D. Breitz. 1989. Ambient and transient bubble spectral densities in quiescent seas and under spilling breakers. J. Geophys. Res., 94, 12751-12759.

Medwin, H. and A.C. Daniel, Jr. 1990. Acoustical measurements of bubble production by spilling breakers. J. Acoust. Soc. Am., 88, 408-412.

Measurements of total gas saturation at a range of wind conditions

Peter Bowyer and David Woolf [1)]

[1)] School of Ocean and Earth Sciences, European Way, Southampton, U.K.

Abstract

Total gas saturation was measured at the Meetpost Noordwijk Tower (MPN) off the Dutch Coast for two periods of about one month as part of the ASGAMAGE experiment and in Lough Mask, Ireland for a period of ten weeks in the winter. Variations in total gas saturation were driven by changes in temperature of the water column, bubble induced supersaturation and variations in atmospheric pressure. The gas saturation was modelled by calculating the air sea flux and comparing the resulting timeseries with the observations. The model results weakly constrain the transfer velocity and bubble induced supersaturation. Transfer velocity and bubble induced supersaturation are both reduced for the lake experiment.

1 Introduction

Total gas pressure can be measured at sea by measuring the pressure inside a silicon membrane (Anderson and Johnson 1992) tube (Bowyer,1996). Total gas pressure in the ocean follows atmospheric pressure. Nitrogen is usually near equilibrium with the atmosphere; but where oxygen concentration varies, it can contribute significantly to the variability in the total gas pressure. In the presence of breaking waves bubbles carried below the surface can force supersaturation when they dissolve (Thorpe, 1982). Temperature changes act to change saturation through changes in solubility. Farmer and MacNeil (1993) have observed bubble induced supersaturations in coastal conditions.

For a well mixed layer of depth d in contact with the atmosphere, the flux of gas from the atmosphere to the ocean may be expressed as

$$F = K_w (C_a - C_w + S_b)$$

where K_w is the transfer velocity, often expressed in cm/hr, C is the atmospheric concentration times the Henry's Law constant, C_w the concentration of the gas in the water and S_b the supersaturation induced by bubble dissolution. Since

$$F=h\, dC/dt,$$

if C_a and S_b are constant, C_w approaches (C_a+S_b) with a time constant $\tau=h/K_w$.
For a depth of 17m, and a transfer velocity of 20cm/hr, τ is 85 hours. Similarly, for a step change in C_a or S_b, C_w approaches the new equilibrium with the same time constant. If C_a or S_b changes for a for a shorter period than several τ, equilibrium is never reached. This might be the case for a depression moving across a measurement site, bringing high winds, low air pressure (C_w and high bubble induced supersaturation (S_b)for a day or two.

The gas saturation (G) is usually expressed in atmospheres: 100% saturation implies that the sum of the partial pressures of the dissolved gases is 1 standard atmosphere, or 1012mB. $G=C_w/\alpha$
where α is the solubility in kg/(m^{3}atmosphere), so

$$dG/dt=(d(C_w)/dt)/\alpha-Gd(\alpha)/d.$$

Combining the above,

$$dG/dt=(P_a-G+S)/\tau-D(\alpha)/dt.(G/\alpha)$$

where P_a is the atmospheric pressure (in %) and S is the equilibrium supersaturation in atmospheres. The change in solubility with temperature is close to -2%/°C, so

$$dG/dt=(P_a-G+S)/\tau+0.02G.dT/dt$$

where T is the temperature.

Since dT/dt may be on average consistently positive or negative for periods much longer than τ, it may cause the long term average saturation to be out of equilibrium, e.g. for a period of autumnal cooling.

In these conditions, the behaviour of the gas saturation may be governed by the heating or cooling of the water column, with the shorter term variations in τ and S modulating the flux of gas into or out of the water.

2 Instruments

Two self recording total gas saturation meters were built at N.U.I., Galway. The design was simple: a 3" outside diameter ABS tube and union formed the case. A pressure sensor (Radionics, Ltd. Dublin, 0-15p.s.i., differential) was connected to the membrane via a thin bore metal tube which passed through the bulkhead of the casing via a Swagelok connector . A silicon tube acted as a membrane. The instruments were deployed at depths of 5 and 12m. To withstand the hydrostatic pressure, tubing of outside diameter 3mm and inside diameter 0.5mm was used. This tubing was tested to the required pressure by enclosing it in a length of vacuum tubing filled with water and increasing the pressure using a syringe, while observing the silicon tube under a
dissecting microscope. Little change in size was observed. Then the experiment was repeated with the tube connected via a water filled pipe to a pressure gauge. The pressure increased by <5% for an external pressure of 6 atmospheres. The response time of the instruments was
tested by immersing their membranes in a solution of sodium sulphite. The e-folding time was about 25 minutes. The signal from the pressure sensor was amplified using an instrumentation amplifier (Analogue Devices AD624) and recorded at 40 minute intervals on a Tinytalk 8
bit data logger (Radionics, Dublin). This data logger switched on the sensing circuit 300mS before a measurement to conserve power.
The pressure sensor recorded the pressure difference between the air inside the ABS tube and the gas inside the silicone membrane, which was in equilibrium with the gas in the water. The pressure and temperature inside the tube was recorded when the tube was sealed before deployment and subsequently calculated from the in situ temperature of the tube.

Temperature was recorded by YSI 6000 probes which were mounted adjacent to the total gas meters. These instruments recorded water temperature with a sensitivity of 0.1 °C and were calibrated before the deployment.

For the Mask deployment , the self recording temperature sensor consisted of a precision temperature sensing chip (LM135, Radionics, Dublin), connected to a data logger. The instrument was calibrated before and after deployment and found to be accurate to 0.2°C.

Meteorological parameters were recorded on the MPN tower as part of the ASGAMAGE experiment (Oost, 1998)

3 Deployment

For both deployments two TGMs were deployed at depths of 5 and 12m on the sensor pole on the SW corner of the MPN tower. The tower is located in 17m of water 9km off the Dutch coast in a region of freshwater influence (the Rhine plume, described e.g. in de Ruijter et al, 1992).
Tidal currents in the region are quite rectilinear (major axis of the tidal ellipse is about 10 times the minor ellipse) with a tidal excursion of up to 15km at springs. The water column was occasionally stratified in the spring deployment and usually well mixed for the autumn deployment.

The deep sensor failed in the second deployment.

Lough Mask is a lake of approximately 10km x 10km, situated in County Mayo, Ireland. Its mean depth is 17m but, because the lake is divided into a shallow Eastern half and a deep Western half, there is a strong topographically controlled flow regime in the lake which causes rapid mixing, especially for winds orientated along its axis, i.e. SW-NE (Bowyer 1999).

For the lake deployment, one gas TGM with an internal temperature logger was deployed at a depth of 10m in the deepest part of Lough Mask.

4 Results and data analysis

Air pressure inside the ABS tube was calculated from the YSI temperatures. Then the pressure inside the silicone membranes was calculated from the recorded signal (pressure difference across the pressure sensor).

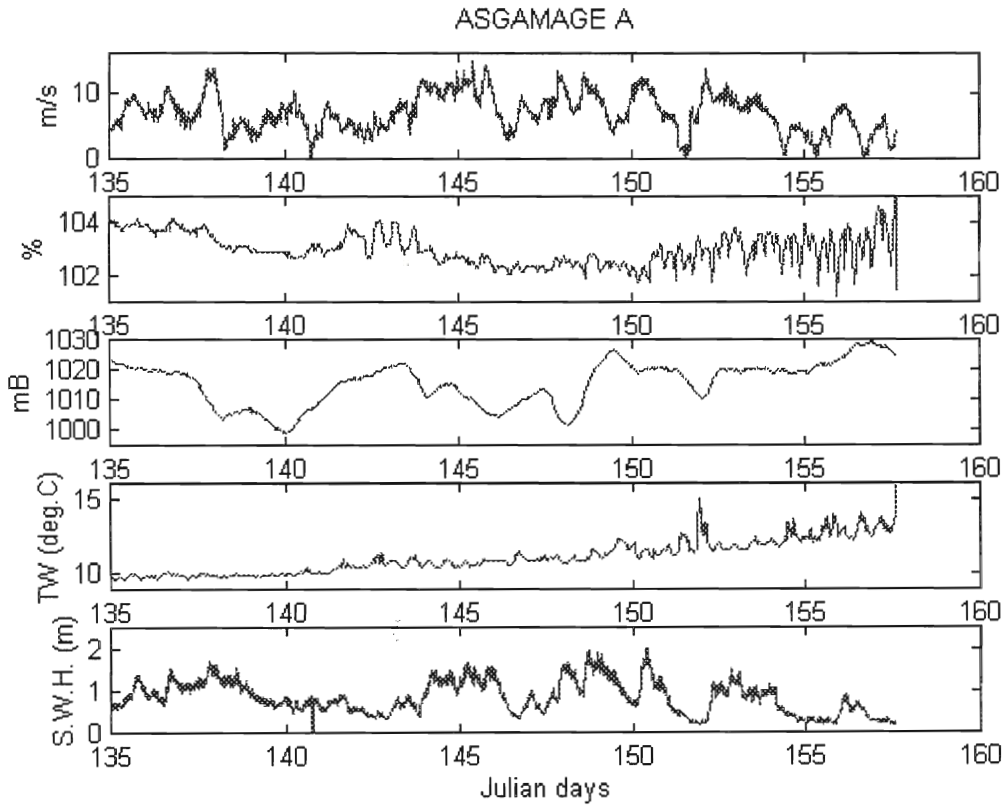

Figure 1: Conditions during the first ASGAMAGE deployment (May-June, 1996). X axis is day number.)

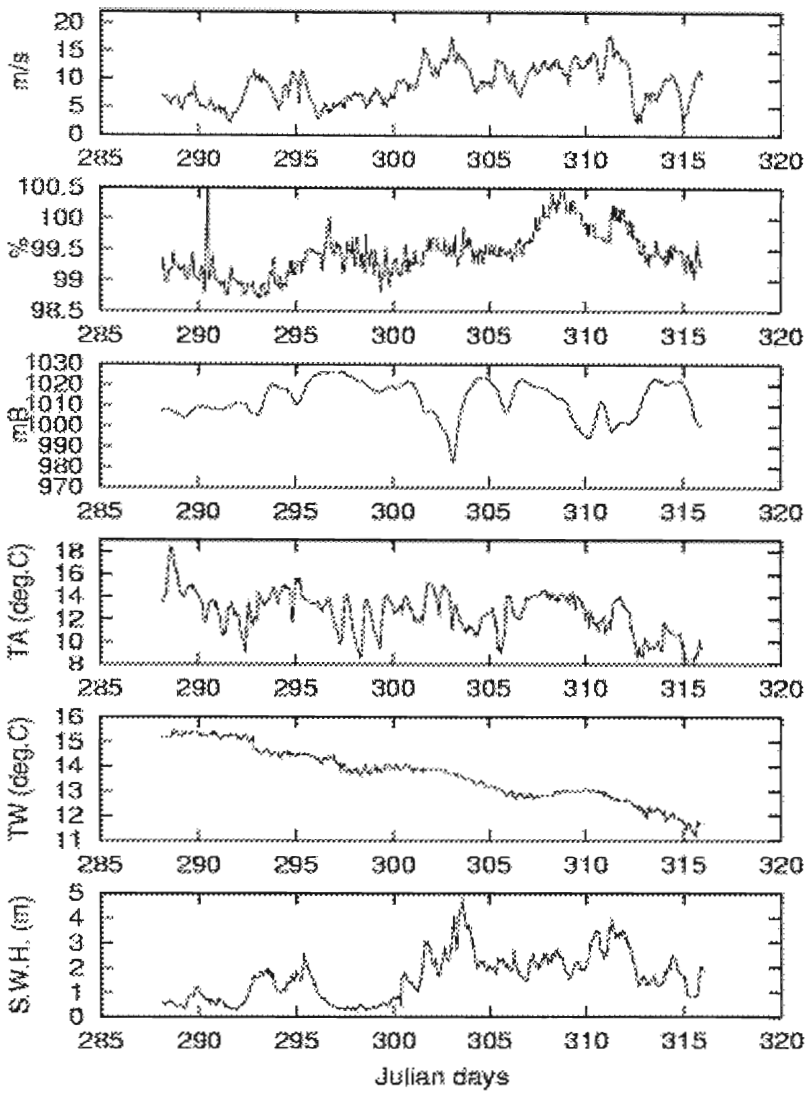

Figure 2: Conditions for the Autumn deployment.

For the spring data (figure 1), supersaturation is apparent in the data, which is expected from the rise in water temperature but possibly of biological origin. Towards the end of this deployment, differences in temperature and saturation indicate the presence of stratified conditions.
For the Autumn deployment (figure 2), winds were higher and the water column was cooling. The spike in gas saturation on day 290 occurred when the sensor pole was lifted out of the water for a short period.

Tidal signals were removed by filtering the data using a 12 hour low passfilter. Figure 3 shows the filtered and unfiltered data.

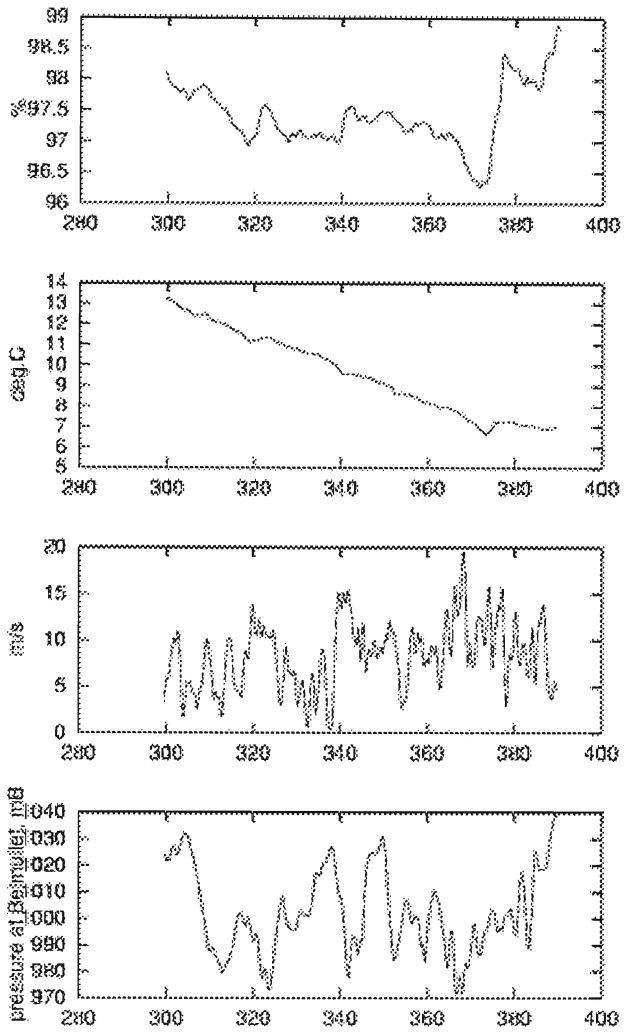

Figure 3: Conditions for the Lough Mask deployment. Windspeeds are from Belmullet, 60 miles NE of the Lake.)

For each dataset the dependence of the gas saturation on the rate of change of the water temperature is clear. Brief warming periods in the ASGAMAGE B (day 308)and Mask (day 375) deployments are associated with increases in gas saturation. At the same time, the air sea gas flux is controlled by the air sea concentration difference, which depends strongly on the air pressure and less strongly on the gas saturation, the bubble induced supersaturation, which depends strongly on windspeed, and the transfer velocity, which depends on windspeed.

Filtered timeseries of windspeed, air pressure and gas saturation were used as the basis for a model. This model is based on similar work by Woolf (1996) and fits the observed gas saturation in terms of the air-water pressure difference, transfer velocity and bubble induced supersaturation.

Here, both transfer velocity (k) and bubble induced supersaturation (b) are assumed to vary as the square of the windspeed: $k=k_{10}(U_{10}/10)^2$ and $b=s_{10}(U_{10}/10)^2$. The coefficients s_{10} and k_{10} are varied and a timeseries of gas saturation calculated using the above equations. For each set of values of (k_{10},s_{10}) the mean square difference between the model predictions and the observed data is calculated.

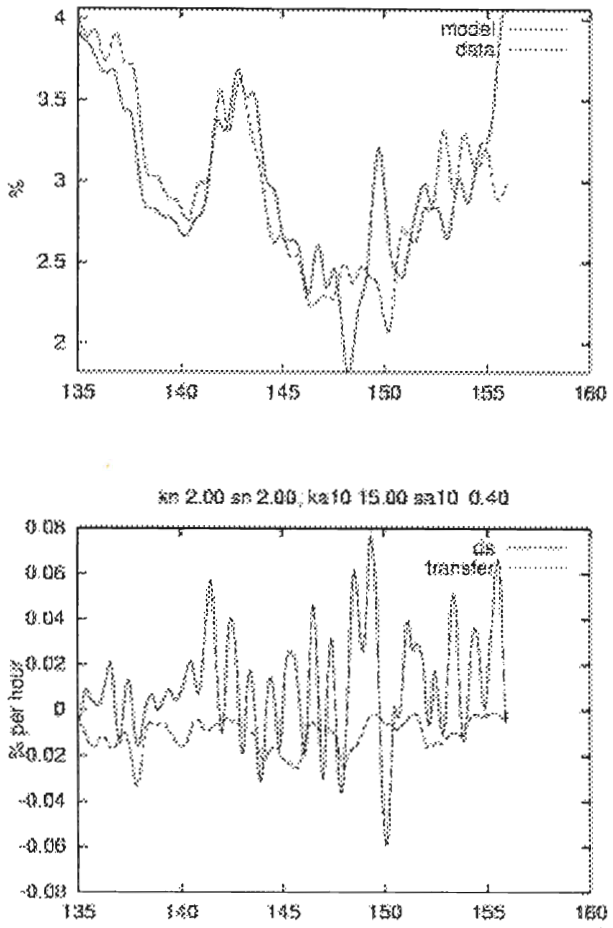

Figure 4: Model results from ASGAMAGE A. Top panel shows data and model output. Bottom panel shows ds, 2dT/dt, the change in saturation due to the change in temperature of the water column, and the change in saturation due to the transfer of gas across the air sea interface.

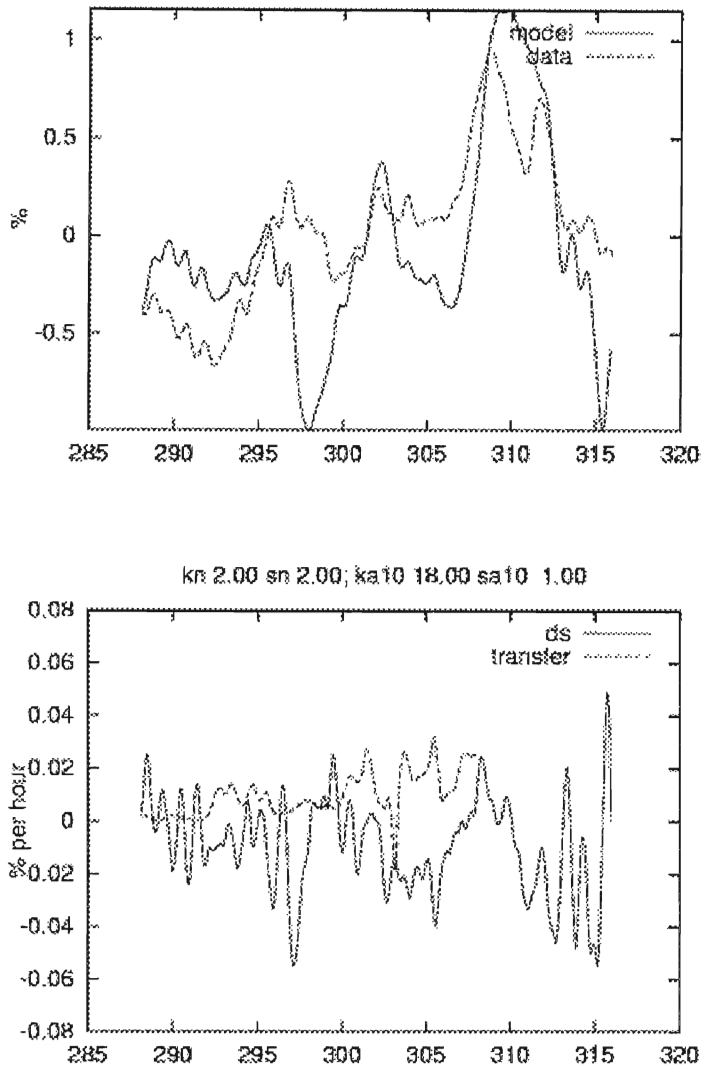

Figure 5: Model results and data from ASGAMAGE B, October-November 1996.

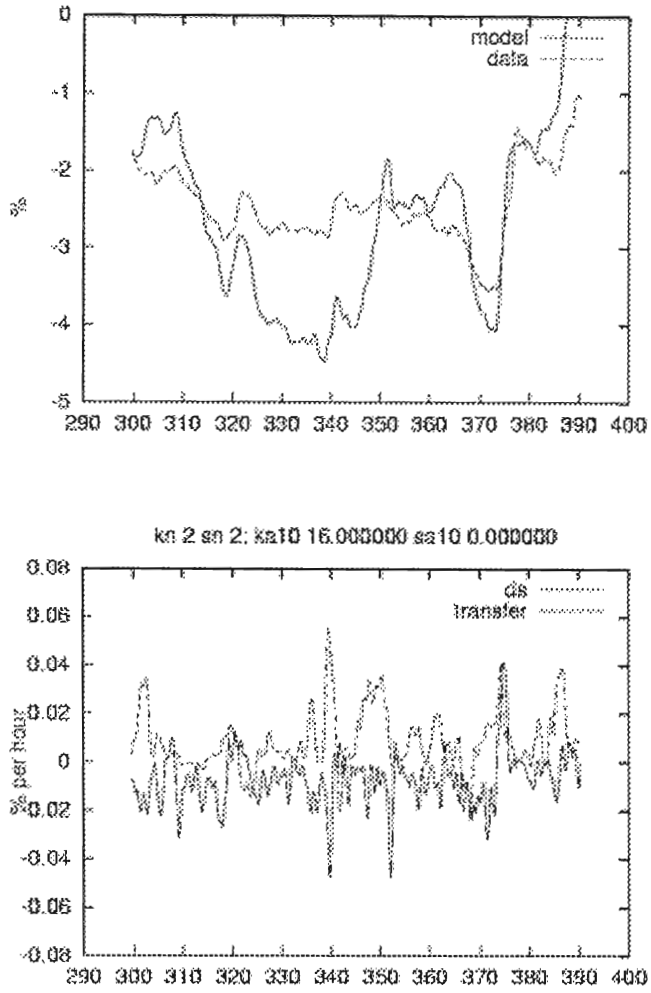

Figure 6: Model results and data for Lough Mask deployment, winter 1997/8. Note that the day numbers greater than 365 indicate January 1998.)

5 Discussion

5.1 Advection at the North Sea site.

Short term changes in measured water temperature tend to be dominated by advective terms. For example, temperature changes of 0.5°C/hr occur on many occasions; in a well mixed water column of 17m depth, this corresponds to a heat flux of about 10KW., compared to measured values of O(100)W/m^2. In addition, variations in gas saturation of the order of 0.5% were apparent in the gas saturation signal. Therefore the gas, temperature, wind and pressure signals were smoothed to remove the tidal component before the model was run.

As an alternative to this approach, current meter data from the site were used to produce a timeseries of longshore displacement. Changes in gas concentration and temperature were calculated between periods of equal longshore displacement. These changes were close to the smoothed data.

The tidal excursion at the North Sea site is of the order of 10km, while the residual current is of the order 5cm/s, so the smoothed data represents the mean gas saturation and temperature of a 10km long patch of water measured at a position which moved at 5km/day with respect to the water column. Over

an experiment of 30 days, the effective 'measuring site' therefore moved about 150 km with respect to the water column. Advective changes in the signals can therefore
be expected. The model's ability to predict rates of change of gas saturation should be less affected.

5.2 Sensitivity of the model

A contour plot of the mean square difference between the model and the Autumn MPN observations is shown in figure 7. The best fit between

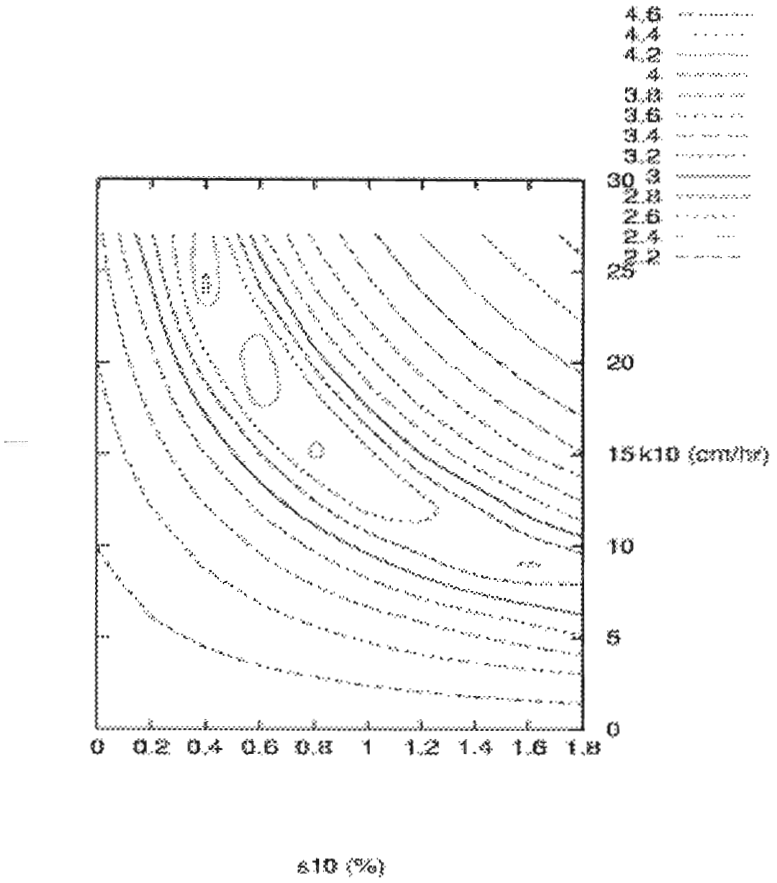

Figure 7: Residuals from the model for ASGAMAGE B. Contours are log10 (mean square difference between the model and the data). s_{10} is the bubble induced supersaturation (s) at 10m/s, k_{10} is the transfer velocity (k_w) at 10m/s. Both s and k_w are assumed to vary as the square of the windspeed.

the model and the data is found at about k_{10}=23cm/hr and s_{10}=0.4%, but lower k_{10}'s in combination with higher s_{10}'s also give a good fit. This is probably a result of the dataset being from a period of water column cooling. On average the water column is subsaturated and there is a net flux into the water column (see figure 2).
This flux increases with windspeed and the model can do this by increasing either k or s. On the other hand, the residuals from the ASGAMAGE A model, where the water column was warming, show good agreement for a range of k_{10}'s which increase with higher s_{10}.

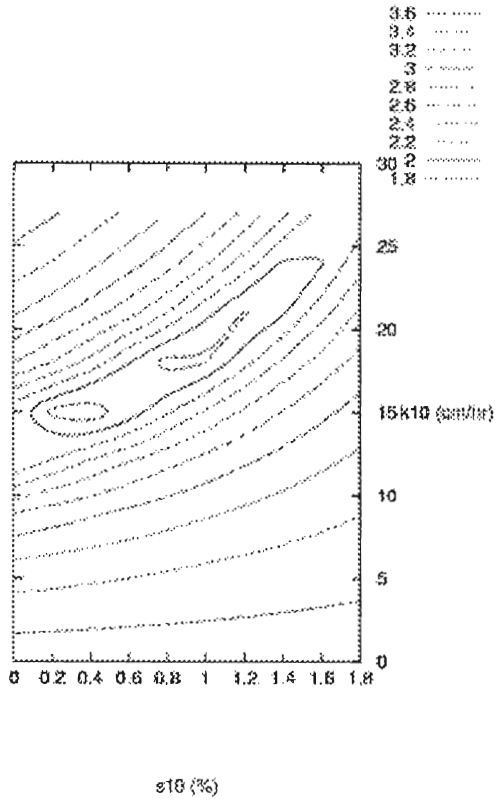

Figure 8: Contour plot of ^{10}log of the mean square deviation of the model and data, ASGAMAGE A.

If it is assumed that the variations in transfer velocity and bubble induced supersaturation are the same for both ASGAMAGE deployments, the range of possible k_{10}'s and s_{10}'s which are a good fit to both datasets is much smaller.
This can be shown from figure 10, where the best fit to both datasets is k_{10}=17cm/hr and s_{10}=0.6%,

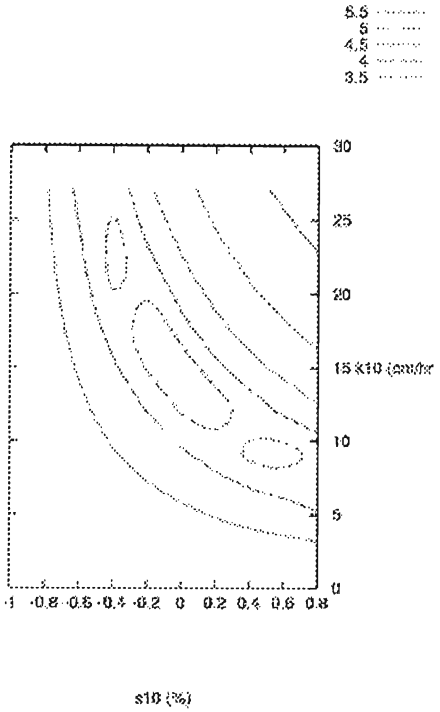

F igure 9: Residuals from the Mask deployment. Contours as for figure 7.

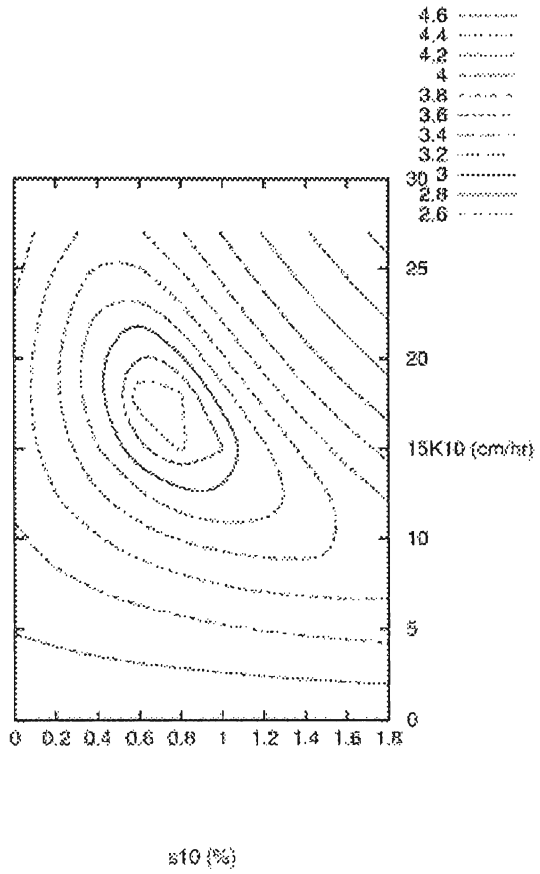

Figure 10: Contour plot of the log of the sum of the residuals from figures 8 and 9

5.3 Comparison of results with other data

The best fit transfer velocity, adjusted to Schmidt number 600, assuming a $Sc^{-1/2}$ relationship is given by $0.14(U_{10})^2$ (cm/hr), which is rather less than with Waninkhof's 1993 parameterization and is comparable to Liss and Merlivat (1983). However the values obtained here are not sufficiently sensitive to decide between the parameterizations, if indeed that is a worthwhile activity . The value for the supersaturation, $0.006(U_{10})^2(\%)$ is somewhat smaller than other estimates (Woolf, 1993).

The above results are all based on the assumption that both the supersaturation and transfer velocity vary as $(U_{10})^2$.

Assuming the value for k_{10} is the same in Lough Mask, figure 9 indicates that the wind induced supersaturation for the fresh water case is smaller than for the other deployments. This is consistent with the relative scarcity of small bubbles in fresh water (e.g. Thorpe, 1982). These bubbles have a low rise speed and are therefore more easily carried to depth where they dissolve, causing the supersaturation.

6 Conclusions

Time series of total gas saturation measurements were obtained at the MPN tower in the Southern North Sea during the ASGAMAGE experiment and in Lough Mask during winter 1997/8. In the spring, the water column was slightly supersaturated, while in the autumn, there is a slight subsaturation. In the lake, saturation shows a rapid increase for a short period of warming following a prolonged cooling. This was modelled assuming parabolic variation of transfer velocity and gas supersaturation for the and the best fit for the model was obtained with a k_w similar to that obtained by Liss and Merlivat and a supersaturation which was given by $0.006(U_{10})^2$.

Acknowledgements
This work was supported by the EU ASGAMAGE Project, MAS3-CT95-0044. The assistance of K.N.M.I and Rijkwaterstaat was essential as was that of Tom Furey and Tom Creaven and Marcel Cure.

References

Anderson, M.L., and B.D. Johnson, 1992: Gas transfer: A gas tension method for studying equilibration across a gas-water interface. J Geophys. Res., 97, C11, 17899-17904.

Bowyer, P.A. 1996: Total gas saturation measurements off Inisheer: Final Report, MAST CT930056m 'The investigation of the influence of bubbles on air sea interaction', 1996, Brussels, DGXII

De Ruijter, W.P.M., A. Van der Grissen and F.C. Groenendijk, 1992: Current and density structure in the Netherlands coastal zone. Pp 529-550, in Dynamics and exchanges in estuaries and the coastal zone, ed. D. Prandle, A.G.U., Washington.

Keeling, R. F., 1993: On the role of large bubbles in air-sea gas exchange and supersaturation in the ocean. Journal of Marine Research; 51(2); pp 237-271.

Liss, P.S. and L. Merlivat. 1986. Air-sea gas exchange rates: introduction and synthesis, in The Role of Air-Sea Exchange in Geochemical Cycling, P. Buat-Menard, ed., D. Reidel Pub. Co., Dordrecht, Holland, 113-127.

Oost, W. A., 1994: The ASGASEX experiment. Technical Reports - Royal Netherlands Meteorological Institute; TR-161; 29 pp.

Thorpe, S.A. 1982. On the clouds of bubbles formed by breaking wind-waves in deep water, and their role in air-sea gas transfer. Phil. Trans.R. Soc. London, A304, 155-210.

Wanninkhof, R., 1993: Gas transfer experiment on Georges Bank using two volatile deliberate tracers. Journal of Geophysical Research; 98(C11); pp 20,237-20,248.

Woolf, D. K., 1993: Bubbles and the air-sea transfer velocity of gases. Atmosphere-Ocean; 31(4); pp 517-540 .
Woolf, D.K., 1986: Model of gas exchange (MAST report CT930056, DG12, Brussels)

ASGAMAGE Final Report

Contribution of
University of East Anglia, School Of Environmental Sciences,
University of Newcastle upon Tyne, Dept of Marine Sciences and Coastal Management, and
CCMS - Plymouth Marine Laboratory

Partners 8 and 9

1. PARTICIPANT INFORMATION:

Partner: School Of Environmental Sciences,
University of East Anglia (UEA)

Co-Partner: Dept of Marine Sciences and Coastal Management,
University of Newcastle upon Tyne (NUT)

Associated Partner: CCMS - Plymouth Marine Laboratory,
Natural Environment Research Council (PML)

Principal Investigators: Dr. P. D. Nightingale
CCMS - Plymouth Marine Laboratory
Prospect Place, Plymouth, PL1 3DH
Tel. 44 1752 633439, Fax. 44 1752 633101
E-mail P.Nightingale@pml.ac.uk

Dr R.C Upstill-Goddard
Department of Marine Sciences and Coastal Management,
University of Newcastle upon Tyne
Ridley Building, The University
Newcastle upon Tyne, NE1 7RU, UK
E-mail Rob.Goddard@newcastle.ac.uk

Prof. P.S. Liss & Dr. G. Malin
School Of Environmental Sciences, University of East Anglia
Norwich, NR4 7TJ, UK
E-mail P.Liss@uea.ac.uk , G.Malin@uea.ac.uk

Investigators Employed on ASGAMAGE

M.I. Liddicoat	PML
S. Leigh	UEA
Dr. M. Helmer	UEA
G. Henry.	NUT

Personnel Involved in ASGAMAGE activities but not directly funded:

Dr. W. Broadgate	UEA
G. Lee	UEA
Dr. G. Uher	NUT
F. Carse	UEA/PML
T. Sjoberg	PML/UEA
Dr. P. Schlosser	Lamont Doherty Earth Observatory (LDEO)
D. Ho	LDEO
Dr. W. Helder	Netherlands Institute for Sea Research (NIOZ)
Dr. J. Den Daas	NIOZ
M-L. Lauria	Department of Oceanography, University of Southampton (SUDO)
Dr. R. Downer (BODC)	British Oceanographic Data Centre, Proudman Oceanographic Laboratory.
Dr. P. Taylor	Southampton Oceanography Centre (SOC)
Dr M. Yelland	SOC
D. Teare	Research Vessel Services, Southampton Oceanography Centre (RVS)
R. Lloyd	RVS

2: OBJECTIVES

Task 1
Co-ordination of shipboard activities in support of the ASGAMAGE programme.

Task 2
Measurements of sea-air gas transfer velocities as a function of wind speed with the triple tracer technique during a two-week period in October 1996.

Task 3
Measurements of dissolved oxygen concentrations, total gas and the concentrations of a range of important marine biogenic gases (DMS, CO_2, halocarbons and non-methane hydrocarbons) in sea water and air.

3. EXPERIMENTAL METHODS

3.1. Measurements of transfer velocity using multiple tracers

3.1.1 The technique

Theoretically, it should be possible to be routinely measure gas transfer velocities at sea by deliberately and simultaneously releasing two tracers, one inert but volatile, the other inert but non-volatile. Concentration measurements for the volatile tracer would then be used to assess k_w, with corrections for dispersive dilution determined from measurement of the conservative tracer. However, at the time of the first dual tracer experiments to determine k_w in 1989 (Watson et al. 1991), an "acceptable" conservative tracer, i.e. one that was non-toxic, non-radioactive and detectable in trace

quantities, had not been identified. Although conservative tracers such as rhodamine-B had been developed for tidal dispersion studies (e.g. Talbot and Talbot 1974), quoted limits of detection were impractical for our purposes (rhodamine-B is also designated a class 1 carcinogen).

An alternative "dual tracer technique" was therefore developed in which two volatile tracers with a large diffusivity contrast, in this case ^3He and SF_6, were released to seawater and their concentrations monitored with time as they escaped to the atmosphere at different rates. In this case it is the difference between the two transfer velocities (i.e. $k_{3He} - k_{SF6}$) that is actually determined from the equation shown below;

$$k_{3He} - k_{SF6} = [\ln (r_1/r_2) \times h] / t_2 - t_1$$

where r_i = $^3He/SF_6$ concentration at time t_i

h = mean depth of the water column.

Clearly it is necessary to have a knowledge of how k_{SF6} and k_{3He} are related in order to obtain an estimate of k for either gas. Traditionally transfer velocities have been related to a power law dependence on the Schmidt number (Sc.) shown below;

$$k_{SF6}/k_{3He} = (Sc_{SF6} / Sc_{3He})^n$$

where Sc. = kinematic viscosity of seawater / molecular diffusivity of the gas.

Modelling work (Ledwell, 1984), laboratory studies (Jahne et al., 1987) and lake experiments (Watson et al., 1991) all show that the value of n is expected to be -0.5 at wind speeds greater than 3.6 m s^{-1}. In calculating our results, we have assumed that this dependence is correct for wind speeds above 3.6 m s^{-1} and have corrected all values of k derived from the $^3He/SF_6$ tracer pair to Sc. 600. If bubbles/breaking waves are important in gas exchange at then our interpretation may be too simple, although the modelling work of Woolf (1995) has indicated that the Sc. dependency of He and SF_6 will remain close to -0.5 in the presence of bubbles.

Ideally however, one of the tracers deployed should be non-volatile. Until recently, a suitable marine tracer had not been identified. Microbial tracers have been used to investigate sewage dispersion in coastal waters (Pike et al. 1969) and to trace the movement of contaminating microbes in groundwater systems (Keswick et al. 1982). Bacterial spores were used in these studies as they persist in the water in their metabolically inactive state and have better detection limits than commonly used chemical tracers. They are considered to be innocuous in use, incapable of growth in the environment and unlikely to interfere with the natural population. These characteristics suggested to us that bacterial spores could be an ideal conservative tracer for use in gas exchange studies in open seawater and we first used them in this context during Challenger Cruise 99A in 1993 (Nightingale et al. 1999). Data obtained on that cruise facilitated the direct calculation of k_w for SF_6 and ^3He independently of each other and allowed us to determine the Schmidt number dependence of gas transfer, a significant advance on our previous capabilities. During the ASGAMAGE experiment our aim was to improve on our first results by using a higher initial spore concentration, minimising sample storage/handling

and carrying out experiments to investigate whether spores are truly conservative with respect to light exposure and micro-zooplankton grazing.

Rhodamines WT and Sulpho-G are representative of a new generation of non-toxic tracer "dyes" which can be analysed at high dilution using improved techniques of analysis (Suijlen and Buyse 1994). Rhodamine WT is susceptible to mild photo-degradation and as such is not strictly conservative. However, by measuring its ratio to rhodamine sulpho-G which has a different photochemical loss rate, any non-conservatism can be corrected for. By deploying these compounds in conjunction with the other three tracers, we aimed to generate additional sets of estimates of k_w for SF_6 and ^3He. Thus, it would be possible for the first time to compare directly k_w determined with three different combinations of tracers.

3.1.2 Release

Our preferred method of deployment is to dissolve the tracers in a known volume of water and then pump this water into the sea to create the tracer-enriched patch. Although this is time-consuming and the mass of tracer deployed is limited by the size of the tank, it avoids loss of gas to the atmosphere via direct bubbling of seawater and ensures that the ratio of the tracers is initially constant throughout the patch. The deployment was complicated by the use of the multiple tracers, as the rhodamines had to be prepared in a manner that was mutually exclusive for the preparation of the gaseous tracers.

Eight units of Biotrace ™, each containing $1 * 10^{14}$ spores of Bacillus globigii var. Niger (BG) per 2 litres of suspension, were added to one steel tank (~ 2500 dm^3). This was then filled with freshwater adjusted to a salinity of about 35 $^{o}/_{oo}$ by addition of sodium chloride. The tank was then sealed and saturated with SF_6 using the method described by Upstill-Goddard et al. (1991) over a period of about 24 hours. A known volume of ^3He was subsequently added to the headspace in the tank and this re-circulated through the water phase.

Sulpho rhodamine G and rhodamines WT have unique preparation requirements that interfere with the gas saturation procedure. Therefore, they were prepared separately. 25 kg of rhodamine WT (20% solution) was added to 50 kg of tapwater in a 1000 dm^3 steel tank, with continuous stirring via a submersible recirculation pump. 75 dm^3 of CH_3OH and 10 kg of rhodamine sulpho-G powder were then added and the tank filled to volume with ambient seawater and sealed.

The release site was closer to the Meetpost Noordwijk than our previous studies (Watson et al. 1991 and Nightingale et al. 1999) but specifically chosen to be away from any low saline water close to the coast. Unfortunately, this area of the North Sea is heavily used and allowance had to be made for possible movement of the patch either towards shipping lanes or the many gas production platforms in the vicinity.

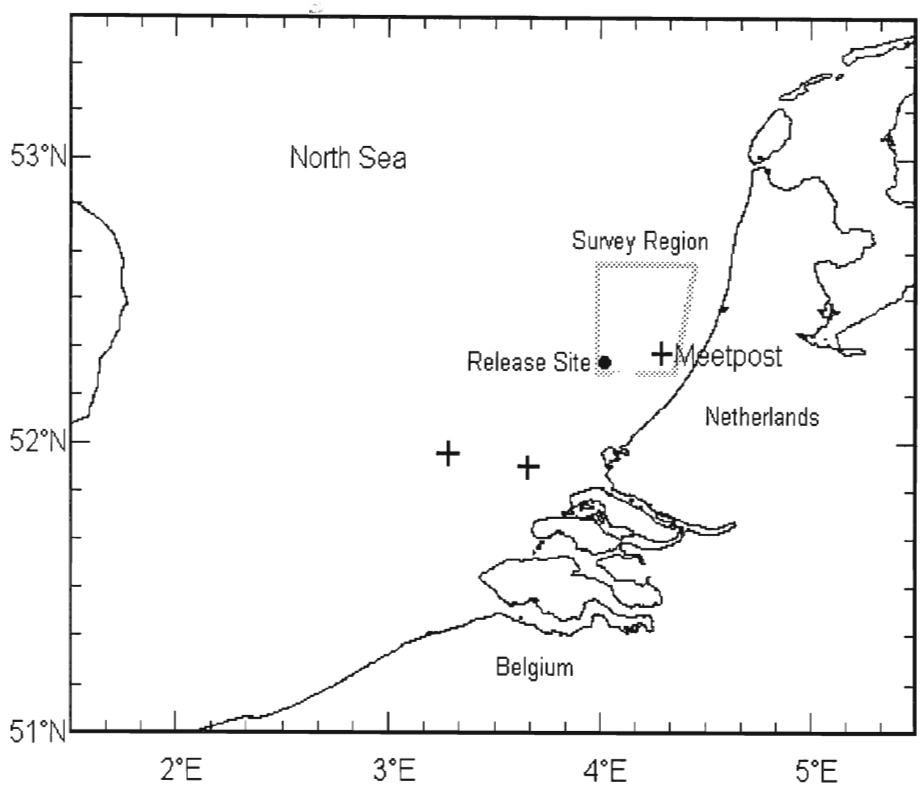

Figure 1. The tracer release site.

3.1.3 Analytical

Sulphur hexafluoride

An automated on-line analytical system, capable of SF_6 analysis with a four minute repeat time, was used to obtain a near real-time representation of the patch while the ship was underway. The system is described in detail by Upstill-Goddard et al. (1990) and Law et al. (1998). The output from this system was interfaced to a GPS and the resultant information plotted for use as a first approximation to reduce the effects of the tidal oscillation. These continuously updated plots were used as a further aid in navigating the ship around the patch. Samples were collected for analysis from the centre of the patch. Vertical profiles of SF_6 were determined using the method of Law et al. (1994).

3-Helium

Samples were collected and stored in sealed copper tubes for the analysis of ^3He on return to land by staff from LDEO according to the method of Ludin et al. (1997).

Bacillus globigii

Seawater samples were collected from the CTD rosette or over-side pump supply into sterile 1.3 L polystyrene roller bottles. Samples were analysed immediately or after storage for up to 12 hours in the ship's constant temperature laboratory at ambient seawater temperature (approx. 15°C). A number of replicate samples were taken, and returned to UEA to test the effect of storage on determination of spore numbers. In all 598 individual spore analyses were carried out following the method outlined by Pike et al (1969). For CTD and pump samples, 10 replicate samples of between 100 and 500 cm^3

volume were dispensed into sterile containers using sterile measuring cylinders. Our original intention had been that glass and plasticware would be used only once to prevent sample cross-contamination. However, the spore concentration decreased more rapidly than we had anticipated and it was necessary to wash and reuse the larger volume bottles. For samples from experiments, 5 replicates were taken and analysis volumes were generally 25 to 30 cm^3. All aliquots were heated to 63°C for 30 minutes in a water bath to induce full spore germination and reduce the background bacterial flora. The heated seawater was then filtered through disposable sterile analytical test filter funnels, containing 47mm diameter 0.45 • m pore size gridded cellulose nitrate filters. To ensure complete removal of spores from the bottles, they were rinsed with autoclaved seawater which was also passed through the filter. The filters were removed using sterile forceps and incubated on Petri-Pads soaked in sterile recovery medium containing tryptone. The petri dishes were incubated in the dark at 30°C for 18 to 20 hours before counting the orange/brown pigmented colonies characteristic of *Bacillus globigii.* Counts were repeated after a further 6 to 10 hours.

Rhodamines

Following tracer deployment, samples (140 in total) were collected in replicate in opaque glass 500 cm^3 screw cap bottles and stored in "dark boxes" for subsequent analysis at the Netherlands National Institute of Sea Research (NIOZ). The measurement technique is described in detail by den Daas et al. (1997).

4. Results

4.1 Task 1. Co-ordination of shipboard activities

Funds were obtained from the ACSOE core project to support both the core and infrastructure costs of the use of the Royal Research Ship Challenger, her officers and crew and the purchase of 4 star service support from the Research Vessel Services (RVS). The absence of a suitable meteorological package on the ship was identified as critical and following discussions between UEA and RVS , together with advice from the group of Peter Taylor at SOC, a permanent and reliable instrument set was installed on the ship. An initial cruise planning meeting was held at SOC on 2/5/96 in order to identify cruise infrastructure requirements and facilitate the formulation of a detailed cruise programme. Staff from the British Oceanographic Data Centre (BODC) were contacted and kindly agreed to manage the data collected during the cruise and to be responsible for its subsequent archiving. BODC also operate a quality check on oceanographic data.

Mobilisation on the ship was undertaken from 14 - 16 October, the vessel sailed on 16 October and was operating in the vicinity of the release site and the Meetpost from 17 October until 31 October with the exception of one period of poor weather from 27 to 29 October. Some surveys and CTD stations were also made close to the Meetpost in support of their activities. Data has been archived by BODC. Full details of the cruise and the data collected are given in the Cruise Report for Challenger 129 (Upstill-Goddard et al. 1997).

4.2 Task 2. Deliberate multiple tracer experiment

Measurements of air-sea gas transfer velocities were made using multiple tracers. Specifically these were, sulphur hexafluoride (SF_6), 3-helium (^3He), spores of the bacterium *Bacillus globigii* var. *niger (BG)*, rhodamine sulpho-G and rhodamine WT. The use of the two rhodamine tracers was a departure from the work plan as their successful use in marine tracer studies had not previously been known to the PIs. It was felt that their inclusion might benefit the overall aims of the project by allowing an independent and direct calculation of ^3He and SF_6 transfer velocities.

4.2.1 Wind data

Wind data are potentially available from the ship-board cup anemometer, a sonic anemometer on the ship operated by SOC and a cup and several sonic anemometers on the Meetpost. The wind record from the ship's cup anemometer is shown in Figure 2. During the very high wind period from 29 to 30 October the RRS Challenger was forced to leave the study area and shelter off the UK coast. As a result, we do not have ship wind data at the tracer site for this period. We therefore made a comparison of ship versus platform wind speeds. The sonic anemometers deployed by the other ASGAMAGE participants on the Meetpost were not operative throughout the whole of our experimental period, only the cup anemometer was. Dr. Wiebe Oost had therefore made a comparison between the platform cup anemometer and the KNMI sonic and developed a calibration of $U_{10n}(\text{sonic}) = 0.8062 * U_{10}(\text{Meetpost}) + 0.8237$ for the whole of the October/November ASGAMAGE B period.

As the cup anemometer is the same instrument we have used in previous gas exchange studies (Nightingale et al. 1999), we wished to further compare the two instruments. Thermal stability effects were removed from the data by correction to an equivalent wind speed at 10m height under neutral air boundary conditions (U_{10n}). This was achieved by estimating the bulk stability parameter Z/L (where Z is the measurement height and L is the Monin-Obukhov length) from air and seawater temperatures as described by Large and Pond [1981] using the Stanton numbers for unstable and stable stratification proposed by Large and Pond [1982]. The functional dependence of the neutral drag coefficient (C_{Dn}) on U_{10n} was taken from Oost et al. [1998] who derived the relationship from datasets collected on the Meetpost during a previous study. The results of this inter-comparison are shown in Figure 2.

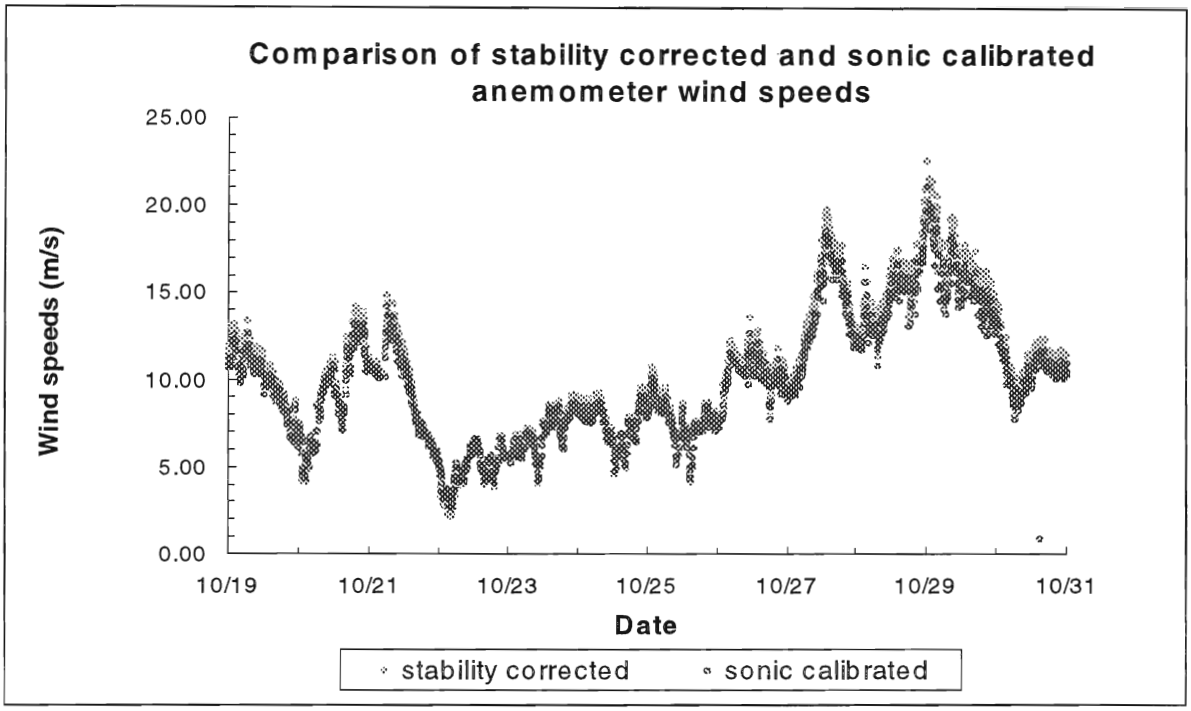

Figure 2

We observed only a mean difference of only 3% between the two interpretations of the cup-anemometer data, unlikely to be significant given that the sonic derived calibration was over a longer time period than the tracer study. We have therefore used the stability corrected cup anemometer data from the platform in interpreting our dual tracer results.

Rather worryingly, Figure 3 shows that the new wind set on the Challenger is still over-estimating wind speeds as compared to the platform. We have not used the latter dataset.

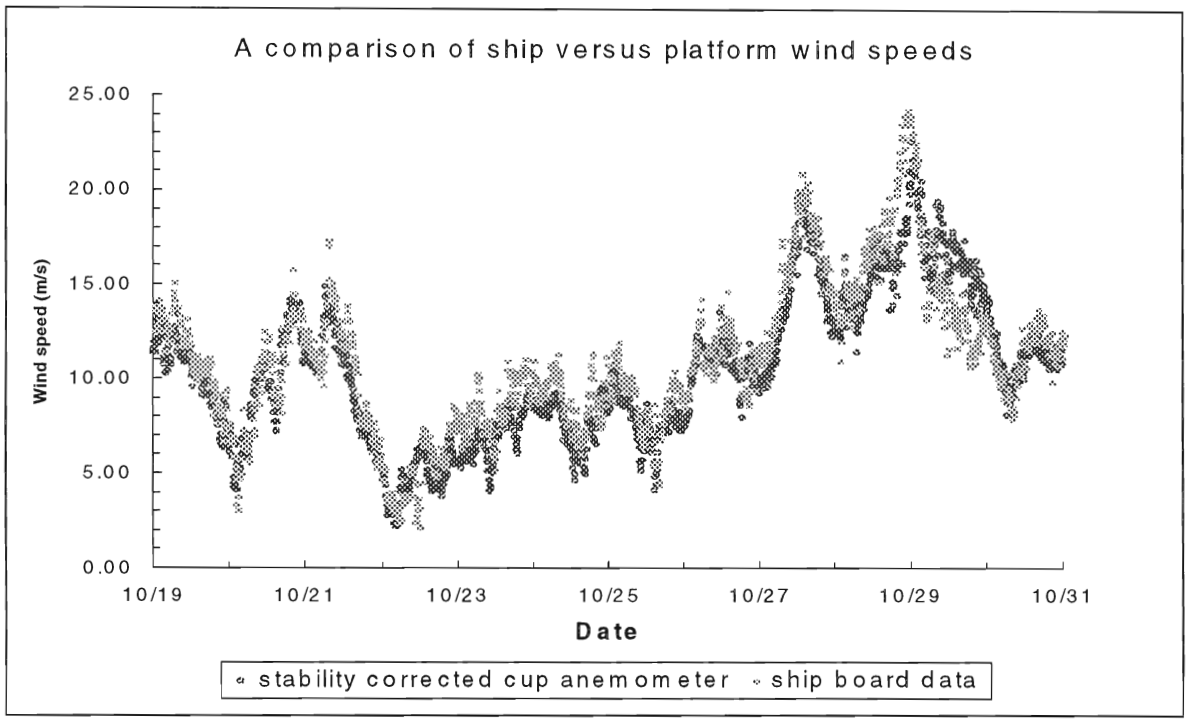

Figure 3.

4.2.2 . Conservative Tracers

The purpose of the bacterial spores and the fluorescent tracers, sulpho rhodamine G and rhodamine WT, deployed during the experiment was to monitor the degree to which the two gaseous tracers were lost from the "patch" by dispersion. In order to do this successfully it was necessary to account for the well-known photolytic losses of the rhodamine compounds. These losses, which are generally small but nonetheless significant, were evaluated using a method based on ratio measurements (by HPLC) of the two tracers with time (Suijlen and Buyse, 1994). The method involves detailed mathematical descriptions of patch dispersion dynamics and photolytic decay rates. These are summarised in den Daas et. al. (1997) and in view of space limitations it seems inappropriate to reproduce them here. All data have been extensively analysed and an exhaustive statistical treatment has been given by den Daas et al. (1997). Because of space considerations, only the most salient features of the data are described here.

With the exception of one or two stations, both tracers were homogeneously distributed through the water column. Analysis of the mean relative standard errors of the rhodamine measurements were close to ± 4 %, based on data from all "usable" stations. In practice, 4 from a total of 19 ratio measurements were deemed "unusable" on the basis that their standard errors were unacceptably high (up to ± 10 %), most likely as a consequence of contamination, either at collection or during analysis (den Daas et al., 1997). Observed time distributions of the two tracer concentrations post-release generally corresponded closely to model predictions based on earlier tracer release experiments, implying that the sampled stations closely represented the patch centre. Two stations not fitting these predictions were excluded from subsequent analysis (one of these also failed to meet the standard error criterion, above).

The precessions of the ratio determinations were better than those of the individual concentration measurements in all cases. Because of this, any effects due to water column inhomogeneity are in practice eliminated. Importantly, the tracer ratio was constant with time within the precision of the measurements. Subsurface light intensities computed using data from meteorological stations along the Dutch coast indicated that photolysis rates for sulpho rhodamine G were indistinguishable from the analytical scatter, whereas for rhodamine WT the cumulative photo-decay was about 4 % by the end of the experiment (den Daas et. al., 1997). Based on this approach, photolysis correction factors were applied to each of the individual measurements.

Figure 4 shows the ratio of *Bacillus globigii* spores to rhodamine WT concentrations uncorrected for photolytic losses over the course of the experiment.

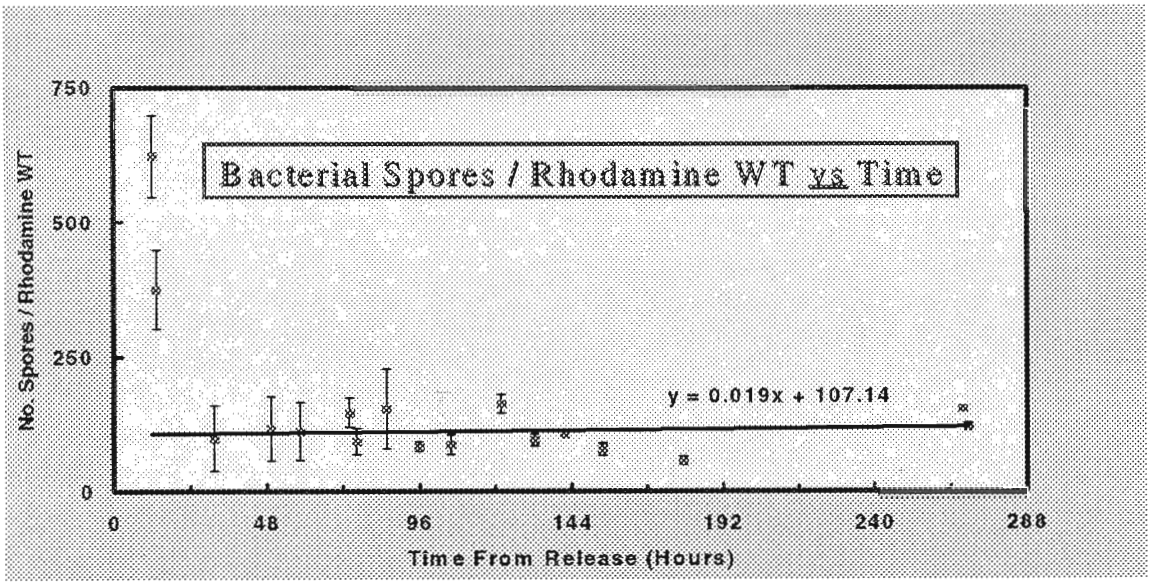

During the first 24 hours of the experiment the ratio fell sharply, presumably due to an initial small-scale inhomogeneity of the tracer distribution caused by the two-tank deployment procedure and which was apparently rapidly attenuated by subsequent mixing. The mean trend line through the remaining data is consistent with the photolytic losses of rhodamine WT discussed above. With this taken account of, the data demonstrate that the two tracers are conservative, at least with respect to each other, during all but the initial stages of the deployment.

4.2.3 Volatile Tracers

In all 17 vertical casts were made for SF_6 and ^3He during the tracer experiment. Recent modelling work by Cor Jacobs (one of our KNMI partners) has suggested that there might be significant near surface gradients in the 3He/SF6 ratio under some conditions (see contribution by KMNI). We have therefore examined our data in order to see if we can identify a reduction in this ratio in our surface samples as compared to the remainder of the water column.

Figure 5. Plot of all SF6 samples obtained from vertical profiling.

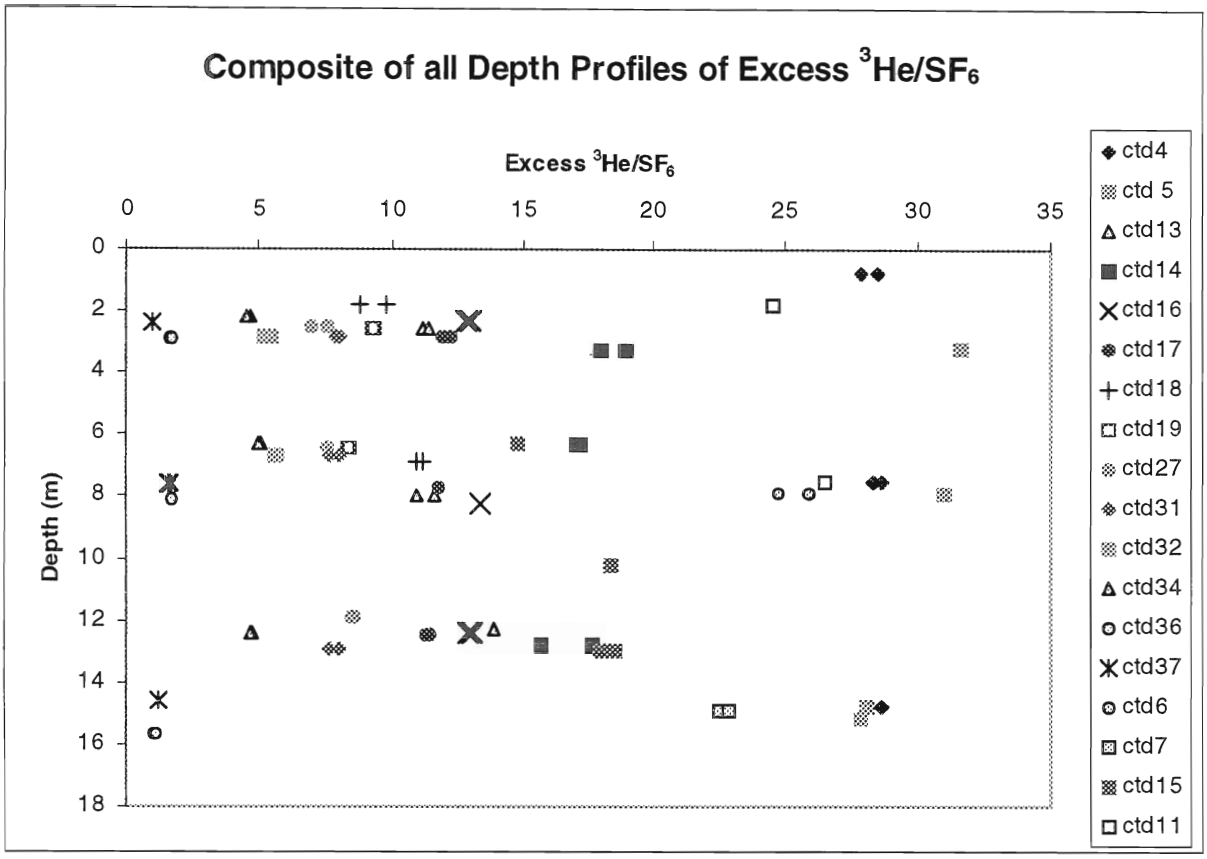

Additionally, a plot of the depth profiles used in the derivation of air-sea gas transfer velocities is shown in Figure 6.

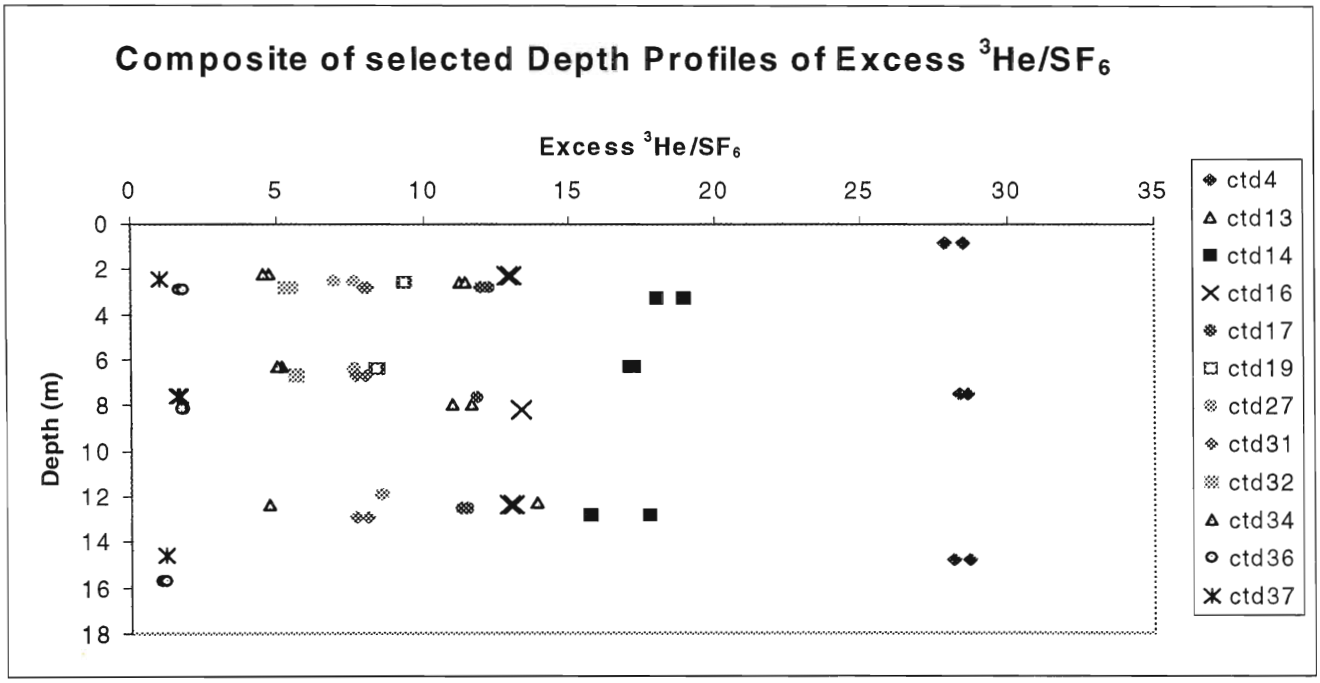

We found no evidence for consistent gradients in the $^3He/SF_6$ ratio through the water column. However, as discussed by Nightingale et al. (1999) the variability in the data is greater than would be predicted from analytical errors suggesting that mixing is a complex process. A more thorough comparison of the model k_{600} values output by the KNMI with dual tracer data with detailed near surface profiles ought to be a priority in future experiments.

4.2.4 Estimates of k_{600}

Estimates of k_{600} were derived from linear regressions through mean values (as determined from vertical profiling) of ln $^3He/SF_6$ versus time. During the course of the experiment part of the tracer patch (typical salinity of 34) mixed with lower salinity water. This was something of a surprise as the tracer patch was laid some distance further from the coast than the Meetpost platform. It therefore seems very likely that the platform was under the influence of lower salinity water (the Rhine plume) for most of the experiment. We have not used profiles from this part of the patch in our data interpretation although all mean values of ln $^3He/SF_6$ are shown in Figure 7 for completeness.

Figure 7

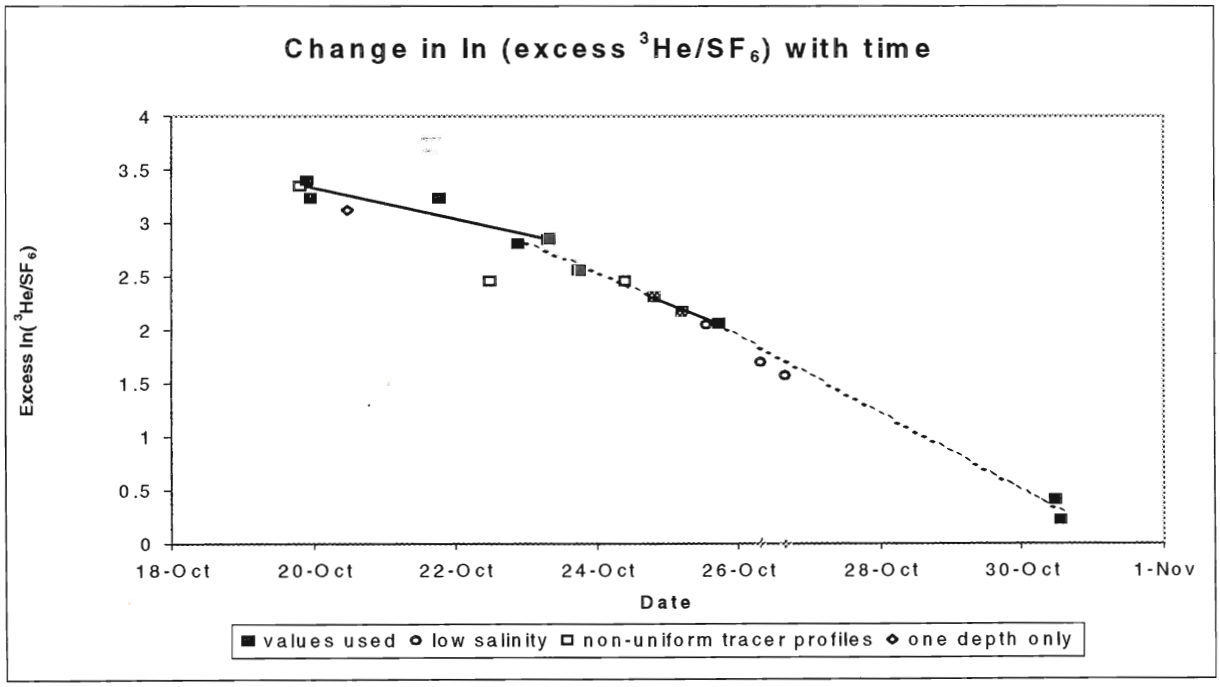

The linear fits shown above were used to derive four estimates of k_{600}. These are shown below and compared to the parameterisations of Liss and Merlivat (1986) and Wanninkhof (1992).

Figure 8. Estimates of k_{600} derived using multiple tracers.

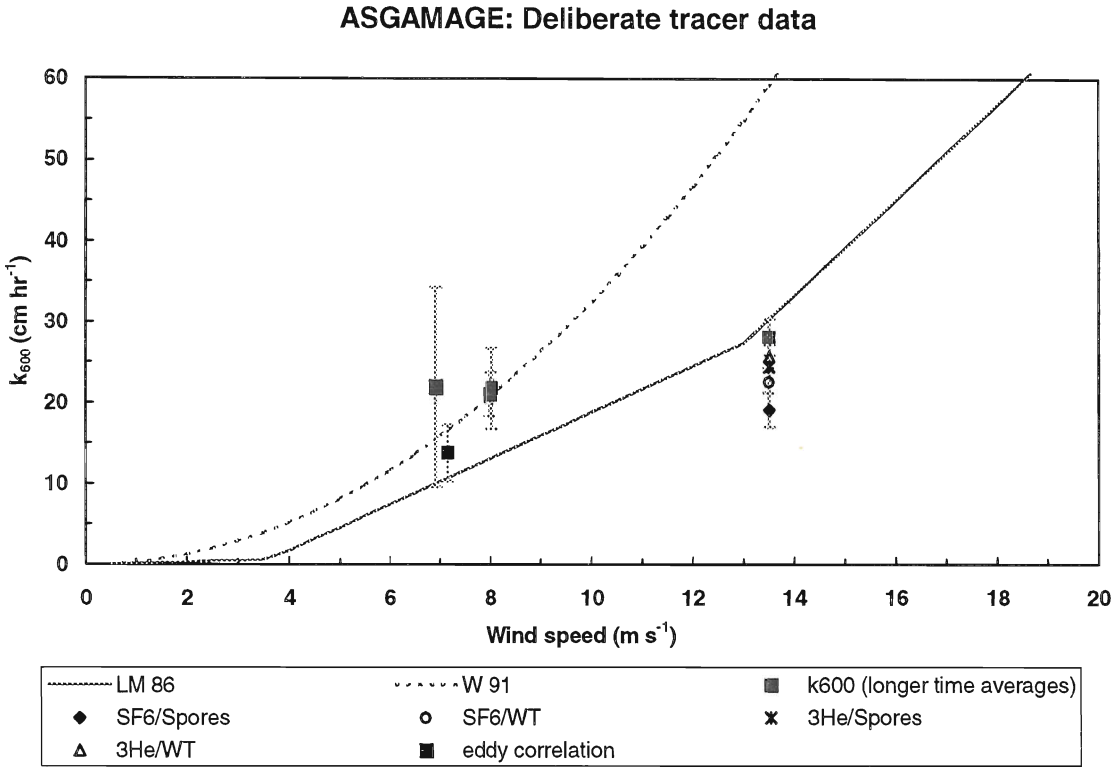

Also shown are four other estimates of k_{600} derived from the conservative tracers for the high wind speed period towards the end of the tracer experiment. The use of multiple tracers has been successful and allows us to derive estimates of n (the Schmidt number dependence) of –0.56 and -0.62 using the rhodamines and bacterial spores respectively.

Shown for comparison is the average value for k_{600} determined by the KNMI eddy correlation group during the first measurement period of the dual tracer experiment. The error bar is the standard error of the eddy correlation derived estimates. The agreement between the techniques is somewhat reassuring although we should caution that this was the only period over which flux measurements from the ship and from the platform overlapped.

In Figure 9 we compare the deliberate tracer derived estimates of k600 with our other experiments in the southern North Sea and with other shallow water dual tracer experiments.

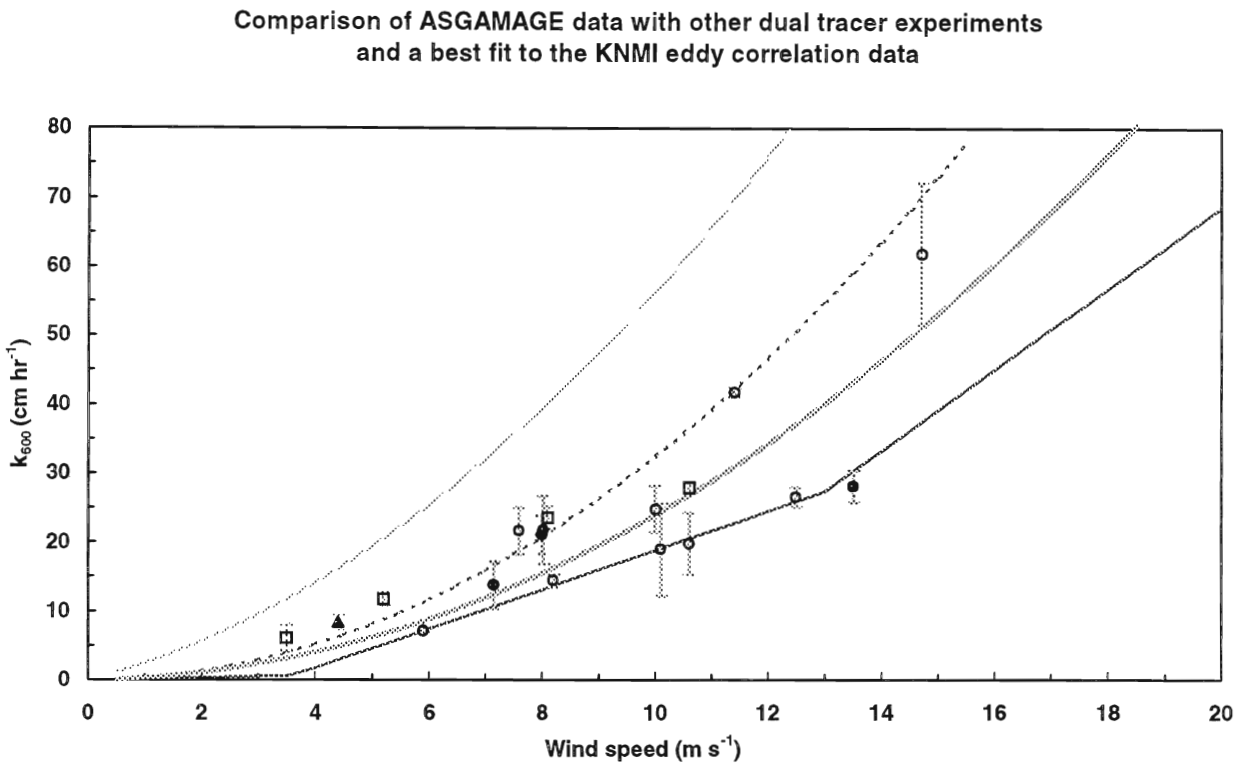

Dual tracer data: Open squares (Asher and Wanninkhof, 1998), open triangle (Wanninkhof et al. (1997), Open circles (Nightingale et al. 1999). Parameterisations of Wanninkhof 1992 (dashed line) and Liss and Merlivat (solid black line). Fits to dual tracer data of Nightingale et al. 1999 (dark grey line) and KNMI EC data (light grey line).

As can be seen from the plot, the new estimates of k_{600} are in good agreement with previous dual tracer studies and scatter between the Liss and Merlivat (1986) and Wanninkhof (1992) parameterisations. Also shown is a best fit to the other dual tracer data (Nightingale et al. 1999). There is a discrepancy between a simple polynomial fit to the total eddy correlation dataset for ASGAMAGE B and the dual tracer data although we should caution that the data were mostly obtained under different experimental conditions.

We have not been able thus far to improve on wind speed only parameterisations of k_{600} although we will continue to investigate the extensive datasets accumulated by other participants on the Meetpost as part of the ASGAMAGE experiment. However, deconvolved wind speed only fits to dual tracer derived estimates of k_{600} already explain 80% of the total variance (Nightingale et al. 1999).

4.3 Task 3. Other measurements on board RRS Challenger

Prior to the start of the cruise it was decided that the sonar systems mounted on a quadrupod operated by (SUDO/SOC/UCG) which were to be deployed from the ship would be switched to the platform. There were restrictions on the use of this equipment from the Challenger which made it difficult for it

to be used in rough weather. The total gas senors were also redeployed to the platform. However, a whole host of other measurements were made during Challenger Cruise 129. These are summarised below and some brief results from studies on carbon monoxide, methane and non-methane hydrocarbons are presented in a little more detail.

4.3.1 Non-tracer measurements made as part of ACSOE/ASGAMAGE

Underway (i.e. continuous) measurements

Water Based:	Depth, sea surface temp, salinity, optical attenuance, Total suspended matter, fluorescence, oxygen, ADCP
Meteorological:	Wind speed (cup anemometer), wind direction, air temperature (wet bulb plus dry bulb), barometric pressure, solar radiation, PAR, wind stress (Taylor and Yelland).

Underway (5 mins – 5 hrs)

Chemical:	Dissolved oxygen, chlorophyll, non-methane hydrocarbons (NMHC) air and water), carbon monoxide (CO), nutrients, suspended matter, methane (CH_4) (air and water).

Vertical Profiling

Physical:	Depth, salinity, temperature, transmission, PAR (upwelling and downwelling)
Chemical:	Fluorescence, oxygen, NMHC, CH_4, CO, nutrients,
Biological:	Chlorophyll, phytoplankton species,

All data is available from the British Oceanographic Data Centre.

4.3.2 Carbon monoxide in Coastal and Shelf waters

Surface dissolved and atmospheric CO were measured as part of a gas exchange study (EC ASGAMAGE) in the southern North Sea ($52^0$17N 004°18E) during October 1996. Surface waters were generally slightly supersaturated, although periods of undersaturation were observed in association with high atmospheric CO of continental origin (mean atmospheric CO 165.8+/-123.6 ppbv). Diurnal trends resulting from photo-production were not apparent, with CO instead varying inversely with salinity (see Fig.6). The source of this may be the lower Scheldt estuary (see Fig.5) as the estuarine plume is transported along the Dutch coast to the site of the ASGAMAGE study. Association of methane with low salinities in the German Bight also suggests the Scheldt as source (De Wilde *et al,* 1995); similarly the Orinocco river has been reported to influence surface CO across the south-eastern Caribbean (Jones and Amador, 1993). It is apparent that estuarine input is primarily determining the coastal/shelf source strength, regardless of whether the CO originates directly from the Scheldt estuary or indirectly from photo-degradation of terrestrial DOC. The atmospheric flux, calculated using the Liss and Merlivat (1986) wind speed-transfer velocity relationship, was relatively

low (10.8 +/- 27.8 nmol/m2/h) with the region acting as a sink during periods of elevated atmospheric CO.

Figure 10. Diurnal measurements of carbon monoxide.

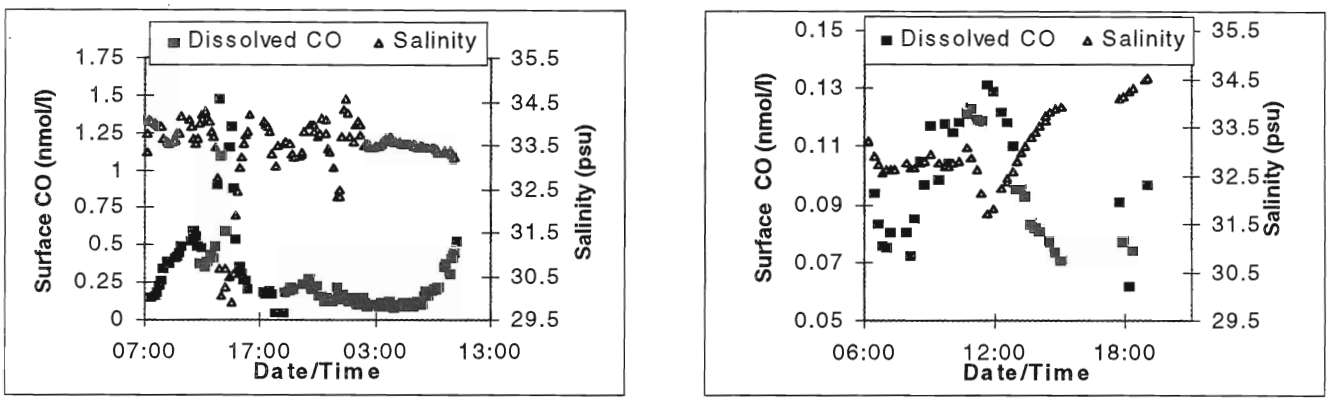

4.3.3 Methane and Nitrous Oxide

Dissolved and atmospheric CH_4 were analysed by single phase equilibration gas chromatography with flame ionisation detection, using an automated version of an apparatus designed for the simultaneous measurement of CH_4 and N_2O (Upstill-Goddard et al., 1996). Unfortunately, severe chromatographic interferences by SF_6 made N_2O measurements impossible and these had to be abandoned. Analytical precisions for CH_4 in water samples and air were better than $\pm$ 1 % (Upstill-Goddard et al., 1996). Results of the CH_4 analyses are presented in Figure 11, where they are plotted as percent saturations vs salinity (100% saturation $\equiv$ atmospheric equilibrium). Clearly, North Sea waters off the Dutch coast are highly CH_4 supersaturated and their CH_4 burden decrease s with increasing salinity. A polynomial function best describes the relationship. These data can be most convincingly explained as arising from continental inputs via the Rhine-Scheldt estuaries, in agreement with previous findings in this region (e.g. Scranton and McShane, 1991) and the form of the relationship can be viewed as indicative of significant CH_4 removal within the estuarine zone, by air-sea gas exchange and/or microbial oxidation. The degree to which the riverine CH_4 signal may be modified during estuarine mixing can be estimated from the tangent of the CH_4-salinity plot at seawater endmember salinity extrapolated to zero salinity by linear regression (Boyle et al., 1974), which yields the effective river water CH_4 saturation as modified by estuarine removal, i.e. ~ 60 nmol l^{-1}. The actual riverine end member CH_4 saturation for the Rhine-Scheldt can be estimated by extrapolating the polynomial fit toward zero salinity. The equivalent river water concentration estimated in this way is ~7500 nmol l^{-1} , which implies the removal of the riverine CH_4 signal in the Rhine-Scheldt estuaries to be almost quantitative. For comparison, Scranton and McShane (1991) estimated CH_4 concentrations in the Rhine-Scheldt to be in the range 500-5000 nmol l^{-1} based on linear extrapolations of offshore-inshore transects, and De Wilde and Duyzer (1995) report 500 nmol CH_4 l^{-1} for the outer Scheldt. Subsequent combination of these data with the tracer-determined gas transfer velocities will enable us to construct a detailed coastal zone budget for this important greenhouse gas.

4.3.3 Non-Methane Hydrocarbons

Isoprene (2-methyl 1,3-butadiene) is reactive hydrocarbon with a lifetime of about 4 hours in the atmosphere where it affects the balance of oxidants, such as the hydroxyl radical and ozone. The major source of atmospheric isoprene is terrestrial plants. However, recent work has shown that isoprene is also input from surface seawater and that production is closely associated with biological activity (Broadgate et al., 1997). During the ASGAMAGE experiment the concentration of isoprene in the surface water generally decreased as the wind speed increased. Variations within the patch are likely to be due to changes in the biology in the patch (linear regression of isoprene and chlorophyll, r^2 = 0.45) and salinity which indicates isoprene does not have a riverine source.

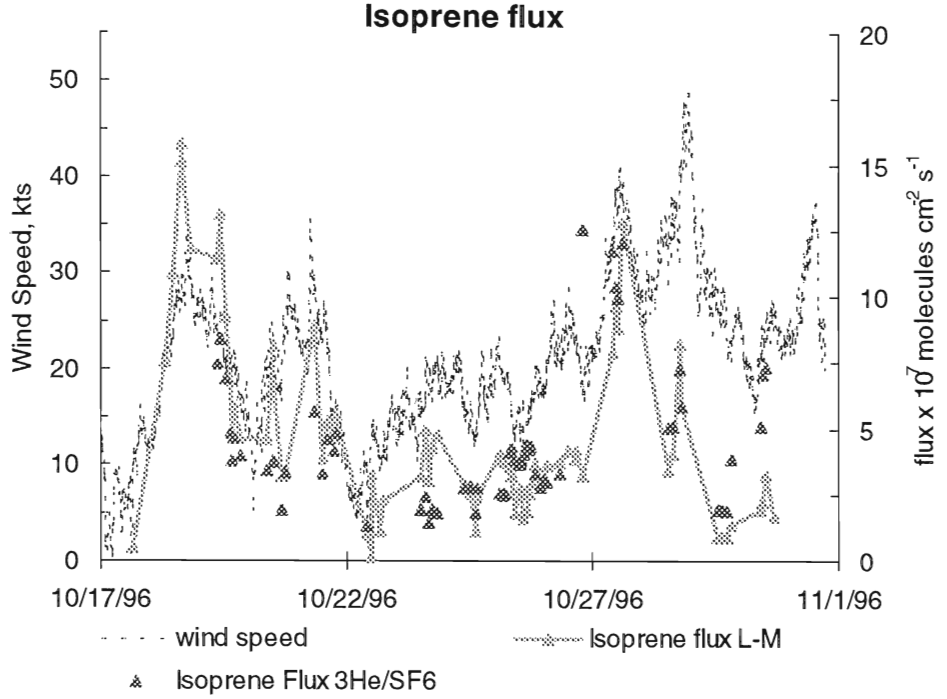

There is good agreement between the flux of isoprene to the atmosphere calculated by the Liss-Merlivat relationship and that calculated using the estimates from tracer technique. The exception is the period of very high winds towards the end of the experiment when the ship was sheltering off the coast of England.

The loss of isoprene to the atmosphere was calculated from the average flux over the period (using the wind speeds measured on the ship and the Liss-Merlivat relationship) and compared with the measured loss in the water column. An *in situ* net production rate of isoprene was calculated to be 1.7 pmol l^{-1} dy^{-1}. This is a crude approximation but represents the first calculation of *in situ* production of isoprene in the ocean.

Acknowledgements

Many of the personnel involved in this study were funded under the UK Natural Environment Research Council (NERC) Atmospheric Chemistry Studies in the Oceanic Environment (ACSOE)

Community Research Programme and in particular NERC grant GST/02/1278. ACSOE also funded the use of the RS Challenger in this project.

References:

Asher, W.L., and R. Wanninkhof, The effect of bubble-mediated gas transfer on purposeful dual-gaseous tracer experiments, *J. Geophys. Res.*, *103*, 10555-10560, 1998.

Boyle, E., A. R. Collier, A. T. Dengler, J. M. Edmond, A. C. Ng and R. F. Stallard (1974). On the chemical mass-balance in estuaries. Geochim. Cosmochim. Acta **38,** 1718-1728.

Broadgate, W. J., P.S. Liss and S.A. Penkett, "Seasonal emissions of isoprene and other reactive hydrocarbon gases from the ocean", *Geophys. Res. Letts.*, **24** (21), 2675 - 2678, 1997.

Cardenas L.M., J.F. Austin, R.A. Burgess, K.C. Clemintshaw, S. Dorling, S.A. Penkett and R.M. Harrison (1998), Correlations between CO, NOy, O3 and non methane hydrocarbons and their relationships with meteorology during winter 1993 on the North Norfolk coast, UK. Atmos. Environ. 32 3339-3351.

den Daas, J. H., Suijlen, J. M. & Helder, W. 1997. Measurements of sulpho rhodamine G and rhodamine WT concentrations in seawater samples taken during the multiple tracer experiment ASGAMAGE (1996). *Nederlands Instituut voor Onderzoek der Zee Technical Report No. 21,* 20 pp.

Erickson, D. J. 1989. *Global Biogeochemical Cycles.*305-314.

Evans, W.F.J and E. Puckrin. 1995. *Geophys. Res. Lett.* 22(8): 925-928.

Gameson, A.L.H. 1986. Editor. Tracers for the Water Industry. Water Research
Centre, Marlow

Harder , J. 1977. *Marine Geology.* 137:13-23.

Hedges, J.I., Hatcher, P.G., Ertel, J.R., K.J. Meyers-Schulte. 1992. *Geochem. Cosmochim. Acta.* 56:1753-1757.

Johnston, J.E. and T.S. Bates. *Global Biogeochemical Cycles.*10:347-359.

Jones R.D and J.A. Amador,. 1993. *J. Geophys. Res.* 98:2353-2359.

Jahne B., K.O. Munnich, R. Bosinger, A. Dutzi, W. Huber and P. Libner (1987), On the parameters influencing air-water gas exchange, J. Geophys. Res. 92 1937-1949.

Keswick, B.H., Wang, D-S. & Gerba, C.P. (1982). The use of microorganisms as ground water tracers: a review. Groundwater 20, 142-149. (1982)

Ledwell J.J., (1984) The variation of the gas transfer velocity with molecular diffusivity, in; Gas transfer at water surfaces, eds. W. Brutsaert and G.H. Jirka, Riedel.

Liss, P.S., and L. Merlivat, Air-sea gas exchange rates: introduction and synthesis, in *The role of air-sea gas exchange in geochemical cycling*, edited by P. Buat-Menard, pp. 113-127, D. Reidel, 1986.

Ludin A., R. Weppernig and P. Schlosser, Mass spectrometric measurement of helium isotopes and tritium in Tracer Oceanography edited by P. Schlosser AGU Monograph.

Nightingale, P.D., G. Malin, C.S. Law, A.J. Watson, P.S. Liss, M.I. Liddicoat, J. Boutin and R.C. Upstill-Goddard, In-situ evaluation of air-sea gas exchange parameterisations using novel conservative and volatile tracers Global Biogeochemical Cycles (submitted).

Pike, E.B., Bufton, A.W.J. and Gould, D.J. (1969). The use of Serratia indica and Bacillus subtilis var niger spores for tracing sewage dispersion in the sea. J. Appl. Bacteriol., 32, 206-216.

Talbot, J.W. and Talbot, G.A. (1974). Rapp. P.-V. Reun. Cons. Perm. Int. Explor. Mer 167, 93

Scranton, M.I. and K. McShane (1991). Methane fluxes in the southern North Sea: the role of European rivers. Cont. Shelf. Res. **11,** 37-52.

Suijlen, J.M. and Buyse, J.J. (1994). Potentials of photolytic rhodamine WT as a large scale water tracer in a long-term experiment in the Loosdrecht lakes. Limnol. Oceanogr., 39, 1411-1423.

Upstill-Goddard, R. C., Watson, A. J., Wood, J. and Liddicoat, M. I. (1991). Sulphur hexafluoride and helium-3 as seawater tracers: deployment techniques and continuous underway analysis for sulphur hexafluoride. Anal. Chim. Acta, 249, 555-562.

Upstill-Goddard, R. C., A. P. Rees and N. J. P Owens (1996). Simultaneous high-precision measurements of methane and nitrous oxide in water and seawater by single-phase equilibration gas chromatography. Deep Sea Res., **43**, 1669-1682.

Upstill-Goddard R.C., J. Barnes, W. Broadgate, F. Carse, R. Downer, D. Ho, M-L. Lauria, S. Leigh, G. Malin, P. Nightingale, T. Sjoberg and G. Uher. The ASGAMAGE experiment, 16 October- 1st November 1996: Gas transfer velocities and biogenic gas fluxes in the southern North Sea. NERC CRUISE REPORT : *Challenger* 129.

Wanninkhof, R., Relationship between wind speed and gas exchange over the ocean, *J. Geophys. Res.*, *97*, 7373-7382, 1992.

Wanninkhof, R., G. Hitchcock, W.J. Wiseman, G. Vargo, P.B. Ortner, W. Asher, D.T. Ho, P. Schlosser, M.-L. Dickson, R. Masserini, Fanning K., and J.-Z. Zhang, Gas exchange, dispersion and biological productivity on the west Florida shelf: results from a lagrangian tracer study, *Geophysical Research Letters*, *24*, 1767-1770, 1997.

Watson, A. J., Upstill-Goddard, R. C. and Liss, P. S. (1991). Air-sea exchange in rough and stormy seas measured by a dual tracer technique. Nature 349, 145-147.

de Wilde, H.P.J. and J. Duyzer (1995). Methane emissions off the Dutch coast: Air-sea concentration differences versus atmospheric gradients. In B Jahne and E.C. Monahan (eds.), *Air-Water Gas Transfer*, pp. 763-773. AEON-Verlag,

Woolf D.K., (1997) Bubbles and their role in gas exchange, in The sea surface and global change, eds P.S. Liss and R.A. Duce Cambridge University Press.

ASGAMAGE Final Report

Contributions of BIO Scientists in ASGAMAGE-B

Partner 10

Coordinating Investigator:

Mr. R.J. Anderson
Ocean Circulation Section,
Bedford Institute of Oceanography,
1 Challenger Drive, P.O. Box 1006 Dartmouth, N.S.
Canada B2Y 4A2
Phone: + 1 902 426 3584; FAX + 1 902 426 7827
E-mail: AndersonR@mar.dfo-mpo.gc.ca

Measurements of wind stress, heat, humidity and CO_2 fluxes.

Robert J. Anderson and Stuart D. Smith

The field experiment

During ASGAMAGE B a team from the Bedford Institute of Oceanography installed an eddy flux system on the MPN boom. The system consisted of a Kaijo Denki DAT-300 sonic anemometer, micro-thermistors and an ERC Lyman-alpha (ultraviolet) humidity sensor, connected to a PC computer-based data logging and analysis system. An infrared CO_2 sensor that was to have been part of this system was unfortunately not ready in time. Instead, signals from the KNMI IFM and NOAA Oak Ridge infrared H_2O and CO_2 sensors were connected to the BIO data logger in parallel with their own respective data systems. Data from a KNMI aspirated Lyman-alpha H_2O sensors, KNMI sea surface temperature and wave wire were also logged on the BIO system. Data from an Advanet infrared CO_2 and H_2O sensor operated by TNO were also logged at times.

Eddy fluxes of momentum, heat, water vapour and CO_2 have been calculated from time series data logged with the BIO system, using the BIO sonic anemometer, thermistors and humidity sensor. The aspirated KNMI sensors worked most of the time, while the OAKR sensor and BIO Lyman-alpha data were useful only in the absence of rain. The OAKR sensor claims a resolution of 20 $\mu g/m^2 s$ for a 1 hour average CO_2 flux. All IR CO_2 sensors at times gave some indications of contamination by accumulation of sea salt or moisture, and on windy days we expect the best results to come from periods just after the sensors were cleaned.

The BIO data system, which logs and gives preliminary results on-line, worked well during the entire experiment. A total of 323 data runs were logged and processed in wind speeds of 3-16 m/s, wind directions from 171-331 degrees. During ASGAMAGE-B there was a fairly constant upward ΔpCO_2, which would drive an upward flux of CO_2 from sea to air.

ANALYSIS RESULTS

The BIO analysis results

The large data set collected was somewhat reduced by applying some restrictions on data quality and by limiting the analysis of data from certain sensors to conditions in which they perform adequately. These include limits on wind speed; $4 < U < 18$m/s; acceptable wind direction 200-330 degrees to reduce land effects and flow distortion; relative humidities < 90%; and lack of precipitation for open-path infrared and ultraviolet sensors that require clean and dry optics. Data runs selected for re-analysis were corrected for tide height, tidal

currents, mean humidity, mean CO_2 concentrations in sea and air, phase shifts due to horizontal sensor separation, sensor recalibration, Webb density terms and crosstalk with humidity. W. Kohsiek at KNMI has provided H_20/CO_2 crosstalk values for the IFM sensor.

The BIO analysis results provide intercomparisons among the eddy flux sensors operated by several groups, using single analysis method. This will allow any systematic differences in eddy flux results of the various participating groups to be resolved between sensor differences on the one hand, and data logging or analysis differences on the other hand.

Wind stress results

Good agreement between direct eddy flux measurements and "dissipation" estimates of the wind stress (Fig 1). Values of the neutral drag coefficient as a function of wind speed.agree with our earlier studies at other sites (Smith, 1988; Anderson, 1993) and the revised HEXMAX values (Oost, 1998) for the same site, but are lower than the HEXMAX values (Smith et al, 1992).

Sensible heat and water vapour fluxes

The neutral heat flux coefficient C_{TN} (Fig 2) is found to have more scatter than the HEXMAX results (DeCosmo et al, 1996) and it does not depend end on wind speed. There was good agreement amongst the infrared and ultraviolet humidity sensors. The neutral humidity flux coefficient averaged for the various sensors (Fig 3) is also in agreement with the HEXMAX results (DeCosmo et al, 1996) and is again found to be independent of wind speed.

CO_2 fluxes

Analysis of CO_2 fluxes as logged by the BIO system revealed systematically higher upwards CO_2 fluxes calculated with the NOAA Oak Ridge sensor than with the KNMI IFM sensor. As a result testing was carried out to identify possible cross-talk of the CO_2 signals with variations in water vapour. Certain filters applied to the KNMI IFM sensor functioned better than others in removing water vapour cross-talk. Eventually a heater was added to the mirror in the infrared optical path of the NOAA Oak Ridge sensor to prevent contamination of the mirror by a thin, invisible film of water. This modification is resulting in improved performance of this sensor in subsequent marine experiments. Figure 4 shows the computed CO2 gas transfer velocity plotted against the neutral wind speed at a height of 10m. Corrections have been applied for the Webb term and various filter dependent water vapour crosstalks for the KNMI IFM sensor.

Acknowledgement

We wish to thank Dr. W.A. Oost, the KNMI team and the European Commission's Marine Science and Technology Programme (MAST III) for the support and cooperation that have made possible our participation in this original and highly productive experiment.

References

1. Smith, S.D., 1988; Coefficients for sea surface wind stress, heat flux and wind profiles as a function of wind speed and temperature. J.Geophys.Res.,V93,C??, 15467-15472.

2. Anderson, R.J., 1993: A Study of Wind Stress and Heat Flux over the Open Ocean by the Inertial Dissipation Method, J.Phys. Oceanogr., 23,2153-2161.

5. DeCosmo, J., K.B. Katsaros, S.D. Smith, R.J. Anderson, W.A. Oost, K. Bumke, and H. Chadwick.,1996; Air-sea exchange of water vapour and sensible heat: The Humidity Exchange Over the Sea (HEXOS) results, J. Geophys. Res., V101,C5, p12001-12016.

3. Oost, W.A., 1998: The KNMI HEXMAX stress data- A reanalysis. Boundary-Layer Meteorol. 86, 447-468.

4. Smith, S.D., R.J. Anderson, W.A. Oost, C. Kraan, N. Maat, J. DeCosmo, K.B. Katsaros, K.L. Davidson, K. Bumke, L. Hasse and H.M. Chadwick, 1992: Sea Surface Wind Stress and Drag Coefficients: the HEXOS Results, Boundary-Layer Meteorol. 60, 109-142.

6. Wanninkhof, R., 1992: Relationship between wind speed and gas exchange over the ocean. J. Geophys. Res., Vol. 97, C5, p7373-7382.

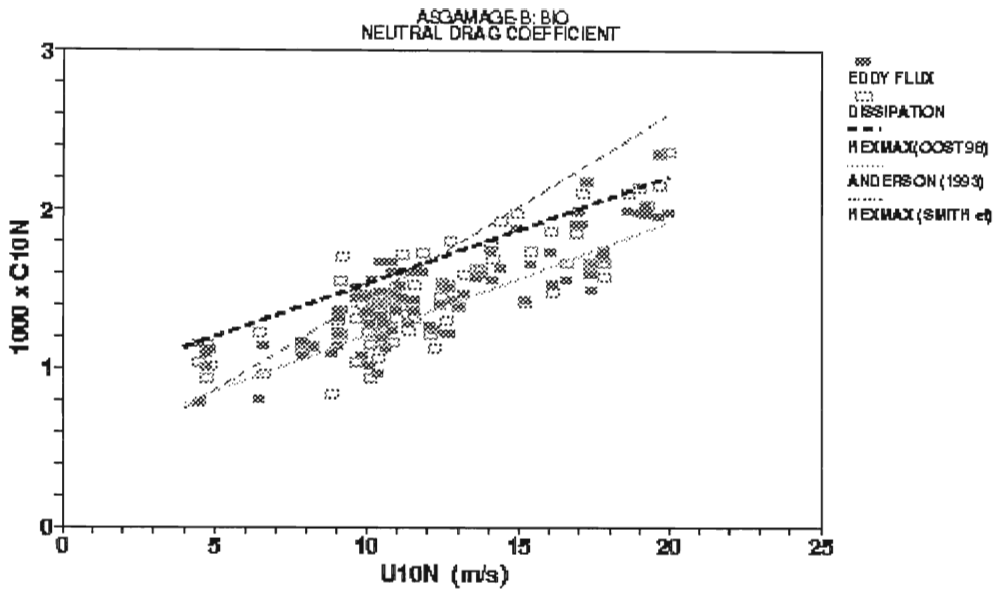

Figure 1. Neutral Drag Coefficient plotted against neutral wind speed at 10m. Closed boxes are eddy correlation and open boxes are inertial dissipation results.

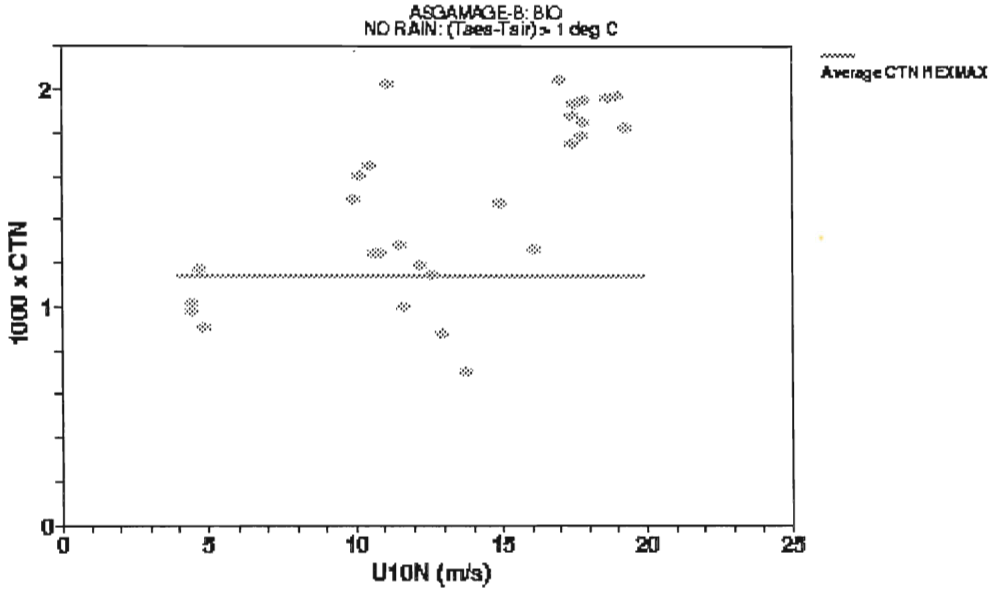

Figure 2. Neutral heat flux coefficient plotted against neutral wind speed at 10m for Tsea-Tair>1C.

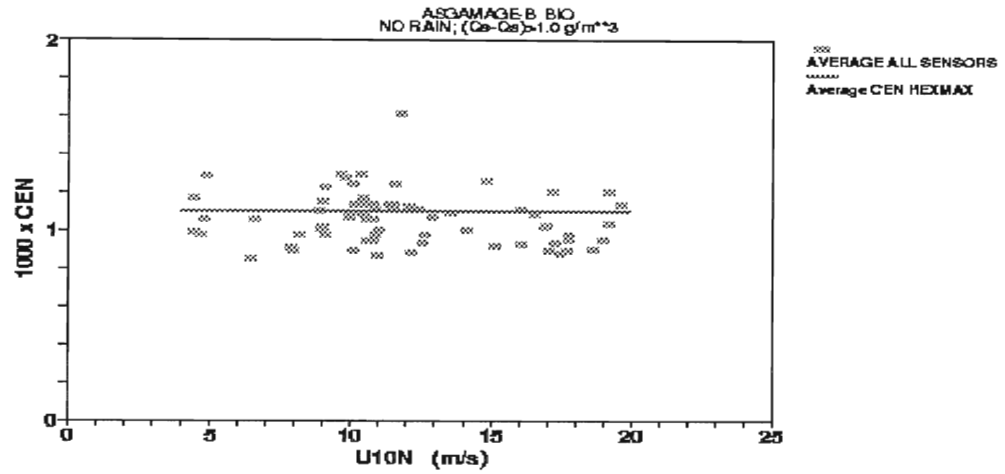

Figure 3. Neutral latent heat flux coefficient plotted against neutral wind speed at 10m for (Qsea-Qair)>1 g/m^3. Coefficient calculated for average flux from all available sensors. HEXMAX line (Decomos et al) for comparison.

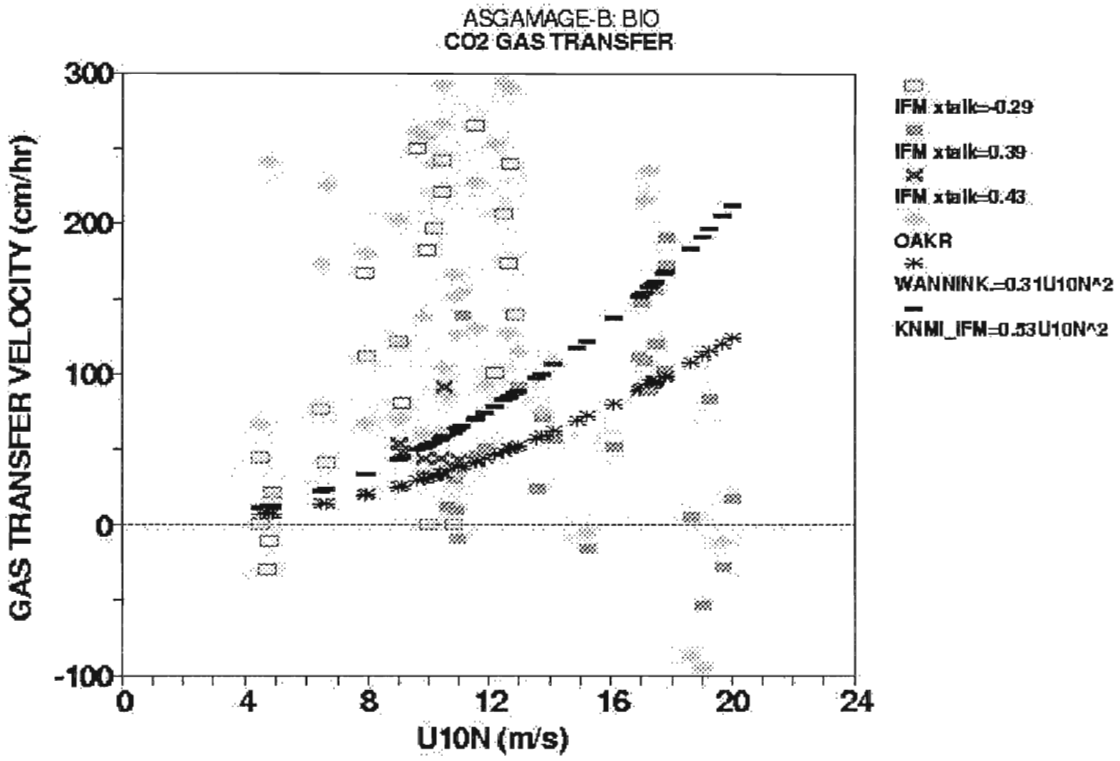

Figure 4. CO2 gas transfer velocity plotted against neutral wind speed at 10m. NOAA Oak Ridge sensor (+) shows much more scatter than the KNMI IFM sensor. Wanninkhof (1992) and KNMI preliminary lines shown for comparison.

ASGAMAGE Final Report

Contributions of NOAA Scientists in ASGAMAGE-B

Partner 11

Coordinating Investigator: Dr.Ch.W.Fairall
R/E/WP7 (Wave Propagation Laboratory)
NOAA/ETL (Environmental Technology Laboratories),
325 Broadway, Boulder CO 80303, USA
Phone: + 1 303 497 3253; FAX + 1 303 497 6978
E-mail: cfairall@etl.noaa.gov

Contributors:

Jeffrey E. Hare
Cooperative Institute for Research in Environmental Sciences (CIRES), University of Colorado Boulder and NOAA/ETL

Christopher W. Fairall
National Oceanic and Atmospheric Administration (NOAA) Environmental Technology Laboratory (ETL), Boulder Colorado

The Air-Sea Interaction Group at the NOAA Environmental Technologies Laboratory (ETL) was pleased to participate in the Autumn 1996 ASGAMAGE-B experiment. The ETL involvement was driven by the current need to make direct covariance measurements of the flux of trace gases (in particular, carbon dioxide) over the sea. These measurements are needed in order to quantify the gas fluxes, to identify the controlling environmental parameters, and to create parameterizations of gas transfer for use in larger scale models of atmospheric flow.

This experiment represented a unique collaboration between U.S. and Canadian scientists and our European Union (EU) - sponsored colleagues, which nabled the sharing of resources, expertise, and scientific knowledge between the trans-Atlantic participants. It is hoped that cooperative scientific endeavors such as ASGAMAGE will continue to prosper during this critical period in environmental investigation.

The NOAA deployment on the Meetpost Noordwijk (MPN) platform was a collaborative effort between the ETL scientists and Richard Dissly, Pieter Tanns, and Jim Smith of the Climate Monitoring and Diagnostics Laboratory (NOAA/CMDL). The ETL scientists have a strong history in marine surface layer turbulence measurements. The CMDL group has developed a sensitive closed-path CO2/H2O gas analyzer, and ASGAMAGE-B provided the first opportunity to deploy that system in the field. ETL brought a workstation-based data acquisition system to the platform, an open-path CO2/H2O infrared gas analyzer, which was developed at the NOAA Air Resources Laboratory in Oak Ridge Tennessee, and a fast-response infrared hygrometer, manufactured by the Ophir Corporation in Colorado.

The ASGAMAGE-B deployment on the MPN provided a rich, diverse scientific environment within which collaboration between North American and European scientists was facilitated. For example, data streams were shared between various groups and a variety of instruments were deployed on the platform, which provided for real-time comparison of the different measurement techniques. Among the groups which generously shared resources with NOAA included: the Royal Netherlands Meteorological Institute (KNMI), TNO Physics and Electronics Laboratory, Bedford Institute of Oceanography (BIO), and Ris National Laboratory (Denmark).

Although the CMDL gas analyzer system experienced some difficulties in its initial field trial, valuable experience was gained which was carried into subsequent experimental endeavors by both

the NOAA laboratories. Some significant results from experimental efforts undertaken by ETL scientists subsequent to the ASGAMAGE-B experience can be found in Edson et al. (1999, J. Atmos. Oceanic Technol., submitted).
Also, ETL has collaborated with KNMI on the characterization of different designs of the open-path infrared gas analyzers, and the results of this work have been reported in Kohsiek (1999, Boundary-Layer Meteorology, submitted). An additional significant realization gained from ASGAMAGE-B was the discovery of the utility of heating the mirrors of the Oak Ridge gas analyzer.

As a result of the participation in ASGAMAGE-B and other gas-flux measurement campaigns, ETL has taken efforts to determine the proper calibration and utilization of the open- path water vapor sensors. This information is vital to the interpretation of the open-path CO2 flux measurements due to the errors induced by the effects of thermal and water vapor fluctuations in the measurement path (Webb, et al., 1980, Quart. J. Royal Meteor. Soc., v106, 85- 100). In addition, this instrumentation is important for the measurement of H2O, as the flux of water vapor over the sea is a very important component in the total heat budget and in the turbulence structure of the marine atmospheric surface layer.

In addition to the participation in the staging of ASGAMAGE-B on the MPN, ETL was also an active participant in the two post-experimental workshops. During the first of these workshops, which was held on September 22-25, 1997 at KNMI headquarters in DeBilt, the Netherlands, Jeffrey Hare presented a talk entitled "NOAA/ETL Water Vapor Measurements During ASGAMAGE-B" by Hare and Fairall. The final workshop was held in Brussels on January 6-7 1999, an invited talk entitled "Results from the GASEX-98 Experiment," by Hare, Fairall, Edson, and McGillis was presented to the ASGAMAGE-B participants.

KNMI-PUBLICATIES, VERSCHENEN SEDERT 1995

Een overzicht van eerder verschenen publicaties, wordt verzoek toegezonden door de Bibliotheek van het KNMI, postbus 201, 3730 AE De Bilt, tel. 030 - 2 206 855, fax. 030 - 2 210 407; e-mail: biblioth@knmi.nl

▼ KNMI-PUBLICATIE MET NUMMER

150-28 Sneeuwdek in Nederland 1961-1990 / A.M.G. Klein Tank
180a List of acronyms in environmental sciences : revised edition / [compiled by P. Geerders and M. Waterborg]
181b FM12 SYNOP internationale en nationale regelgeving voor het coderen van de groepen 7wwW1W2 en 960ww; derde druk
183-1 Rainfall in New Guinea (Irian Jaya) / T.B. Ridder
183-2 Vergelijking van zware regens te Hollandia (Nieuw Guinea), thans Jayapura (Irian Jaya) met zware regens te De Bilt / T. B. Ridder
183-3 Verdamping in Nieuw-Guinea, vergelijking van gemeten hoeveelheden met berekende hoeveelheden / T.B. Ridder
183-4 Beschrijving van het klimaat te Merauke, Nieuw Guinea, in verband met de eventuele vestiging van een zoutwinningsbedrijf / T.B. Ridder a.o.
183-5 Overzicht van klimatologische en geofysische publikaties betreffende Nieuw-Guinea / T.B. Ridder
184a Inleiding tot de algemene meteorologie : studie-uitgave ; 2e druk / B. Zwart, A. Steenhuisen, m.m.v. H.J. Krijnen
185a Handleiding voor het gebruik van sectie 2 van de FM 13-X SHIP-code voor waarnemers op zee / KNMI; KLu; KM
186-I Rainfall generator for the Rhine Basin: single-site generation of weather variables by nearest-neighbour resampling / T. Brandsma a.o.
187 De wind in de rug: KNMI-weerman schaatst de Elfstedentocht / H. van Dorp
188 SODA workshop on chemical data assimilation: proceedings; 9-10 December 1998, KNMI, De Bilt, The Netherlands

▼ TECHNISCH RAPPORT = TECHNICAL REPORT (TR)

170 DARR-94 / C.P.G. Lomme
171 EFEDA-91: documentation of measurements obtained by KNMI / W.A.A. Monna a.o.
172 Cloud lidar research at the Royal Netherlands Meteorological Institute KNMI2B2, version 2 cloud lidar analysis / A.Y. Fong a.o.
173 Measurement of the structure parameter of vertical wind-velocity in the atmospheric boundary layer / R. van der Ploeg
174 Report of the ASGASEX'94 workshop / ed. by W.A. Oost
175 Over slecht zicht, bewolking, windstoten en gladheid / J. Terpstra
176 Verification of the WAQUA/CSM-16 model for the winters 1992-93 and 1993-94 / J.W. de Vries
177 Nauwkeuriger nettostraling meten / M.K. van der Molen en W. Kohsiek
178 Neerslag in het stroomgebied van de Maas in januari 1995: waarnemingen en verificatie van modelprognoses / R.Jilderda a.o.
179 First field experience with 600PA phased array sodar / H. Klein Baltink
180 Een Kalman-correctieschema voor de wegdektemperatuurverwachtingen van het VAISALA-model / A. Jacobs
181 Calibration study of the K-Gill propeller vane / Marcel Bottema
182 Ontwikkeling van een spectraal UV-meetinstrument / Frank Helderman
183 Rainfall generator for the Rhine catchment : a feasibility study / T. Adri Buishand and Theo Brandsma
184 Parametrisatie van mooi-weer cumulus / M.C. van Zanten
185 Interim report on the KNMI contributions to the second phase of the AERO-project / Wiel Wauben, Paul Fortuin a.o.
186 Seismische analyse van de aardbevingen bij Middelstum (30 juli 1994) en Annen (16 augustus '94 en 31 januari '95) / [SO]
187 Analyse wenselijkheid overname RIVM-windmeetlokaties door KNMI / H. Benschop
188 Windsnelheidsmetingen op zeestations en kuststations: herleiding waarden windsnelheden naar 10-meter niveau / H. Benschop
189 On the KNMI calibration of net radiometers / W. Kohsiek
190 NEDWAM statistics over the period October 1994 - April 1995 / F.B. Koek
191 Description and verification of the HIRLAM trajectory model / E. de Bruijn
192 Tiltmeting . een alternatief voor waterpassing ? / H.W. Haak
193 Error modelling of scatterometer, in-situ and ECMWF model winds; a calibration refinement / Ad Stoffelen
194 KNMI contribution to the European project POPSICLE / Theo Brandsma a.o.
195 ECBILT a coupled atmosphere ocean sea-ice model for climate predictability studies / R.J. Haarsma a.o.
196 Environmental and climatic consequences of aviation: final report of the KNMI contributions to the AERO-project / W. Wauben a.o.
197 Global radiation measurements in the operational KNMI meteorological network: effects of pollution and ventilation / F. Kuik
198 KALCORR: a kalman-correction model for real-time road surface temperature forecasting / A. Jacobs
199 Macroseismische waarnemingen Roswinkel 19-2-1997 / B. Dost e.a.
200 Operationele UV-metingen bij het KNMI / F. Kuik
201 Vergelijking van de Vaisala's HMP233 en HMP243 relatieve luchtvochtigheidsmeters / F. Kuik
202 Statistical guidance for the North Sea / Janet Wijngaard and Kees Kok
203 UV-intercomparison SUSPEN / Foeke Kuik and Wiel Wauben
204 Temperature corrections on radiation measurements using Modtran 3 / D.A. Bunskoek, A.C.A.P. van Lammeren and A.J. Feijt
205 Seismisch risico in Noord-Nederland / Th. De Crook, H.W. Haak en B. Dost
206 The HIRLAM-STAT-archive and its application programs / Albert Jacobs
207 Retrieval of aerosol properties from multispectral direct sun measurements / O.P. Hasekamp
208 The KNMI Garderen Experiment, micro-meteorological observations 1988-1989; instruments and data / F.C. Bosveld a.o.
209 CO2 in water and air during ASGAMAGE: concentration measurements and consensus data / Cor M.J. Jacobs, Gerard J. Kunz, Detlev Sprung a.o.
210 Elf jaar Cabauw-metingen / J.G. van der Vliet
211 Indices die de variabiliteit en de extremen van het klimaat beschrijven / E.J. Klok
212 First guess TAF-FGTAF: semi-automation in TAF production / Albert Jacobs
213 Zeer korte termijn bewolkingsverwachting met behulp van METCAST: een verificatie en beschrijving model-uitvoer / S.H. van der Veen
214 The implementation of two mixed-layer schemes in the HOPE ocean general circulation model / M. van Eijk
215 Stratosphere-troposphere exchange of ozone, diagnosed from an ECMWF ozone simulation experiment / Harm Luykx
216 Evaluatierapport Automatisering Visuele Waarnemingen Ontwikkeling Meestsystemen / Wiel Wauben en Hans de Jongh
217 Verificatie TAF en TREND / Hans van Bruggen
218 LEO - LSG and ECBILT coupled through OASIS: description and manual/A. Sterl
219 [nog niet verschenen]
220 Back-up modellering van windmeetmasten op luchthavens / Ilja Smits

▼ WETENSCHAPPELIJK RAPPORT = SCIENTIFIC REPORT (WR)

95-02 Internal variability of the ocean generated by a stochastic forcing / M.H.B. van Noordenburg
95-03 Applicability of weakly nonlinear theory for the planetary-scale flow / E.A. Kartashova
95-04 Changes in tropospheric NOx and O3 due to subsonic aircraft emissions / W.M.F. Wauben a.o.
95-05 Numerical studies on the Lorenz84 atmosphere model / L. Anastassiades
95-06 Regionalisation of meteorological parameters / W.C. de Rooy
95-07 Validation of the surface parametrization of HIRLAM using surface-based measurements and remote sensing data / A.F. Moene a.o.
95-08 Probabilities of climatic change : a pilot study / Wieger Fransen (ed.) a.o.
96-01 A new algorithm for total ozone retrieval from direct sun measurements with a filter instrument / W.M.F. Wauben
96-02 Chaos and coupling: a coupled atmosphere ocean-boxmodel for coupled behaviour studies / G. Zondervan
96-03 An acoustical array for subsonic signals / H.W. Haak
96-04 Transformation of wind in the coastal zone / V.N. Kudryavtsev a.o.
96-05 Simulations of the response of the ocean waves in the North Atlantic and North Sea to CO2 doubling in the atmosphere / K. Rider a.o.
96-06 Microbarograph systems for the infrasonic detection of nuclear explosions / H.W. Haak and G.J. de Wilde
96-07 An ozone climatology based on ozonesonde measurements / J.P.F. Fortuin
96-08 GOME validation at KNMI and collaborating institutes / ed. P Stammes a.o.
97-01 The adjoint of the WAM model / H. Hersbach
97-02 Optimal interpolation of partitions: a data assimilation scheme for NEDWAM-4; description and evaluation of the period November 1995 - October 1996 / A.Voorrips
97-03 SATVIEW: a semi-physical scatterometer algorithm / J.A.M. Janssen a.o.
97-04 GPS water vapour meteorology . status report / H. Derks a.o.
97-05 Climatological spinup of the ECBILT oceanmodel / Arie Kattenberg a.o.
97-06 Direct determination of the air-sea transfer velocity of CO2 during ASGAMAGE / J.C.M. Jacobs, W. Kohsiek and W.A. Oost
97-07 Scattering matrices of ice crystals / M. Hess, P. Stammes a.o.
97-08 Experiments with horizontal diffusion and advection in a nested fine mesh mesoscale model / E.I.F. de Bruijn
97-09 On the assimilation of ozone into an atmospheric model / E.Valur Hólm
98-01 Steady state analysis of a coupled atmosphere ocean-boxmodel / F.A. Bakker
98-02 The ASGAMAGE workshop, September 22-25, 1997 / ed. W.A. Oost
98-03 Experimenting with a similarity measure for atmospheric flows / R.A. Pasmanter and X.-L. Wang
98-04 Evaluation of a radio interferometry lightning positioning system / H.R.A. Wessels
98-05 Literature study of climate effects of contrails caused by aircraft emissions / V.E. Pultau
99-01 Enhancement of solar and ultraviolet surface irradiance under partial cloudy conditions / Serdal Tunç
99-02 Turbulent air flow over sea waves: simplified model for applications / V.N. Kudryavtsev, V.K. Makin and J.F. Meirink
99-03 The KNMI Garderen experiment, micro-meteorological observations 1988-1989: corrections / Fred C. Bosveld
99-04 ASGAMAGE: the ASGASEX MAGE experiment final report / ed. W.A.Oost